CR 151753

BARNES

ADVANCED MULTISPECTRAL SCANNER (AMS) STUDY

PROJECT 2738

(NASA-CR-151753) ADVANCED MULTISPECTRAL SCANNER (AMS) STUDY Final Report (Barnes Engineering Co., Waltham, Mass.) 217 p HC A10/MF A01 CSCL 14B

N78-29424

Unclas
G3/35 27223

FINAL REPORT, MA 183T
Under NASA/JSC Contract
NAS 9-15323

Submitted to:

NASA
Lyndon B. Johnson Space Center
Houston, Texas 77058

June 30, 1978

BARNES ENGINEERING COMPANY
44 Commerce Road
Stamford, Connecticut 06904

TABLE OF CONTENTS

TABLE OF CONTENTS
(Continued)

TABLE OF CONTENTS
(Continued)

LIST OF ILLUSTRATIONS

LIST OF ILLUSTRATIONS
(Continued)

LIST OF TABLES

1.0 INTRODUCTION

Barnes Engineering Company, Stamford, Connecticut, performed a study of an Advanced Multispectral Scanner for NASA, Lyndon B. Johnson Space Center, Houston, Texas. The study was made under Contract NAS 9-15323, of one year nominal duration, to be completed April 14, 1978.

This final report, MA 183T, is submitted in compliance with the data reporting requirements of DRL T-1377. The report includes the analyses and studies performed by Barnes, and presents the required data, preliminary design specifications, and recommendations. It complies with the Statement of Work (SOW) for Advanced Multispectral Scanner, dated September 30, 1976, and with directions from the Technical Monitor at NASA, Houston.

The Table of Contents provides a clear picture of the organization of the report. To facilitate location of the specific task items called for by the Statement of Work, the SOW paragraphs are indicated in parentheses in the table.

2.0 THE MULTISPECTRAL SCANNER PERFORMANCE OBJECTIVE

To provide a baseline for this discussion of the study objectives, Section 1.0, Scope, of the SOW is transcribed here.

1.0 SCOPE

This effort is for a study and a preliminary design specification for an advanced multispectral scanner for use in an aircraft for remote sensing data collection in the 1980 time frame. The contractor shall provide conceptual sketches, data and supporting information to describe the subject instrument. The study shall address state of the art instrumentation in the technology common to aircraft multispectral scanners. The product of the study shall be a comprehensive report and specifications which will fully define the instrument. All areas of interest to scanner design shall be detailed as portions of the study. For each area an approach is to be selected based on supportable arguments (charts, data, narrative discussions, performance record or other information).

In discussing this statement of scope in a meeting at NASA Houston, the point was emphasized that the approach was not to be "blue sky," that the "state of the art" was to be manufacturable and not a one-of-a-kind success in a research program. This clarification was important to the subsequent study. It provided a set of guidelines that encouraged concentration on the details and difficulties of the surely achievable, rather than a diffusion of effort into the broad area of the possible.

The problem of clearly defining the performance objective in quantitative terms proved to have some difficulties. For example, the attempt to tie down the optimum spectral regions of the entire multispectral scanner did not succeed because of there being no clear agreement among the users in the remote sensing field. Therefore, the approach was taken that, as long as the optics, detectors, and general systems configurations considered would tolerate simple changes in spectral bandpass, it was unnecessary to define the particular intervals during the study.

The performance objective then becomes more tractable to definition. In Table 2-1, the performance objectives are summarized. These objectives also represent the general final system specifications.

TABLE 2-1. AMS PERFORMANCE OBJECTIVES

Angular Coverage	±60° from nadir, perpendicular to line of flight
Element Angular Resolution	1 x 1 milliradian nominal, 0.4 - 1 μm 2 x 2 milliradian nominal, 1.8 - 14 μm
Sensitivity	3.5% or better contrast* at λ_c = 0.4 μm 0.3% or better contrast* at λ_c = 0.8 μm 1°K or better NET** at λ_c = 3.8 μm 1°K or better NET** at λ_c = 10 μm
Spectral Coverage	0.4 μm to 14 μm in selectable intervals
V/H Rate Range	0.025 to 0.25 rads/sec.
Automatic Roll Correction	±8.7°
Environmental Operation	-22°F to 110°F
High Reliability, Maintainability	

* Under Typical Scene Conditions:

Sun Angle	45°
Average Earth Reflectance	20%
Average Atmospheric Transmissions	80%

** At 300°K Limited by Background Subtraction

3.0 SELECTION OF THE SCANNER PRINCIPLE

In the past, selection of a scanner principle always involved extensive and detailed considerations of whirling mirrors, motors, bearings, lubricants and shock and vibration analyses. This was because, after careful evaluation of the state-of-the-art of detector arrays, it was correctly decided that such arrays were not really available for inclusion in operational hardware, relegating electronic scanning to the future. Therefore, the survey of mechanical scanners would be undertaken.

Now, however, the large scale detector array is available as an off-the-shelf commercial component from the silicon technology industry and great progress has been made in the devices for longer wavelengths. Also, large and continuing government support has appeared for the infrared detector arrays, greatly increasing the probability of the availability of flightworthy devices by the 1980 era.

The argument for the superiority of the pushbroom concept over the single-element mechanical scanner is a simple one. In the present case, we would compare two thousand individual detectors in an array, each scanning an instantaneous field of one by one milliradian, with a single one-milliradian detector scanning the same two thousand field elements consecutively. The minimum theoretical advantage of the array elemental sensitivity would be $(2000)^{1/2} \cong 45$. This is an enormous increase in sensitivity in a technology that pays large premiums to gain factors of two (by antireflection coating all optical surfaces, for example).

It might be thought that the factor of 45 could be regained by increasing the optical collector area by that factor. This is not so when we consider optimum optical design, however. When the optical system is scaled up, the

detector must increase in size to subtend the same field of view. This increases its noise as the square root of area, so the required increase of factor 45 is to the diameter, not the area. If we assume that the volume (and mass) of an optical system increases as a power somewhat greater than two of its diameter, the mass advantage is of the order of 10^4. This is overwhelming and shows clearly why so much effort has been put into the development of large-scale linear (and areal) detector arrays.

Before closing the door on mechanical scanner systems, the possible advantages of intermediate schemes, mechanically scanning small-scale arrays of, say, 100 detectors was investigated. While no formal scanning system was employed, an extended discussion of the pros and cons, considering sensitivity, size, data handling, roll compensation, image rotation, V/H compensation and/or speed control, etc., led to the conclusion that a hybrid system combined the worst, rather than the best, of each system and the static pushbroom system was the method of choice.

This decision eliminated the necessity of making an extensive study of mechanical scanning systems. However, a new task immediately appeared. The detector array technology was restricted to planar arrays, usually for very high angular resolution over small to moderate field angles. Fields of 60° to 120° can hardly be called moderate. The problem is to transfer the energy from a 120° field of view to a flat focal plane, using a fast optical system with resolution of the order of one milliradian. Apparently considerable ingenuity and effort would be required, since to our knowledge no such optical system exists.

Also considered were the advantages of using an area array, e.g., 1000 elements wide and 10 deep with a signal processing technique commonly referred to as TDI. This approach is particularly useful in military applications where extremely high sensitivities are required, since the S/N is improved by the $\sqrt{n}$, which for the above example would be 3.2 times. However, for the AMS application such an improvement is of marginal value when the data processing complexity is considered. As discussed in Section 4.4, with only 1000 elements, the internal data rate is on the order of 10 MHz; increasing the number of detector elements by n also must increase the data rate by n. In addition, the ground data reduction process becomes enormous when effects of aircraft yaw must now be calibrated out of the data. Consequently, the AMS system was based on the use of linear arrays.

In summary, the availability of large-scale linear detector arrays makes the pushbroom static scanner principle the clear choice. The task then becomes one of determining the best method of employing these arrays, rather than whether or not to employ them.

4.0 DETAILS OF THE AMS DESIGN

In this section we discuss in detail the design considerations and tradeoffs required to establish a candidate design for the AMS. As discussed in Section 2.0, the design presented is modular in construction and allows for operational flexibility. Two optical sensor modules have been studied; one covers the short wavelength region and the other the long wavelength region.

4.1 Detectors and AMS System Design Considerations

4.1.1 Detector Types

Short Wavelength Detectors

At the present time there are three types of short wavelength detector arrays using charge transfer technology. Two of these are CCD devices and CID devices. Both technologies are monolithic, that is, the photon detection and the charge readout processes are fabricated on the same silicon chip. A third type of array is composed of an array of silicon diodes coupled to a silicon CCD shift register. This latter device is called a hybrid. Either area or linear arrays are commercially available.

A CCD is basically a metal-oxide-semiconductor structure which can detect and store minority carrier charge packets in localized potential wells at the $Si-SiO_2$ interface. The CCD can transfer charge packets in discrete time increments via the controlled movement of potential wells. The change is detected at an output node via capacity coupling. (See Ref. 3).

A CID is quite similar to the CCD with regard to the detector and integration processes. The major difference between the two is in the transfer or readout process. Whereas the CCD is a serial readout device, the CID is a random access device. It reads out the charge stored in a potential well by injecting it into the bulk at the end of an integration time. These carriers recombine at the substrate contact and generate a current flow in the external circuit which is read out in an x-y fashion.

Fairchild is presently offering several types of buried channel monolithic devices for sale commercially, e.g. CCD131, whereas Reticon is offering at present a hybrid device, e.g. CCPD1024, which uses a surface channel CCD shift register. See Appendix C and reference 21. General Electric is presently offering for sale a series of CID's.

Long Wavelength Detectors

Long wavelength detector arrays also can be classified in two distinct types: monolithic and hybrid.

There is apparently at the present time only one type of monolithic device being seriously developed: Extrinsic Silicon CCD's. However, other monolithic devices exist in the laboratory. See Ref. 23. The extrinsic silicon CCD has been popular because it borrows heavily from the mature silicon CCD technology associated with short wavelength CCD detectors. Its major drawback from an operation sense is its required low operation temperature. These devices usually operate between 25°K and 40°K, with 55°K a sought-after goal. As shown in reference 18, using a single stage Stirling Cooler, with a one watt heat load, 100W of power are required to reach a 40°K operating temperature with the power increasing quite rapidly the lower the desired temperature.

There is also a good deal of work going into hybrid devices using conventional long wavelength detectors and operating at 77°K or greater. Table 4-1 was prepared to identify the various detector types, their developers, and some of their salient performance characteristics, including cooling requirements.

For the most part, the work being done in this area is either proprietary or classified. Consequently no spec sheets exist for these detectors and performance is deduced from published literature, private communications, and specific knowledge of IR detectors used in hybrid configurations.

TABLE 4-1. SUMMARY OF LONG WAVELENGTH CTD DETECTOR ARRAY TECHNOLOGY

Developer	Technology Under Development	Spectral Region (μm)	Operating Temp.	Array Size	Detector Element Size	Remarks
General Electric	Hybrid CID, InSb	3 - 5	77°K	32 x 32	4 mils 2 mils	Devices available now, smaller detectors probably under development
Honeywell	Hybrid: pV MCT/Si CCD	3 - 5 8 - 12	140°K 77°K	270 x 8	Several mils	Linear array and mosaics; fabrication due Fall 1979
Hughes	Classified					
Rockwell	Extrinsic Si Si:Ga Si:In	 3 - 5 8 - 14	 25°K			Most work is in area arrays
SBRC	Hybrid { InAsSb InGaSb MCT (PV) MCT (PC)	3 - 5 8 - 12	77°K	32 x 32	4 mils	135°K operation predicted in future. 200 el x 16 el arrays available soon. D* 5×10^{12} achieved
TI	Hybrid MCT					
Westinghouse	Extrinsic Si Si:In	3 - 8	40°K		3 - 4 mils	Linear array under development, smaller detector element sizes too.

4.1.2 Detector Noise

All of the detector types discussed in Section 4.1.1 have a number of noise sources in common, regardless of whether we are considering a short wavelength or a long wavelength detector array. Rather than attempt to delve deeply into this subject which has been extensively investigated in the literature, we will restrict the discussion in this section to the most significant noise sources and their effect on system performance.

Many references discuss this topic. Reference 3 has a particularly good summary of CCD noise sources in tabular form; Figure 4-1 reproduces that table. All noise sources in CCD's can be divided into three categories: input, integration and transfer, and output. Before discussing the table, however, it would be informative to identify the relationship between noise equivalent power (NEP) and noise equivalent signal charge (NES) since we use the former in subsequent discussions. It can be shown that

$$NEP\Big|_{\lambda = \lambda_c} = NES\left(\frac{hc}{\lambda_c}\right)\left(\frac{1}{\eta}\right)\left(\frac{1}{t_I}\right)^{\frac{1}{2}}$$

where

$\frac{hc}{\lambda_c} = \frac{1.98 \times 10^{-19}}{\lambda_c}$ = photon energy $\left[\frac{\text{Joules}}{\text{photon}}\right]$ at $\lambda_c[\mu m]$

η = quantum efficiency [electrons/photon] at λ_c

t_I = integration time [sec]

For example, using the conditions listed in Figure 4-1 with $\eta = 0.1$ at 1 μm and assuming correlated double sampling to eliminate reset noise (see section 4.1.3) is employed, then

$$NEP\ (\lambda_c = 1\ \mu m) = 1.1 \times 10^{-15}\ w/\sqrt{Hz}$$

which is quite reasonable for this 1×10^{-6} cm^2 detector element.

SUMMARY OF CCD NOISE SOURCES

OPERATION	PROCESS	VARIANCE (Number of electrons)^2			
			SURFACE CHANNEL	BURIED CHANNEL (20°C)	BURIED CHANNEL (-50°C)
INPUT	PHOTON NOISE	n_s			
	FAT ZERO INPUT	$\frac{kT}{e^2} C_{I \cdot N}$	1.6×10^4	0	0
INTEGRATION AND TRANSFER	FAST INTERFACE STATES	$mkT N_{FIS} A$	4×10^6	0	0
	SLOW INTERFACE STATES	$mkT N_{SOS} A \ln(\tau/\tau_s)$ if $\tau >> \tau_s$	1300	0	0
		$m \frac{2kT}{e} N_{SOS} A(\tau/\tau_s)$ if $\tau << \tau_s$			
	BULK STATES	$mn_s \frac{N_t}{N_D}(1 - e^{-\tau/\tau_e}) e^{-\tau/\tau_e}$ if $\frac{14 n_s}{AN_D} > L_D$			
		$\frac{m}{14} AL_D(1 - e^{-\tau/\tau_e}) e^{-\tau/\tau_e}$ if $\frac{14 n_s}{AN_D} < L_D$		<35	<35
	DARK CURRENT	n_{dark}	10^4	10^4	50
OUTPUT	RESET AMPLIFIER	$\frac{kT}{e^2} C_{O \cdot N} + \left(\frac{C_{O \cdot N}}{e}\right)^2 \frac{8kTB}{3g_m}$	1.6×10^4	1.6×10^4	1.6×10^4
	CORRELATED DOUBLE SAMPLING	$\left(\frac{C_{O \cdot N}}{e}\right)^2 \frac{8kTB}{3g_m} + \left(\frac{C_{O \cdot N} i_n}{g_m e}\right)^2 B$	320	320	320
	DISTRIBUTED FLOATING GATE AMPLIFIER	$\frac{ef_c I_0}{0.4(g_m')^2 \mathcal{R}^2 M}$	100	100	100

n_s = number of signal electrons collected in a CCD cell,
$C_{I \cdot N}$ = input node capacitance,
m = number of positions involved in the process; i.e., for integration, $m = 1$; and for transfer m is the number of transfers,
A = area of a CCD gate,
N_{FIS} = fast interface-state density,
N_{SOD} = area density of slow oxide states,
τ = time a charge packet is under a gate,
τ_s = time constant of slow oxide states located at the $Si\text{-}SiO_2$ interface,
N_t = volume density of bulk traps in the silicon,
N_D = doping density of the buried channel,
τ_e = emission time constant of the bulk traps,
L_D = extrinsic Debye length in the channel,
n_{dark} = number of electrons added to a charge packet during integration and transfer due to dark current,
$C_{O \cdot N}$ = output node capacitance,
B = bandwidth of the output circuit,
g_m = transconductance of the output amplifier, and
i_n = equivalent noise current of the off-chip amplifier in amps/(Hz)$^{1/2}$
M = number of distributed amplifier stages,
$\mathcal{R}$ = responsivity of the floating gate in volts per electron,
g_m' = transconductance of the floating gate amplifier
I_0 = bias current of each floating-gate amplifier stage.

$C_{I \cdot N} = 0.1$ pf
$m = 1000$
$N_{FIS} = 10^{10}$ cm^{-2} (eV)$^{-1}$
$A = 10^{-6}$ cm^2
$N_{SOS} = 3 \times 10^{11}$ cm^{-2} (eV)$^{-1}$
$\tau_{integrate} = 1/30$ s
$\tau_{transfer} = 10^{-6}$ s
$\tau_s = 10^{-6}$ s
$N_t = 2 \times 10^{11}$ cm^{-3}
$N_D = 2 \times 10^{16}$ cm^{-3}
$L_D = 4 \times 10^{-6}$ cm
$C_{O \cdot N} = 0.1$ pf
$B = 4$ MHz
$g_m = 250$ micromhos
$i_n = 1$ pa/(Hz)$^{1/2}$
$M = 12$
$\mathcal{R} = 5$ microvolts per electron
$g_m' = 10$ micromhos
$I_0 = 10^{-6}$ amps

Figure 4-1 Summary of CCD Noise Sources (after Reference 3)

Referring again to Figure 4-1 , we see listed the magnitudes and expressions for the components of the noise equivalent charge for two CCD process technologies: surface channel and buried channel. Reticon uses the former in their CCPD 1024 device and Fairchild uses the latter in their CCD 131 device. For the situation analyzed in the figure, it is apparent that the buried channel device's major noise source is the dark current charge accumulated over the integration time when correlated double sampling is used to eliminate the reset noise. Consequently, as the figure shows, cooling the device is quite effective, since it reduces the current and therefore the noise equivalent charge associated with this process.

Now suppose we reduce, in the above example, the integration time from 1/30 sec. to 880 μsec; increase the bandwidth from 4 MHz to 7.5 MHz; and reduce the off-chip noise equivalent current from 1pa/$\sqrt{\text{Hz}}$ to 0.33pa/$\sqrt{\text{Hz}}$. Then the resulting noise equivalent signal charge using the equations in Figure 4-1 decreases from 100 electrons to 21 electrons, as follows:

$$\text{NES} = \left[\left(\frac{880\mu s}{33ms}\right) 10^4 + \left(\frac{7.5}{4}\right) 70 + \left(\frac{7.5}{4}\right)\left(\frac{.33}{1}\right)^2 250 \right]^{\frac{1}{2}}$$

$$= \left[\underset{\text{dark current}}{264} + \underset{\text{on chip preamp}}{131} + \underset{\text{off-chip amp}}{51} \right]^{\frac{1}{2}} = 21 \text{ electrons}$$

due to:

This result indicates that the predominant noise source under these particular conditions is the dark current noise. Since the signal charge build-up is directly proportional to the integration time and the noise equivalent charge, NES, is essentially proportional to the square root of this time, then the S/N is proportional to the square root of the integration time. This fact is exploited and

discussed in detail in section 4.4.1.3. The conditions used for this calculation were specifically selected since they correspond to the worst case situation for the AMS as discussed in section 4.1.4.

Another type of noise that is prevalent in a CCD is pattern noise. This noise manifests itself as a non-uniform spatial pattern "riding" on the output of each video sample from the array. It has a fixed portion usually produced by clock feed-through and bias charge variations; it also has a variable portion produced by dark current non-uniformity. The effects of this noise source on the processed video signals are minimized through the choice of appropriate sampling times and through direct removal in the ground data reduction process which is discussed in Section 6.2.

Although the above discussion concerned itself with CCD's, CID's also exhibit similar noise properties because of the similar process by which signal charge is detected. However, the output capacitance of a CID is the capacitance of the row and one column if all other columns are floated during the readout process. The output capacitance of a CCD, on the other hand, is only the capacitance of a reversed biased diode. Therefore, for a similar on-chip preamplifier configuration, the CID readout is noisier than that for a CCD and is probably preamplifier noise limited. Correlated double sampling, as discussed in section 4.1.3, may also be used for CID's to eliminate $\frac{KT}{C}$ noise and 1/f noise.

Unlike the short wavelength detector arrays, which see no background generated photon noise, the long wavelength detector arrays, whether monolithic or hybrid, are sensitive to this background radiation and generate significant photon noise. In such cases it is the goal of the detector and system design to achieve background limited performance (BLIP). For an Si:In extrinsic silicon CCD detector, for example reported in reference 18, BLIP was nearly attained in a 16-element time delay integration (TDI) mode. For a linear array, it is expected that this early array design would be a factor of 4 away from BLIP behavior.

4.1.3 Correlated Double Sampling

Figure 4-2 shows the typical output circuit for a CCD array. After the voltage change associated with each signal charge in read, the gate node is reset to some voltage V_R through the MOSFET switch. Since the switch has resistance, the Johnson noise produced by it appears across the capacitance associated with the node. When the switch is opened, a sample of this noise is stored on the capacitor. This noise voltage has been shown to be equal to (Ref. 3)

$$V_{nc} = \left[\frac{KT}{C}\left(1 - e^{-2t/RC}\right)\right]^{\frac{1}{2}}$$

where K = Boltzmann's constant

T = absolute temperature

C = node capacitance

R = resistance associated with node, with switch open.

Typically, RC is on the order of 100 ms. If resetting the output node is performed at a 5 MHz rate, i.e. every 200 ns, then

$$V_{nc} = \sqrt{\frac{KT}{C}}$$

which is essentially constant over this period. This reset noise is sometimes referred to as KT/C noise.

Therefore, to eliminate this reset noise from the next signal sample, that is, level B in Figure 4-2 , all we must do is measure level A and subtract it from level B. This procedure is referred to as correlated double sampling (CDS).

To implement CDS the circuit shown in Figure 4-19 is used. The clamp switch is closed during the period that the output node is being reset, and its capacitor charges to a voltage corresponding to the noise. When the next signal sample, B, appears at the output of the video buffer, the stored clamp voltage, A,

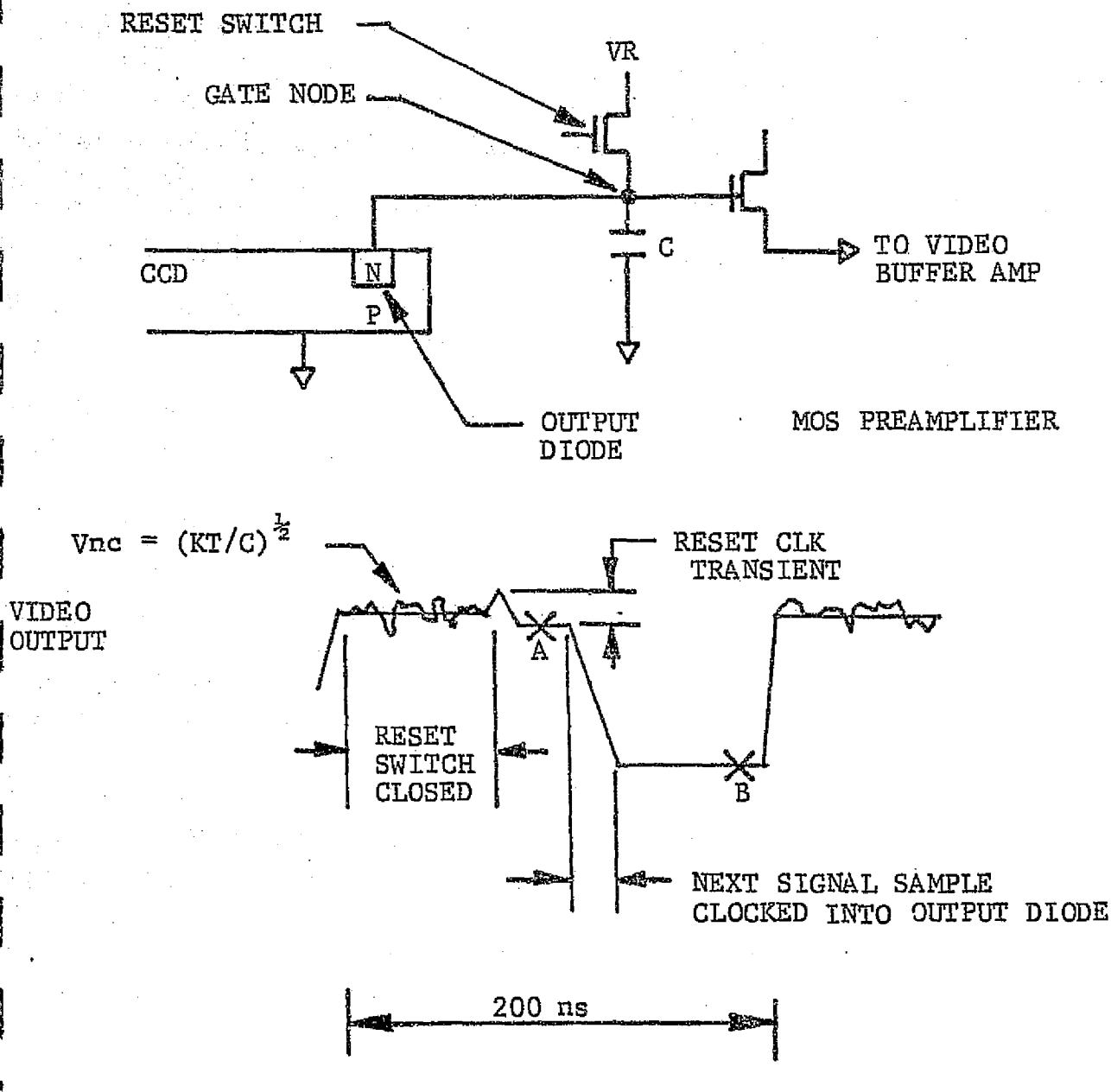

Figure 4-2 CORRELATED DOUBLE SAMPLING

subtracts from it, removing the KT/C noise. The resulting difference voltage is then sampled by a sample/hold circuit prior to A/D conversion. Since CDS takes the difference between two signals very close together in time, it also eliminates any 1/f noise present at the output of the array and buffer amplifier.

4.1.4 AMS System Design for the Short Wavelength Sensors

In order to study the tradeoffs between the various optical and electronic system parameters and system performance for the short wavelength sensors, Figure 4-3 was prepared.

Two CCD devices were investigated as part of this phase of the study; one is manufactured by Fairchild and the other by Reticon. The Fairchild CCD 121H detector array was used as the basis upon which Figure 4-3 was developed because of the completeness of the specifications associated with that device. But that device has 1728 detector elements as compared to the selected CCD 131 which is a 1024 element device. Since both devices are made by the same manufacturer and use the same technology, we have assumed that the detector parameters derived for one apply equally to the other, e.g., NEP (121 H) = NEP (131).

Although data provided by Reticon for their CCPD 1024 detector array indicates that its performance is superior to that of the Fairchild device especially at short wavelengths, there is reason to doubt the validity of some of the verbally provided data. Consequently, a conservative approach was taken and the AMS short wavelength sensor was developed about the CCD 131 with adequate system performance being achieved as discussed below. Nevertheless, one of the first tasks during the next phase is to evaluate the performance of both the Fairchild and Reticon devices in a "side-by-side" test in a controlled laboratory environment.

Referring again to Figure 4-3 , the major sensitivity parameter is $A_0 \theta^2$; where A_0 is the effective collecting area of the optical system and θ is its resolution. This parameter is plotted along the X axis in the figure.

Also identified on this axis and plotted against $A_0\,\theta^2$ is a range of optical T/nos. as discussed in Section 4.3.1.1. The T/no. is a calculated function of the detector area and optical system efficiency. That is:

$$T/\quad = \left[\frac{\frac{\pi}{4}\, d^2/A_0\,\theta^2}{(\text{OPT EFF})}\right]^{1/2}$$

The detector area, d^2, for the CCD 131 is 13 μm x 13 μm; as discussed in Section 4.3.4 the optical efficiency is expected to be approximately 50%.

Using the data on the CCD 131 provided by Fairchild, see Appendix C the performance parameters shown in Table 4-2 were generated. These, in turn, were used to calculate the minimum signal-to-noise ratio for the sensor as a function of, $A_0\,\theta^2$, see Figure 4-3. The S/N ratio is given by

$$S/N \quad = \left(\frac{B\sqrt{2}}{NEP\sqrt{V/H}}\right) A_0\,\theta^{5/2}$$

The minimum signal-to-noise ratio occurs when the V/H rate is maximum, the detector NEP is maximum and the scene brightness B is minimum. This equation is plotted for two spectral bands, i.e., $\lambda_c = 0.42\,\mu m$ and $\lambda_c = 0.8\,\mu m$ in Figure 4-3. These bands were selected since they correspond to the minimum and maximum detector sensitivities under worst case conditions. See Table 4-2. In order to evaluate the ability of the system to measure a 1% contrast, B was set at $0.01 \times B_{typ}$ and the resulting S/N plotted vs $A_0\,\theta^2$. However, before we use these results, the maximum integrator time, t_I, for each detector element in the array must be considered. t_I is given by:

$$t_I = \frac{E_S}{B_{max}} \quad \frac{d^2}{A_0\,\theta^2}$$

where: E_S is the saturation exposure associated with the particular CCD device selected and d^2 is the area of each of its detector elements.

In addition, it is a function of the maximum scene brightness B_{max}. Using Table 4-2 t_I was plotted vs $A_0 \theta^2$ for the worst case B_{max}, which occurs in Band 9 ($\lambda_c = 0.8\mu m$).

Note too, that the integration time and the number of CCD photosites establish the A/D conversion rate. This is because the charge stored in all of the array elements must be transferred and read out in a time which must not exceed t_I. Therefore for an N element array the maximum allowed A/D conversion time, t_c, is given by:

$$t_c = \frac{t_I}{N}$$

where: N = 1024 for the CCD 131. This parameter is also plotted in Figure 4-3.

Now in order to maximize a sensor's signal-to-noise ratio, we would want the fastest optical system, i.e., lowest possible T/no. However, without "stopping down" the system, making the optics faster requires that the detector element integration time be made shorter. This, in turn, requires a faster digitization rate and a faster CCD clocking rate.

The optical system developed in Section 4.3 for the short wavelength sensor has a T/no. of 1.1, which is as fast as is optically practical. Referring again to Figure 4-3 , we see that for this T/no., the signal-to-noise ratio is 3.5:1 for the most sensitivie band, $\lambda_c = 0.8\mu m$ and 0.28:1 for the least sensitive band, $\lambda_c = 0.42\mu m$. Since making the optics faster is not possible,

we can only improve the short wavelength signal-to-noise ratio by reducing the detector's NEP, all other things being equal. As indicated above, this may be a realistic possibility, if the Reticon CCPD 1024 array is as sensitive as the informally provided data indicates. However, until the laboratory tests comparing the performance of the two devices, as mentioned above, is complete we will assume the use of the Fairchild device.

Consequently, under the worst case brightness condition and at $\lambda_c = 0.4\mu m$, the minimum resolvable contrast (S/N = 1) expected for the AMS is 3.5%. However, as the center of the spectral band moves toward $0.8\mu m$, the contrast improves and is approximately 0.3% at $\lambda_c = 0.8\mu m$.

As was mentioned above, each photosite can accumulate only a certain amount of charge before saturation occurs. The charge buildup in the photosite is a direct function of the integration time, t_I, scene brightness, B, and the temperature of the array.

For the T/1.1 optical system selected, the maximum allowable integration time, t_I, for the maximum scene brightness, B_{max}, is $100\mu s$. Correspondlingly, for a scene of typical brightness, B_{typ}, the integration time may be as long as $880\mu s$. As a result of these short integration times, the temperature of the array has negligible affect on the amount of charge accumulated due to photosite leakage current.

At the end of the integration time, the charge accumulated in the photosites is dumped into a serial transfer register on the chip. As mentioned above, this charge must be read out in a time less than or equal to t_I Since t_I varies with wavelength, in order to have a constant readout rate for all sensors in the AMS system, we have used the shortest t_I (which occurs at $0.4\mu m$). Therefore, referring to Figure 4-3 , we see that for

the T/1.1 system the readout rate corresponds to 10 MHz, or each video sample occurs in 100 ns. Since this analog video data is ultimately digitized as described in Section 4.4.2, the A/D converter must also convert each sample at a 10 MHz rate.

As indicated above, the Fairchild CCD 131 must be read out at a 10 MHz rate in this application. Referring to Table 4-2 we see that for the Reticon device the maximum integration time is approximately three times longer than for the Fairchild device at the same center wavelength. This difference is due in part to the fact that the saturation exposure quoted for the CCPD 1024 device is approximately two times larger than that for the CCD 131 device and the area of the Reticon device is 1.5 times larger. If we assume that this factor of 3 holds for the worst case spectral band, i.e., 0.4 μm, then the read out rate would be approximately 3.3 MHz for the Reticon device. This read out rate is approaching the maximum allowable rate for the device which is 5 MHz. This situation will also have to be looked at carefully when considering the performance of the two devices in the next phase.

The signal-to-noise information plotted in Figure 4-3 was derived from the data in Table 4-2. As indicated in Table 4-2, the signal-to-noise ratio is the ratio of the minimum signal power to the detector NEP at a particular wavelength. The NEP is derived from detector information given on its spec sheet, e.g., the noise equivalent exposure, NEE, the area of the detector, and the integration time used in the measurement of the noise equivalent exposure. In addition, there is a term that is referred to as the noise bandwidth (NBW). The noise bandwidth is equal to $\frac{1}{2\,t_I}$. This equivalency stems from the fact that the data output from each photosite

is sampled by the A/D converter once every t_I seconds and stored in memory. This process is equivalent to that of an analog sample and hold circuit which is updated every t_I second. The transfer function of this type of circuit is equivalent to that of a $\frac{\sin x}{x}$ filter which has an equivalent noise bandwidth, NBW, equal to $\frac{1}{2\,t_I}$.

As discussed in Section 4.4.1.3, averaging the output of each detector element over the dwell time T_d, results in a S/N which is equivalent to that which would have been produced if the array integration time, t_I, were allowed to extend to T_d. Therefore, the S/N calculations which are presented in Table 4-2 use an equivalent noise bandwidth of $\frac{1}{2\,T_d}$. Since T_d is equal to $\frac{\theta}{V/H}$, where θ is the pixel resolution and V/H is the V/H rate of the aircraft, then the expression for the S/N in Table 4-2 equates to that in Figure 4-3.

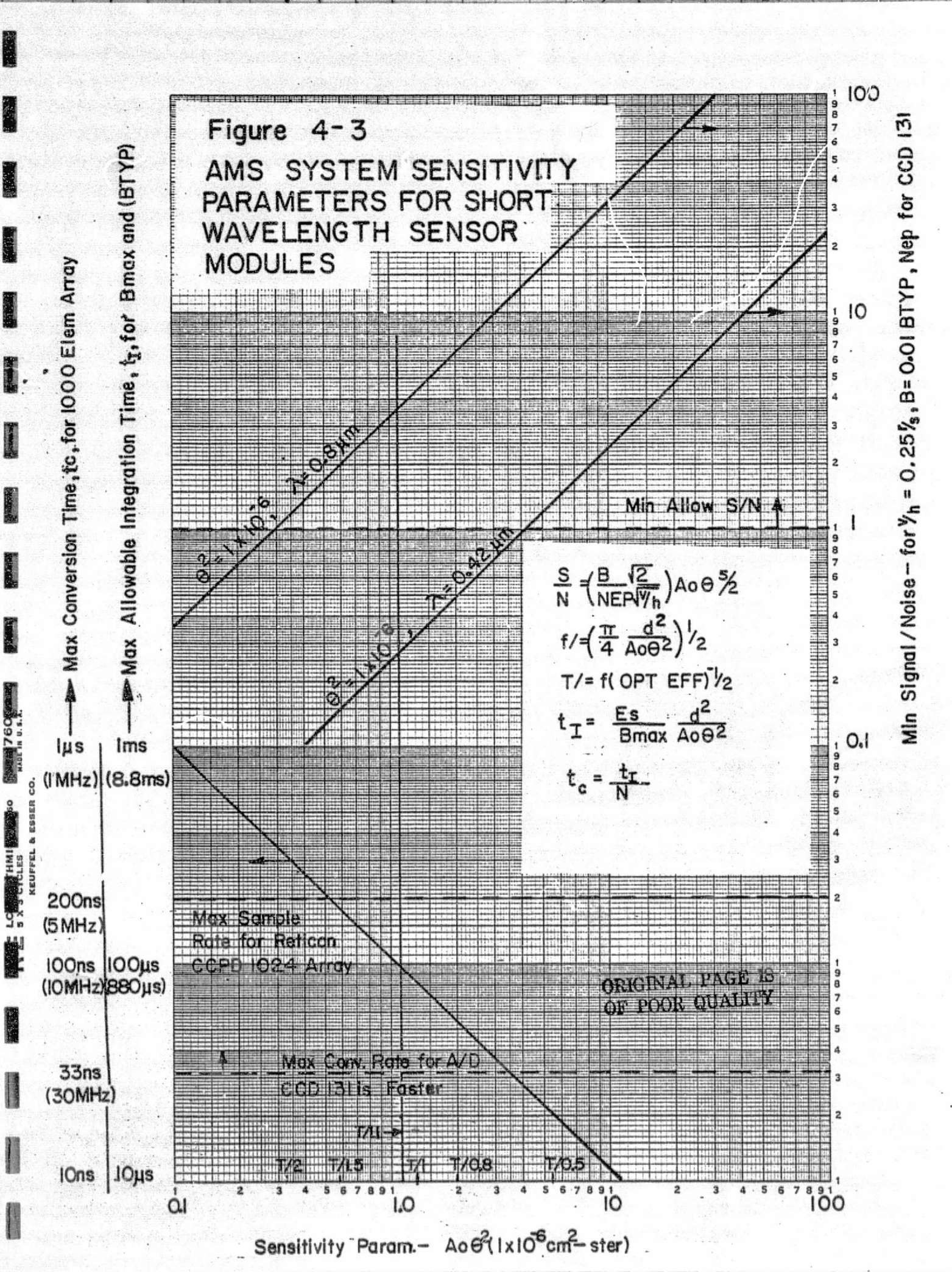
Figure 4-3
AMS SYSTEM SENSITIVITY PARAMETERS FOR SHORT WAVELENGTH SENSOR MODULES
Max Conversion Time, t_c, for 1000 Elem Array
Max Allowable Integration Time, t_I, for Bmax and (BTYP)
Min Signal / Noise – for η_h = 0.25, B = 0.01 BTYP, Nep for CCD 131
$\frac{S}{N} = \left(\frac{B}{NEP\sqrt{\eta_h}}\right) A_o\theta \sqrt{2}$
$f/ = \left(\frac{\pi}{4}\frac{d^2}{A_o\theta^2}\right)^{1/2}$
$T/ = f(\text{OPT EFF})^{-1/2}$
$t_I = \frac{E_s}{B_{max}}\frac{d^2}{A_o\theta^2}$
$t_c = \frac{t_I}{N}$
$\theta^2 = 1 \times 10^{-6}$, $\lambda = 0.8\mu m$
$\theta^2 = 1 \times 10^{-6}$, $\lambda = 0.42\mu m$
Min Allow S/N
1µs (1MHz)
1ms (8.8ms)
200ns (5MHz)
100ns (10MHz)
100µs (880µs)
33ns (30MHz)
10ns
10µs
Max Sample Rate for Reticon CCPD 1024 Array
Max Conv. Rate for A/D
CCD 131 is Faster
T/1.1
T/2
T/1.5
T/1
T/0.8
T/0.5
ORIGINAL PAGE IS OF POOR QUALITY
0.1
1.0
10
100
Sensitivity Param. – $A_o\theta^2$ (1×10^{-6} cm^2 – ster)

TABLE 4-2

SHORT WAVELENGTH SENSOR - S/N PERFORMANCE PARAMETERS FOR FAIRCHILD CCD 121H/CCD 131

(1) Band No.	(2) Center Wavelength λ_c (μm)	(3) Rel. Responsivity	(4) Noise Equiv. Exposure NEE (nJ/cm^2)	(5) Noise Equiv. Power NEP (x 10^{-13} w/$\sqrt{Hz}$)	(6) Min. Sig. Pwr. P_s (pw) for $A_0\theta^2$ = 1 x 10^{-6} st-cm^2	(7) S/N min. for $A_0\theta^2$ = 1 x 10^{-6}-st-cm^2 & V/H = 0.25 r/s	(8) Sat. Exp. S_E (nJ/cm^2)	(9) Max. t_I
1	0.42	0.17	5.9	4.3	1.19	0.25	941	1.51 ms
2	0.47	0.30	3.3	2.4	1.61	0.60		
3	0.51	0.45	2.2	1.6	1.98	1.11		
4	0.55	0.6	1.67	1.2	1.80	1.34		
5	0.59	0.73	1.37	1.0	1.73	1.55	219	242 μs
6	0.63	0.82	1.22	0.89	1.65	1.66		
7	0.67	0.9	1.1	0.80	1.55	1.73		
8	0.72	1.0	1.0	0.73	1.44	1.76		
9	0.81	1.0	1.0	0.73	2.77	3.4	160	110 μs
10	0.99	0.43	2.3	1.67	1.34	0.72		

FOR RETICON CCPD 1024

5	0.59	0.85	0.17	0.062	1.65	25	420	703 μs

NOTES ON COLUMN (N)

(3) Rel. Responsivity = $\frac{\mathcal{R}_\lambda}{\mathcal{R}_{pk}}$

(4) (5) $NEP = \frac{NEE}{t_I \sqrt{NBW}} A_D$

NEP = Noise Equivalent Power (w/$\sqrt{Hz}$)

NEE = Noise Equivalent Exposure in NBW (nJ/cm^2, rms)
= 1 nJ/cm^2, rms in 280 Hz for CCD 121H

A_D = Detector Photosite Area = 2.2 x 10^{-6} cm^2 for CCD 121H

t_I = Integration Time = 1.78 ms for CCD 121H

NBW = Noise Bandwidth = $\frac{1}{2 t_I}$ = 280 Hz for CCD 121H

(6) $P_{s_{min}} = B_{min} (A_0 \theta^2)$

B_{min} = 0.01 B_{typ} (see Table 4-4.)

A_0 = Collecting Area = 1 cm^2

θ^2 = Instantaneous FOV
= (1 mrad)^2 = 1μ-ster

Let $A_0 \theta^2$ = 1 x 10^{-6}-ster-cm^2

(7) $\left.\frac{S}{N}\right|_{min} = \frac{P_{s_{min}}}{NEP \sqrt{NBW}}$

$NBW = \frac{1}{2 t_I} = \frac{1}{2 T_d}$

$T_d = \frac{\theta}{V/H}$

$\sqrt{NBW} = \sqrt{\frac{V/H}{2\theta}}$

for θ = 1 mr, V/H = 0.25 r/s

NBW = 125 Hz

(8) $S_{E_\lambda} = \frac{\mathcal{R}_{pk}}{\mathcal{R}_\lambda} S_{E_{pk}}$

$S_{E_{pk}}$ = 160 nJ/cm^2 for CCD 121H

(9) $t_{I_{max}} = \frac{S_{E_{min}}}{P_{max}} A_D^2$

$P_{max} = B_{max} (A_0 \theta^2)$

A_D = 1.69 x 10^{-6} for CCD 131

$S_{E_{min}} = S_{E_\lambda}$ (λ_c = 0.8)

4.1.5 AMS System Design for the Long Wavelength Sensor

The optical design of the long wavelength sensor module, which is described in Section 4.3.9, achieves the same 60° field of view as had been achieved for the short wavelength sensor. The long wavelength design is based on the availability of a detector array with 512 elements, 4 mils by 4 mils in area and on 4 mil centers. This geometry corresponds to an optical resolution of 2 mrad for each element in the array. The optical design in Figure 4-12 just achieves this resolution and consequently linear detector arrays, if available, with larger numbers of elements would not result in any higher optical resolution.

Based upon the information available at this time on long wavelength detector arrays, see Table 4-1, we believe that the 4 mil, 512, element array represents a realistic size that certainly will be available in 1980 era.

The major difference between detector arrays operating in the long and short wavelength spectral regions is the level of background radiation present. If we assume that most objects and natural scenes that the AMS will view have an average temperature of 300°K, then a black body at this temperature will emit radiation equivalent to that of the background. Consequently, the background radiation emitted in the short wavelength region below, say, 1 μm will be quite negligible; but increases rapidly as the spectral bandpass of the sensor moves toward longer wavelengths. For example, the radiant emittance of a 300°K background at 10 μm is over 10^6 greater than at 1 μm.

This long wavelength background radiation generates signal charge in the detector array which for these long wavelengths and large fields of view may totally mask the dark current in each detector element. As was shown in Section 4.1.4, it was this detector dark current which produced the predominant

system noise. In the case of the long wavelength detectors, it is the background current which contributes to system noise and as a design goal predominates it producing BLIP behavior.

One other aspect of the large background generated signal is that its charge adds directly to the leakage current charge and consequently may limit the maximum integration time, t_I, of the detector array. Since most of the literature on long wavelength devices is sketchy to say the least, probably due to its present developmental nature coupled with its confidential status, the saturation charge capacity or alternately the maximum exposure time is barely mentioned. Of the literature listed in Section 9.0, only one reference (23) cites this parameter. It is stated for several monolithic devices; one being an In Sb device operated at 77°K, over a spectral band of 3.5 - 4.2 μm, with a 30° FOV. Under these conditions t_I is 5.8 msec. as determined by the background level.

Since the integration time is directly proportional to the elemental detector's field of view (solid angle), then for a 2π steradian field of view, the maximum integration time would become:

$$t_I = 5.8 \text{ ms} \quad \frac{2\pi(1 - \cos 15°)}{2\pi}$$

$$t_I = 197 \mu s$$

For this particular device, the leakage current generated charge would saturate the device in 2.1 sec. Consequently as expected, the background radiation determines the maximum integration time.

Alternately let us consider a hybrid device. We will assume operation in the 8 - 14 μm window region using a photovoltaic Hg Cd Te detector array coupled to a silicon CCD. This is a common arrangement.

If we assume that the active area of each element in the CCD array is 50% of its total area, than for a 25 μm square element its active area is 3.13×10^{-6} cm^2. The maximum charge density of a CCD is set by the dielectric strength of the $Si\ 0_2$ gate insulator and is 10^{13} el/cm^2. Consequently, the resulting saturation charge of the CCD array is 3.13×10^7 electrons. If each element of the Hg Cd Te detector is 4 mils square, then the total area of each element is 10^{-4} cm^2. As indicated in Reference 12, a similar device had a background current of 200 nA for a 180° FOV. Now

$$200\,nA = 2 \times 10^{-7} \frac{C}{sec} = \frac{2 \times 10^{-7}}{1.63 \times 10^{-19}} \frac{el}{sec} = 1.23 \times 10^{12} \frac{el}{sec}$$

Therefore, the maximum integration time for this device is:

$$t_I = \frac{3.13 \times 10^7}{1.23 \times 10^{12}} = 25.4\,\mu sec.$$

If the area of each element in the CCD were increased, thus increasing its charge capacity, or if the leakage current of each Hg Cd Te detector is reduced, then t_I would increase proportionately.

In any event, the maximum integration time here is not too different than the 100 μs used for the short wavelength sensors, see Section 4.1.4.

However, whereas the maximum brightness B_{max} in the short wavelength scene set the maximum integration time, it is the background radiation that sets it in the case of the long wavelength sensors. Therefore in order to process the scene variations in the 2 mrad field of view of the long wavelength sensor riding on this background level, signal subtraction must be performed. But care must be taken in this process because the usual non-uniformity between detector elements in the array may produce artifacts in the processed signal that are larger than the scene variations.

For a 0.1°K change in scene temperature at 300°K in a spectral region from 3.5 μm - 4.2 μm, the signal produced at the detector with an f/1.5 optic will be 0.1% of the background radiation in the same spectral region. Similarly for the 8 μm - 14 μm region, the signal is only 0.02% of the background radiation.

Therefore, if the signal processing is to measure these signal variations, a level must be subtracted from the signal output of each detector element, which results in a signal difference, wherein the signal variation is made larger than 0.4% (corresponding to one LSB of the 8 bit A/D which follows).

This subtraction process will be done digitally by storing the required levels to be subtracted in a ROM (read only memory) and using a high precision DAC (digital to analog converter) to perform the actual subtraction at the buffer amplifier input, see Sections 4.4.1.2 and 4.4.2.2.

In order to quantitatively determine long wavelength sensor system performance, we shall calculate the noise equivalent temperature difference, NET, for detector arrays in the 3.5 - 4.2 μm and 8 - 14 μm regions. The NET will use those sensor parameters established in Section 4.3.9 as follows:

$$NET = \frac{\sqrt{A_d\ (NBW)}}{A_0\ \theta^2\ \eta\ D^*}$$

where:

A_0 = Effective area of collecting optics = 7.9 cm^2

θ^2 = IFOV = 4×10^{-6} ster

η = Optical efficiency including obscuration = $(0.5)\ (0.95)^6 = 0.37$

$\frac{\Delta T}{\Delta N}$ = Slope of 300°K blackbody

$$= 1 \times 10^5 \frac{°K}{w/cm^2\text{-ster}}, \quad 3.5 - 4.2\mu m$$

$$= 5 \times 10^3 \frac{°K}{w/cm^2\text{-ster}}, \quad 8 - 14\mu m$$

D^* = $1 \times 10^{10}\ cm^2\ Hz^{1/2}\ w^{-1}$ (Typical both regions)

A_d = Area of elemental detector = $(4\ mil)^2 = 10^{-4}\ cm^2$

$NBW = \frac{1}{2\ T_d} = \frac{1}{8\ ms} = 125\ Hz$

Note that the noise bandwidth is the same as that in the short wavelength sensor case because the predominant noise source is the detector noise and digital averaging will also be performed, see Section 4.1.4. Hence:

$NET = 0.1°K$, $3.5 - 4.2\mu m$

5×10^{-3} °K, $8 - 14\mu m$

These NETs are quite low even though a conservative D* was used in the calculation. This result points out why electronically scanned CCD detector arrays are superior to their electro-mechanical counterparts. It is due to the fact that the NBW for the array approach is much lower than for the mechanical approach.

4.2 Methods of Spectral Isolation

The study of spectral isolation methods could be a very extensive one if complete and in-depth coverage were attempted (Ref. 10.25). Consequently in this section, we will examine only those methods which apply to the AMS application with a view toward determining their advantages and compatibility with linear detector arrays covering large field angles.

In general, optical spectral isolation can be divided into dispersive and non-dispersive methods. In dispersive methods an optical element deviates the path of a beam of polychromatic radiation through an angle which is a function both of the wavelength of the components of the beam, and the angle of incidence of the original beam. The latter fact means that the original beam must have small divergence, which in turn means the object space must be imaged onto a small field stop, such as a slit, before dispersion.

This possibility was pursued, with the thought in mind that the scanner collecting optic could image a swath on a slit in the focal plane, and then the slit would be reimaged on a number of detector arrays. In principle, this would permit the use of many detector arrays with only one, or a few, collectors and dispersion elements. In fact, it turned out that, after passing through the slit, the divergence of the rays behind the focal plane made the scheme impractical except for very small arrays, of the order of ten elements. Thus, to cover 120° across the flight path, very large numbers of collector optics and/or dispersion elements would be required. Also the secondary optics required behind each focal plane to redirect the dispersed energy to the detector arrays became prohibitively complex. The conclusion is that dispersion elements, as a means of using common collector optics and multispectral detector arrays is not practical in other than narrow field-angle systems.

Non-dispersive spectral isolators include absorption filters and multi-layer interference filters. Absorption filters are relatively low resolution devices, transmitting comparatively broad regions of the spectrum and absorbing the unwanted remainder. They depend on the intrinsic absorption properties of the bulk material of which the filter is made. While some flexibility of bandpass, wavelength and shape can be achieved by stacking and/or varying thicknesses, in general sharp cutoff narrow-band filtering at specified wavelengths cannot be achieved with absorption filters. Interference filters, on the other hand, can be manufactured to meet exacting requirements of passband and transmission, far superior to those obtained by absorption filters. Multilayer filters with high transmission, narrow pass-band, sharp cutoffs and wide regions of rejection get quite expensive. However, for applications such as the AMS, which requires only moderate resolution, these filters are quite practical. Combinations of interference filters and absorption filters can be employed, where the out-of-band rejection is accomplished by the inexpensive absorption filter. This tends to simplify the design and complexity of the interference filter, reducing costs.

Absorption type filters are also subject to changes in transmission when exposed to strong ultra-violet radiation. Kodak Wratten filters, for example, are less stable than color glass filters such as the common Schott and Corning types. The tendency of the filters is to increase in opacity with exposure. Filters of this type have been in use for many years and information about the susceptibility to "solarization" is available from the manufacturers.

Both absorption and interference filters are also subject to changes in transmittance with changes in temperature. For certain Schott filters (Ref. 10), the shift is of the order of 1 Å per kelvin toward longer wavelengths with increasing temperature, between 10° and 90°C. Interference filter passbands are also shifted to longer wavelengths as temperature increases. The displacement is smaller than for color glass filters, of the order of $5 \times 10^{-5} \lambda_0$ per kelvin, where λ_0 is the nominal, or peak-transmission wavelength. In both types of filters when the bandpass is moderate to wide, the effect is slight and a first-order correction with temperature should be adequate.

The shape and position of the filter bandpass also changes with angle of incidence in both types of filters. Again, however, the effect is small for filters of moderate passband and when the angle is less than 5° from normal, it is negligible. Thus as described in Section 4.3.8.3, the optical surface was selected for the interference filter coating with the need to minimize the incident angles in mind.

Other methods of spectral isolation were also considered. These included polarization filters, Christiansen filters, reststrahlen reflection plates, scatter plates, conductive screens, interferometers, and spectrally-selective detectors.

The first five of these are similar in function to the absorption and interference filters already discussed, in that they transmit a desired spectral interval of radiation while rejecting the rest. The mechanism of rejection is different, but there is no advantage in cost or performance in the AMS application. (Reference 10 gives succinct, practical descriptions of the principle and performance of these filters.)

Interferometers and spectrally-selective detectors are different in kind from the other spectral isolation methods discussed. Since these are conceptually attractive, some time was spent in considering their practicality.

The principle of the use of an interferometer in multispectral scanning can be described as follows: Suppose that a Michelson interferometer with a large collecting optic and a detector with wide spectral sensitivity were aimed at nadir from an aircraft. If the Michelson was scanned in path-difference) rapidly, a series of interferograms would be generated at the detector output. The Fourier Transform of each of these interferograms would be the spectrum of the ground area that the detector was pointed at during each scan interval. From these spectra a number of strip maps one detector field-of-view wide could be made. The number of maps would depend on the interferometer spectral resolution and the region of spectral sensitivity of the detector. Now, if a number of additional detectors were lined up in a linear array in the focal plane of the interferometer, we would have a push-broom interferometric scanner, capable of producing a complete set of flight strips in all of the resolved spectral regions simultaneously.

This is the ideal, but examination of the practicality shows that the optical problems of beamsplitting, path changing, recombining and then introducing the radiation to an array of detectors covering, say, 30° to 60° is prohibitive. Second, the data rate and sampling requirement becomes impossible with today's technology. And finally, it appears that unless essentially all the spectral information is needed, interferometry is not worth while. That is, if only a small number, say 10 or 20, spectral channels are required, the interferometer has little or no sensitivity advantage and a great number of optical-mechanical difficulties. Therefore, the interferometer concept was abandoned.

As for spectrally-selective detectors, the attraction there would be to avoid the expense, installation, and losses due to filters. There are several mechanisms possible in producing spectrally-selective detectors. One is the use of materials with different band-gaps as the junctions of a diode. Essentially, long wave radiation is transmitted, producing no signal; short wave radiation is absorbed before it reaches the junction, producing no signal, but intermediate wavelength radiation is absorbed in the junction producing hole-election pairs and thus a useful signal. Ideally then, having produced such detectors, they would be assembled (or produced) in arrays and the band-gaps would be "turned" either electrically, thermally, or magnetically, to produce spectral sensitivity in the desired region.

As of 1978, it is unrealistic to expect the useful production and availability of such detector arrays in the near future. While on a laboratory basis, these detectors have been produced in single units, no demand has materialized to encourage manufacture.

Therefore, our conclusion is that conventional broad-spectrum detector arrays used with interference filters for spectral isolation is the preferred, practically available, state-of-the-art choice.

4.3 Optical Design

The candidate optical designs for both the short wavelength and long wavelength sensor modules are shown in Figure 4-10 and Figure 4-12 respectively. In the following sections the various tradeoffs, problem areas, and design considerations particular to these designs are discussed and rationale given for their choice. Table 4-3 summarizes these designs.

4.3.1 General Specifications for Short Wavelength Sensor Modules

Spectral Coverage	0.4 to 1.0 μm
Total Field of View Desired	120° (achieved in two 60° sensor modules)
Resolution	1 milliradian
f/no.	f/0.8

4.3.2 Discussion of Design Tradeoffs

The basic optical element which allows both large field angles and high resolution at low f numbers is the spherical reflector. The reason for this property is that the sphere has no particular optical axis as shown in Figure 4-4 . Consequently, spherical aberration is the only aberration which occurs for directions A and B in the figure; this aberration is independent of field angle ψ.

Fortunately, spherical aberration can be highly corrected while maintaining independence from field angle by using refracting shells which are concentric with the spherical reflector as shown in Figure 4-5 . The shell introduces very little negative power into the system, while the negative surface of the shell introduces spherical aberration opposite to that caused by the spherical reflector. As a result, such a system can easily be corrected to a 1 milliradian resolution for an f/0.8 optical speed. This was in fact

done, and the resulting spot diagrams appear in Appendix B. Because a spherical reflector introduces less spherical aberration than an equivalent refracting element, no systems which used refractors only were considered in this study.

Although a 120° field of view was desired and is possible, the system stop will cause considerable vignetting (50%) at the field-extremes as shown in Figure 4-6 . Consequently, it was decided to limit the total field of view of each sensor to 60° with an attendant 13% vignetting at the field extremes which was considered quite tolerable. Therefore, two sensor modules would be required to cover the full 120° field of view.

4.3.3 CCD/Optics Interface

If a curved array of detecting elements could be found and used at the image surface, the basic optical system design concept would now be complete. However, silicon wafer technology does not presently lend itself to fabricating non-planar geometries. In fact, presently available CCD image devices, like the Fairchild CCD 131 and the Reticon CCPD 1024, are available only in standard "dual in line" (DIP) packages. As a result, each CCD array is straight, flat and is surrounded by an obscuration-producing substrate, lead assemblies, etc., which makes it unsuitable for mounting directly in the image surface as shown in Figure 4-5 . Thus a means of field flattening must be implemented. Three field flattening techniques were considered: (a) refractors, (b) reflectors, and (c) fiber optics.

The refractor approach quickly fails due to the very low f number desired. This approach works well for highly corrected multi-element photograph objectives where each element contributes a little to field flattening.

The reflector approach easily flattens the field but difficulty is experienced in secondary mirror obscuration. A reflector flattener system could be developed, but with somewhat slower optical speed, power, and resolution than the fiber optic approach which is described subsequently. However, as discussed in Section 4.3.6, the reflector approach is the only practical approach for the long wavelength sensors.

4.3.4 Fiber Optics Field Flattening Approach

The basics of the fiber optics approach are shown in Figure 4-7. Since the fiber optics bundle is a thin blade in the plane of the paper, very little light is blocked out of the entrance pupil by the fibers. The blade could be supported by thin stalks perpendicular to the plane of the paper. If fiber optics were available for the entire required spectral coverage (0.4μm - 14μm), then this field flattening technique could be used for both the long and short wavelength sensors. However, at present, only short wavelength coverage can be accomplished with the above fiber optics system. In the near future, it is expected that IR fiber optics will become generally available. In the meantime, an alternate and practical optical design approach for the long wavelength sensors is necessary and this approach is described in Section 4.3.6.

Figure 4-8 is a sketch of the fiber optics array required as part of the focal plane assembly for the short wavelength sensors. Two fabrication problems are anticipated.

The first is the arrangement of the fibers with their axes lying along radial lines in the focal surface while maintaining an adequate packing and mating factor; the significance of this problem is as follows:

The f/0.8 optical speed represents an acceptance angle of 72°. If the ends of individual fibers could be square to the optical axis, all of the f/0.8 bundle is easily accepted. At the ends of the field, the fibers will have to be turned somewhat to face the f/0.8 bundle or else the acceptance angle will be exceeded with loss of light in the cladding as shown in Figure 4-9 . Wedging the edges of a fiber reduces the acceptance angle for one side of the f/0.8 bundle.

The second problem was the mechanical interface between the CCD detector array and the fiber optics bundle. Since the optical rays leave the bundle at a divergent angle, the fiber ends must be situated closer than 1/2 the elemental detector width (6.5 μm for the CCD 131) to the detector surface so as not to result in significant energy spillover and sensitivity degradation.

As the letter in Appendix C reveals, we have contacted Galileo, Inc. of Sturbridge, Mass., manufacturers of fiber optics to review the above requirements and obtain a quotation for this fiber optic array. As indicated, a positive response as to the array's manufacturability was obtained using 13 μm square fibers arranged in a line array. (Their response applies to 16 μm fibers as well.) The above-stated requirement for fibers lying along radial lines will be achieved by slitting one edge of the fiber bundle into a discrete number of flat elements as shown in Figure 4-8 . The end of each flat element is then ground into a cylindrical radius of 1.3 cm. Each element is then epoxied parallel to a radial direction with the bundles overlapping as required to allow clearance for the converging bundles. With this approach, the end fibers in each elemental bundle will only be a few degrees from the radial orientation, thereby minimizing the loss of aperture in the converging optical beam, due to rays escaping through the cladding in the fiber.

Regarding the interface between the fiber bundle and the CCD array: In discussions that we have had with Galileo, they have suggested that the fibers could physically touch the CCD elements and/or be optically coupled to the elements (i.e., "immersed") by using a transparent epoxy. The final approach will be decided upon in the detailed design phase.

In view of the above discussion, we believe the fiber optic focal surface transfer element is a practical component for incorporation into the candidate short wavelength sensor module. It is further noted that as a result of the fibers being the same size as each photosite in the CCD array, that the MTF of the system will not be influenced by the fiber optic transfer element. In addition, it is conservatively estimated that the optical efficiency of the fiber optic will be 50%. Consequently, the effective f number or the equivalent T number of the system, given f/0.8, will be at worst:

$$T/ = \frac{0.80}{\sqrt{0.5}} = 1.1$$

4.3.5 General Specifications for Long Wavelength Sensor Modules

Spectral Coverage	1.0 μm to 14 μm
Total Field of View	60°
Resolution	2 milliradian
F Number	f/1.5

4.3.6 Discussion of Design Tradeoffs

As mentioned before, long wavelength infrared transmitting fibers are not currently available. However, it is worth noting that Hughes Aircraft Company is presently working on classified research programs on IR transmitting fibers which use polycrystalline core techniques and which cover

the visible through 35 μm spectral regions. Since these fibers are pushing the state-of-the-art at present, we have elected to present the more conservative reflective field flattening approach for the long wavelength sensor. When long wavelength fiber technology matures, then the sensor approach defined for the short wavelength sensors may be directly utilized with its advantages of higher resolution and lower f/no.

Of the several possible arrangements which use a reflecting field flattener, the approach shown in Figure 4-11 presently appears most promising.

The flat first surface reduces the input field angle presented to the second surface without introducing any aberrations to a collimated input bundle. The second surface then acts as a spherical reflector in the same manner as discussed for the short wavelength design. The bundle reflected from the second surface is again reflected from a field flattener coating imbedded in the refracting medium. A narrow slot in the reflecting coating of the second surface allows an exit bundle to form a flattened image plane with a lower f number than that reflected from the field flattener coating.

In this manner, aberrations are held to a minimum without resorting to correction surfaces. The negative curvature of the field flattener does remove some spherical aberration caused by the second surface but at the larger field angles it introduces off-axis aberrations which can only be reduced by means of auxiliary correction surfaces not shown in the figure. As shown in Appendix B , this system has a 2 milliradian blur circle for an f/1.5 exit bundle.

If the field flattening coating is a 50 - 50 beamsplitter, 75% of the input energy is lost. As shown in Figure 4-12, a more efficient method uses a 100% reflecting strip which cuts a slot in the entrance pupil. This will reduce the loss to approximately 57%. A combination method which uses 50 - 50 and 100% reflecting strips can reduce the loss to 50%. The effective f/no. or I/no. is then:

$$T/no. = \frac{1.5}{\sqrt{0.5}} = 2.1$$

Other tradeoffs are possible which could produce approximately T/2.5 at 1.5 milliradian resolution. This system would require correction surfaces which produce off-axis aberrations opposite to those caused by the field flattener in order to reduce the blur circle for 60° input field angles. There is evidence that combinations of various refracting media would be needed to achieve this end. In addition, there is not a wide variety of material available in the long wavelength regions for all-weather, easily fabricated systems.

An elaborate multi-element corrector on the style of a low f/no. wide angle photograph objective is considered to be unsuitable for purposes of this study. Thus different types of optical corrections produce different types of point spread functions which might have "needle-nose" tops with wide skirts, etc. These point spread functions are more satisfactory for photographic purposes than for long wavelength sensors. The wide skirt of such a point spread function presensitizes the film in photograph systems, while in the long wavelength case, it produces noise. Choice of the final correction configuration will be selected during the detail design phase.

4.3.7 Opto-Mechanical Considerations

In this section we address the practical mechanical and material aspects in implementing the optical design into a realizable sensor for both the short and long wavelength regions.

4.3.8 Short Wavelength Sensor Design

Figure 4-10 shows the construction of the candidate short wavelength sensor. It shows a feasible mechanical packaging of the fiber optics and the concentric corrector shell approach which was discussed in the previous sections. The diagrams of the basic elements which were referred to those discussions closely parallel the final design shown in Figure 4-10 For this sensor module, the optical material will be Pyrex glass for the mirror and a suitable high index glass such as Schott SF 15 for the Bouwers corrector shell. Since all surfaces are spherical and the optics dimensions are relatively small as shown in the figure, no significant fabrication problems relative to the glass elements are anticipated.

The spherical reflector and corrector shell are mounted in a lens cell forming a complete subassembly which moves as a unit when aligning the optical system to the fiber optics input end. The spherical reflector and shell are aligned to each other by shimming these optical elements in the lens cell. This "hard adjust" is much more stable and permanent than adjusting screws, especially in a shock and vibration filled environment such as would be experienced in an aircraft. A special set of alignment procedures is not offered at this time. However, Section 5.3.1 discusses general concepts on various alignment methods and procedures.

Interference filters are used to select a narrow band in each spectral region. Since these filters have a small acceptance angle, they should be deposited on one of the curved surfaces of the candidate optical system instead of using a separate plane surface window. This will allow these filters to operate efficiently at large field angles. To avoid unwanted spectral wavelengths from filling the optical interior, it is best to use one of the corrector surfaces for the interference filter (see Figure 4-5). The interior (negative) surface is best for abrasion protection and minimum handling considerations.

A flexible boot or an epoxy seal may be used between the output end of the fiber optics and the corrector lens cell so that all optical surfaces except the first (which acts as a window) would be sealed from moisture and dust. This seal could be made flexible enough to accommodate changes in barometric pressure without the need for breathers and driers. Alternatively, the entire sensor could be installed in a separately sealed container with a window to include electronics in a sealed environment.

Except for the long wavelength regions where fiber optics are not presently feasible, the system shown in Figure 4-10 is the best approach for a "push broom" multispectral scanner. Any application of this system would involve routine developments which do not border on state-of-the-art techniques. There is not, however, a specific mechanical packaging which would be ideal for all wavelengths. Most systems would be based upon the design shown in Figure 4-10 but consideration of fine details would lead the final configuration to differ slightly for different wavelengths. Consequently, the amount of detail presented in Figure 4-10 is sufficient for purposes of this study.

4.3.9 Long Wavelength Sensor Design

Figure 4-12 shows a practical mechanical implementation of the long wavelength sensor modules incorporating the reflecting field flattener approach discussed in Section 4.3.6 . In general, many of the mechanical aspects and alignment adjustments are similar to those discussed for the short wavelength module. Two notable exceptions are the selection of long wavelength materials because of the thickness of the optics and the need for cryogenic cooling of the CCD detector array.

The "solid reflector" optical design shown in Figure 4-11 for the long wavelength sensor modules is composed of relatively thick elements. In order to minimize attenuation of the long wavelength energy by the relatively thick optics, an optical material with low bulk absorption in the 3 - 5μm and 8 - 14μm regions is required. The design shown in Figure 4-12 has been ray traced for a refractive index of 1.7, which is representative of various long wavelength transmissive, low absorption optical materials. See Appendix B.

In the 3 - 5μm wavelength region, several materials can be used: sapphire, calcium fluoride, or barium fluoride. All of these have low bulk absorption in this wavelength region and have good optical fabrication characteristics and good environmental durability. In the 8 - 14μm region, the choice of materials with low bulk absorptivity is more limited and unfortunately, many of these materials, such as Na Cl, KC l, KBr, Cel and KI are hygroscopic. The only other materials exhibiting low absorption in the 8 - 14μm region which are not hygroscopic are germanium, Zn Se (IRTRAN 4) and Cd Te (IRTRAN 6). However, germanium is relatively expensive and must be antireflection coated to maximize its optical throughput; Zn Se and Cd Te are even more expensive and have an index of 2.4. Furthermore, an optical system using the "solid reflector" concept shown in Figure 4-13 when implemented in germanium (index = 4), becomes very thick, which makes it both expensive and heavy, in addition to which, the long optical path theough the germanium will result in some attenuation of the 14μm radiant energy.

In the event that any of the hygroscopic materials are used, the evacuation seal will be placed at the entrance aperture of the system, where a relatively thin germanium or Zn Se window can be located to define the vacuum-air interface for the dewar. Alternatively, if germanium or Zn Se is

used for the optics, the vacuum-air interface will be situated just ahead of the detector-array so that the germanium or Zn Se optics will act as the dewar window. The final choice of material for the optics will depend upon a detail tradeoff study to be conducted in the design phase for the instrument using such considerations as: ray-trace-determined optical resolution, manufacturing tolerances, vacuum sealing interface characteristics, relative coating difficulties, and overall optical throughput.

TABLE 4-3

OPTO-MECHANICAL CHARACTERISTICS OF SELECTED
SINGLE WAVELENGTH MULTISPECTRAL SCANNER DESIGN

Characteristics	Short Wavelength Sensor Module	Long Wavelength Sensor Module
Spectral Coverage	0.4 to 1 μm	1 μ to 14 μm
No. of Spectral Bands per Sensor	1	1
Means of Spectral Sorting	Interference Filter	Interference Filter
Field of View Width per Sensor	60°	60°
Max. Blur Circle Diameter	1 milliradian	2 milliradians
T/	1.5	2.2
Equivalent Focal Length	13.3 mm	52.0 mm
CCD Detector Array	1024, 13 μm square elements	512, 0.004" square elements
Weight of Complete Assy.	1.2 lbs.	6.0 lbs.
Housing Material	Al. Aly.	Al. Aly.
Field Distortion (θ Map)	2% max.	2% max.
Dewar Hold Time	----	12 Hrs.

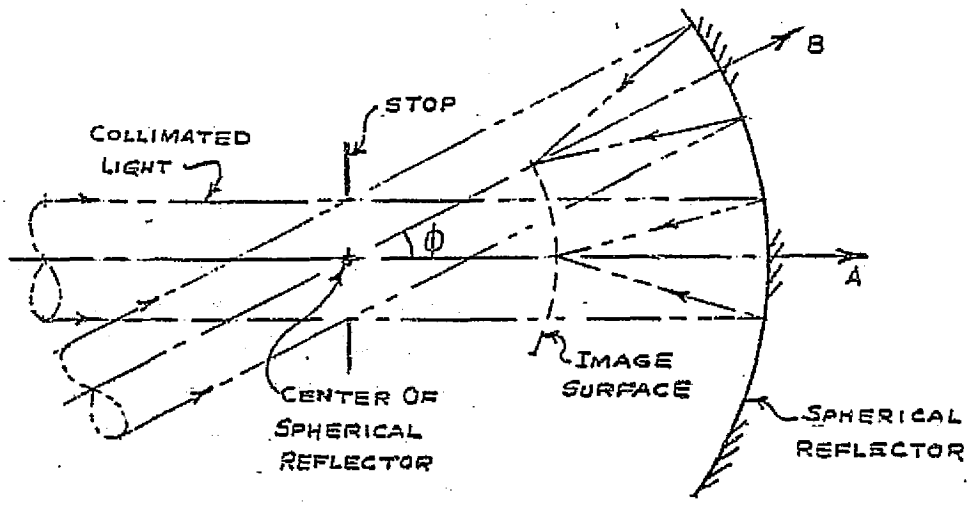

Figure 4-4 SPHERICAL REFLECTOR

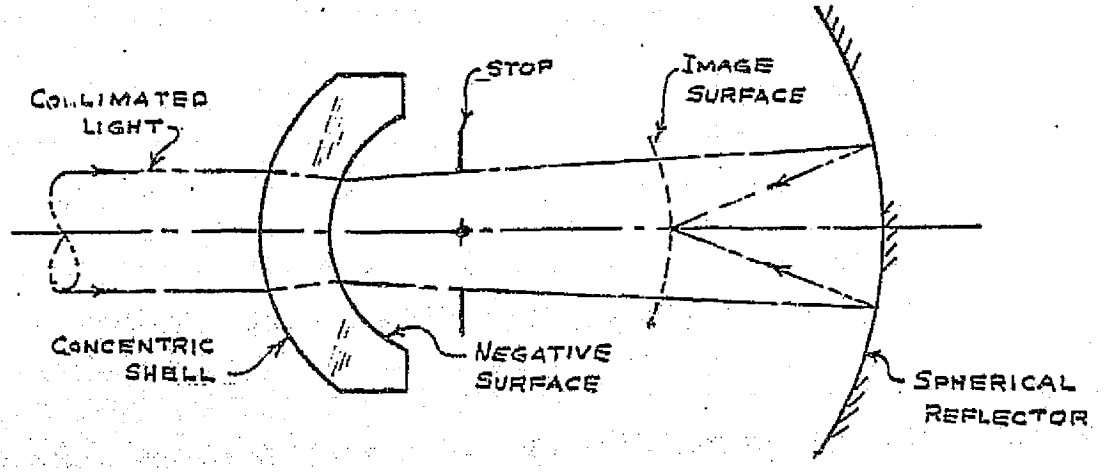

Figure 4-5 SPHERICAL ABERRATION CORRECTION

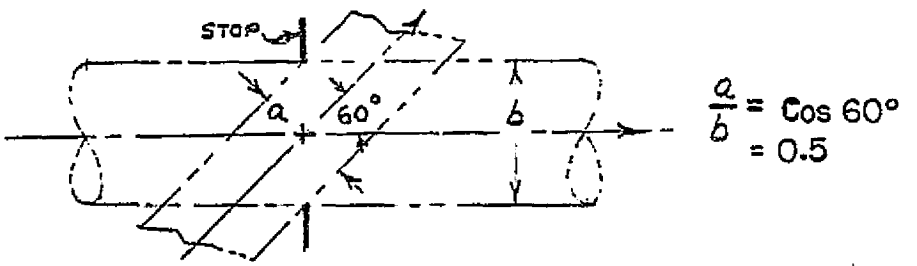

Figure 4-6 VIGNETTING FOR A 120° FOV

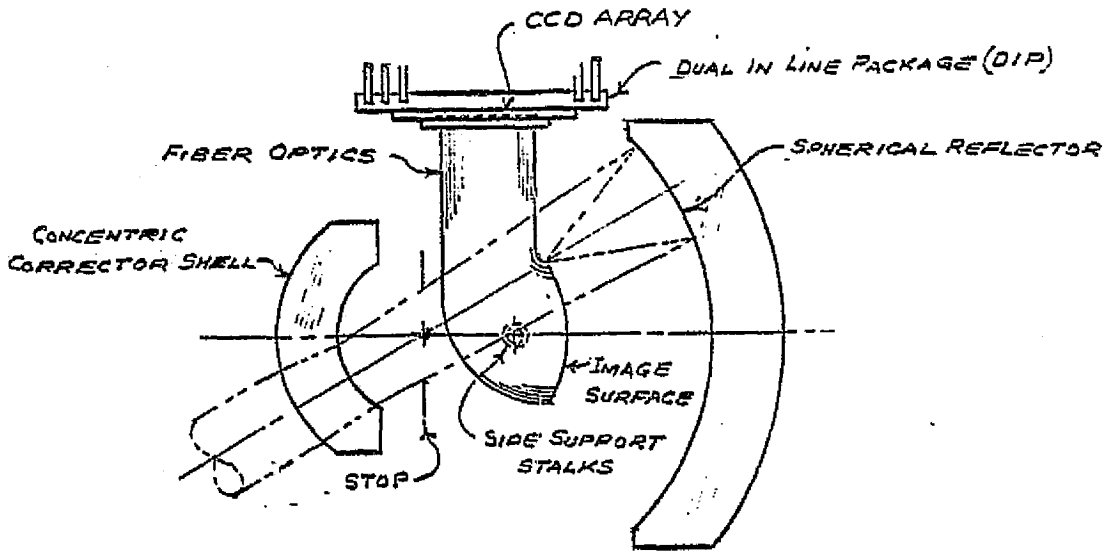

Figure 4-7 FIBER OPTICS APPROACH

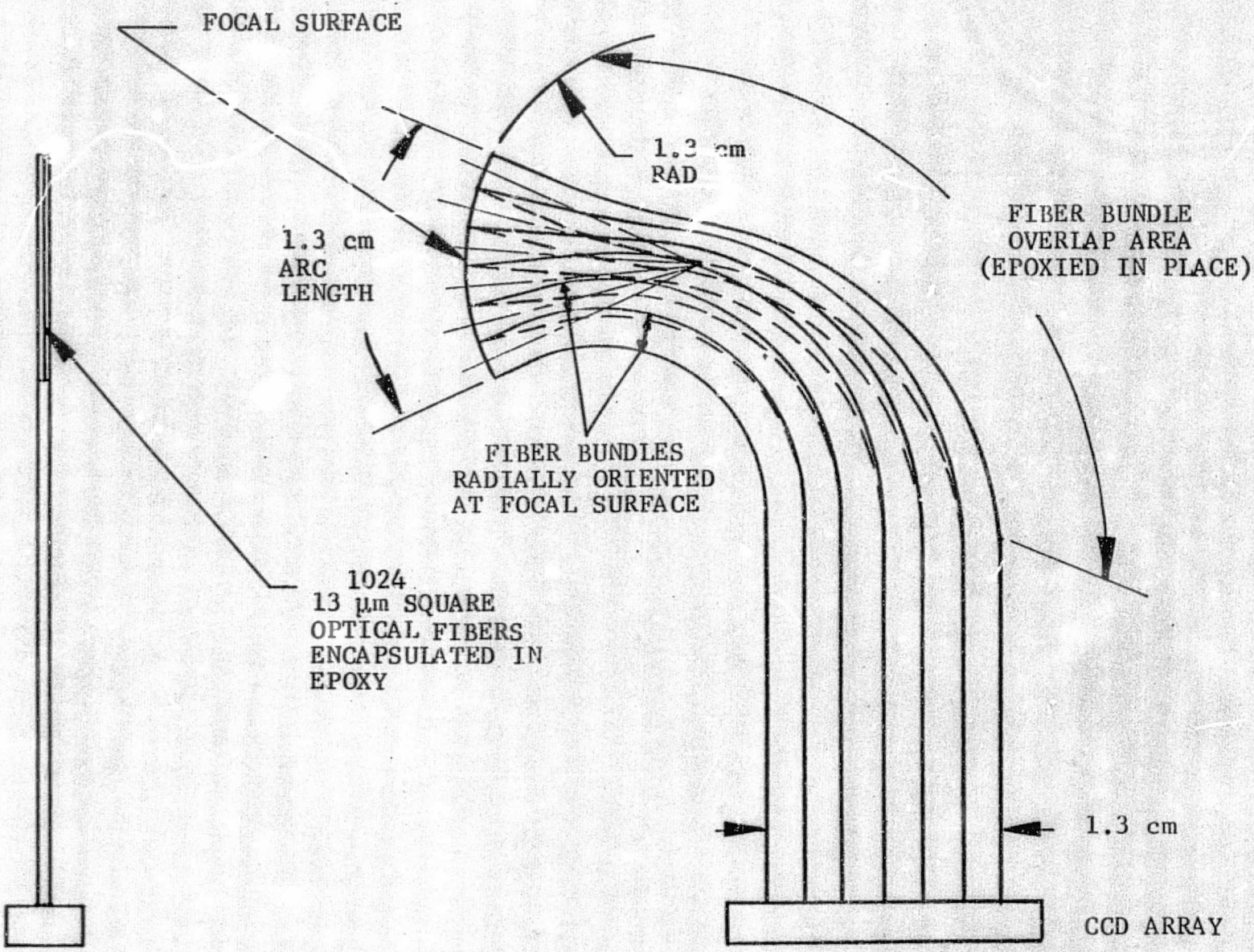

Figure 4-8

FIBER OPTICS ARRAY FOR SHORT WAVELENGTH SENSORS

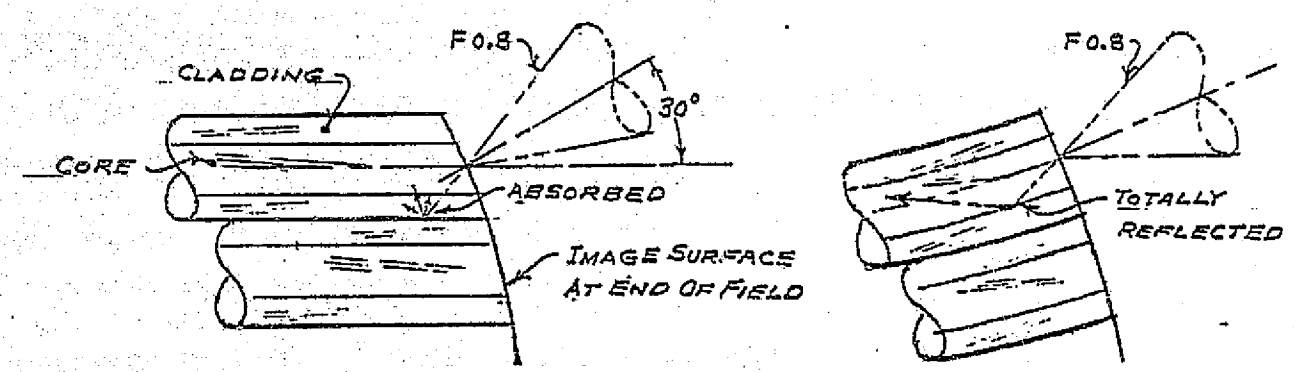

Figure 4-9 FIBER OPTIC GEOMETRY

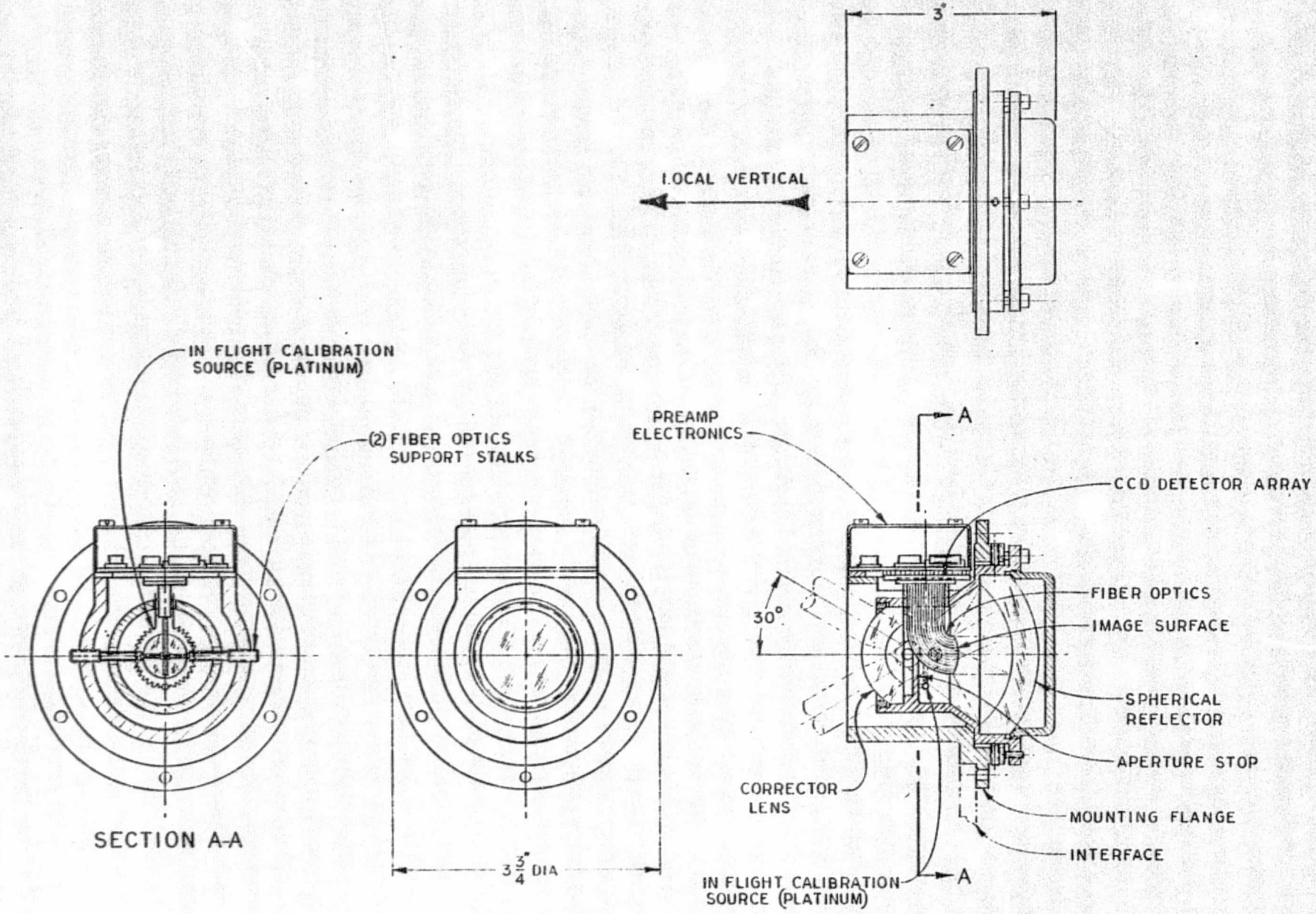

FIGURE 4-10

ADVANCED MULTISPECTRAL SCANNER SENSOR MODULE

FOR 0.4 TO 1.0 μm WAVELENGTHS

BARNES ENGINEERING COMPANY
STAMFORD, CONNECTICUT

C273800-4002-1

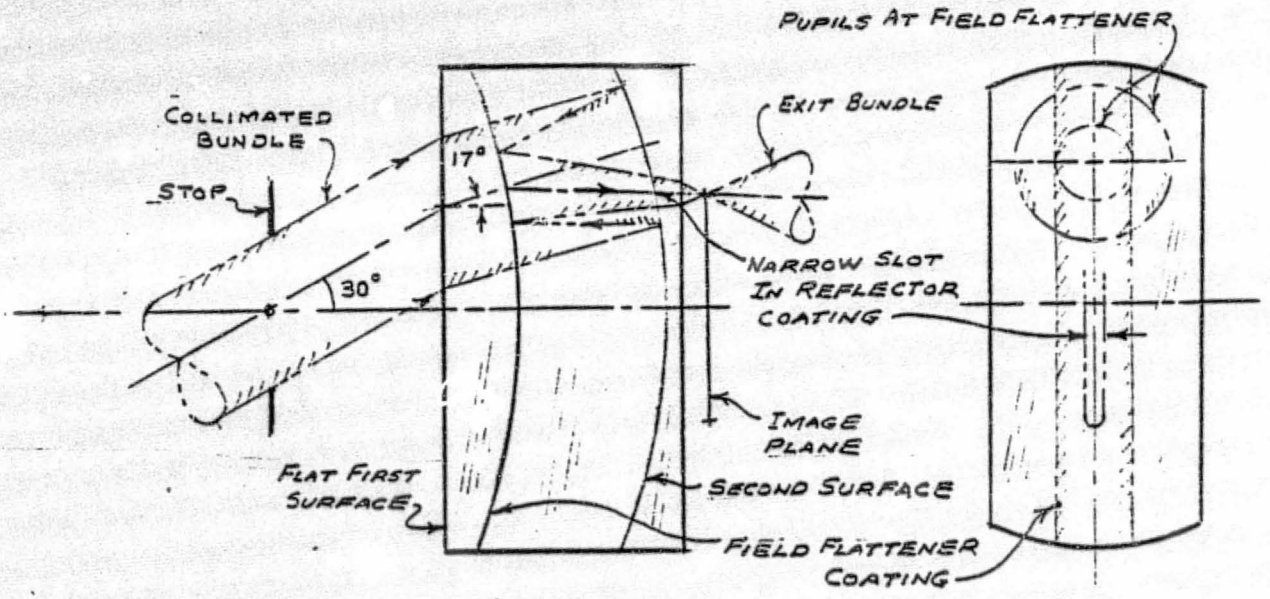

Figure 4-11 LONG WAVELENGTH FIELD FLATTENER APPROACH

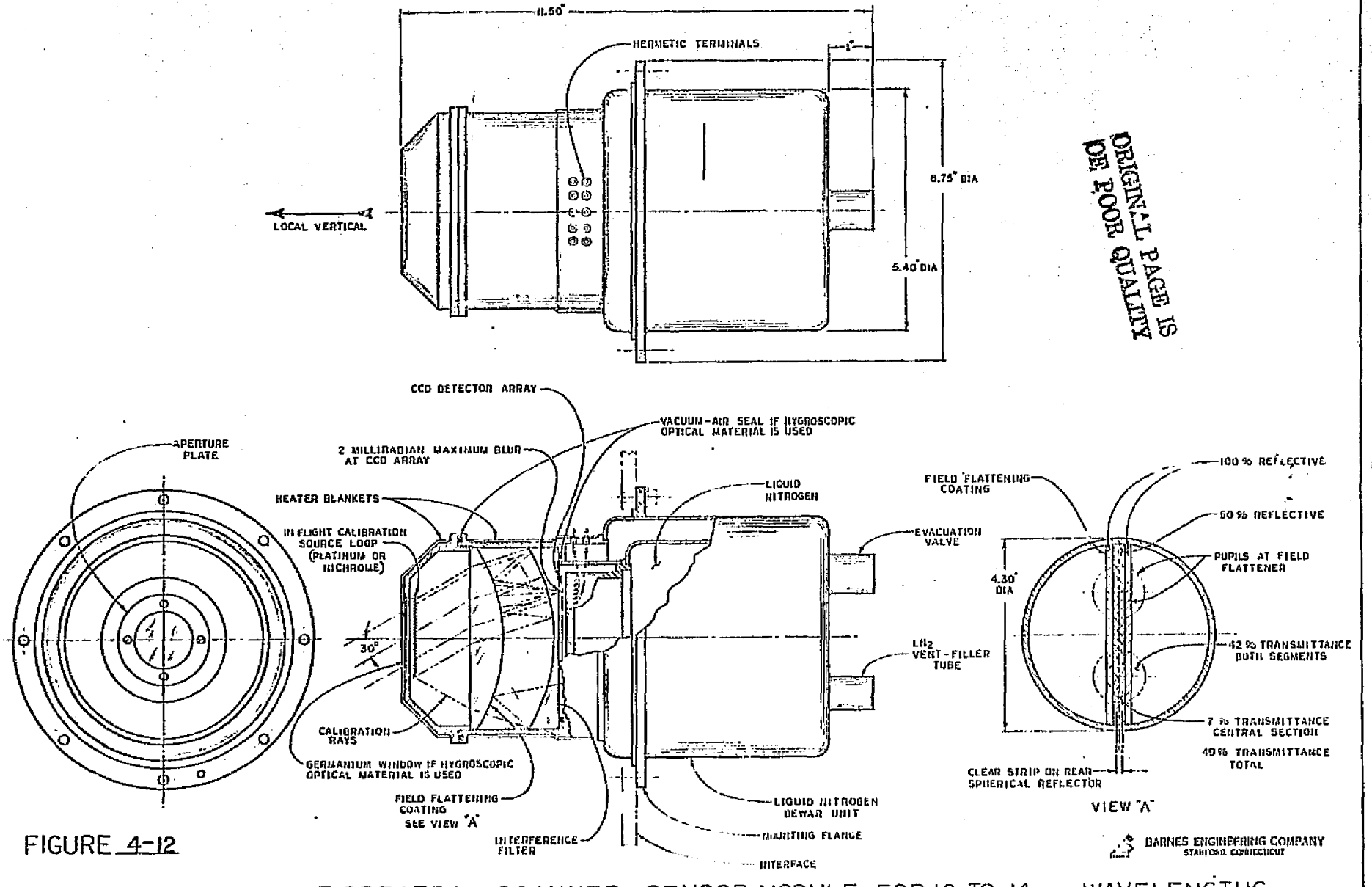

FIGURE 4-12

ADVANCED MULTISPECTRAL SCANNER-SENSOR MODULE FOR 1.8 TO 14 μM WAVELENGTHS

D 27[illegible]-400-400[illegible]

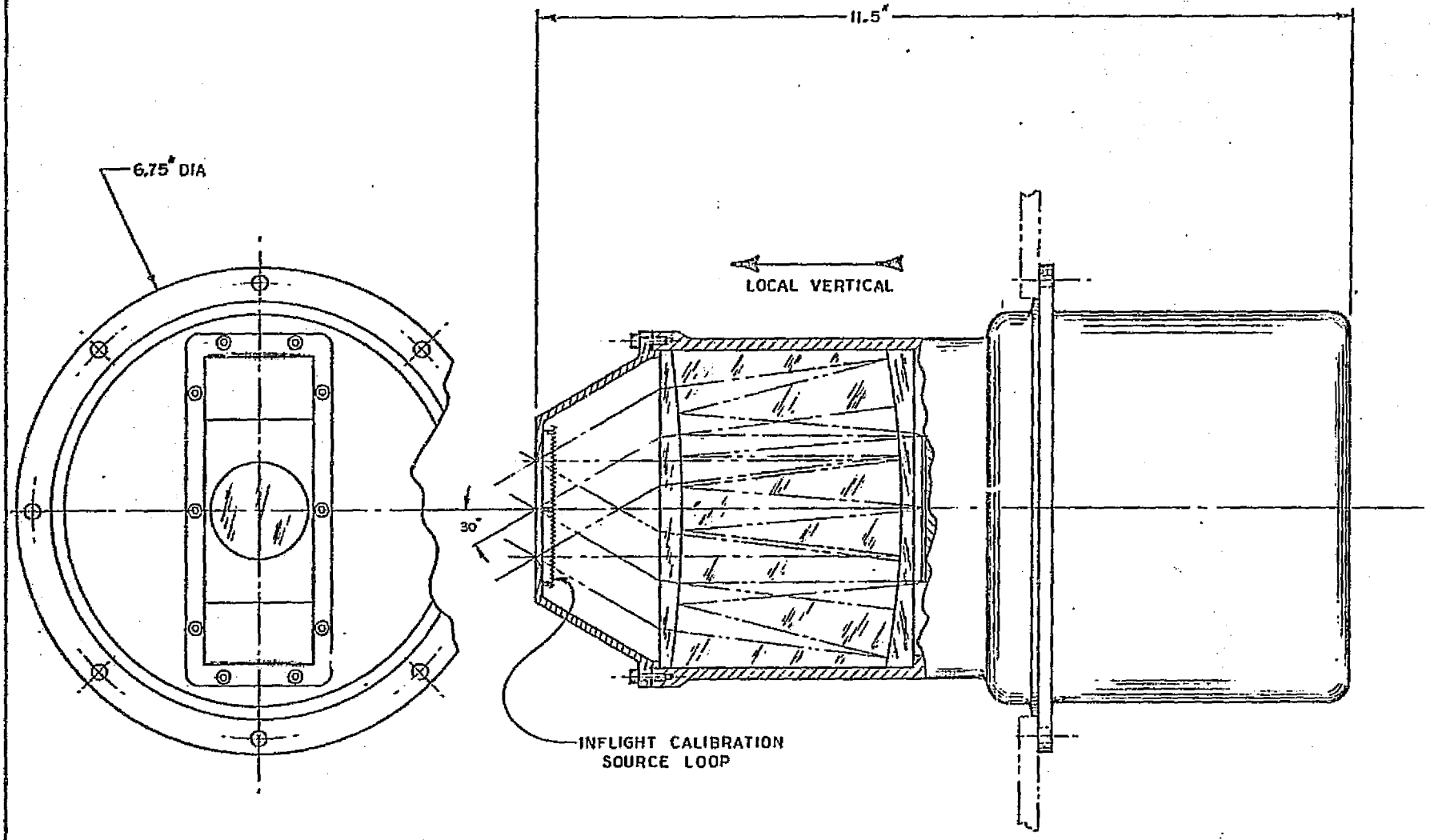

FIGURE 4-13 ADVANCED MULTISPECTRAL SCANNER SENSOR MODULE

FOR 1.8 TO 14μM WAVELENGTHS

GERMANIUM OPTICS APPROACH

BARNES ENGINEERING COMPANY
STAMFORD, CONNECTICUT

C 273800-4003-1

4.4 Electronics

In this section, we will describe the electronics design which is required to support each sensor module in the AMS system. A key feature of this design is its modularity which permits up to 24 sensor modules to be utilized at any one time. This artificial limit is set by the data handling capabilities of the selected tape recorder; of course more than one tape system could be employed to provide additional capability.

The purpose of this section is not to present a final electronics design for the AMS, but to provide a detailed systems description of the required electronics, along with system considerations, which may be used as a design guide in the next phase.

Figure 4-14 is a block diagram of the overall AMS system. With regard to the electronics, it shows the relationship between each of the independent sensor modules and its post electronics and the portions of the AMS system that are common to all. Unless otherwise noted, we shall refer to a sensor module and its corresponding post electronics as if it were one unit called a sensor module. With very few exceptions, the electronics design associated with a short wavelength sensor module is identical with that of a long wavelength sensor module. However, these differences will be identified, as appropriate, in the sections which follow.

As shown in Figure 4-15 each sensor module consists of a set of collecting optics, an in-flight calibration source, a CCD linear image array, a clock interface and temperature monitors. In the case of the long wavelength sensors, cryogenic cooling of the CCD array is also provided. The

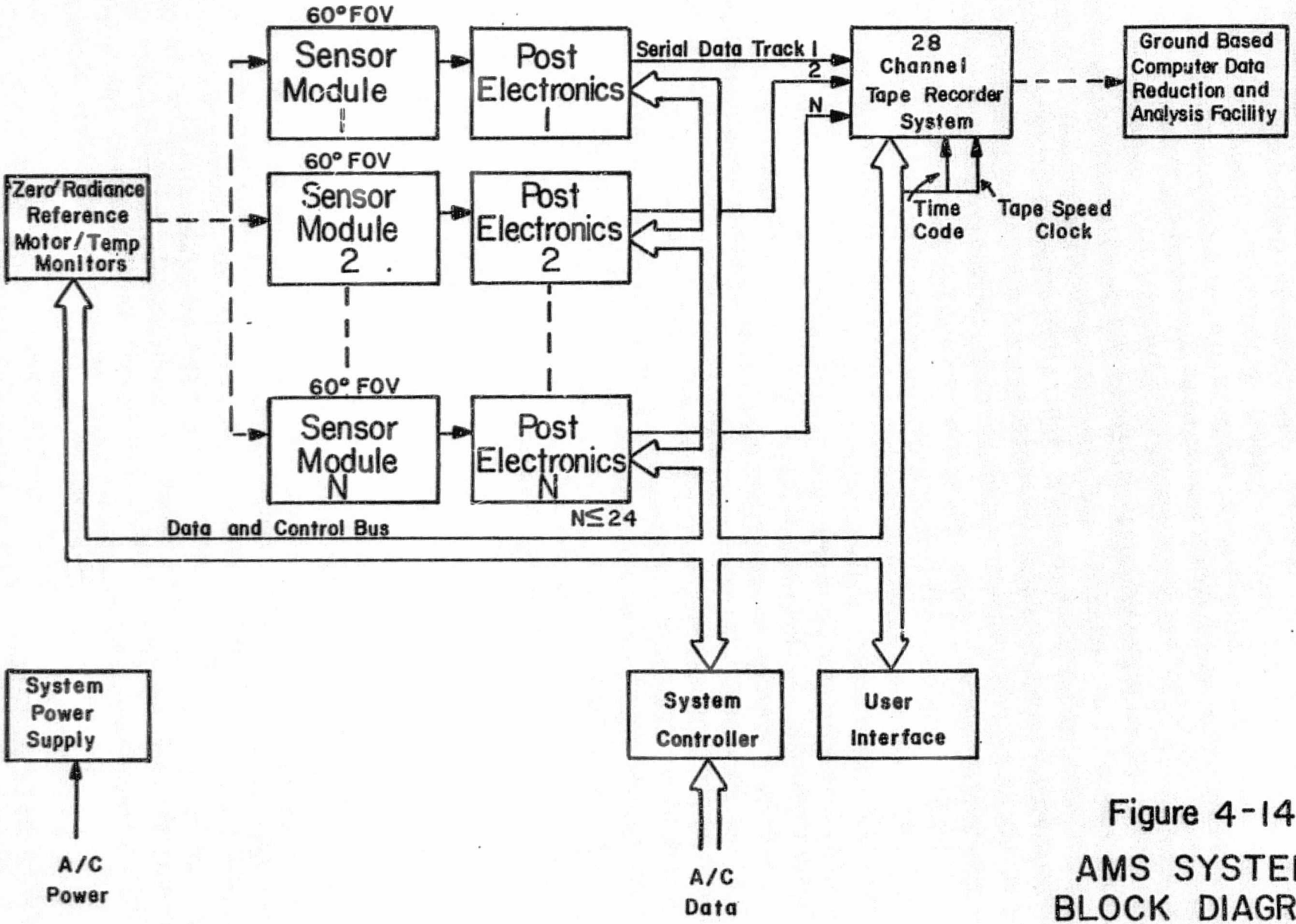

Figure 4-14

AMS SYSTEM BLOCK DIAGRAM

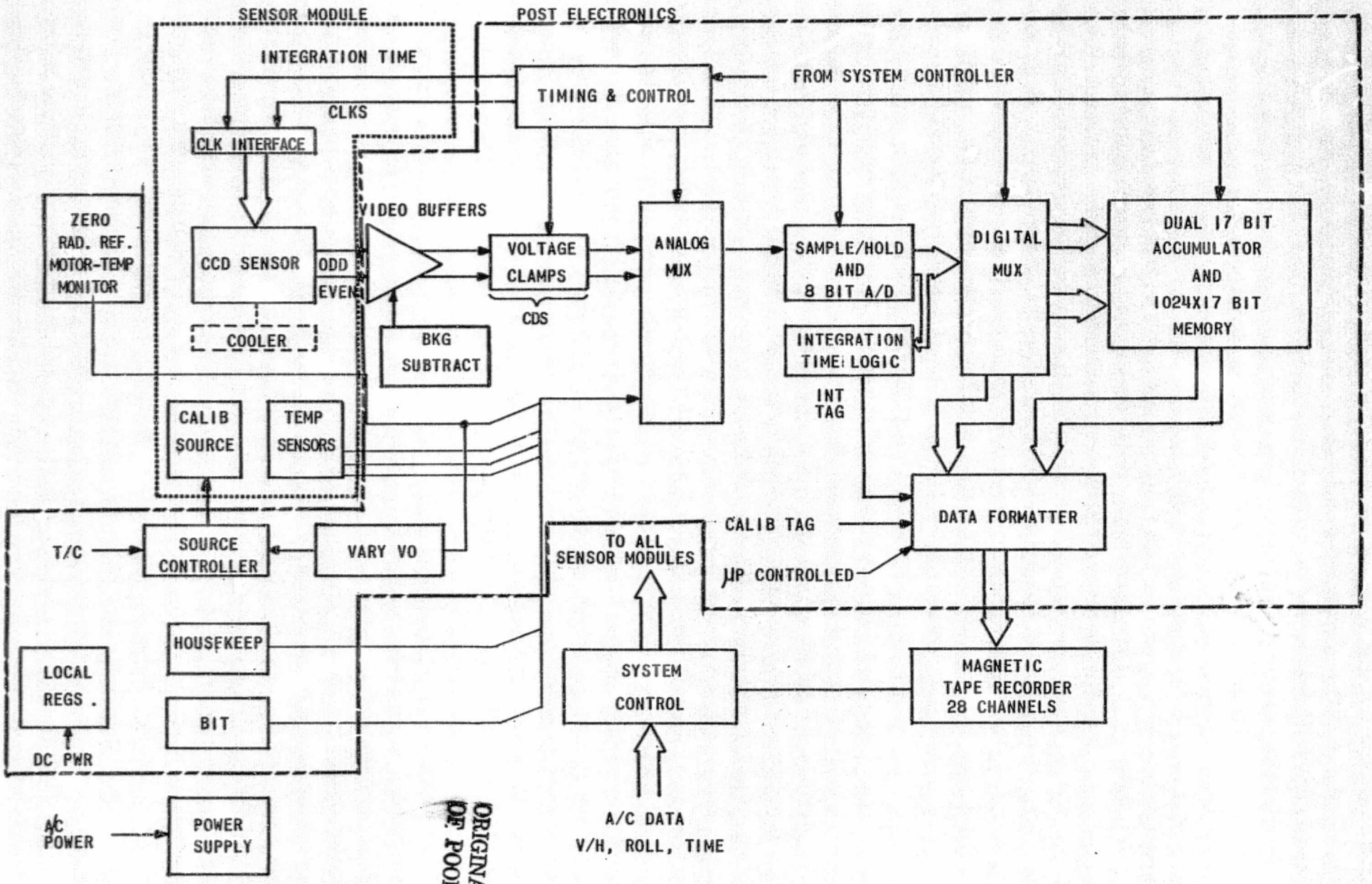

Figure 4-15
BLOCK DIAGRAM
SENSOR MODULE AND POST
ELECTRONICS

corresponding post electronics consists of an analog video signal processing chain, a digital signal processing chain with roll and V/H rate compensation and a block which formats the data prior to recording on tape. In addition, there is a timing and control block which provides all of the timing for the module in synchronism with commands and clocks sent from the common system controller. Housekeeping and BIT (built-in-test) data are multiplexed with radiometric data from the CCD array during the periodic in-flight calibration sequence. Each sensor module receives its dc power from the system power supply and locally regulates it.

Again referring to Figure 4-14, the formatted serial data output of each sensor module is fed to its uniquely allocated track on the system's multi-channel tape recorder. In addition to the 24 data channel inputs, the recorder stores IRIG time code information and the tape speed clock on two of its four available auxiliary channels. Other aircraft information relevant to data reduction may be stored on the other two channels. The recorder's tape speed is varied by the system controller in accordance with the aircraft's V/H rate to achieve constant data packing density. The data stored on tape is subsequently reduced and analyzed in a ground-based computer facility. It is at this facility that the calibration data taken during the ground calibration of the system is applied to the data recorded during flight.

In order to synchronize the operation of all of the sensor modules in the system, a common Microprocessor based system controller is utilized. Its clock is used as the system master clock. This controller accepts roll angle, IRIG time code and V/H rate data from the aircraft data interface. It uses this data to ultimately provide roll compensation and V/H rate correction for the data outputted from each sensor module.

One of the main tasks of the system controller is to support the user interface function shown in Figure 4-14. Although this function is not fully defined at this time, some of its important features are:

(1) Allows monitoring go-no go status of tape recorder channels

(2) Permits manual activation of an in-flight calibration sequence

(3) Allows selection of in-flight calibration duration and frequency

(4) Allows a health check of each sensor module in the system to be made

(5) Displays various temperature monitor points, e.g., detector array temperatures or reference source temperatures, etc.

Periodically, the system controller places the system in an in-flight calibration mode. This is done either automatically or manually as mentioned above. In this calibration mode, a "zero" radiance reference is placed in front of each sensor module. This reference may take the form of either the protective aperture covers on the system pod or a reference "flag" on the sensor module itself. In addition, the system controller activates the in-flight calibration source in each sensor module and commands each module to multiplex in with the radiometric data housekeeping, BIT and temperature data.

The electronic system considerations, detailed operation and inter-relationship between the various blocks mentioned above are described in the following sections.

4.4.1 Electronics System Considerations

4.4.1.1 Dynamic Range Considerations for Short Wavelength Sensors

As shown in Table 4-4 , the range of diffuse reflectance varies approximately 2.3:1 over the short wavelength bands being investigated. The largest and worst case sensor irradiance B_{max}, from a CCD array saturation point of view, occurs in band 9 (λ_c = 0.81 μm) when the sun is normal to the scene (ϕ = 90°) and with 100% atmospheric transmission (τ = 1) and while "looking" at a near perfect diffuse reflectance (ρ = 1). If maximum integration time t_I is selected based upon this irradiance, then in order to just resolve a 1% contrast change in a typical scene B_{typ} (i.e., sun angle ϕ = 45°, atmospheric transmission τ = 0.8, average scene reflectance ρ = 0.2) the dynamic range required is 884:1. Since it would be desirable to digitize the data from both a signal processing and data handling point of view, a 10 bit A/D would be required. However as Figure 4-3 shows, the maximum allowable t_I for this worst case B_{max} condition is 100 μs. This, in turn, requires that the signal output corresponding to each pixel in the 1024 element array be digitized at a 10 MHz rate. Unfortunately, 10 bit A/D converters with 100 ns conversion times to not exist at present; however, 8 bit converters do. See Section 4.4.2.1.

Therefore, in order to accommodate this large dynamic range, while at the same time not saturating the CCD array photosites nor compromising the 1% (of typical scene) contrast resolving capability of the system, the following approach is suggested:

TABLE 4-4

EXPECTED DIFFUSE REFLECTANCE IN THE
SHORT WAVELENGTH SENSORS

Band No.	λ_c (μm)	$\Delta\lambda$ (nm)	B_{max}* (w/cm^2-ster x 10^{-3})	B_{typ}** (w/cm^2-ster x 10^{-4})
1	0.42	28	1.05	1.19
2	0.47	35	1.43	1.62
3	0.51	43	1.75	1.98
4	0.55	40	1.59	1.80
5	0.59	40	1.53	1.73
6	0.63	40	1.46	1.65
7	0.67	40	1.37	1.55
8	0.72	40	1.27	1.44
9	0.81	94	2.45	2.77
10	0.99	78	1.18	1.34

Assumed solar flux density at earth = 0.1 w/cm^2

* B_{max}: Sun Angle $\phi = 90°$
Average Earth Reflectance $\rho = 1$
Average Atmospheric Transmission $\tau = 1$

** B_{typ}: $\phi = 45°$
$\rho = 0.2$
$\tau = 0.8$

Each CCD array will be operated in an automatic exposure control mode. This mode of operation is realized by adjusting the integration time t_I of the array in proportion to the average brightness of the scene, while keeping the readout rate constant. Naturally, provision could also be made for manual adjustment. This form of control is possible since the signal output of each photosite is directly proportional to t_I.

Suppose that t_I is set near 880 μsec. so that under the typical scene conditions, B_{typ}, ($\phi = 45°$, $\tau = 0.8$, $\rho = 0.2$) the signal output of each pixel is near saturation. Then by digitizing each pixel output into an 8-bit word, measurements with contrasts of at least 1% may be realized. Now suppose that the average brightness of the scene increases to the worst case condition B_{max} ($\phi = 90°$, $\tau = \rho = 1$), then the integration time must be reduced to 100 μs to prevent pixel saturation as indicated in Figure 4-3.

To adjust the integration time, the pixel outputs of each line scan will be digitally compared to a threshold value. When the number of threshold exceedances goes above a given value, the integration time will be made shorter. A similar process will be gone through to increase the integration time for less bright scenes. See Section 4.4.2.1. Due to the unpredictable nature of a scene, only two integration times are recommended, e.g., 100 μs and 880 μs. Manual selection is also possible.

In order to allow data reduction to be performed with variations in the integration time, each data word stored on tape will contain an integration time tag as explained in Section 4.4.1.7.

4.4.1.2 Dynamic Range Considerations for Long Wavelength Sensors

The dynamic range required to be handled by the signal processing for the long wavelength sensors is directly proportional to the ratio of the maximum background radiation, B_{max}, to the noise equivalent radiance, $NE\Delta N$. (Note: the $NE\Delta N$ is related to the NET discussed in Section 4.1.5 by the slope of the blackbody curve $\frac{\Delta T}{\Delta N}$.) For the 3.5 μm - 4.2 μm band, the dynamic range is 1000:1 for a 0.1°K change, as indicated in Section 4.1.5. Similarly for the 8 μm - 14 μm band, the dynamic range is 5000:1.

Thus in order to achieve a NET of 0.1°K or better using an 8 bit A/D converter, the background level must be subtracted to reduce the dynamic range to at least 256:1.

Since the 8 bit A/D converter which ultimately follows has an accuracy of 0.4%, the level subtracted, V_{SUB}, and the subsequent gain, G, in the video buffers must have the following relationship with the background, V_{BKG} and the signal ΔV:

$$G\ (V_{BKG} + \Delta V - V_{SUB}) \geq 0.004$$

This defines the gain G required provided the subtraction error is small. If the subtraction error $(V_{BKG} - V_{SUB})$ is ϵ, then if we want $\frac{\epsilon}{\Delta V}$ to be smaller than 10%, then the background level must be matched to within one part in 5×10^4 in the worst case (8 - 14μm). That is:

$$\epsilon = 0.1\ \Delta V = (0.1)\ (2 \times 10^{-4})\ V_{BKG}$$

$$\epsilon = \frac{V_{BKG}}{5 \times 10^4}$$

This result for an NET of 0.1°K is not practically realizable because:

(1) The adjustment cannot be done with 512 analog voltage divider bias networks for each detector array.

(2) The speed requirements allow only a 12 bit resolution (one part in 4096) digital to analog converter to be used (see Section 4.4.2.2)

and (3) The background temperature will change that much even with a temperature controlled background.

Therefore, it appears at present that only a 1°K NET may be realized even though the detector array per se is capable of more precision. However, this should be adequate for the AMS application.

Note in passing that ac coupling, although inviting to consider and easy to implement, introduces a difficulty in that the true value of the signal is lost in the process.

4.4.1.3 Impact of CCD Noise Mechanism on Short Wavelength Signal Processing

It is established in Section 4.1.2 that the signal to noise ratio at the output of the CCD array for each photosite is proportional to the square root of the integration time, $\sqrt{t_I}$. It is further shown that this ratio is not degraded by subsequent wide bandwidth amplification since the major noise source is dark current noise. Consequently, one would be tempted to allow the integration time to increase to the full resolution element dwell time, T_d, in order to maximize the S/N, See Table 4-5. However, as is shown in Figure 4-3, pixel saturation occurs much sooner. For the candidate T/1.1 system and the brightest scene expected B_{max} in the short wavelength band ($\lambda_c = 0.81\,\mu m$), the maximum allowable integration time is only 100 μs. Even for the typical scene B_{typ}, t_I = 880 μs max., see Table 4-5.

Fortunately, as a result of the nature of the CCD noise, these short integration times are not a limitation on system sensitivity provided that we integrate or average the signals in each photosite over the entire dwell time. As a consequence, the integration time of the CCD may be made independent of the V/H rate dependent dwell time. This is quite an important result. We will, however, vary the CCD integration time with scene brightness to achieve a form of automatic exposure control as explained in Section 4.4.1.2.

This important observation can be seen as follows: If the signal at the end of an integration period is S_I and the noise is N_I, where $S_I = a\,t_I$ and $N_I = b\,\sqrt{t_I}$, then the S/N at the end of the integration time is:

$$\left(\frac{S}{N}\right)_I = \frac{a}{b}\,\sqrt{t_I}$$

If we now define m as the ratio of the dwell time, T_d, to the integration time, t_I, i.e.,

$$m = \frac{T_d}{t_I}$$

then, averaging m signal samples and m noise samples gives:

$$S_{av} = \frac{m}{m} S_I = \frac{T_d}{t_I} \frac{a}{m} t_I = \frac{a}{m} T_d$$

since the signals add linearly, and

$$N_{av} = \frac{\sqrt{m}}{m} N_I = \sqrt{\frac{T_d}{t_I}} \frac{b}{m} \sqrt{t_I} = \frac{b}{m} \sqrt{T_d}$$

since the noise increases as the square root of the number of samples.

Therefore, the signal to noise of the average is:

$$\left(\frac{S}{N}\right)_{av} = \frac{a}{b} \sqrt{T_d}$$

which is the same result as had each pixel been integrated over the entire dwell time without the photosite saturation restriction!

As Table 4-5 shows, the number of averages, m varies with both V/H rate and scene brightness. Since we cannot average fractions of a sample, the numbers in parenthesis represent practical values.

The required averaging is implemented digitally as described in Section 4.4.2.1. Basically, the averager consists of an accumulator and a memory. 8 bit words from the A/D converter, which represent the signal outputs of each photosite in the CCD array, are added to the corresponding

pixels from the last line which was previously stored in memory; the result of each addition is then returned to its corresponding memory location. After m cycles, the memory contains in each location the sum of the outputs for that pixel over the dwell time.

The maximum bit length of the adder and the memory location is a direction function of m. The maximum number each memory location will contain is 2^8 x m. Therefore as Table 4-5 shows, a 17 bit word is required to handle the largest case. Although the averaging process requires the sum in each memory location to be divided by m, this is done on the ground to reduce the burden on the sensor electronics. However, the word length associated with the final data in each memory location will be divided by 2 to shorten the word length to a convenient 16 bits. Before outputting the contents of this memory to the tape formatter, roll compensation as explained in Section 4.4.1.5 is applied.

It should be mentioned that analog techniques for averaging were considered and discarded. First, classic analog averaging cannot be practically done because 1024 storage elements (integrators) would be required. Second, CCD shift registers similar to the CCD 321A by Fairchild, although having more than sufficient analog storage elements, cannot be used since they cannot, by themselves, accummulate over the required signal dynamic range. Use of external attenuation, $\frac{1}{m}$, to implement the averaging algorithm:

$$\frac{1}{m} \sum_{L=1}^{m} a_i = \frac{a_1}{m} + \frac{a_2}{m} + \frac{a_3}{m} \cdots\cdots \frac{a_m}{m}$$

is not practical for large m because of S/N degradation. Thus digital averaging or actually, accumulation, is recommended.

TABLE 4-5

RELATIONSHIP BETWEEN T_d, t_I and V/H RATE

For Short Wavelength Sensors, θ = 1 mrad, T/1.1

Parameter \ V/H Rate	0.25 rad./sec.	0.025 rad./sec.
Dwell Time T_d	4 ms	40 ms
Max. Allowable Integration Time, t_I		
for B_{max}	100 μs	100 μs
for B_{typ}	880 μs	880 μs
Number of Averages in T_d, m		
for B_{max}	40	400
for B_{typ}	4.55 (4)	45.5 (45)
Required Max. Bit Size of Accumulator		
for B_{max}	14	17
for B_{typ}	(10)	(14)

4.4.1.4 Impact of CCD Noise Mechanism and Background Radiation on Long Wavelength Signal Processing

The subject of this section is adequately covered in Sections 4.1.5 and 4.4.1.2 respectively, with specific design recommendations described in Section 4.4.2.2. In addition, many of the discussions pertinent to the short wavelength sensor signal processing apply equally well to the long wavelength sensors too.

4.4.1.5 Roll Compensation Considerations

Each sensor module, as shown in Figure 4-16 , is designed to cover a nominal 60° (58.7°) field of view, this is true for either the short or the long wavelength sensors. In order to cover a 100° FOV, two modules must be employed.

In the short wavelength sensors, the 100° FOV corresponds to 1744 pixels out of a maximum of 2048. Similarly for the long wavelength sensors, the 100° FOV corresponds to 872 pixels out of a maximum of 1024. Thus for aircraft roll angles of less than or equal to ±8.7°, roll compensation can be realized by simply deleting from the final data outputted from each sensor, as explained below, those pixels which lie outside the 100° FOV. Figure 4-17 depicts this situation.

As described in Section 4.4.2.1, the digital accumulator in each short wavelength (long wavelength) sensor contains in its memory 1024 (512) numbers each of which represents the sum of the signal outputs, over the dwell time, of a given pixel in the sensor's CCD array. Since the pixel locations to be deleted in the outputted data are a linear function of roll angle, then only the location in memory at which data outputting should end need be kept track of to implement roll compensation. For example, if the roll angle were 1°, then data in memory locations 855 through 1024 would be deleted in one of the two short wavelength sensors covering the 100° FOV, while locations 889 through 1024 would be deleted in the other. Thus a simple "look up" table stored in ROM, whose pointer updated once every dwell time, would contain the last addresses to be outputted from memory for a given roll angle. For the above example, these addresses would be 854 and 888.

Figure 4-16
AMS SCAN GEOMETRY

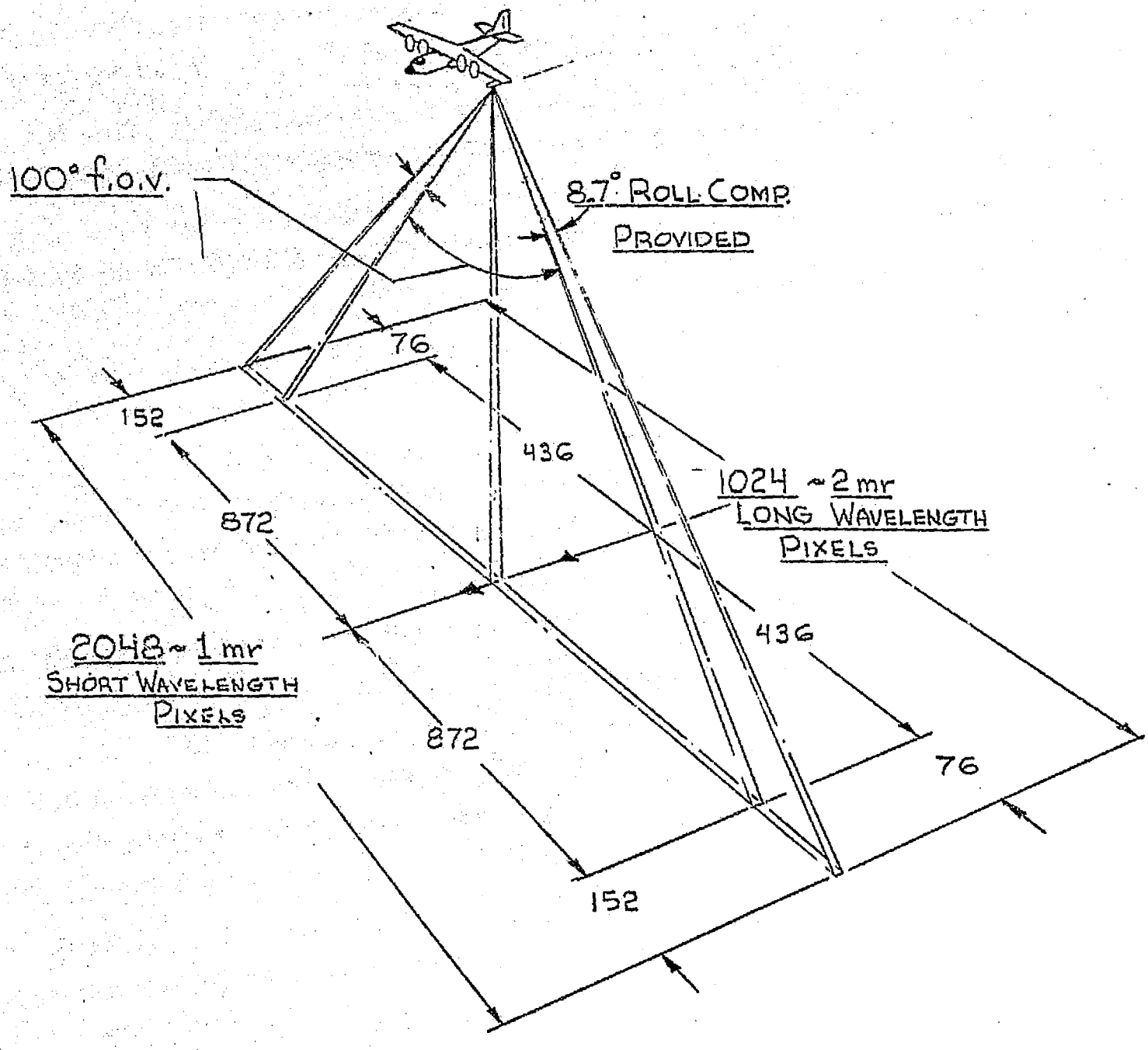

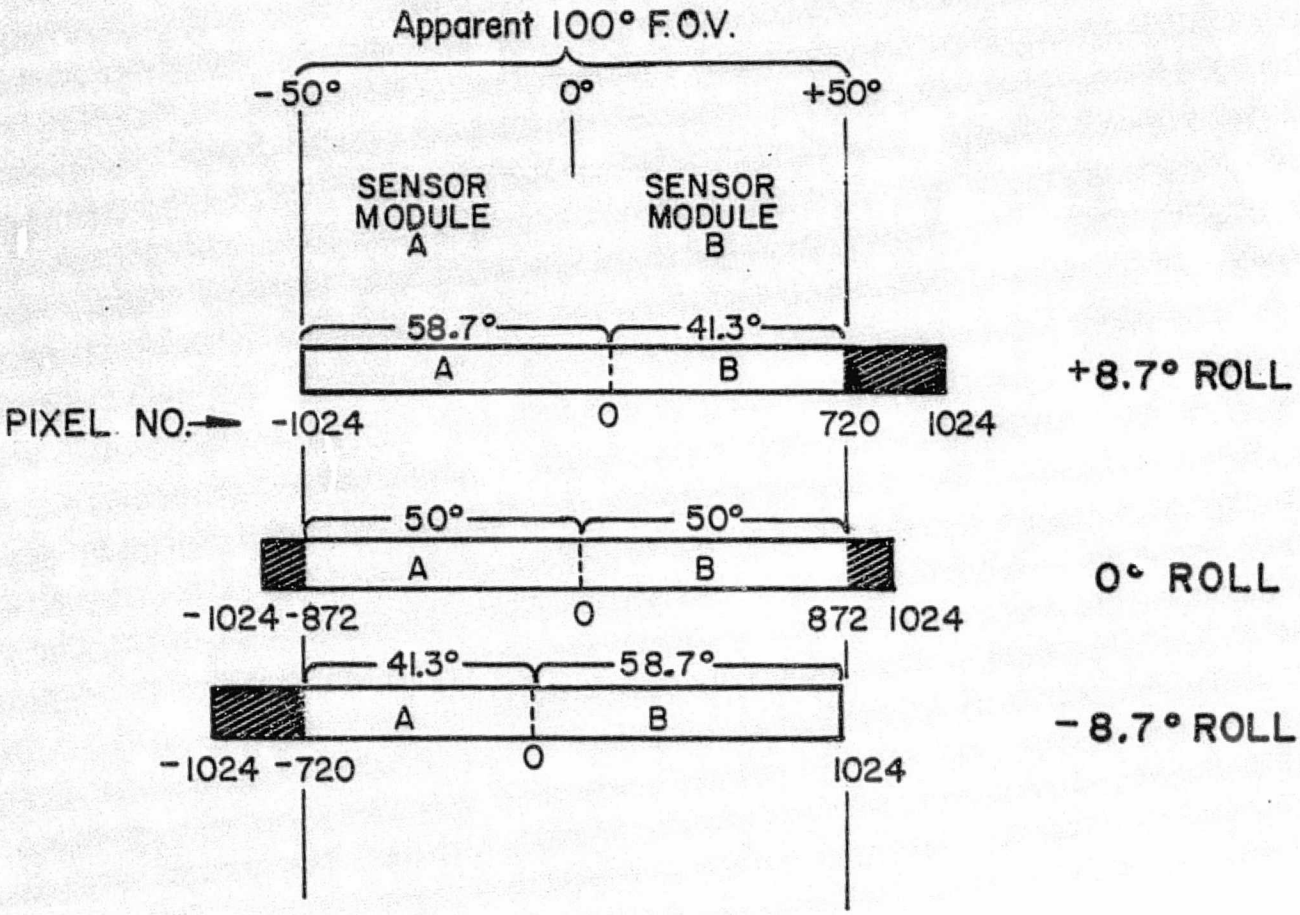

Figure 4-17 ROLL COMPENSATION SCHEME – SHORT WAVELENGTH SENSORS 100° F.O.V.

4.4.1.6 Output Data Rates

As indicated in Section 4.4.1.3, a digital averager is required to preserve the S/N inherent in the CCD data collected over a "scan" dwell time. Although the accumulator processes the data from an entire array, i.e., over the 60° FOV, it only outputs data corresponding to a 50° FOV in accordance with the roll angle compensation discussion of Section 4.4.1.5. Consequently, 872 data words are outputted from the accumulator for the short wavelength sensor and 436 data words are outputted for the long wavelength sensor over the scan dwell time T_d. Since T_d varies with the V/H rate, so will the output data rate. Table 4-6 lists the data rates expected for the short and long wavelength sensors. We have assumed, for the purposes of tape recorder formatting, which is discussed subsequently, and for common digital accumulator design, that the output data word length is fixed at 16 bits.

TABLE 4-6

AVERAGER OUTPUT DATA RATES

FOV θ	1 mrad	2 mrad	1 mrad	2 mrad
V/H Rate	0.25 rad./sec.		0.025 rad./sec.	
Data Rate (K words/sec.)	218	109	22	11
Maximum bit Length in Memory ÷ 2	16	16	16	16
Maximum bit Rate (M bits/sec.)	3.49	1.74	0.35	0.176

NOTE: 1 16 bit Word = 2 Bytes, eg, 218 K words/sec. = 436 K Bytes/sec.

4.4.1.7 Tape Recorder Considerations

As shown in Figure 4-14 , we have assumed that the primary means of storing the data collected from each sensor module during a flight will be via an on-board tape recorder system. Alternatively, the data could be telemetered to earth over a radio link. However, this alternative would also require a tape system, if the receiving stations were not always in range of the aircraft during its mission run.

The types of tape systems that are generally available are: digital data recorders, instrumentation recorders and video recorders.

Digital tape recorders have the advantage that they are directly computer compatible. That is, the tape may be read into a computer without any preprocessing in IBM format. The Pertec T1000 tape driver with F6250 tape formatter is an example of such a system, see appendix. At 125 ips and a data density of 6250 Bytes/sec., it is capable of 781K Bytes/sec. The maximum data rate required by a sensor module is 436K Bytes/sec. (see Table 4-6). At this transfer rate, a "scan" of the scene corresponds to a 4 ms dwell time. If the tape is 2400 ft. long, then the maximum record time is:

$$\text{Record Time} = (2400 \text{ ft.})\left(12 \frac{\text{in.}}{\text{ft.}}\right)\left(6250 \frac{\text{Bytes}}{\text{in.}}\right)\left(\frac{1}{436\text{K} \frac{\text{Bytes}}{\text{sec.}}}\right)\left(\frac{1 \text{ min.}}{60 \text{ sec.}}\right)$$

$$= 6.9 \text{ minutes}$$

If start/stop and formatting is taken into account this time reduces to approximately 3.5 minutes. This is only for one 50° FOV spectral band! Consequently, this type of recorder system is impractical.

As a practical alternative, the Ampex AR-1700 airborne high density digital recording system, with Miller digital recorder electronics, for example, appears to be appropriate; see appendix. This system can record image data on up to 24 tracks; one track being alloted to each sensor module. In addition, ancillary data may be recorded on any one of 4 additional tracks, e.g., IRIG time code and the data clock which varies with V/H rate. This latter clock is also used to vary the tape speed in order to achieve a constant bit packing density. As Table 4-6 shows, a maximum transfer rate of 3.49 M bits/sec. is required in the worst case. This recorder system is capable of 4 M bits/sec. at a data density of 33.3K bits/in. With 10,500 feet of tape available, the maximum record time would be 17.5 minutes. This is reasonable when one considers that 12, 100° FOV, sensor channels are being recorded simultaneously.

Video recorders presently available, e.g., Arvin Echo VRR-421, see appendix, have bandwidths to 6 MHz which will handle the 3.49 M bit/sec. sensor data rate. They also have a channel available for timing information. Record time is 60 min. These systems are not at present adequate for recording multi-sensor data. However, work on 80 M bit/sec., 50 min. recorders is going on at Bell and Howell under classified contract. This type of recorder is of interest because it will be able to handle multi-sensor data and provide long recording times.

In light of the above, we have assumed the use of a multi-track instrumentation recorder like the AR1700. Figure 4-18 shows a possible data format for the serial data input on one track.

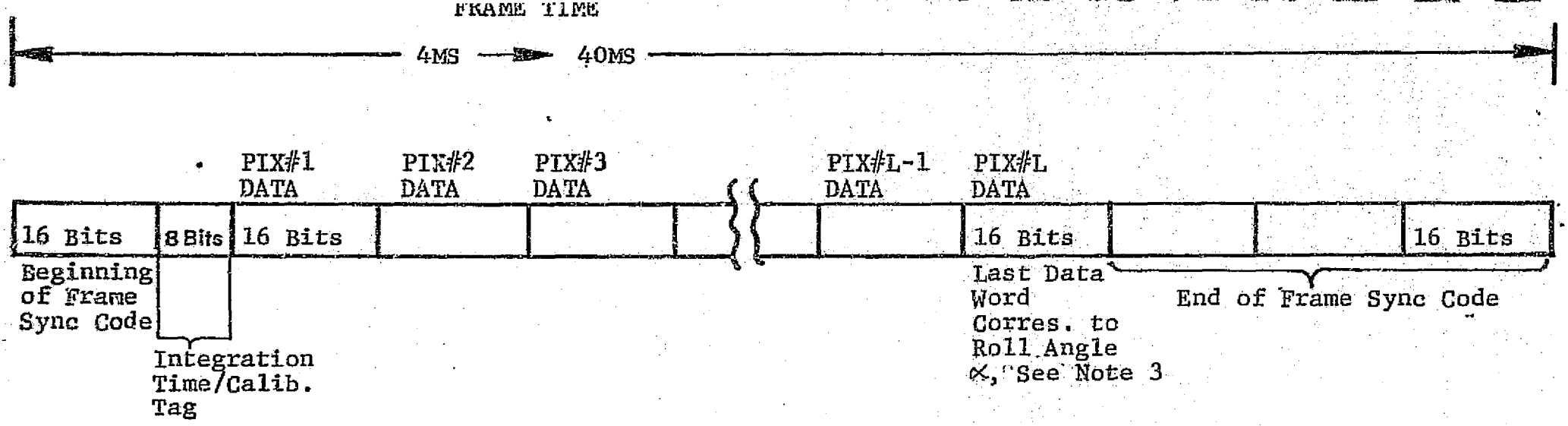

NOTES:

1. TRACK NO. IDENTIFIES SENSOR MODULE
2. EACH FRAME REPRESENTS M CCD ARRAY SCANS; $40 \leq M \leq 400$.
3. FOR SHORT WAVELENGTH SENSORS, $L \doteq 872 \pm 17.5\alpha$;
   FOR LONG WAVELENGTH SENSORS $L \doteq 436 \pm 8.75\alpha$;
   WHERE L IS AN INTEGER, $|\alpha| \leq 8.7°$
4. FRAME TIME VARIES WITH $^{V}/h$ RATE. TO ACHIEVE CONSTANT BIT PACKING DENSITY, RECORDING SPEED IS VARIED WITH $^{V}/h$ RATE.
5. AIRCRAFT DATA, eg, ROLL, V/H, HEADING, IRIG TIME, HOUSEKEEPING, RECORDED ON AUXILIARY TRACK.
6. ONCE EVERY C FRAMES CALIB DATA COLLECTED.

Figure 4-18

SERIAL DATA FORMAT FOR AMS RECORDER

4.4.2 Details of Electronics Design

4.4.2.1 Short Wavelength Sensor Module Electronics Design

Figure 4-15 is a detailed block diagram of the AMS electronics. It is referred to in the discussion which follows.

As described in Section 4.1.4, each sensor module operating in the short wavelength region will utilize a Fairchild CCD 131 linear image detector array. In order to prevent photosite saturation, this 1024 element array is read out at an effective 10 MHz rate. As discussed in Section 4.4.1.1, the array's photosite integration time is switched between 100 μs and 880 μs by the post electronics depending upon the dynamic range of the scene. The CCD 131 requires a number of clocks for operation, see Appendix C. The major portion of these clocks are generated in the sensor module in a block called clock interface in order to minimize cabling and potential EMI problems. The input to the clock interface is from the timing and control (T/C) processor located in the post electronics. Besides outputting the required timing and control signals for the analog and digital processing sections to be described subsequently, the T/C processor outputs the integration and reset clocks for the array. Since each sensor module's T/C processor operates from the system controller's master clock, all clocking within a module is in synchronism with all other modules in the AMS system. This latter feature permits easier EMI control.

The analog video output from the CCD 131 array is actually read out on two lines at a 5 MHz rate; one line outputs all of the even photosites and the other line outputs all of the odd photosites. Each output is fed to a separate buffer amplifier and voltage clamp as shown in Figure 4-19. In order to minimize crosscoupling between video samples in these amplifiers to less than 1 LSB of the 8 bit A/D converter which follows, their bandwidth must be at least 7.5 MHz.

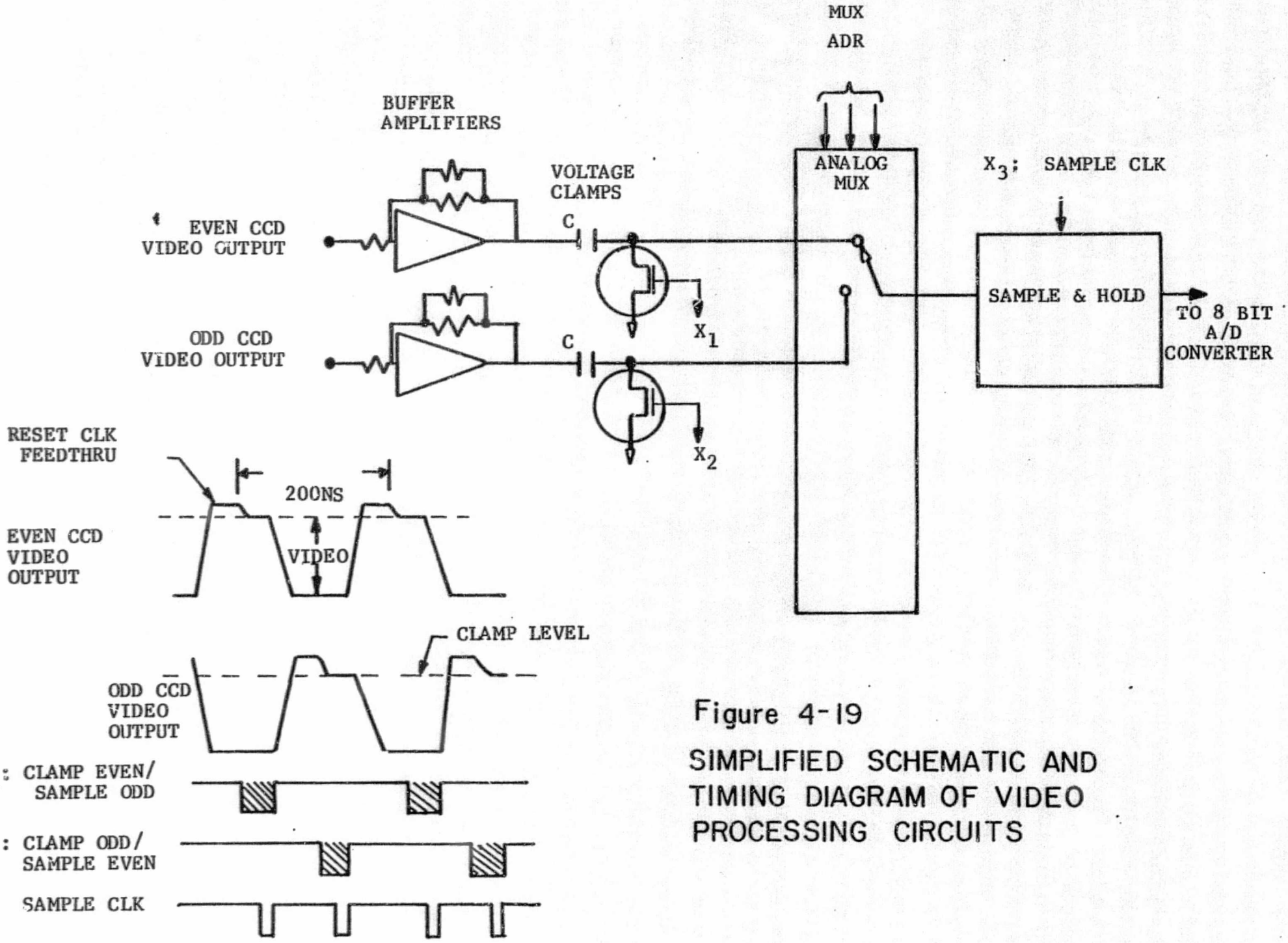

Figure 4-19

SIMPLIFIED SCHEMATIC AND TIMING DIAGRAM OF VIDEO PROCESSING CIRCUITS

The voltage clamps operating in conjunction with the analog multiplexer (MUX) and sample and hold generate a 10 MHz analog signal which is free from reset transients and reset ($\frac{KT}{C}$) noise. These circuits implement, in practice, the correlated double sampling (CDS) technique described in Section 4.1.3. This, of course, is in addition to their primary functions which are described subsequently.

During an in-flight calibration sequence, the various temperature monitor outputs, e.g., CCD array temperature, aperture cover temperature, etc. and other analog housekeeping and BIT (built-in-test) functions are multiplexed into the main data stream through the analog multiplexer (MUX). The output of the MUX is fed to a sample and hold which is also clocked at 10 MHz, see timing diagram in Figure 4-19. The output of the sample and hold circuit is then fed into an 8 bit A/D converter. Because of the high data rates involved, a TRW monolithic video A/D converter Model TDC 1007J is utilized. This device typically does a conversion at speeds to 30 megasamples/second. Since the analog video is clocked at 10 MHz, the A/D will also be clocked at this rate. See appendix for data sheets.

The output of the A/D converter is fed into a digital MUX. During the non radiometric portions of the calibration sequence, e.g., housekeeping, BIT, etc., the data from the A/D converter is outputted directly to a data formatter prior to magnetic tape recording. However, during the radiometric portions of the calibration sequence and during a normal data run of a natural scene, the data from the A/D converter is outputted to a digital averager for further processing.

As described in Section 4.4.1.3, the purpose of this processing is to restore the S/N of the data collected for each pixel to that which would be measured if the integration time could be made as long as the "scan" dwell time without saturation. To achieve this requirement the average must:

(1) Accumulate the sum of each detector element output over a full "scan" dwell time, T_d.

(2) Vary the number of partial sums, m, in accordance with the aircraft's V/H rate.

(3) Output data corresponding to a 50° FOV; compensating for as much as ±8.7° of aircraft roll.

(4) Limit the size of output data word to 16 bits.

To perform these tasks in 100 ns, i.e., the time between video samples, requires a "flip-flop" configuration which uses two accumulators, each with a bit capacity of 17 bits and two memories each of which can store 1024, 17 bit words. Figure 4-20 shows a possible implementation of this requirement.

Each memory is constructed from 1024 x 1 RAM devices similar to the Fairchild 93L425. Typical time for a read and write cycle is 60 ns. Although faster memories exist in ECL technology, we have not chosen them because their low temperature performance is limited to 0°C. Each 17 bit binary accumulator uses 8 SN545281, 4 bit parallel binary accumulators, and 3 SN54182, look-ahead carry generators or similar devices. Typical enter-store and add time is 75 ns. Adding this to the memory read/write cycle time results in 135 ns for adding a current output of the A/D converter from a particular detector element, to the previously stored partial sum for that detector element and then returning the new partial sum to its memory location. Since the A/D converter is outputting data at a 10 MHz rate, i.e., every 100 ns, the

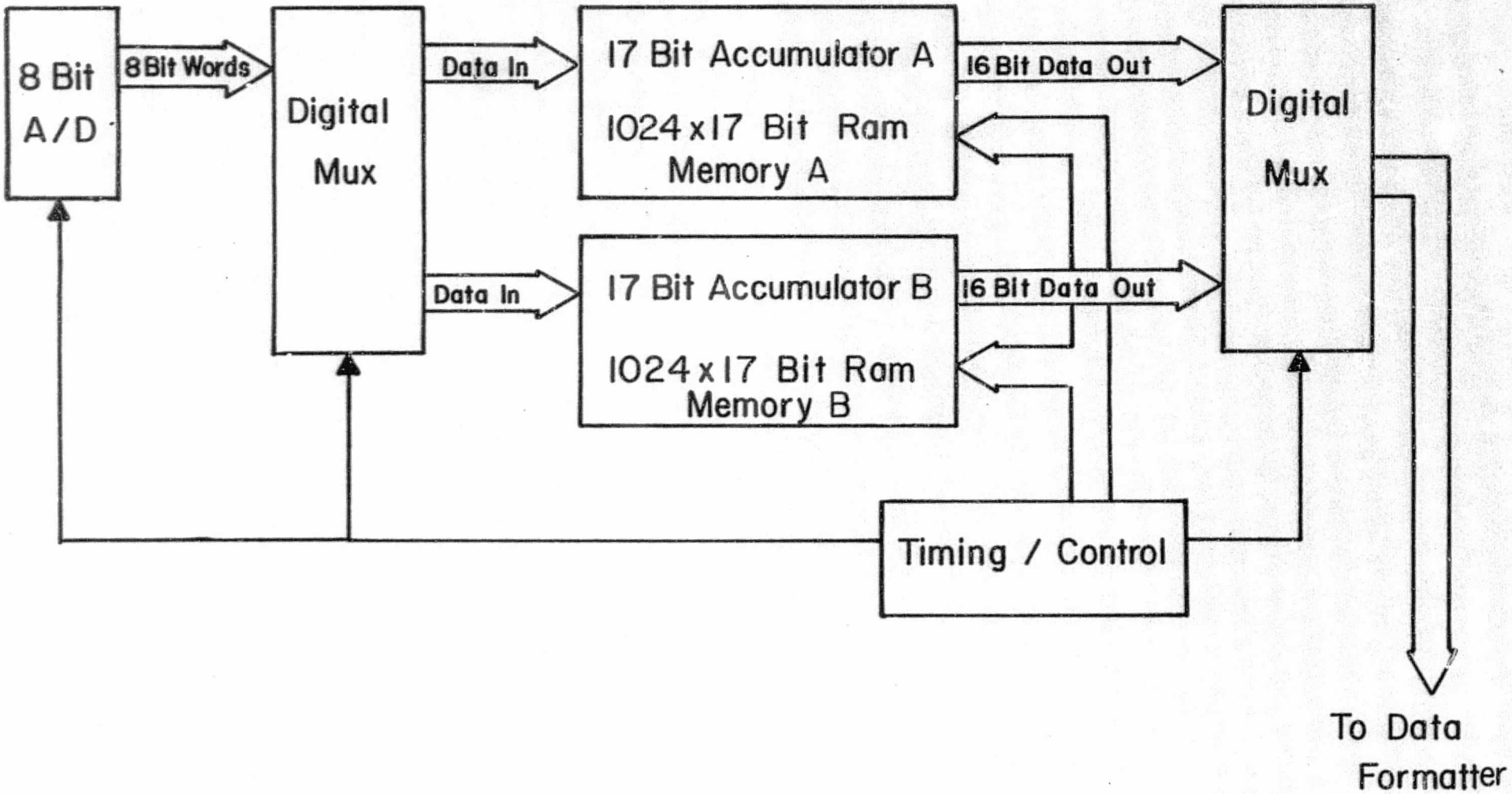

Figure 4-20 FLIP FLOP ARRANGEMENT FOR DIGITAL ACCUMULATORS

above process is too slow for one accumulator/memory. Therefore, in order to provide more processing time using these devices, the dual accumulator/memory configuration shown in Figure 4-20 is recommended. This flip-flop arrangement, by operating on alternate A/D converter outputs, reduces the effective processing rate to 5 MHz and consequently allows 200 ns for the data accumulation process. After m cycles as described above, the sum in each memory location is divided by 2 (shift right) in its corresponding accumulator and each resulting 16 bit word is alternately outputted to the data formatter; thereby reconstructing the 10 MHz data rate. The overall timing and control of the accumulator as well as the sample and hold, A/D converter and multiplexers are under the control of the timing and control processor.

The readout rate of the CCD array is maintained constant regardless of the V/H rate. The only timing parameter that is changed with respect to CCD array operation is the integration time. As described in Section 4.4.1.1, the integration time is varied between one of two levels (100 μs and 880 μs) in order to accommodate the maximum expected scene dynamic range, while permitting contrasts of 1% to be measured. The decision as to which integration time to choose is done automatically in the post electronics by counting the number of exceedances that each digitized output from the array produces over a given dwell time. When this number of exceedances reaches a given number, then the integration time of the array is reduced from 880 μs to 100 μs. Conversely, when the number of exceedances falls below a given number, then the integration time during the next dwell period is increased from 100 μs to 880 μs. The logic that controls the integration time also generates a tag on the formatted and recorded data so that ground data processing can take the integration time change into account.

In order to conserve tape and to lessen the burden on the tape system with respect to data transfer rate, roll compensation is performed in-flight on the data before it is outputted to the tape recorder as described in Section 4.4.1.5. Roll compensation truncates the 60° of radiometric data contained in the digital accumulator such that only data corresponding to 50° is outputted. Roll compensation will be implemented using a ROM in which is stored the last memory address at which data is to be outputted. The selection of this last memory location is a function of the roll rate which addresses the ROM. The roll data is obtained from the aircraft interface and is preprocessed in the system controller which contains the above-mentioned ROM. The system controller, in turn, outputs the roll compensation address to each sensor module's T/C processor.

The roll compensated 16 bit output of the digital accumulator is fed into the data formatter. The purpose of the data formatter is to put the data into a form which will allow subsequent unambiguous data reduction from the recorded data. To do this, the formatter takes the digital data and annotates it with the sync codes, integration time and calibration tags as shown in Figure 4-18.

The implementation of the data formatter, the integration time control logic, as well as the T/C processor in each sensor module will utilize a microprocessor where speed permits; otherwise discrete logic will be utilized.

As is shown in Figure 4-15 the sensor module and post electronics also contain ancillary electronics, e.g., an in-flight calibration source controller, BIT, housekeeping and local voltage regulation.

As described in Section 6.1, the source controller for both the short wavelength and long wavelength sensor modules are essentially the same; that is, it uses a conservation of charge technique to effect temperature control. For the short wavelength sensor, the voltage applied to the source controller's storage capacitor is fixed. Whereas in the long wavelength sensor, if the aperture doors' approach is used as the radiation reference, this voltage is a variable depending on the doors' absolute temperature. To produce a variable voltage, the doors' temperature is measured periodically. The system controller generates a digital word corresponding to the voltage which should be placed on each of the storage capacitors in this system. Alternatively, if the mirror/solenoid approach is used for the long wavelength reference source, then as described in Section 6.1, the storage capacitors are operated with a fixed voltage as in the short wavelength case.

The details of BIT, housekeeping, and local voltage regulation will be worked out in the detailed design phase.

4.4.2.2 Long Wavelength Sensor Module Electronic Design

The design of the electronics for the long wavelength sensor module is nearly identical to that described in Section 4.4.2.1 for the short wavelength sensors. The major difference is the need to perform background subtraction to achieve the desired dynamic range capability as discussed in Section 4.1.5.

Background subtraction is realized in a combination of digital/analog circuitry. Figure 4-21 shows one such implementation. The value to be subtracted from each detector element output is stored in a read only memory (ROM). The stored values are determined during the calibration phase when the sensor is looking at a uniform 300°K blackbody. As a consequence, the subtraction not only subtracts the "dc" background radiation produced signal, but also any fixed pattern noise associated with the detector element being processed. The ROM is controlled by the timing and control logic.

The digital output of the ROM is fed to a high speed, 12 bit resolution digital to analog converter similar to the Data Conversion Products DAC-S. The analog output of the ROM is then subtracted from the appropriate analog video sample from the detector array.

The subtraction is performed at the input to the video buffer amplifiers. Assuming an even/odd output arrangement for the CCDs as in the short wavelength case, an analog MUX is, therefore, provided, see Figure 4-21.

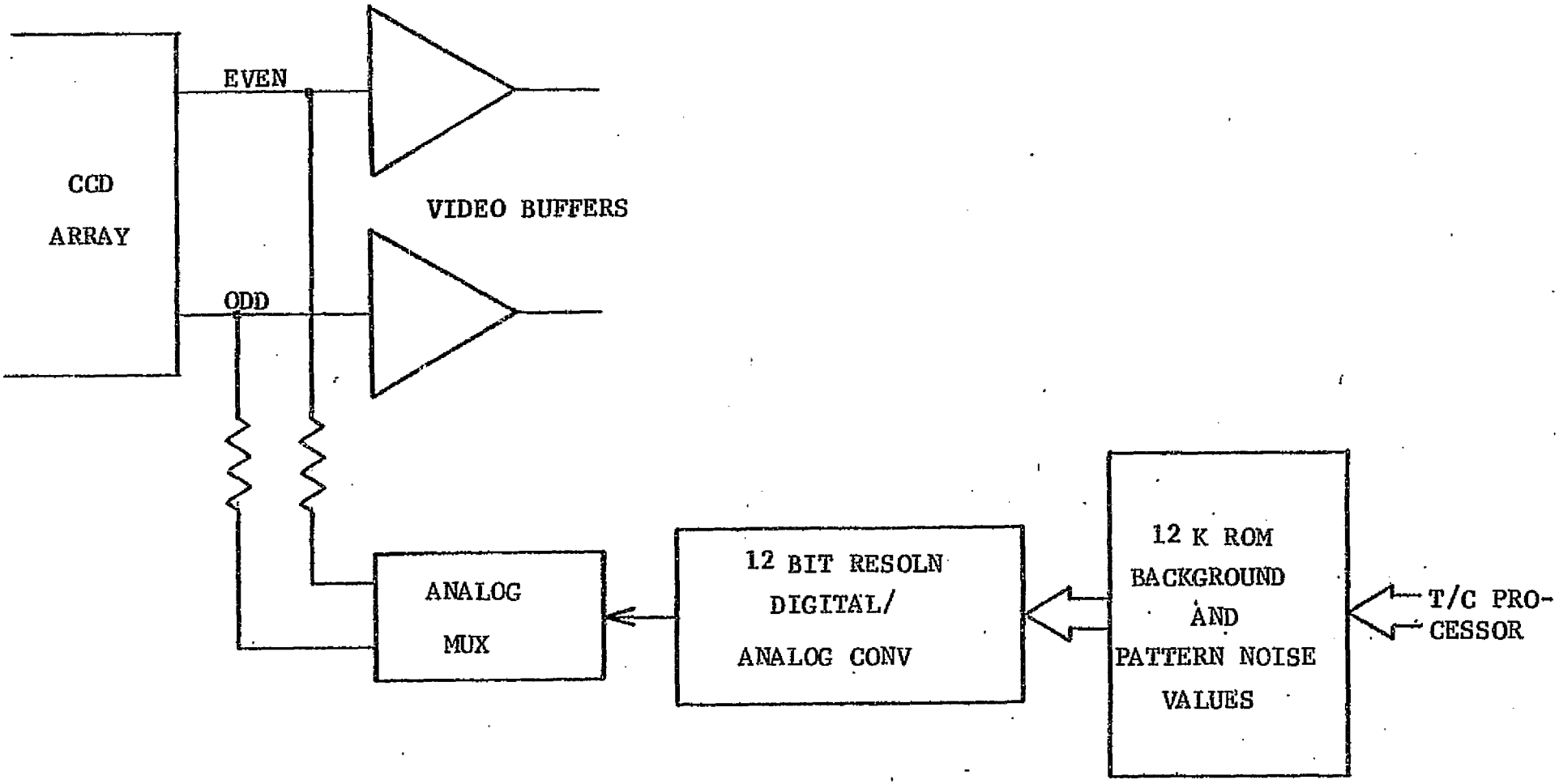

FIG 4-21 IMPLEMENTATION OF BACKGROUND SUBTRACTION IN LONG WAVELENGTH SENSOR ELECTRONICS

5.0 MECHANICAL DESIGN

The AMS System is designed to be modular in configuration thereby allowing for maximum operational flexibility. It is designed to be easily installed in an aircraft using the standard mechanical and power interfaces. Figure 5-1 shows one possible mounting configuration.

This configuration mounts as many as 24 (12 pairs of) sensors in a single pod. The final shape, mounting location and interface to the aircraft will be worked out in the next phase. The configuration presented in Figure 5-1 allows easy access to the sensor modules and electronics package through two access panels permitting facility in system maintenance and subsystem removal. Since all sensor modules are independent in operation, all 24 need not be installed or operational to allow system operation of the remainder. Sliding doors are also provided in the pod design to protect the optics in general and especially during landings and takeoffs. In addition, these doors provide a "zero" reference for the long wavelength sensor, see Section 6.1.4.

Aircraft roll compensation of the data outputted from the system is provided for as described in Section 4.4.1.5. As a consequence of this provision, the data recorded is independent of roll angle within ±8.7°.

5.1 Environmental Considerations

The AMS System is designed to operate in the vibration and shock environment usually experienced in any operational four engine prop-jet. Since the AMS has no moving parts, except perhaps for a calibration solenoid on the long wavelength sensor (see Section 6.1.4), and operates at low voltages, it is therefore not expected to experience difficulties in high altitude applications.

Figure 5-1
AMS SYSTEM MOUNTING CONFIGURATION

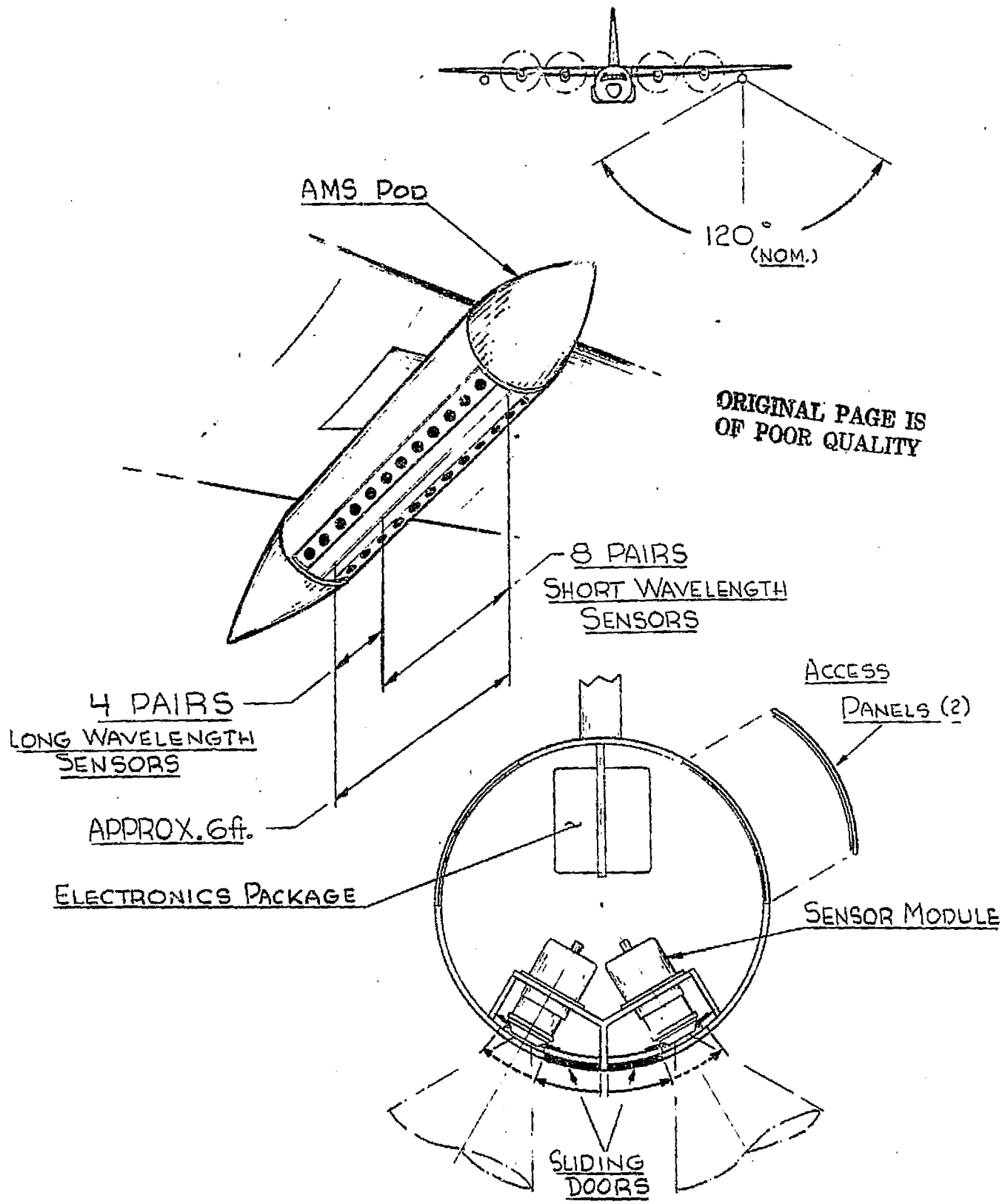

All materials and component parts are selected for high reliability and to withstand storage temperatures of -22°F to 150°F. The cold temperature limit being set by the short wavelength CCD (CCD 131). If -30°F is a firm requirement, either the feasibility of special processing for the CCD 131 must be undertaken or provision for heating the device made. The latter being awkward in storage situations. Under operational conditions, the temperature range of -30°F to 110°F is easily accommodated.

The AMS is designed to operate in a humidity environment ranging from 0 to 100% humidity. All components which are affected by moisture are located in sealed environments within the sensor module, e.g., optical materials which may be hygroscopic, see Section 4.3.9.

As indicated above, condensation on the optics during aircraft descent will not deteriorate the sensors. However, it may affect performance. Provision is made in the sensor module design, see Figure 4-12, to heat the exterior of each sensor module to above the dew point to prevent formation of condensation on the optics.

5.2 Sensor Module Design

As stated in Section 5.0, the AMS System has been designed to be modular. That is, for each 60° F.O.V. spectral band being monitored, there is a corresponding sensor module (with its post electronics). To cover a roll compensated 100° F.O.V., a pair of sensor modules are required. The AMS System can accommodate as many as 12 pairs of modules. All modules are independent, optically and electronically. Thus a very flexible system results. Sections 4.3.7, 4.3.8 and 4.3.9 describe the optical design aspects and 4.4.2.1 and 4.4.2.2 the electronic design aspects.

5.3 Optical Alignment Considerations

5.3.1 Short Wave Sensor Optical Alignment Considerations

In this section we will present some general optical alignment considerations as they apply to the specific sensor design approach discussed in Section 4.3.8. As stated earlier, it is not meant to be a procedure but it is meant to support the design and show that it is practical.

The various optical properties of the optical elements themselves can be used to act as indicators for the positioning of the elements. For example, as shown in Figure 5-2 which shows the fiber optics removed, the pointer and return image coincide only at the center of curvature of the spherical reflector. The overall approach is building up the assembly one step at a time. First, the spherical reflector is positioned alone and carefully checked with a rotary table, alignment telescope, pointer, etc. The corrector shell element is then introduced. If difficulties arise, the elements are reshimmed if necessary, until a complete and checked system is obtained. For those sensor modules which require filters which are opaque to the eye, a clear glass corrector shell, manufactured to the same tight tolerances as the actual corrector shell, will be substitued during this phase of the alignment. Upon completion, the actual corrector shell to be used is introduced.

The complete lens cell subassembly is then assembled to the main housing with all adjustments at mid position. The detector array and fiber optics subassembly is then assembled through the slot at the top so that the spherical end of the fiber optics bundle faces the spherical reflector.

The detector array assembly must be hard mounted to the main housing by means of pins or shoulder screws so that subsequent removal of the unit does not upset the alignment of the fiber optics to the optical system. The input end of the fiber optics and the image surface formed by the optical

C2

system must have the same spherical radius to within the size of one array element. Optical measurement techniques can be used to determine the radius of the optical image; then the fiber optics radius can be adjusted by controlled polishing procedures.

Since the input face of the fiber optics and the image surface are both spheres of the same radius, it is only necessary to make their centers coincide for proper alignment. Consequently, only three degrees of freedom are needed between the two subassemblies. The three adjustments could be divided between the two subassemblies but as Figure 4-10 shows, all three adjustments are on the lens cell. They are essentially X, Y, Z linear adjusts. As stated previously, shim adjusts are always preferred over screw adjust wherever it is convenient or possible.

Although a dummy detector array fiber optics subassembly might be used to monitor the image with a microscope at the output end of the fiber optics as shown in Figure 5-3, it is better to monitor the electrical output of the detector array to verify overall performance of the completed assembly. The general setup shown in Figure 5-3 will be needed during the alignment of the optical image to the fiber optics array. The rotary table eliminates the need for a wide angle high resolution target projector but the entire field cannot be tested simultaneously. Significant portions of the field can be sampled at one time for alignment purposes.

When this adjustment is complete, the side supporting stalks for the fiber optics are inserted and adjusted so that they are within a few thousandths of the fiber optics. This can be monitored by watching the adjustment through the front corrector with a jeweler's loop. The corrector has very little power and acts more like a window. If optically opaque narrow band pass filters are used on the corrector, side looking holes in the main housing and lens cell

will have to be used to watch the feet of these stalks. The electrical output signals, the turns count on the stalk, plus the jeweler's loop would all be used to bring the stalks into contact with the fiber optics without misaligning the system.

Final boresighting of the sensor assemblies consists of aligning the optical axis with a main housing flange. This can be accomplished by a pair of wedged shims (not shown in Figure 4-10) and the general setup shown in Figure 5-3. After the adjust, the shims are pinned to the flange to allow interchangeable installation of any sensor which has a boresighted mounting surface.

5.3.2 Long Wavelength Sensor Optical Alignment Considerations

The purpose of this section is to identify any particular alignment consideration that pertain to the long wavelength sensor design shown in Figure 4-12. Again, it is not meant to be a procedure but to support the design and show that it is practical. Many of the general techniques for aligning long wavelength optical systems apply here, as do some of the considerations discussed in Section 5.3.1.

The sensor is mounted on a back cover plate which can be adjusted for aligning the sensor elements to the optical image plane. A shim is used for axial adjustment. Side screws produce any X, Y adjustments required.

The fabrication of the optics could be treated in the same manner as that used for a simple doublet with both elements of the same index. In case there are cementing difficulties, a small air space between the element would have little effect on the blur circle. Anti-reflection coatings would be needed however.

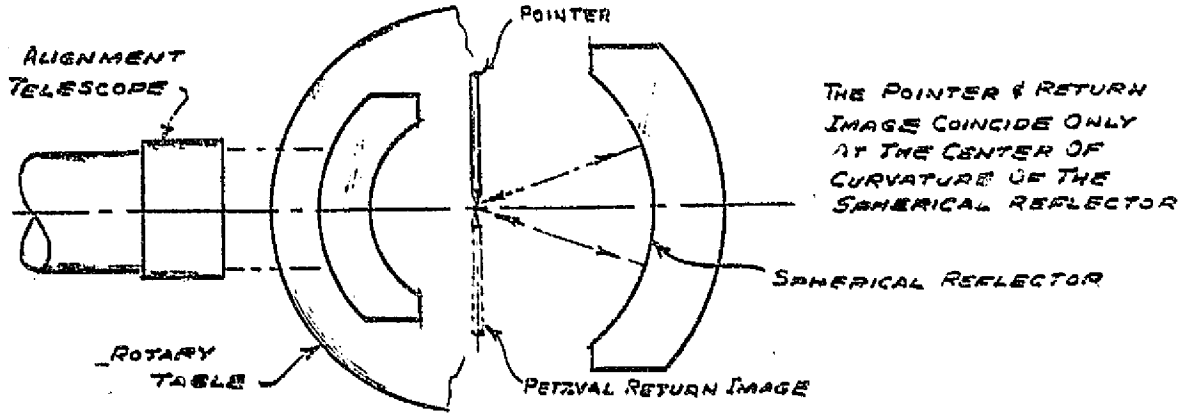

Figure 5-2 SHORT WAVELENGTH ALIGNMENT SET UP

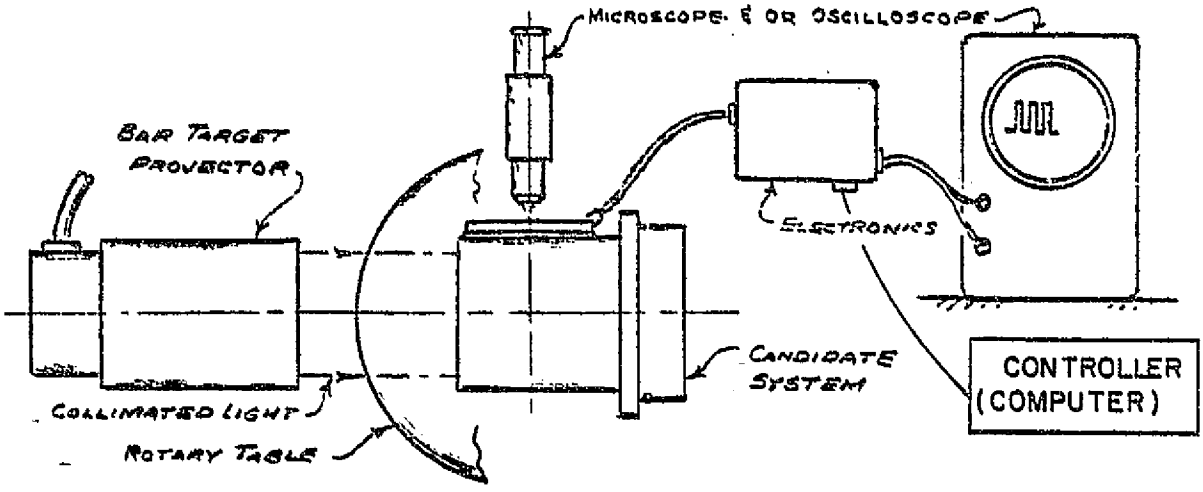

Figure 5-3 GENERAL ALIGNMENT SET UP

If separate elements are used, side screws could be used to adjust them with respect to each other. In addition, the centers of the two spherical surfaces determine an optical axis which must be perpendicular to the flat first surface. General techniques similar to those discussed under the short wavelength approach can be used in this case too.

5.4 Power, Weight and Volume Budget for the AMS System

The AMS System can be characterized as being comprised of four major subsystems. These subsystems and the contribution to the power, weight and size of the total configuration is as follows with reference to Figure 4-15:

(1) Sensor Modules - One of these modules will be required for each 60° spectral band to be monitored. The CCD sensor, the clock interface, and the calibration source will consume 2 watts maximum and require minimal board space and weight. All power will be supplied externally.

(2) Post Electronics - One post electronics unit will be required for each 60° spectral band to be monitored. Each one of these housed subsystems will weigh approximately 15 lbs., consume 58.5 watts, and will be housed in a 7.5" x 10.5" x 12" enclosure. The greatest portion of the power consumption in this system is due to the levels required by the data formatter and the accumulator/memory blocks. Since the data rate to each bank of the dual accumulator/memory is 5 M bytes per second, high speed logic devices were essential in its implementation. High system power consumptions must result when high system throughput rates are required. As the power and configuration breakdown shows in Table 5-1, the wattage consumed by these two high-speed digital subsystems is 41.5 watts which is 71% of the power consumed in the post electronics package.

(3) System Controller - Only one 8080 microprocessor package is required for up to 24 system monitoring channels; each channel, as stated, previously, consisting of one sensor module and one post electronics module. This controller will require 10 watts of power for itself and approximately 20 watts for the aperture door motor drive(s) in the system. This package will reside in an enclosure with dimensions of 4" x 10.5" x 12", and it will weigh 8 lbs.

(4) Power Supply - This package will supply power to each of the three system elements listed previously. In the system's maximum configuration, it will have to supply 1482 watts. A switching supply of this magnitude will weigh approximately 100 lbs. in a 12" x 12" x 24" enclosure. The A/C source supplying this power supply will have to deliver approximately 2.1 Kw to it, assuming a 70% power supply efficiency.

(5) Tape Recorder System - The tape system will also derive its power directly from the support vehicle. Only one unit will be required for 24 channels of information. The Ampex Model AR-1700 will consume 490 watts maximum, weigh 107 lbs., and will be packaged in two militarized enclosures. One enclosure houses the tape system and is dimensionally 20" x 16-1/4" x 15". The second enclosure houses the electronics package and is dimensionally 10" x 10" x 14".

A summary of the data presented above is listed in Table 5-1.

TABLE 5-1

AMS SYSTEM POWER, WEIGHT AND VOLUME BUDGET

I.	Sensor Module	
(a)	Power	2 watts
(b)	Weight (electronics only)	2 lbs.
(c)	Weight (short wavelength) (long wavelength)	3.2 lbs. 8.0 lbs.
(d)	Size (electronics only)	2-1/2" x 4.5" x 6"
II.	Post Electronics	
(a)	Power	58.5 watts
	(1) Data Formatting	15 watts
	(2) Dual 17 Bit Accumulator/Memory	26.5 watts
	(3) Sample & Hold + Integration Time Logic	5.25 watts
	(4) Analog Multiplexer	1 watt
	(5) CCD Timing Generator	3.25 watts
	(6) Sources and Controllers	5 watts
	(7) Assorted Interface IC's	2.5 watts
(b)	Weight	15 lbs.
(c)	Size	7.5" x 10.5" x 12"
III.	System Controller	
(a)	Power	30 watts
	(1) Electronic Control	10 watts
	(2) Motor Drives	20 watts
(b)	Weight	8 lbs.
(c)	Size	4" x 10.5" x 10"

TABLE 5-1

AMS SYSTEM POWER, WEIGHT AND VOLUME BUDGET
(Continued)

IV.	<u>System Power Supply</u>	
(a)	Power Required from Vehicle (except tape system)	2.1 kw max.
(b)	Power Output in Max. Configuration (24 channels)	1482 watts
(c)	Weight	100 lbs.
(d)	Size	12" x 12" x 24"
V.	<u>Tape System</u>	
(a)	Power (from vehicle)	490 watts maximum
(b)	Weight	107 lbs.
(c)	Size	(1) 20" x 16-1/4" x 15" (2) 10" x 10" 14"
VI.	<u>Maximum Systems Power and Weight Specification</u> (For 24 Channel System - 16 Short Wavelength Sensors 8 Long Wavelength Sensors)	
(a)	Power	2600 watts
(b)	Weight	690 lbs.

6.0 CALIBRATION

6.1 In-Flight Calibration

6.1.1 Calibration Philosophy

The purpose of the in-flight calibration source is not to provide an absolute calibration of the system but only to check for gross variations in CCD detector array responsivity and, in general, optical system throughput. In this approach, the calibration source will serve as a transfer standard and consequently will not be designed to be an absolute radiometric reference. We may adopt this calibration philosophy because the in-flight calibration source will be simultaneously viewed by at least 512 CCD detector elements in each sensor module. As a direct result of these large numbers of simultaneous measurements and the monitoring of the temperature of the array as well as that of the aperture cover (to be described subsequently), the state of operation of the array and of the sensor module can be deduced with a high degree of confidence, even if one or more elemental detectors were to fail. This concept cannot be implemented in a single detector or small multi-detector array because of the limited number of independent measurements which can be made. This calibration approach is described as follows:

As part of the ground calibration sequence as explained in Section 6.2, an in-flight calibration of each sensor module is performed and data collected. By correlating the in-flight calibration performance data measured during a normal flight with that data obtained as part of the ground calibration sequence, the health of the sensor module under test can be determined. Further correlations between the spectrally independent sensor modules in the calibration environments can also be made in the same way to provide additional information on which to evaluate sensor performance. It is these correlations taken over large independent numbers of detector elements that permit the transfer standard approach to be utilized.

6.1.2 General Considerations

In any in-flight calibration system, it is an inherent requirement that the calibration be performed against a "zero" reference level. This reference level usually requires the aperture to be covered or the sensor's FOV shifted so that the viewed scene radiance is prevented from reaching the detectors. This is usually achieved by placing a shutter vane in front of the aperture or by moving the detector's FOV onto the reference.

However, in this case, where we would use multiple sensor modules which contain no moving parts, the incorporation of multiple, solenoid-operated shutters does not appear to be a desirable or an optimum solution.

Rather, we would envisage that the protective motorized aperture door covers shown in Figure 5-1 be commanded closed during in-flight calibration. With their inside surfaces insulated and painted black, this would place a relatively constant temperature source at the entrance aperture of all the optical modules; the temperature of the door would be monitored.

For the short wavelength sensors, since this cover will be at ambient temperatures and will emit only in the long wavelengths, this will represent a true, non varying, "zero" background radiance level. On the other hand, the long wavelength sensors will output a d.c. signal proportional to the radiance emitted by the black cover (which is a function of its absolute temperature). However, because each cover's temperature will be relatively constant over the longest expected FOV dwell time (40 ms), due to its high thermal mass, an adequate indication of the long wavelength detector array's uniformity of response can be obtained. This will be done by irradiating each element in the array with a short pulse of radiant energy. The resulting pulse will appear superimposed on this d.c. level at the array's output, so that the absolute d.c. amplitude of this pulse will depend to some extent on

the temperature of the door. (See Section 6.1.4.) The same technique will be utilized for the short wavelength sensors. However, the resulting pulse will be outputted on essentially a zero d.c. level (dark current level) as mentioned above. The implementation of these short radiant energy pulses will be discussed subsequently for the short and long wavelength sensors.

6.1.3 Short Wavelength Sensors

Short wavelength in-flight calibration is achieved by passing a pulse of current through a helical coil of platinum wire mounted inside the aperture stop (see Figure 4-10) with the loop diameter being slightly larger than the aperture dimension. In this way, the entire fiber optic focal surface is flooded equally with source energy and the reflectance of the mirror is checked as well. It is envisaged that the source will be pulsed by discharging a capacitor through it as described below, thereby generating a pulse of "light" energy without using mechanical shutters. The resistance of the calibration source will be set by using the appropriate wire thickness and coil length. The loop resistance-storage capacitor RC time constant will determine the average pulse width of the calibration pulse. The peak energy will be set to obtain a calibration source radiance which will produce in each elemental detector, a signal which lies approximately in the middle of its dynamic range.

The worst case requirement with respect to radiant power of the source for the short wavelength calibration source occurs at 0.42 μm. At this wavelength, the source must produce a radiant power on the aperture of the corresponding CCD array of 6.21×10^{-11} watts. This power corresponds to 50% of the peak radiant power expected at 0.42 μm and consequently exercises the signal processing midway in its dynamic range for the typical scene, B_{typ}, condition. This radiant power, P_D, was calculated as follows:

$$P_D = (DR) [B_{typ} \theta^2 A_0 \eta_0]$$

where:

DR = dynamic range factor = 0.5

B_{typ} = 1.2×10^{-4} w/cm^2-ster (see Table 4-4)

θ^2 = elemental field of view = (1 mrad)^2 = 1μ ster

A_0 = area of collecting aperture = 2.07 cm^2

η_0 = optical throughput = 0.5

$\therefore$ P_D = $0.5 \left[1.2 \times 10^{-4} \times 10^{-6} \times 2.07 \times 0.5 \right] 6.21 \times 10^{-11}$ watts

The calibration source could be constructed in a straightforward manner using a 2 cm diameter loop of helically coiled platinum wire with the helix coil annulus having a projected width of 2 mm. The source, therefore, will have a total area of $\pi \times 2$ cm $\times$ 0.2 cm = 1.25 cm^2 and is conservatively estimated to have an emissivity of 0.4, when the black body cavity action of the wire coils is taken into account.

Provided platinum wire can repeatedly reach a temperature of 1900°K without degradation, this approach will be utilized; alternatives are discussed below. Now, conservatively assuming an optical throughput of 0.5, the radiant power of the source, P_s, seen by each detector in the 0.42μm CCD array is calculated as follows:

$$P_s = \epsilon N_s \Delta\lambda \theta^2 A_s \eta_0$$

where:

ϵ = emissivity of source = 0.4

N_s = emitted radiance of 1900° black body source at 0.42μm = 1.43×10^{-2} w/cm^2-ster-μ

$\Delta\lambda$ = spectral bandwidth = 0.0275 μm

θ^2 = elemental FOV = 1μ ster

A_s = source area = 1.25 cm^2

η_0 = optical throughput = 0.5

$\therefore$ P_s = 9.8×10^{-11} watts

This power is 1.58 times the radiant power, P_D, required. Therefore, a slightly lower source temperature than 1900°K can be used for the in-flight calibration of this sensor.

In the above, we have assumed that the in-flight calibration for each sensor would be carried out at 50% of the expected maximum signal level corresponding to B_{typ} for that sensor. However, one could, in the interest of lowering the source temperature, relax the in-flight source emission requirements on the shortest wavelength sensor by reducing the calibration level to 10% - 20% of its maximum signal value. This is possible since, as shown in Figure 4-3 , the expected worst case noise level will be 3.6% of the maximum signal expected.

Alternatively, we could have used instead of the platinum wire source, a parallel array of "Pinlite" tungsten lamps (see Appendix C) operating at 2400°K. Operating these lamps at temperatures higher than 2400°K greatly reduces their life expectancy. This approach would allow a 45:1 reduction in the surface area of the required source. However, due to the extremely small size of the "Pinlite" lamp filaments, an array of from 50 to 100 "Pinlite" lamps would be required. This results in a difficult fabrication problem with respect to packing this number of lamps in close proximity to the 13 mm diameter aperture periphery.

Two other source configurations under consideration are a specially fabricated annular xenon flash tube or an annular evacuated tungsten lamp. Both approaches require component development.

At the present time, because of its simplicity, we favor the use of the platinum wire source at some reduced dynamic range factor, which provides an adequate safety margin with respect to source degradation.

However, a problem that will have to be addressed in the detail design phase regardless of which approach is finally selected, is the rapid change in radiance at 0.42 μm as a function of source temperature. The cooler the source temperature, the worse the problem. This occurs because this wavelength is situated at the short wavelength edge of the Planck blackbody curve where the spectral radiance varies as a high power of the absolute temperature (in °K) of the source. (See Figure 6-1.) Regardless of the approach, the capacitive discharge scheme for controlling source temperature looks quite attractive for this application as discussed below.

Using this conservation of energy technique, a capacitor, C, is charged slowly to voltage V_0. The energy stored in the capacitor is then $\frac{C V_0}{2}$. Since the peak temperature of the source is established by the energy delivered to it, then we can, by dissipating this energy in the source, precisely control the temperature of the source as a function of time. This scheme has the added advantages of being simple to implement and less demanding with respect to power supply current capabilities.

It should be mentioned before leaving this section that for all other short wavelength sensors, the problems discussed above are eased because the source generates much more spectral radiant energy (for a given source temperature) as the wavelength increases. See Figure 6-1.

6.1.4 Long Wavelength Sensors

As was discussed in Section 6.1.1, the in-flight calibration source for the long wavelength, as well as the short wavelength, sensors is intended to check for gross variations in detector responsivity and optical system throughput.

One possible implementation of this calibration source, see Figure 4-12 is quite similar to that shown for the short wavelength sensors. Here too, a helical coil of platinum wire or nichrome surrounds the aperture stop and is energized by the discharge of a capacitor through its resistance, thus generating a single pulse of radiant energy. This radiant pulse emits rays in all directions some of which lie parallel to the ray bundles focused by the optics on the detector array. Hence, this source configuration checks the throughput of the entire optical system except for the entrance window. As was the case for the short wavelength sensors, this configuration uses no shutters or other moving parts. Again here too, the capacitor and coil resistance values will be set to generate a radiance pulse which will generate an elemental detector signal at some fixed level in its dynamic range.

Using this configuration, the main difference between the long wavelength and the short wavelength source is the lower required source temperature. For the long wavelengths, the maximum diffuse scene temperature expected is only 330°K. Consequently, the source is operated near this temperature and either the platinum wire source, which can be blackened with a high temperature paint, or a nichrome wire source will work quite satisfactorily and reliably. However, unlike the short wavelength source which operates against a "zero" radiance reference background, the long wavelength sensor sees its in-flight calibration source against a background radiance which is a function of the

aperture doors' temperature in this "closed position." The temperature of these covers may vary and be as high as 40°C (110°F). Therefore in order to make the in-flight calibration of the long wavelength sensors meaningful, the peak source temperature will be adjusted in each sensor to produce a signal whose level is fixed at 75% of the maximum signal expected for that sensor.

Expressed in equation form for the long wavelength in-flight calibration source:

$$DR\ N_{max} = N_{bkg} + \Delta N_s$$

where for a 9 μm sensor, for example:

DR = the dynamic range factor = 0.75

N_{max} = 1.6×10^{-3} w/cm^2-ster-μm at the maximum expected radiance of the scene (330°K) at about 9 μm

N_{bkg} = the radiance of the aperture cover ≈ 1×10^{-3} w/cm^2-ster-μm (300°K) at 9 μm

ΔN_s = the required radiance produced by the long wavelength in-flight source at about 9 μm

or $\Delta N_s = DR\ N_{max} - N_{bkg}$

$\therefore \Delta N_s = (0.75)\ (1.6 \times 10^{-3}) - 1 \times 10^{-3} = 0.2 \times 10^{-3}$

Consequently, the in-flight calibration source must increase the radiance of the aperture cover background at 9 μm by about 20%. In other words, the source must make each elemental detector see a 307°K source against a 300°K background in order to achieve the required 75% calibration level.

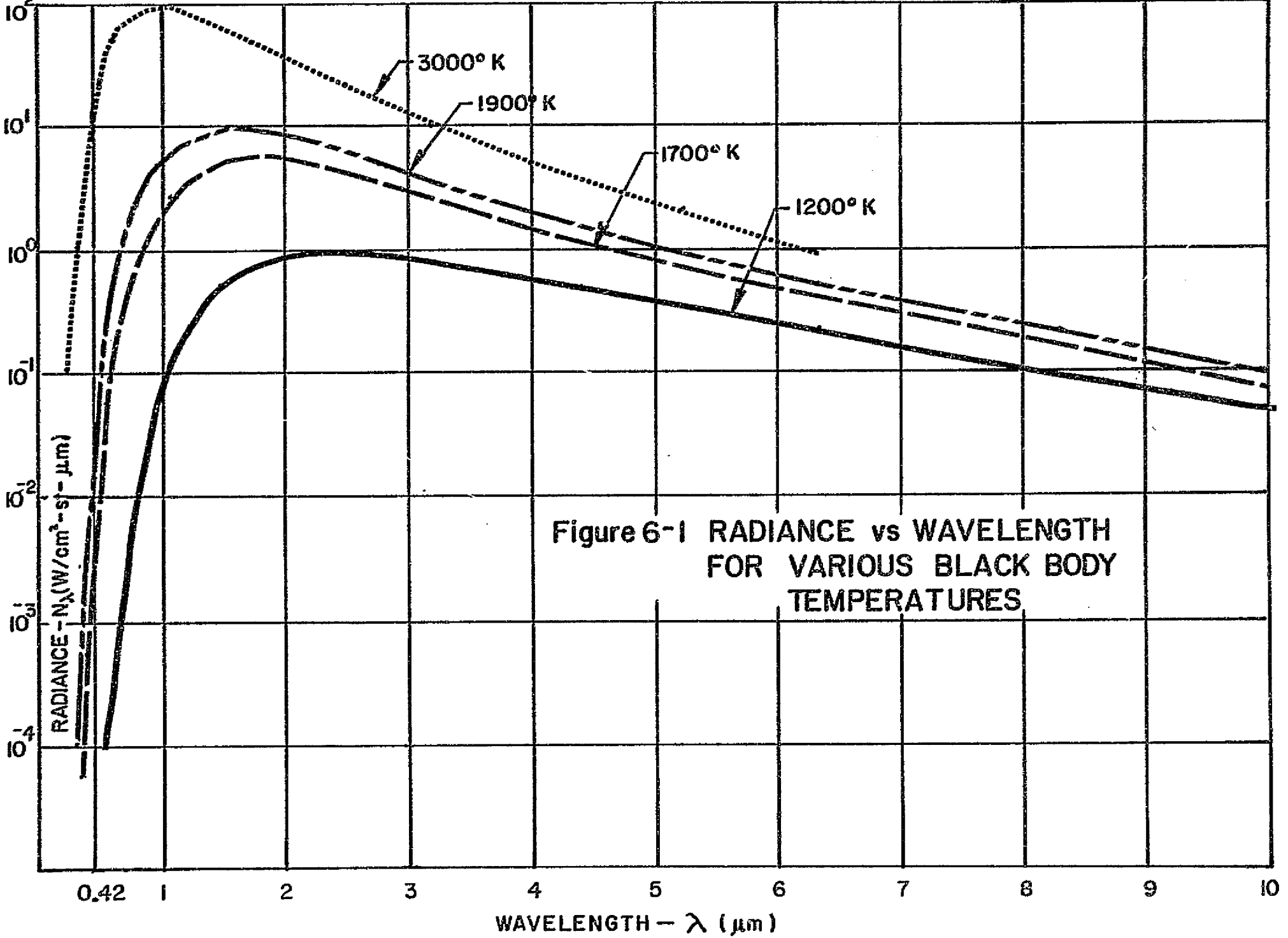

Figure 6-1 RADIANCE vs WAVELENGTH FOR VARIOUS BLACK BODY TEMPERATURES

The major advantage of the above implementation is that it is simple and contains no moving parts. One possible disadvantage, however, is that the background reference radiance is a function of the ambient temperature of the covers. As a consequence, long term comparisons between sensor data must always be corrected for the temperature of this background as well as requiring the electronics to adjust the source capacitance voltage V_0, appropriately to achieve the 75% dynamic range factor.

Aside from insulating, as best as practical, the side of the covers facing the sensors, the only other approach to providing a better controlled and/or closer to zero radiance reference is by using a front surfaced mirror attached to a solenoid. This solenoid would have to be attached to the sensor housing and "swing" the mirror into place for a calibration. With the plane mirror in place at the effective center of curvature of the optic, the cooled detector array sees itself or 77°K so that a cold reference is thereby attained. Although straightforward to implement, it introduces a moving part into a no moving parts system. But it does have the advantage of providing a true long wavelength radiance reference close to zero.

Figure 4-12 , which shows the design of the long wavelength sensor, shows it without a solenoid. Once the thermal interface definition of the aperture doors on the AMS pod are firmed up during the design phase, then a final decision as to which way to proceed may be made.

6.2 Ground Calibration

As discussed in Section 6.1, the purpose of the periodic in-flight calibration is to determine the general health of the AMS system. That is, its primary purpose is to check out each sensor module and the central data acquisition portions of the system in order to determine whether ground

maintenance or recalibration is required or is necessary. The purpose of this section is not to present a detailed calibration procedure but to identify those general requirements which are relevant to the ground calibration of the AMS system.

The ground calibration provides the necessary calibration data which will be used in interpreting the optimum performance from the system. CCD based sensor systems such as this one, because of the large number of detectors in any one array and the number of arrays required (one for each spectral region), require substantially more calibration measurements to be processed than their single, double, or triple detector electro-mechanically scanned predecessors. Fortunately, the built-in data acquisition capability inherent in the AMS system, coupled with the presumably readily accessible ground-based computer processing available, make the large quantity of calibration data needed for ground calibration quite manageable.

A typical calibration setup would contain a calibrated blackbody or lamp source, an unobscured off-axis reflective collimator and a stepper motor-driven single-axis rotary table, which will sequentially illuminate each detector element in the array under computer control. These calibrations would be conducted at various ambient temperatures. The calibrated radiation source used in conjunction with the off-axis collimator would be a 1000°C black body similar to the Barnes Model 11-201T for the near and far IR and a xenon lamp for the shorter wavelengths.

Because of the large number of repetitive measurements required to calibrate the system, a computer must be utilized both to control the calibration sequence, as well as to acquire and reduce data, and output instructions and results to calibration personnel via peripherals.

Provision would be made in the sensor module design to accept a specific set of calibration commands from the computer to allow for a more efficient calibration sequence. For example, it may be desirable to reduce the number of accumulations, m, made during a test run to speed up the ground calibration process. Normally, it is dictated by the V/H rate as described in Section 4.4.1.3. In addition since the sensor modules normally output only 50° of data, it will be necessary to vary the roll angle data input in order to calibrate the sensor over a full 60°. The details of this interface would be worked out in the detailed design phase.

As in any imaging system, the key performance parameters are noise equivalent contrast for the short wavelength sensors or alternatively noise equivalent temperature for the longer wavelength sensors, dynamic range and resolution.

Calibration would be carried out over the entire operational temperature range (-35°C to 44°C) using the temperature monitor outputs from each sensor module to correlate data runs. The calibration over temperature is particularly important with regard to CCD array performance as discussed in Section For each detector element in an array, the following parameters will be directly or indirectly measured:

1. Dark current levels
2. Random detector noise
3. Pattern noise
4. Responsivity
5. Signal dynamic range

During the post flight data reduction process, the data collected in-flight will be corrected for Parameters 1 and 3 above, which offset the measured data in each detector element; and fo. Parameter 4 which varies the gain of the measured data in each detector element. Parameter 2 directly affects the NE$\Delta\rho$ and the NET of the particular sensor module and Parameter 5 is measured indirectly.

In addition, the response of the sensors to the in-flight calibration source will be recorded and correlated to the primary calibration described above. This is done to aid in diagnosing gross changes in sensor performance in-flight.

7.0 LONG WAVELENGTH DETECTOR COOLING

As indicated in Section 4.1.1, the detector arrays which are sensitive in the long wavelength spectral region all require cooling to at least 77°K, with extrinsic silicon detectors requiring cooling to 25°K - 50°K. Although various refrigeration systems exist for achieving temperatures well below 77°K, e.g., Vuilleumier and Stirling, we believe these would prove to be unsatisfactory for an airborne multi-sensor module system like the AMS because of their complexity. Consequently, we have rejected further consideration of extrinsic silicon detectors for the present and have concentrated our study of detector cooling techniques to those which maintain detector temperatures at 77°K or above.

In this category are liquid nitrogen (LN_2) and thermoelectric coolers. A four-stage thermoelectric cooler will practically achieve a cold surface temperature of 220°K with its base at about 60°C. This type of cooler is the most satisfactory for the AMS application, since it requires no operational maintenance. However, the sensitivity or D* of most detectors in the 3 - 5 μm and 8 - 14 μm regions falls off rapidly above 77°K. Although the NET calculations made in Section 4.1.5 indicate that NETs less than 0.1°K may be realized at 77°K, we hesitate to attempt to extrapolate the performance to higher temperatures until better long wavelength detector data is available. Consequently, we will conservatively operate the AMS long wavelength detector arrays at 77°K.

To achieve this temperature several LN_2 cooling techniques are available: manually filled dewars, demand cryostat cooling, constant feed cryostat cooling. For the AMS application, we recommend the manually filled dewar technique. Dewars with various hold times up to 12 hours are practical depending on detector area and power dissipation. As indicated in Figure 4-12, a dewar similar to the CA IR-13 type with a hold time of 12 hours was selected. Access to the dewars for filling is provided by convenient access doors in the AMS mounting assembly, see Figure 5-1. This type of cooling approach has been time-proven to be reliable and with its long hold time should allow for operational flexibility.

The demand and constant feed cryostat systems were not recommended since their operation depends directly on the purity of the gaseous nitrogen used. Because of this and based upon our experience, this type of system is not reliable for flight applications not to mention the "plumbing" required for operation.

8.0 CONCLUSIONS

The design of the AMS system as described in this study represents a practical implementation of a state-of-the-art instrument concept that if not totally manufacturable today will certainly be in the early 1980s.

This design provides a no-moving-parts multispectral scanning capability through the exploitation of linear array charge-coupled device technology and advanced electronic signal processing techniques. It provides a system that has the following major advantages:

- 10:1 V/H Rate Capability
- 120° FOV at V/H = 0.25 rad./sec.
- 1 - 2 mrad Resolution
- High Sensitivity
- Large Dynamic Range Capability
- Geometric Fidelity
- Roll Compensation
- Modularity
- Long Life
- 24 Channel Data Acquisition Capability

These key advantages stem from the AMS's superior optical design which through its unique field flattening techniques allows wide field of view to be achieved at fast f/nos. for both the short and long wavelength regions. In addition, its electronic design allows, through its digital signal averaging technique, maximization of signal to noise performance over the entire V/H rate range.

Appendix A contains a detailed preliminary design specification for the AMS System.

9.0 REFERENCES

[1] Barbe, D. F., "Advanced Infrared Focal Plane Array Concepts," Electro-Optical Systems Design, April, 1977.

[2] Barbe, D. F., "Charge-Coupled Device and Charge-Injection Device Imaging," IEEE Journal of Solid-State Circuits, Vol. SC-11, No. 1, Feb. 1976.

[3] Barbe, D. F., "Imaging Devices Using the Charge Coupled Concept," Proc. IEEE, Vol. 63, No. 1, Jan. 1975.

[4] Bergere, L. M. et al, "Design Study for Advanced IR Focal Planes," General Electric Co. Surface-Based Electronics Products Dept., Syracuse, N.Y. 13201, Feb. 25, 1977.

[5] Burke, H. K., "Charge-Injection Imaging: Operating Techniques and Performance Characteristics," IEEE J. of Solid-State Circuits, Vol. SC-11, No. 1, p. 121, Feb. 1976.

[6] Buss, R. R. et al, "Principles of Low-Noise Signal Extraction from Photo-Diode Arrays," Reticon Corp., Sunnyvale, CA.

[7] Campana, S. B., "Techniques for Evaluating Charge Coupled Imagers," Optical Engineering, Vol. 16, No. 3, May-June 1977.

[8] Elliott, C. T. et al, "Counterdoped Extrinsic Silicon Infrared Detectors," Infrared Physics, Vol. 18, pp 65-71, 1978.

[9] Hall, J. A., "Can Solid State Imaging Devices Replace Television Camera Tubes?" Optical Engineering, Vol. 16, No. 3, p. 224, May-June 1977.

[10] Harris, L., "Filters for the Isolation of Radiant Energy," Monograph No. 2, Eppley Foundation for Research, June 1970.

[11] Hirschberg, I. & Bashe, R., "CCD Imaging Application -- A Modular Approach," Fairchild Camera & Instrument Corp., Imaging Systems Division, Syosset, N.Y.

[12] Iwasa, S., "Direct Coupling of Five-Micrometer (Hg,Cd)Te Photovoltaic Detector and a CCD Multiplexer," Optical Engineering, Vol. 16, No. 3, May-June 1977.

[13] Kim, J. C. et al, "InSb CID Infrared Imaging Devices," General Electric Company,Optoelectronic Systems Operation, Syracuse, N.Y., Oct. 1976.

[14] Kosonocky, W. F. & Sauer, D. J., "Consider CCD's for a Wide Range of Uses," Electronic Design 6, March 15, 1976.

[15] Labinger, R. L., "A Real-Time, Wide-Angle, Solid-State Reconnaissance Camera System for High-Speed, Low-Altitude Aircraft," The Perkin-Elmer Corp., Optical Technology Division, Danbury, Conn. 06810.

[16] Nelson, R. D., "Infrared Charge Transfer Devices -- The Silicon Approach," Optical Engineering, Vol. 16, No. 3, May-June 1977.

[17] Renzelman, R. F., "Study of Infrared Solid State Images Using Cha Transport Devices," Naval Postgraduate School, Monterey, CA : NTIS AD/A-005-736, Dec. 1974.

[18] Schroder, D. K., "Extrinsic Silicon Focal Plane Arrays," Westinghouse Research & Development Center, Pittsburgh, PA. 15235.

[19] Sequin, C. H. et al, "All-Solid-State Camera for the 525-Line Television Format," IEEE J. of Solid-State Circuits, Vol. SC-11, No. 1, p. 115, Feb. 1976.

[20] Sequin, C. H. & Tompsett, M. F., "Charge Transfer Devices," Academic Press, Inc., 1975.

[21] Snow, E. H. & Weckler, G. P., "Self-Scanned Charge Coupled Photodiode (CCPD) Sensor Arrays," Solid State Imaging Devices, SPIE Vol. 116, 1977.

[22] Solomon, A. L., "Parallel-Transfer-Register Charge-Coupled Imaging Devices," Fairchild Camera and Instrument Corp. Research and Development Laboratory, Palo Alto, CA 94304.

[23] Steckl, A. J. et al, "Application of Charge-Coupled Devices to Infrared Detection and Imaging," Proc. IEEE, Vol. 63, No. 1, Jan. 1975.

[24] Vogt, S. S. et al, "Self-Scanned Photodiode Array: High Performance Operation in High Dispersion Astronomical Spectrophotometry," Applied Optics, Vol. 17, No. 4, 15 Feb. 1978.

[25] Wolfe, W. L., "Optical Components," Chapter 7 of "Handbook of Military Infrared Technology," ONR, 1965.

APPENDIX A

PRELIMINARY DESIGN SPECIFICATION FOR AN ADVANCED MULTISPECTRAL SCANNER

1.0 SCOPE

This is a preliminary design specification for an advanced multispectral scanner designed for use on an aircraft for remote sensing purposes. It measures and collects data in a wide field of view, over a range of spectral regions extending from 0.4μm through 14μm, using an electronic scanning technique. One sensor module is required for each 60° spectral region being monitored. All data collected in-flight is stored on magnetic tape for subsequent data reduction purposes.

2.0 APPLICABLE DOCUMENTS

The AMS will be designed to meet the construction, reliability, and quality assurance standards outlined in appropriate NASA and MIL type documents which will be defined and established prior to entering the design phase.

3.0 GENERAL CHARACTERISTICS

3.1 Scanning Mechanism

The AMS uses a pushbroom scanning technique in which a linear array of detector elements is oriented at right angles to the aircraft's line of flight. The detector array is located in the focal plane of an optical system and the ground below is imaged upon the detector array. As the aircraft moves, side by side areas on the ground are scanned in the cross track direction by electronically scanning the array. As a consequence of such an arrangement, all areas on the ground are viewed for the full V/H rate dependent dwell time. See Table 3.1.

3.2 Spectral Selection and Field of View

The AMS uses multiple sensor modules to achieve multi-band spectral coverage over the region from 0.4 μm through 14 μm. That is, one sensor module is required per spectral band. Spectral selection is realized through the use of an interference type filter located in each sensor module.

Each sensor module covers a nominal 60° field of view. Two identical modules would then be required to cover 120°. See Table 3.1.

3.3 Roll Compensation

The AMS data output is roll compensated over ±50° with respect to Nadir, assuming two modules are used per spectral region. This arrangement provides for up to ±8.7° of aircraft roll and is done entirely electronically.

3.4 Detectors

The AMS uses linear detector arrays to achieve its performance. See Table 3-1. In the short wavelength region, a 1024 element CCD linear array is utilized. Each element of the array is 13 μm by 13 μm on 13 μm centers. The array required no cooling.

In the long wavelength region a 512 element hybrid CCD linear array is utilized. In Sb is used for the detector elements in the 3 - 5 μm region and correspondingly Pb Sn Te or Hg Cd Te (PV) in the 8 - 14 μm region. Each element of the array is 100 μm by 100 μm on 100 μm centers. Performance is specified in Table 3-1. Detector cooling is required and supplied via a manually filled, 12 hour capacity dewar.

3.5 Optics

The AMS uses two types of optical designs to achieve its performance: one design is for the short wavelength sensors and the other for the long wavelength sensors. Both designs provide a nominal 60° field of view at a fast f/no. Table 3-2 defines the opto-mechanical parameters for these two designs.

The short wavelength optic is basically reflective and uses a specially designed fiber optic field flattener to interface the CCD array to the optic. It also utilizes a refractive corrector shell to minimize spherical aberration. This design provides an f/0.8 optical system.

The long wavelength optic is also reflective and uses a reflective field flattener approach. This design provides an f/1.5 optical system.

3.6 Electronics

The AMS electronics uses a combination of advanced but presently available analog video and digital signal processing and control techniques. LSI is used as much as possible; depending upon speed considerations either discrete devices or microprocessors are employed.

The AMS electronics are designed to perform the least amount of data processing in-flight, leaving this function to ground based facilities. It does, however, acquire data for as many as 24 sensor modules, formatting and preprocessing the data so that it is suitable for tape recording on its system recorder.

Roll compensation, dynamic range gain changing, background subtraction, calibration sequences, and built-in test sequences are among the processes which are sensed and controlled under microprocessor control. V/H rate changes are also accounted for in the electronics.

Operation of the system does not require all sensor modules to be operative or present. But the design of each post electronics module is identical to all others in the same wavelength region.

Table 3-3 identifies the salient performance parameters and characteristics of each electronic subsystem. See Table 3-4 for power requirements.

3.7 Calibration

The AMS system provides for an in-flight calibration to be performed. The primary purpose of this calibration is to serve as a transfer standard. The data reduction process performed on the ground compares the in-flight calibration data to that taken on the ground under similar conditions. If a fault is identified or calibration is recommended, then a full calibration is performed on the ground using sources, etc. that are traceable to NBS.

3.8 Environmental Considerations

The AMS is designed to operate in an operational aircraft environment similar to that experienced on a four engine prop-jet at altitudes up to 60,000 feet.

The AMS will survive storage and non-operational temperature extremes from -30°F to 150°F. The AMS will perform in spec from -22°F to 110°F.

The AMS will not be damaged by humidity in the range from 0 to 100%. However, optical performance in certain spectral bands will be affected by condensation of water on the optics. Provision is made in the sensor module design to prevent this condensation from forming by heating the elements so affected.

The AMS will survive and operate in spec when shock and vibration levels are encountered similar to those experienced in a four engine prop-jet aircraft.

3.9 Mechanical

The AMS is designed for easy installation in an aircraft utilizing standard interfaces and power. Table 3-4 lists a breakdown of weight, volume and power requirements for the AMS system.

The AMS is designed to be modular, i.e., the system may be expanded from 1 to 12 120° FOV spectral bands by simply adding modules. It is designed to be easy to install, repair and maintain. Covers are provided to protect the optical elements during landings and take-offs.

TABLE 3-1. AMS SYSTEM PARAMETERS/SENSOR MODULE

Aircraft V/H Rate	0.025 r/s to 0.25 r/s
Optical Resolution	
Short Wavelength	1 mr
Long Wavelength	2 mr
Dwell Time/Gnd. Elem.	
Short Wavelength	4 ms - 40 ms
Long Wavelength	8 ms - 80 ms
Field of View (Uncompensated)	60°
Roll Compensation	8.7°
No. of Elements/Array	
Short Wavelength	1024
Long Wavelength	512
Spectral Region of Operation	
Short Wavelength	0.4μm - 1.0μm
Long Wavelength	1.8μm - 14μm
Performance	
Short Wavelength (NE$\Delta\rho$)	3.5% at λ_c = 0.4μm
	0.3% at λ_c = 0.8μm
Long Wavelength (NET)	1°K 3 - 5μm
	1°K 8 - 14μm

TABLE 3-2

OPTO-MECHANICAL CHARACTERISTICS OF SELECTED
SINGLE WAVELENGTH MULTISPECTRAL SCANNER DESIGN

Characteristics	Short Wavelength Sensor Module	Long Wavelength Sensor Module
Spectral Coverage	0.4 to 1 μm	1 μ to 14 μm
No. of Spectral Bands per Sensor	1	1
Means of Spectral Sorting	Interference Filter	Interference Filter
Field of View Width per Sensor	60°	60°
Max. Blur Circle Diameter	1 milliradian	2 milliradians
T/	1.5	2.2
Equivalent Focal Length	13.3 mm	52.0 mm
CCD Detector Array	1024, 13 μm square elements	512, 0.004" square elements
Weight of Complete Assy.	1.2 lbs.	6.0 lbs.
Housing Material	Al. Aly.	Al. Aly.
Field Distortion (θ Map)	2% max.	2% max.
Dewar Hold Time	----	12 Hrs.

TABLE 3-3

ELECTRONICS: PERFORMANCE PARAMETERS AND CHARACTERISTICS

Sensor Module Electronics	Clock Interface Temperature Monitors Calibration Source
Post Electronics Module	Video and digital signal processing and control
Effective Video Signal Bandwidth	Function of V/H Rate: 12.5 Hz to 125 Hz
Video Gain Control	Function of scene dynamic range, two positions controlled by CCD integration time
Digital Processing	8 bit A/D conversion Sample Averaging Digital outputs tape recorder compatible
System Controller	Synchronizes all module processing and clocks, controls calibration sequence, calibration source, BIT, housekeeping
Tape System	24 channels of sensor data 4 channels A/C and ancillary data 17 minutes record time
Calibration Source	Capacitive discharge type; fixed voltage for short wavelength, variable for long wavelength
User Interface	Permits monitoring status of tape system and sensor modules

TABLE 3-4

AMS SYSTEM POWER, WEIGHT AND VOLUME BUDGET

I.	Sensor Module	
(a)	Power	2 watts
(b)	Weight (electronics only)	2 lbs.
(c)	Weight (short wavelength) (long wavelength)	3.2 lbs. 8.0 lbs.
(d)	Size (electronics only)	2-1/2" x 4.5" x 6"
II.	Post Electronics	
(a)	Power	58.5 watts
	(1) Data Formatting	15 watts
	(2) Dual 17 Bit Accumulator/Memory	26.5 watts
	(3) Sample & Hold + Integration Time Logic	5.25 watts
	(4) Analog Multiplexer	1 watt
	(5) CCD Timing Generator	3.25 watts
	(6) Sources and Controllers	5 watts
	(7) Assorted Interface IC's	2.5 watts
(b)	Weight	15 lbs.
(c)	Size	7.5" x 10.5" x 12"
III.	System Controller	
(a)	Power	30 watts
	(1) Electronic Control	10 watts
	(2) Motor Drives	20 watts
(b)	Weight	8 lbs.
(c)	Size	4" x 10.5" x 10"

TABLE 3-4

AMS SYSTEM POWER, WEIGHT AND VOLUME BUDGET
(Continued)

IV.	<u>System Power Supply</u>	
(a)	Power Required from Vehicle (except tape system)	2.1 kw max.
(b)	Power Output in Max. Configuration (24 channels)	1482 watts
(c)	Weight	100 lbs.
(d)	Size	12" x 12" x 24"
V.	<u>Tape System</u>	
(a)	Power (from vehicle)	490 watts maximum
(b)	Weight	107 lbs.
(c)	Size	(1) 20" x 16-1/4" x 15" (2) 10" x 10" 14"
VI.	<u>Maximum Systems Power and Weight Specification</u> (For 24 Channel System - 16 Short Wavelength Sensors 8 Long Wavelength Sensors)	
(a)	Power	2600 watts
(b)	Weight	690 lbs.

APPENDIX B

OPTICAL DESIGN ANALYSES

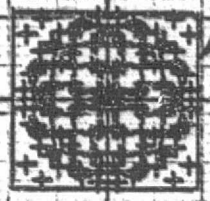

AMS SHORT WAVELENGTH SENSOR SPOT DIAGRAM FOR f/0.8 SYSTEM

CHIEF RAY HEIGHT 0.0000

FOCUS SHIFT 0.000000

1 INCH = 0.100000 MILLIRADIAN

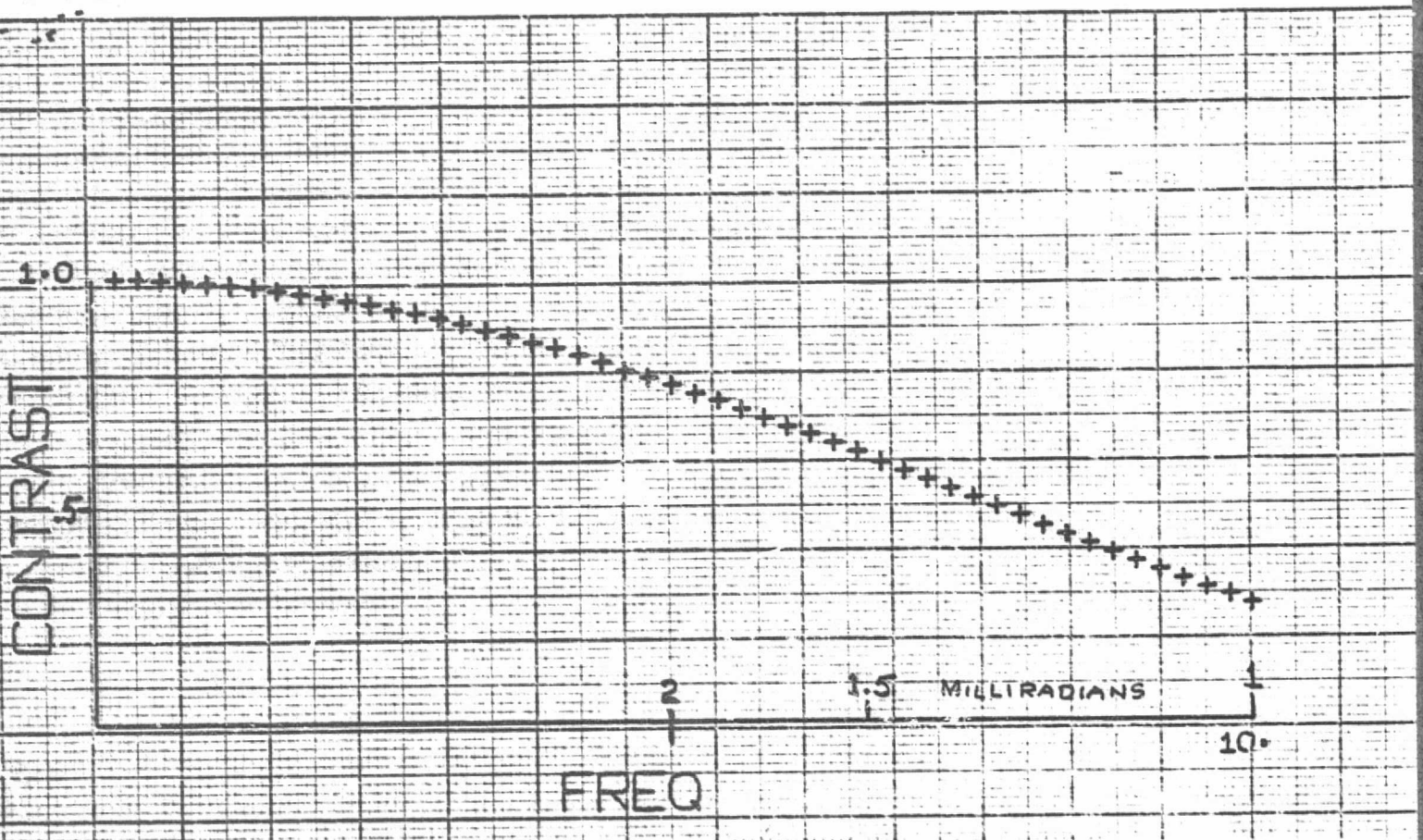

AMS SHORT WAVELENGTH SENSOR
SINE WAVE RESPONSE
AND PHASE RESPONSE FOR
f/0.8 SYSTEM

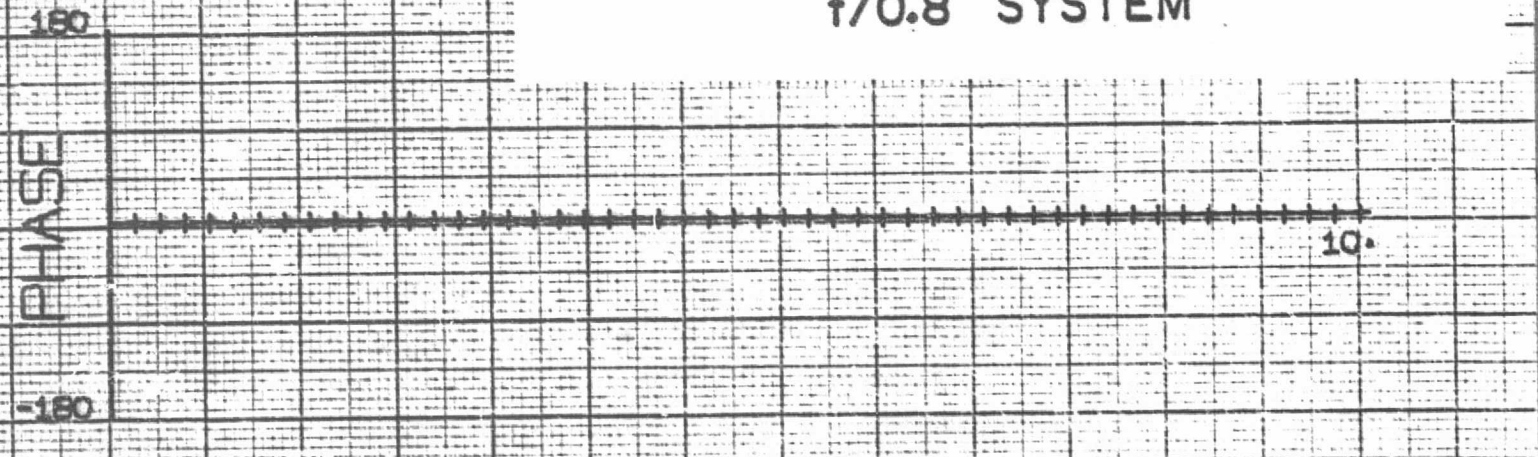

TARGET ORIENTATION	0.0
FOCUS SHIFT	0.000000
FRAC OBJECT HEIGHT	0.0000

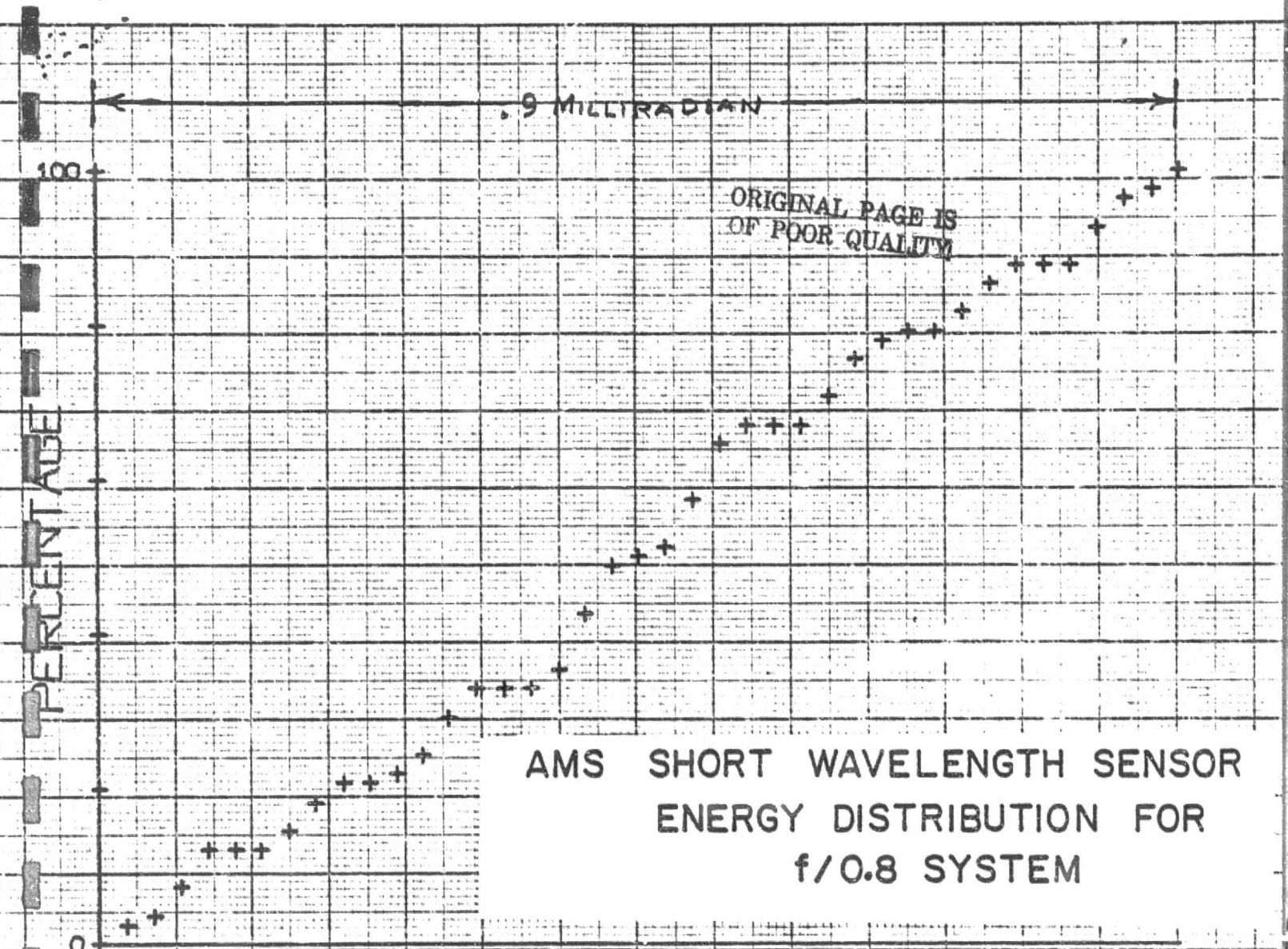

AMS SHORT WAVELENGTH SENSOR
ENERGY DISTRIBUTION FOR
f/0.8 SYSTEM

CHIEF RAY HEIGHT	0.0000
FOCUS SHIFT	0.000000
ORIENTATION ANGLE	0.0

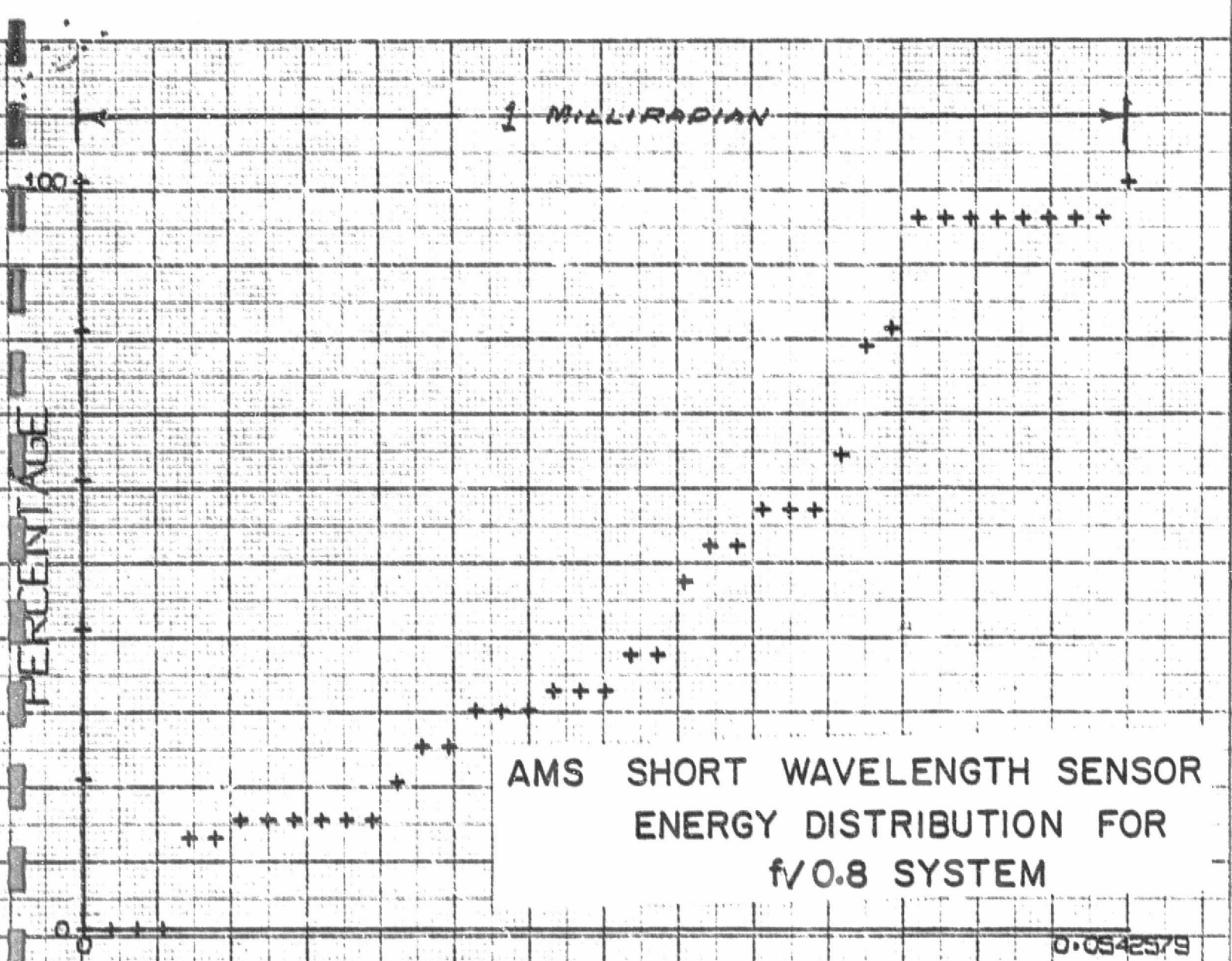

AMS SHORT WAVELENGTH SENSOR
ENERGY DISTRIBUTION FOR
f/0.8 SYSTEM

CHIEF RAY HEIGHT	0.0000
FOCUS SHIFT	0.000000
ORIGIN SHIFT	0.000000

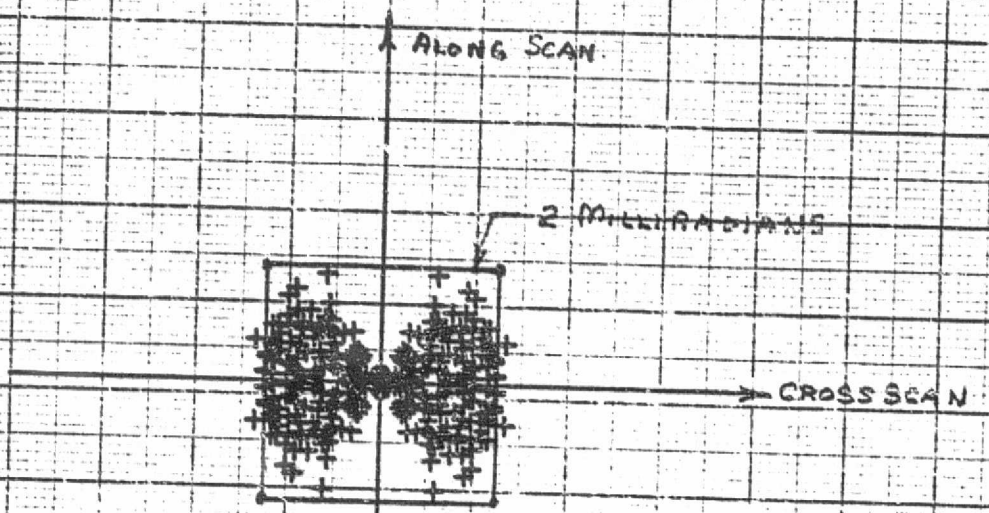

AMS LONG WAVELENGTH SENSOR
SPOT DIAGRAM FOR f/1.5 SYSTEM
0° ENTRANCE ANGLE

CHIEF RAY HEIGHT 0.0000

FOCUS SHIFT 0.500000

1 INCH = 0.200000

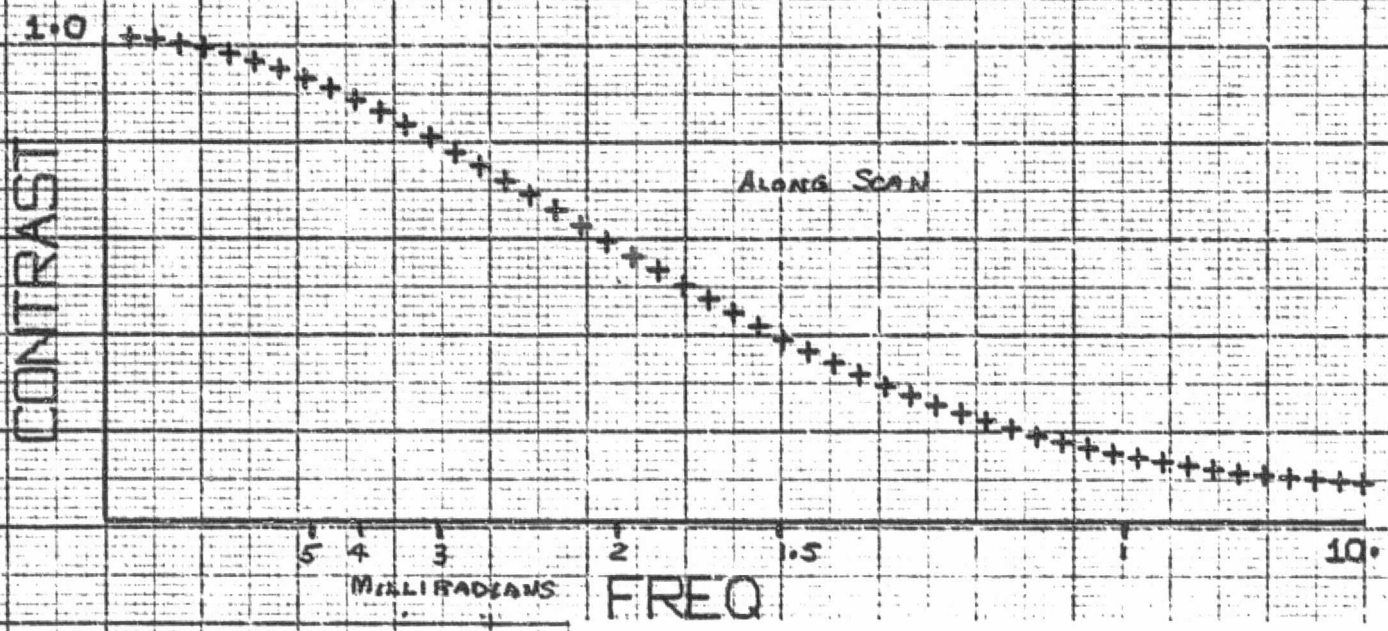

AMS LONG WAVELENGTH SENSOR
SINE WAVE RESPONSE AND PHASE
RESPONSE FOR f/1.5 SYSTEM
0° ENTRANCE ANGLE, ALONG SCAN

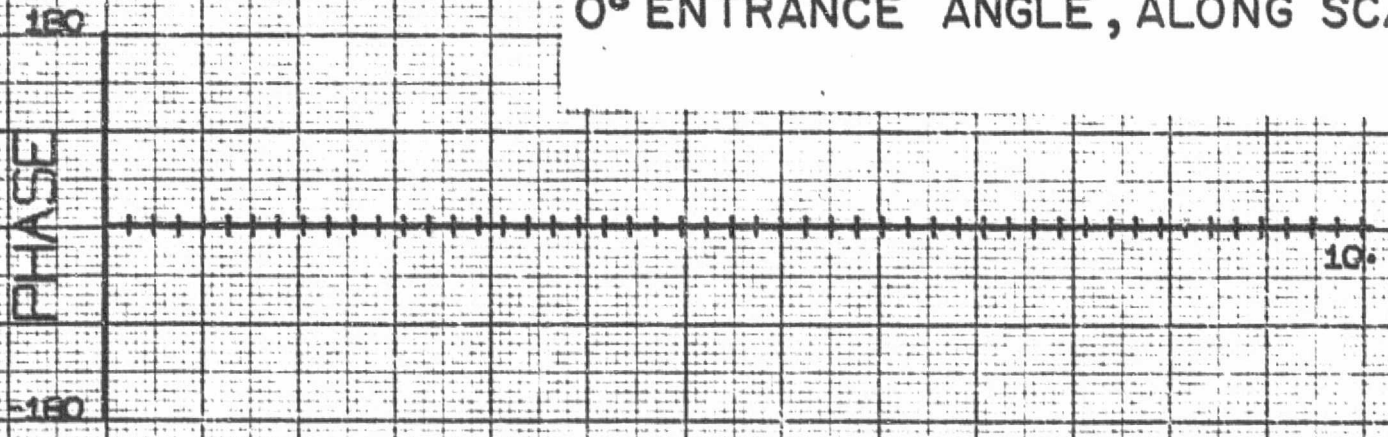

TARGET ORIENTATION	90.0
FOCUS SHIFT	0.500000
FRAC OBJECT HEIGHT	0.0000

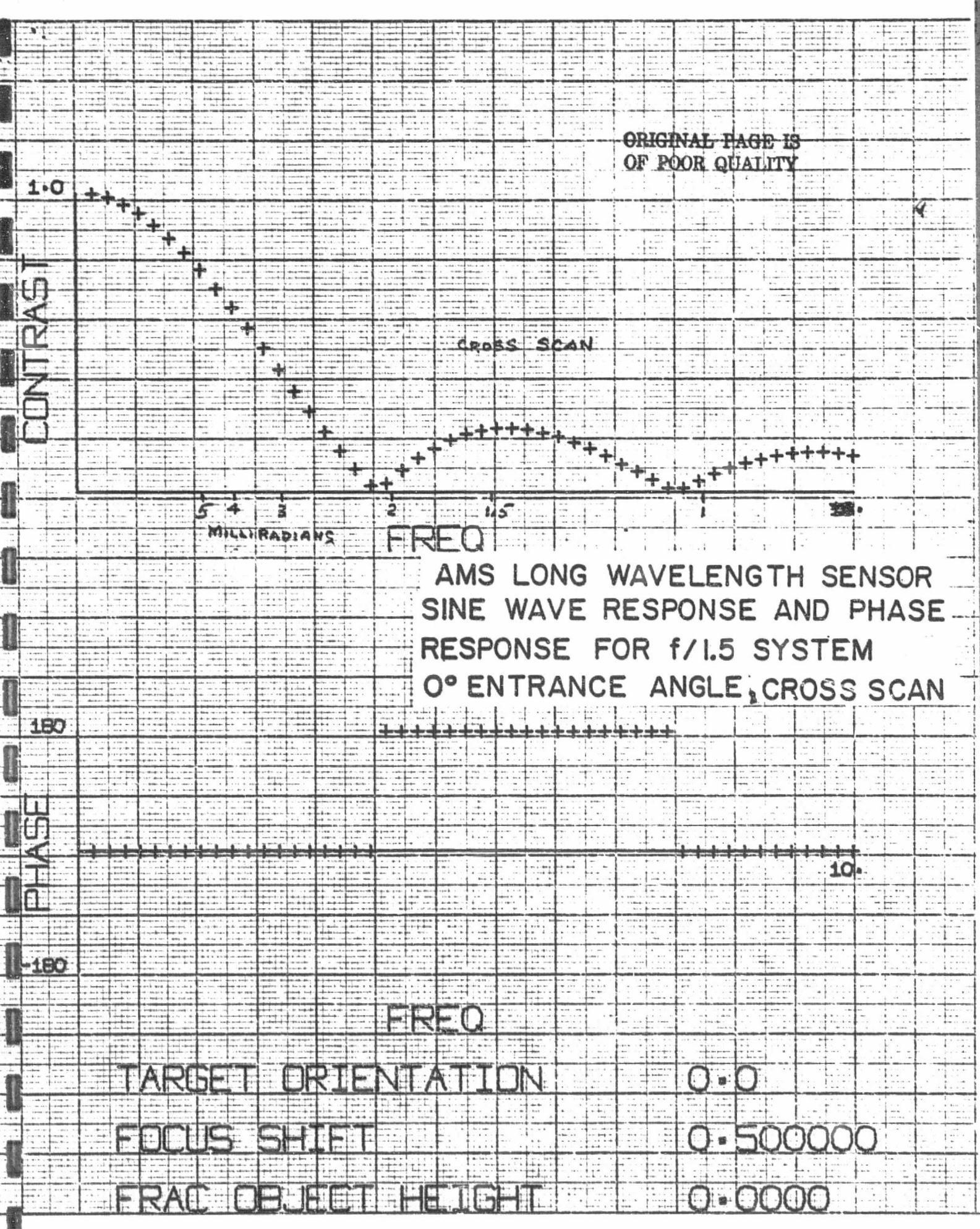

AMS LONG WAVELENGTH SENSOR
SINE WAVE RESPONSE AND PHASE
RESPONSE FOR f/1.5 SYSTEM
0° ENTRANCE ANGLE, CROSS SCAN

TARGET ORIENTATION	0.0
FOCUS SHIFT	0.500000
FRAC OBJECT HEIGHT	0.0000

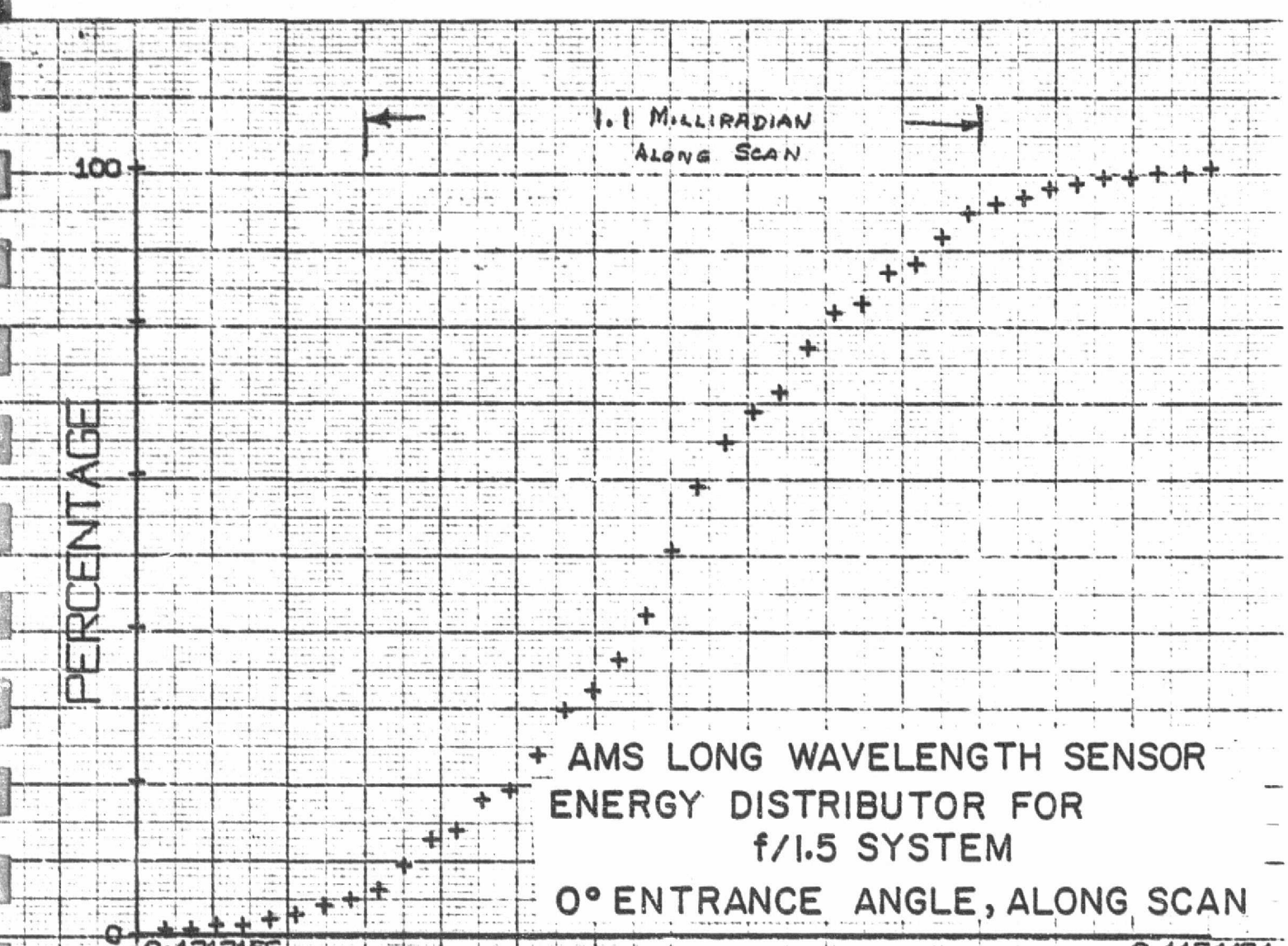

+ AMS LONG WAVELENGTH SENSOR
ENERGY DISTRIBUTOR FOR
f/1.5 SYSTEM
0° ENTRANCE ANGLE, ALONG SCAN

KNIFE POSITION

ENKY

CHIEF RAY HEIGHT	0.0000
FOCUS SHIFT	0.500000
ORIENTATION ANGLE	0.0

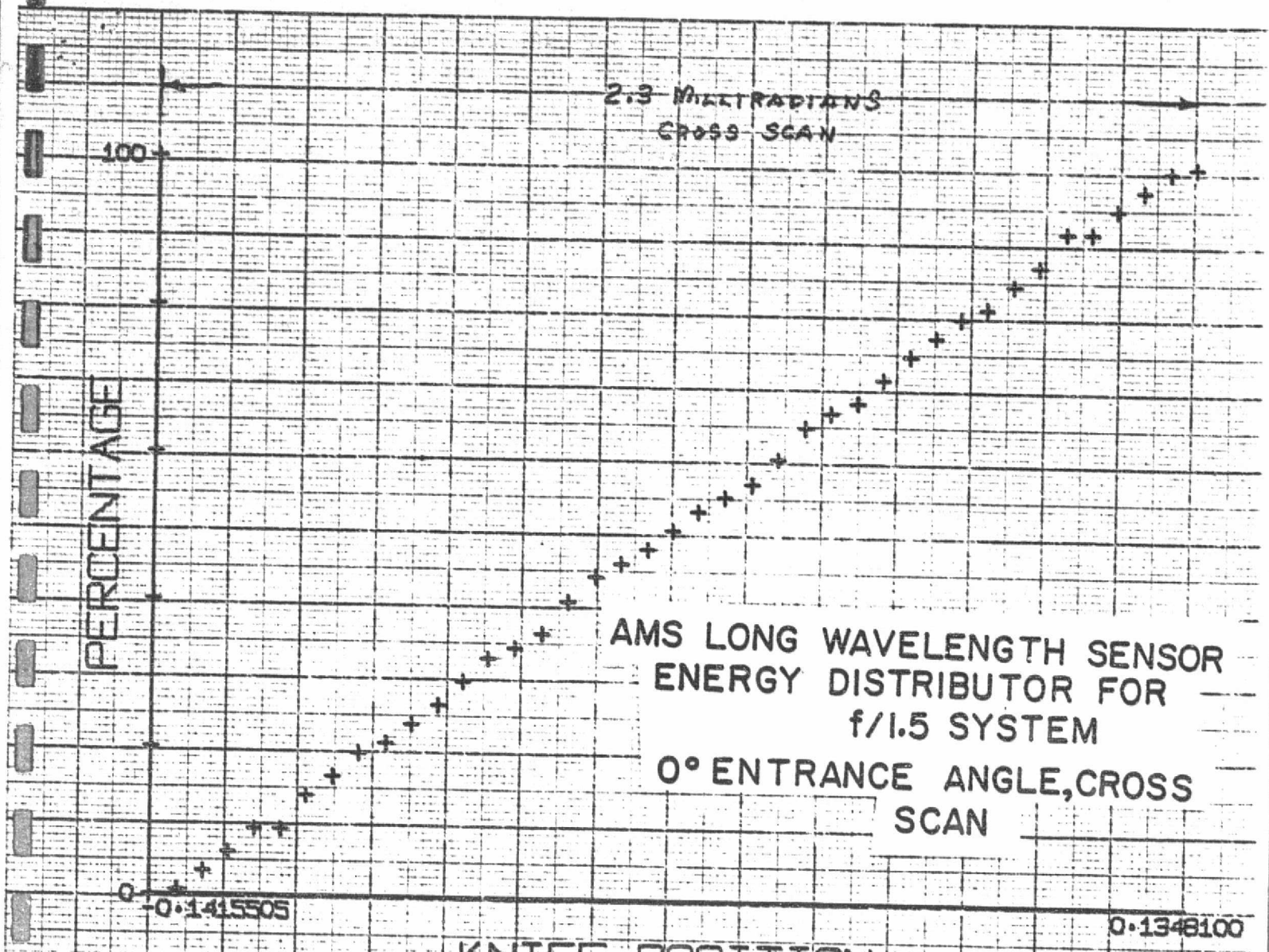

AMS LONG WAVELENGTH SENSOR
ENERGY DISTRIBUTOR FOR
f/1.5 SYSTEM
0° ENTRANCE ANGLE, CROSS
SCAN

CHIEF RAY HEIGHT	0.0000
FOCUS SHIFT	0.500000
ORIENTATION ANGLE	0.0

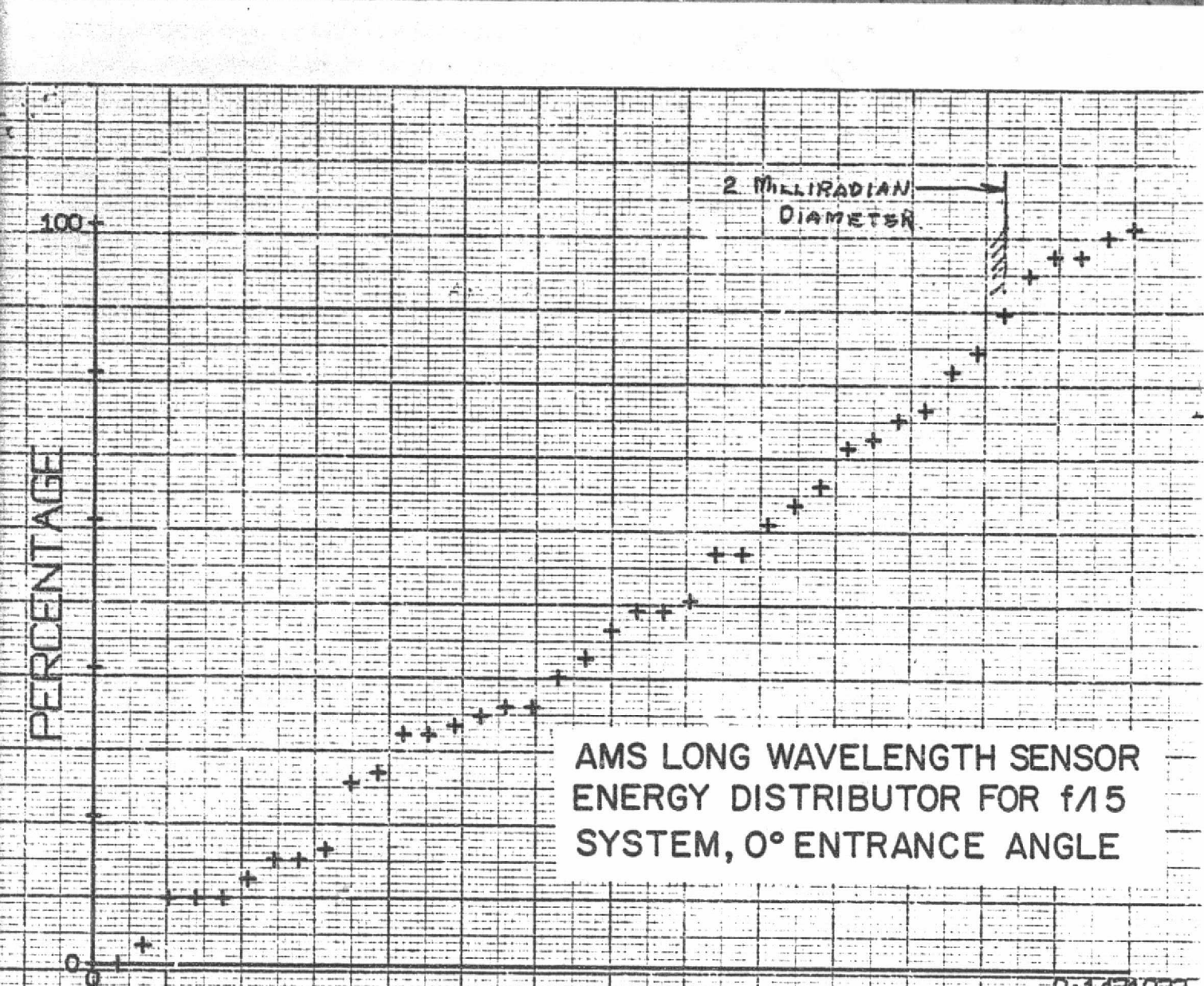

AMS LONG WAVELENGTH SENSOR ENERGY DISTRIBUTOR FOR f/15 SYSTEM, 0° ENTRANCE ANGLE

CHIEF RAY HEIGHT	0.0000
FOCUS SHIFT	0.500000
ORIGIN SHIFT	0.000000

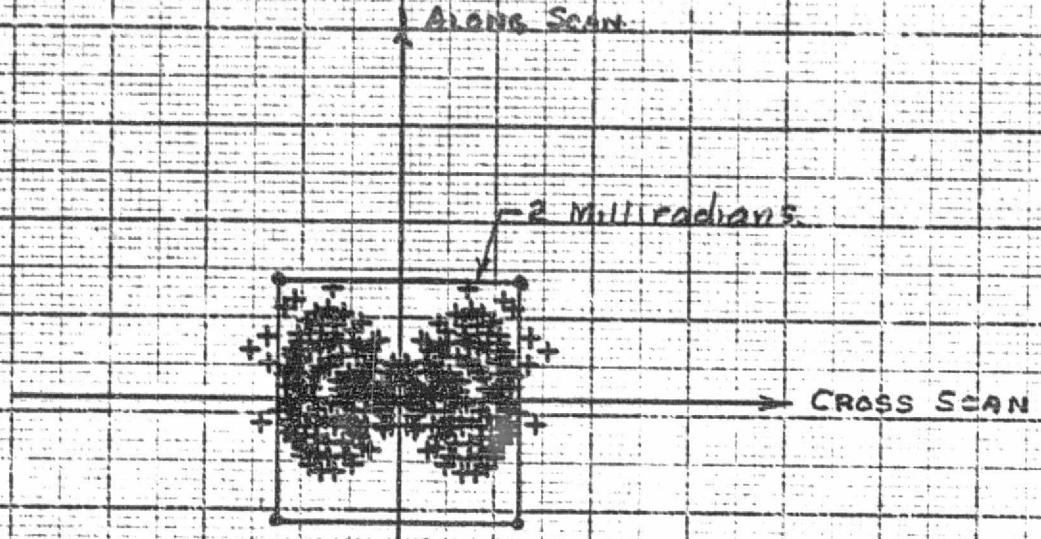

AMS LONG WAVELENGTH SENSOR
SPOT DIAGRAM FOR f/1.5 SYSTEM,
30° ENTRANCE ANGLE.

CHIEF RAY HEIGHT 34.5922

FOCUS SHIFT 0.500000

1 INCH = 0.200000

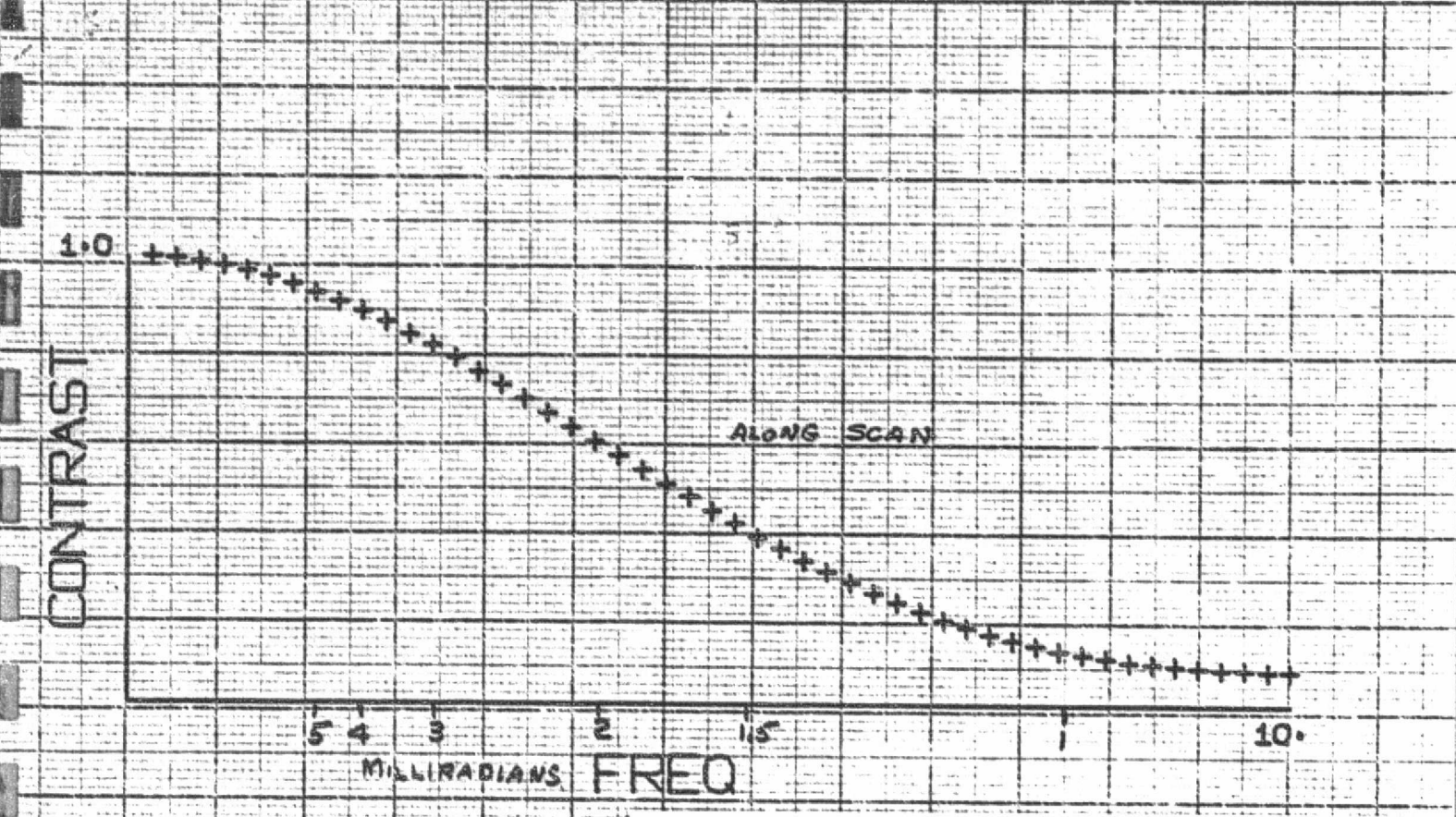

AMS LONG WAVELENGTH SENSOR SINE WAVE RESPONSE AND PHASE RESPONSE FOR f/1 5 SYSTEM , 30° ENTRANCE ANGLE, ALONG SCAN

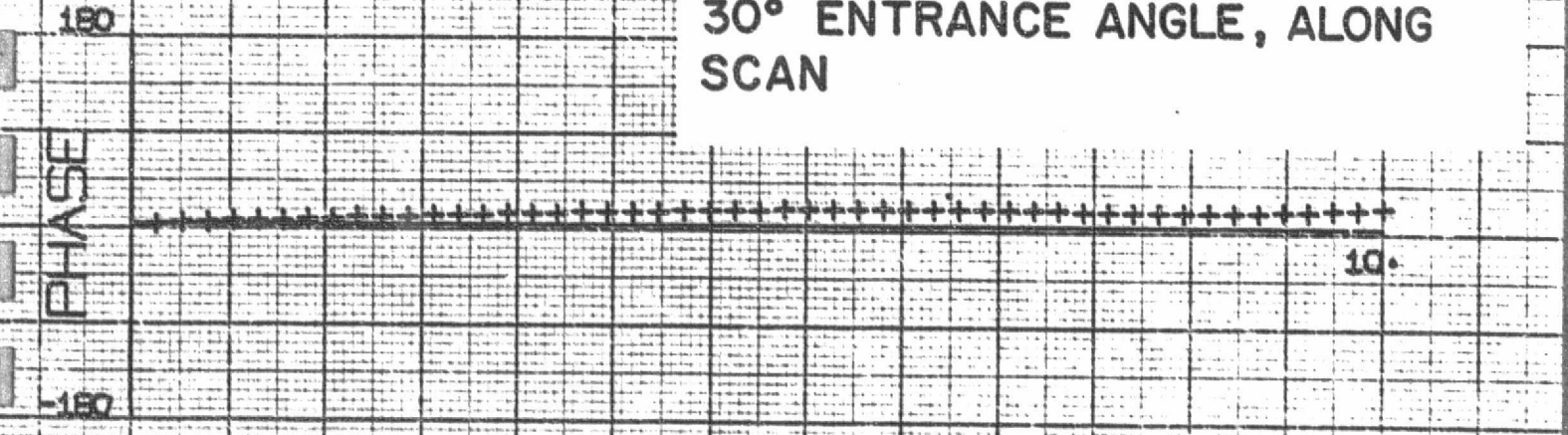

TARGET ORIENTATION	90.0
FOCUS SHIFT	0.500000
FRAC OBJECT HEIGHT	0.5000

AMS LONG WAVELENGTH SENSOR SINE WAVE RESPONSE AND PHASE RESPONSE FOR f/1 5 SYSTEM, 30° ENTRANCE ANGLE, CROSS SCAN

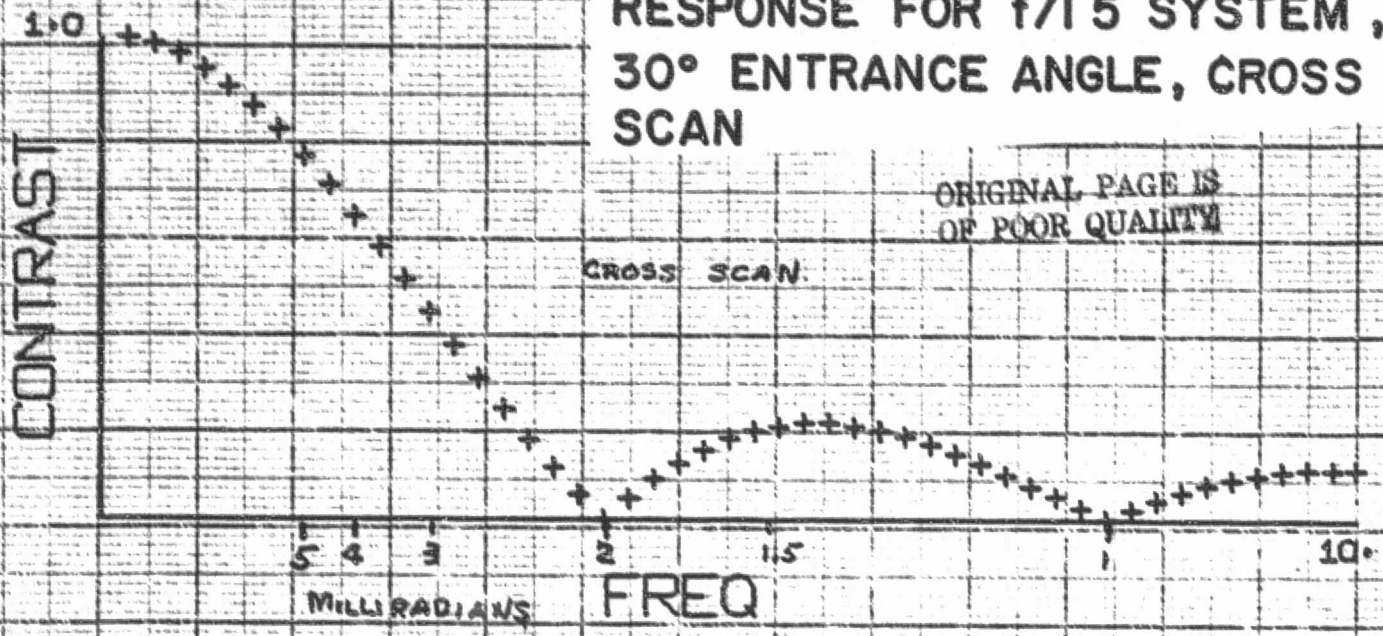

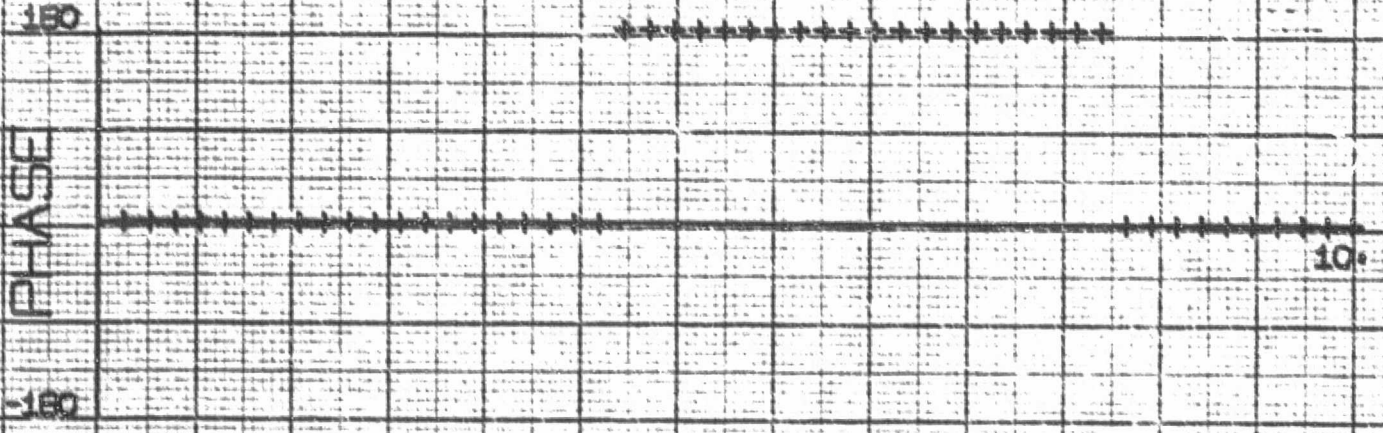

TARGET ORIENTATION	0.0
FOCUS SHIFT	0.500000
FRAC OBJECT HEIGHT	0.5000

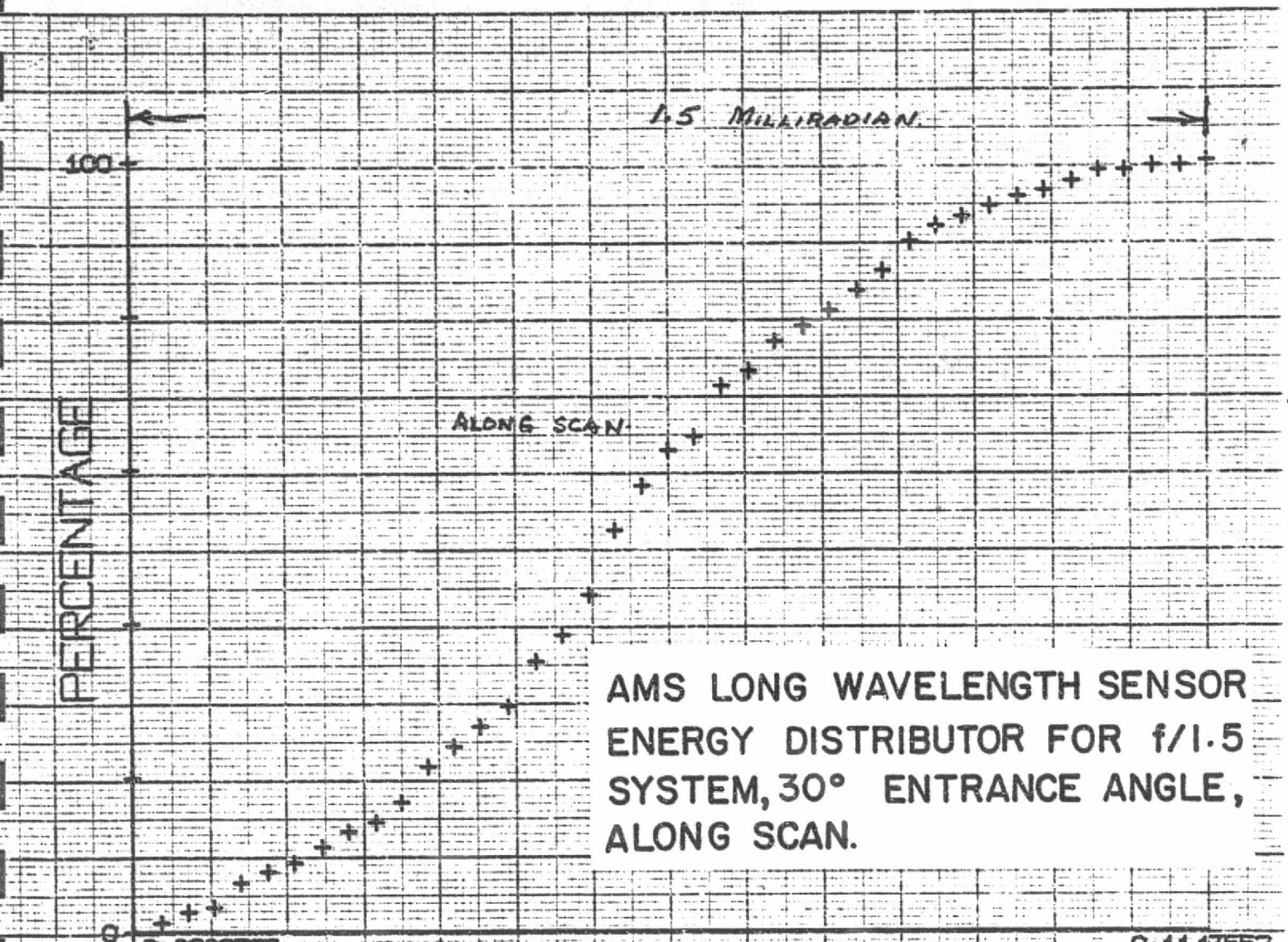

AMS LONG WAVELENGTH SENSOR ENERGY DISTRIBUTOR FOR f/1.5 SYSTEM, 30° ENTRANCE ANGLE, ALONG SCAN.

KNIFE POSITION

ENKY

CHIEF RAY HEIGHT	34.5922
FOCUS SHIFT	0.500000
ORIENTATION ANGLE	0.0

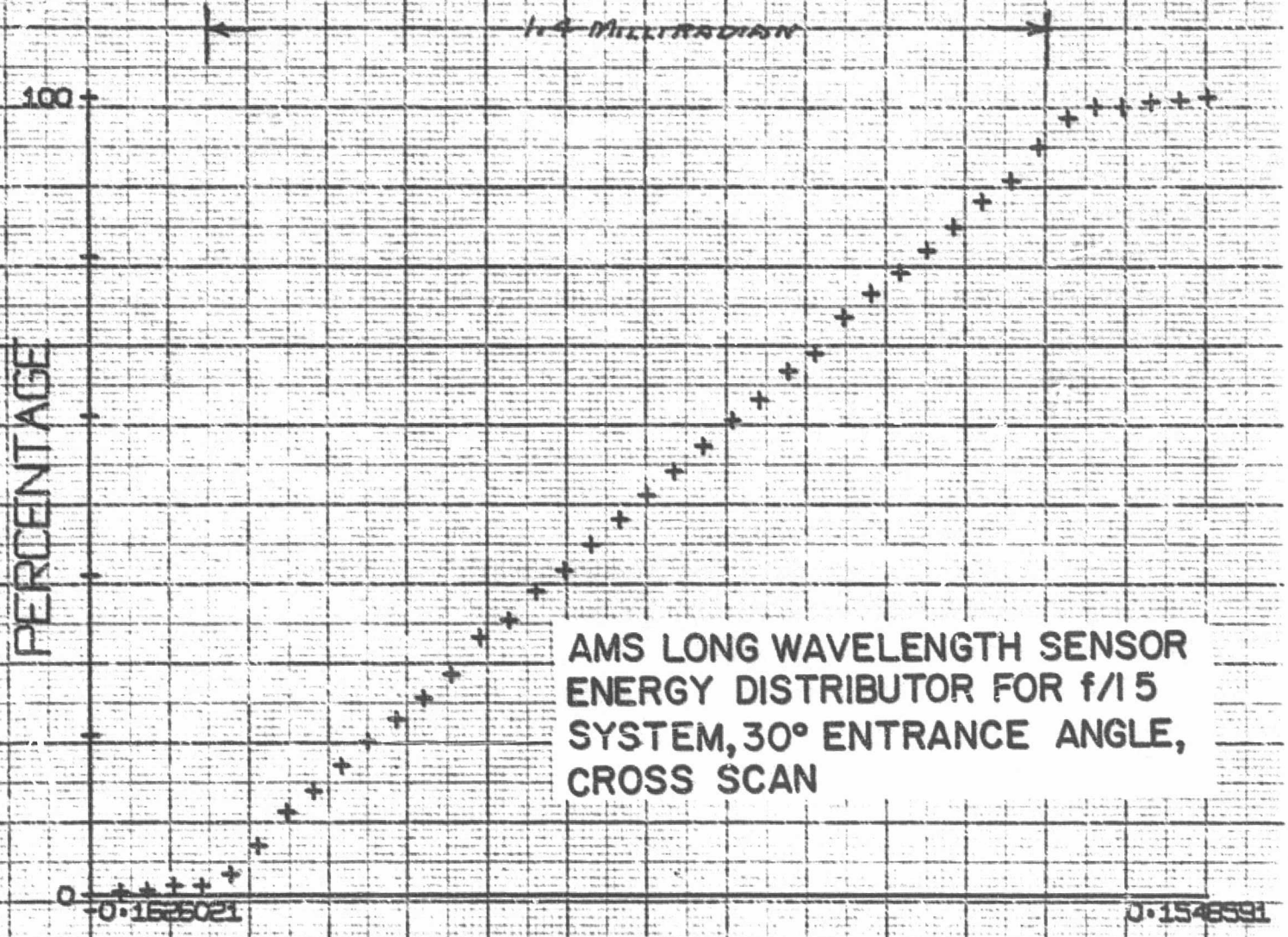

AMS LONG WAVELENGTH SENSOR ENERGY DISTRIBUTOR FOR f/15 SYSTEM, 30° ENTRANCE ANGLE, CROSS SCAN

CHIEF RAY HEIGHT	34.5922
FOCUS SHIFT	0.500000
ORIENTATION ANGLE	0.0

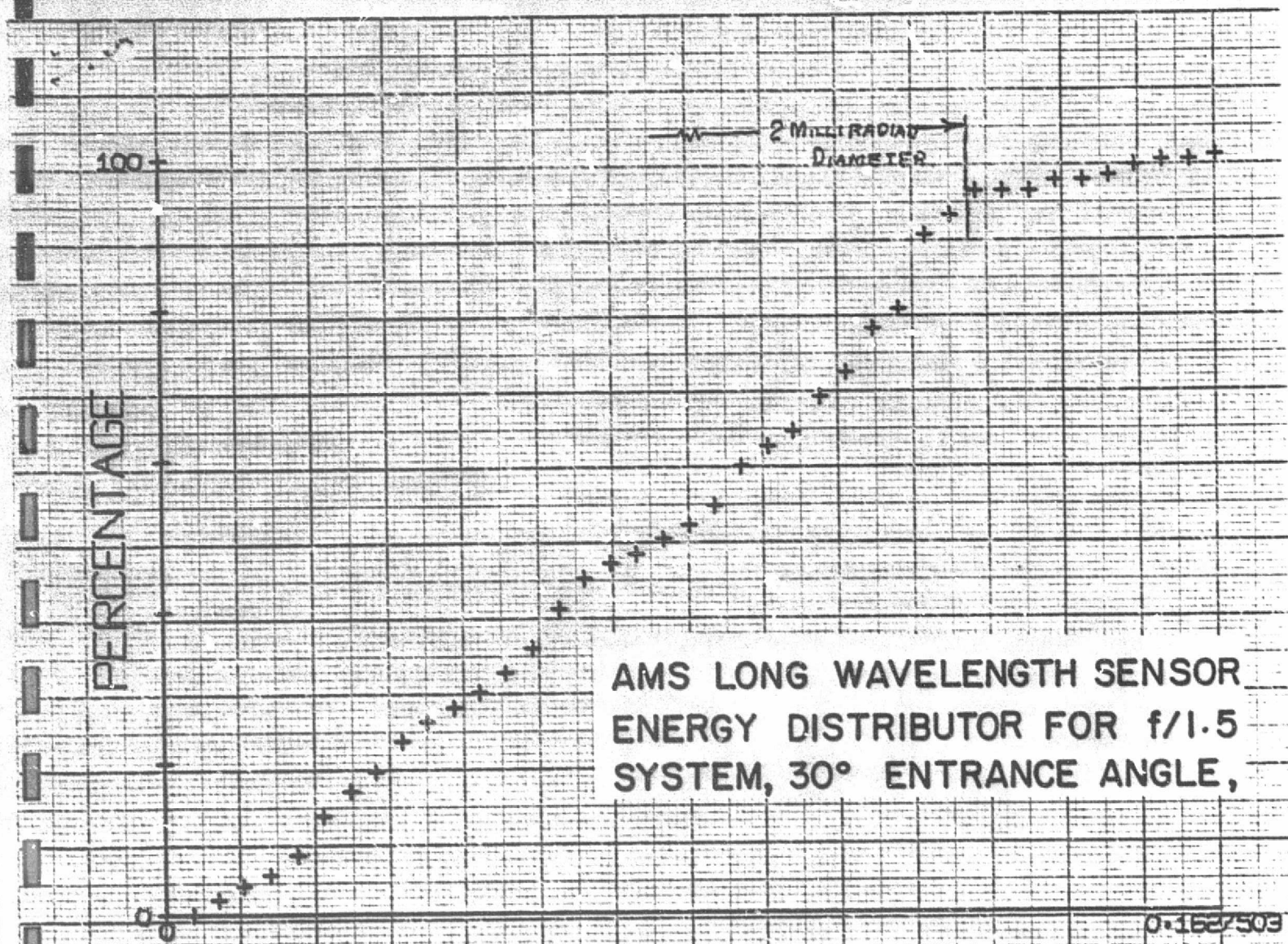

AMS LONG WAVELENGTH SENSOR
ENERGY DISTRIBUTOR FOR f/1.5
SYSTEM, 30° ENTRANCE ANGLE,

CHIEF RAY HEIGHT	34.5922
FOCUS SHIFT	0.500000
ORIGIN SHIFT	0.000000

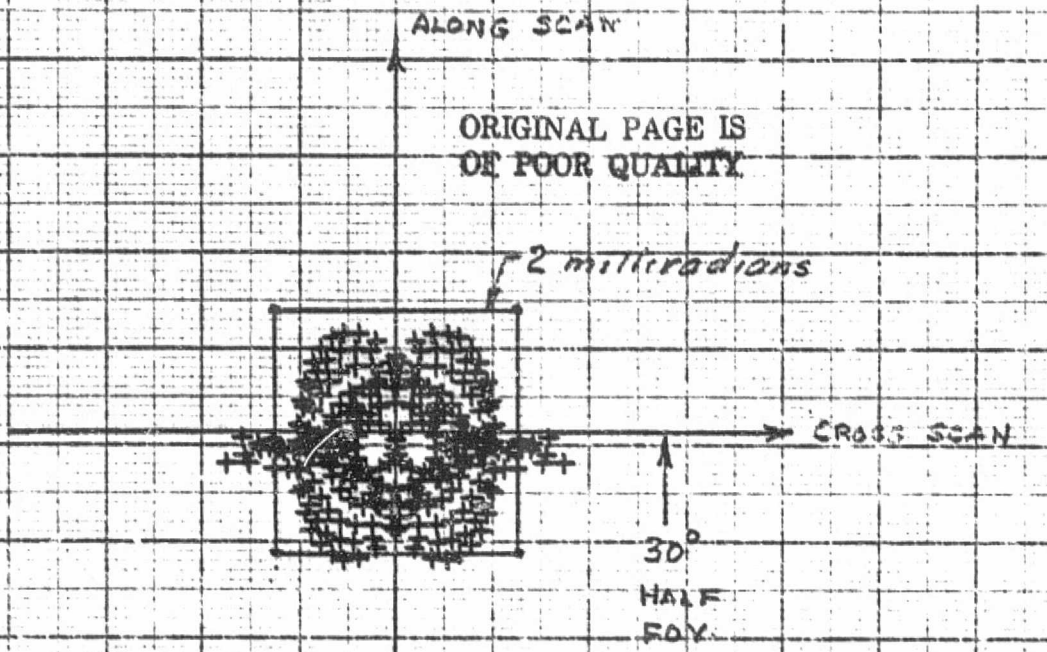

AMS LONG WAVELENGTH SENSOR
SPOT DIAGRAM FOR f/1.5 SYSTEM,
60° ENTRANCE ANGLE.

CHIEF RAY HEIGHT 63.7269

FOCUS SHIFT 0.500000

1 INCH = 0.200000

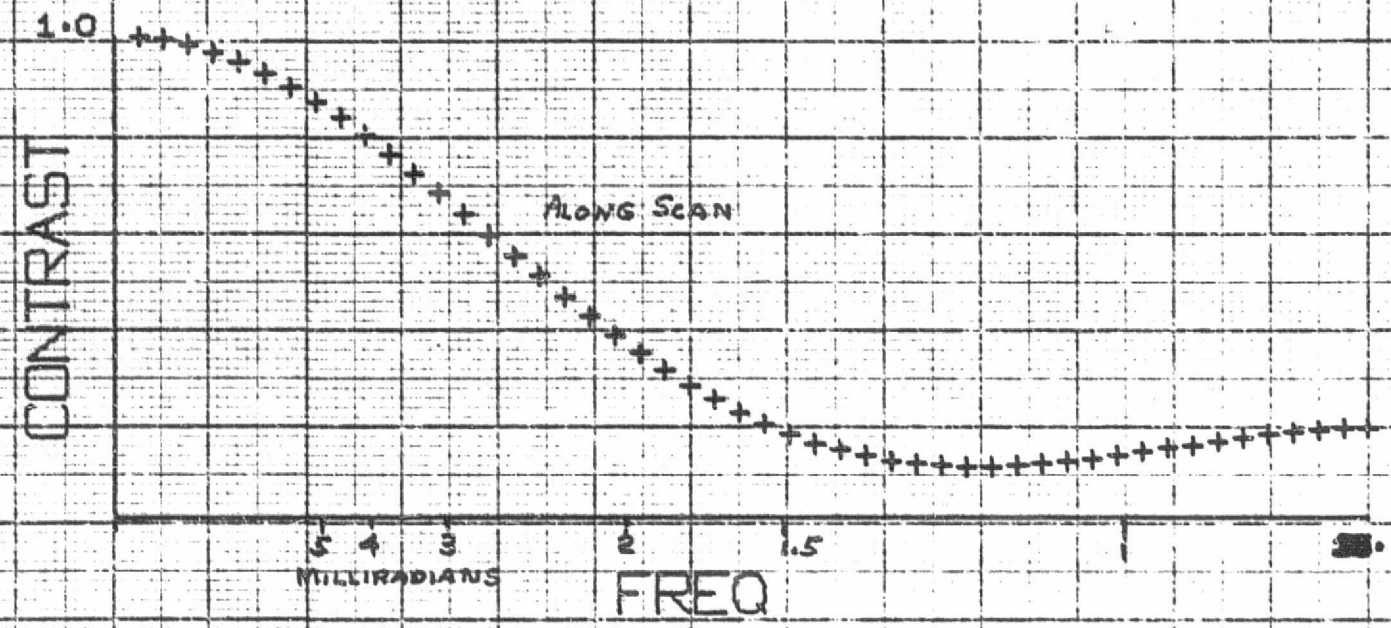

AMS LONG WAVELENGTH SENSOR SINE WAVE RESPONSE AND PHASE RESPONSE FOR f/15 SYSTEM, 60° ENTRANCE ANGLE, ALONG SCAN

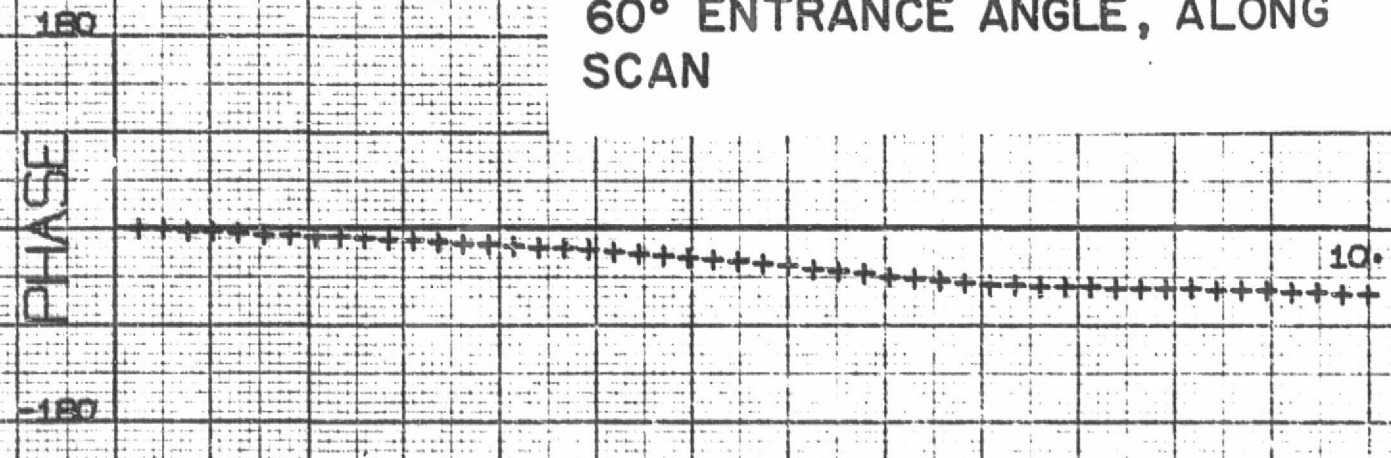

TARGET ORIENTATION	90.0
FOCUS SHIFT	0.500000
FRAC OBJECT HEIGHT	1.0000

AMS LONG WAVELENGTH SENSOR SINE WAVE RESPONSE AND PHASE RESPONSE FOR f/15 SYSTEM, 60° ENTRANCE ANGLE, CROSS SCAN

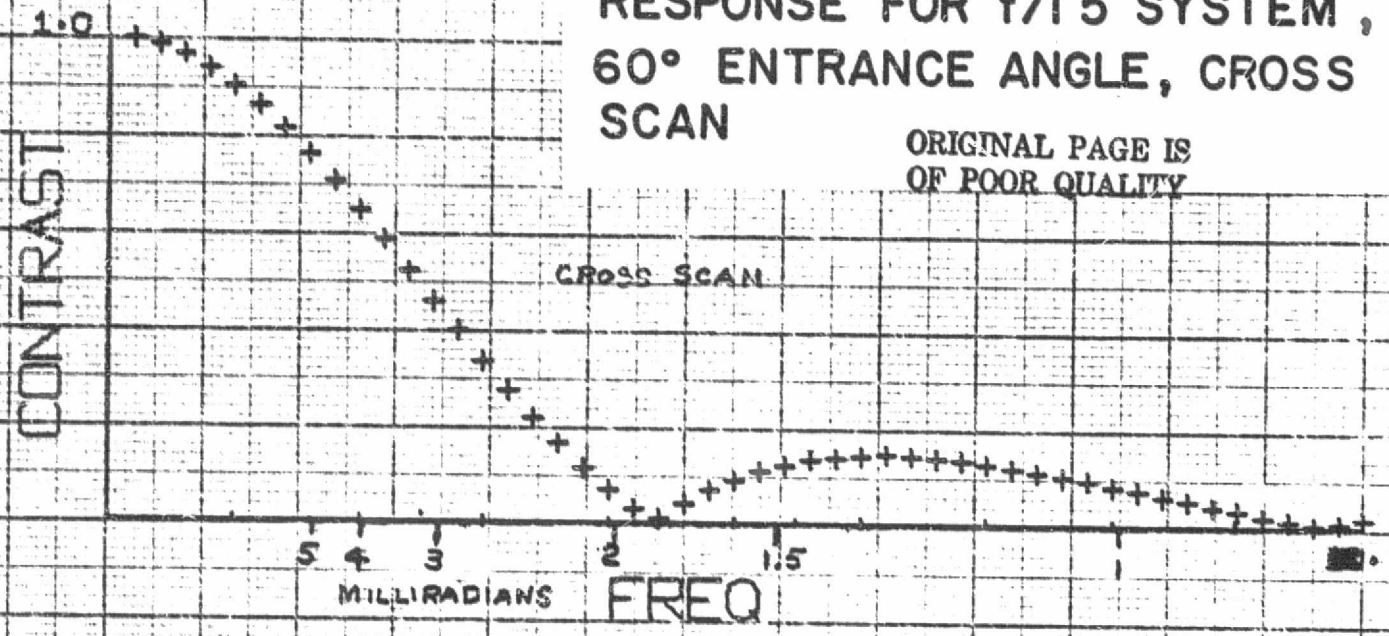

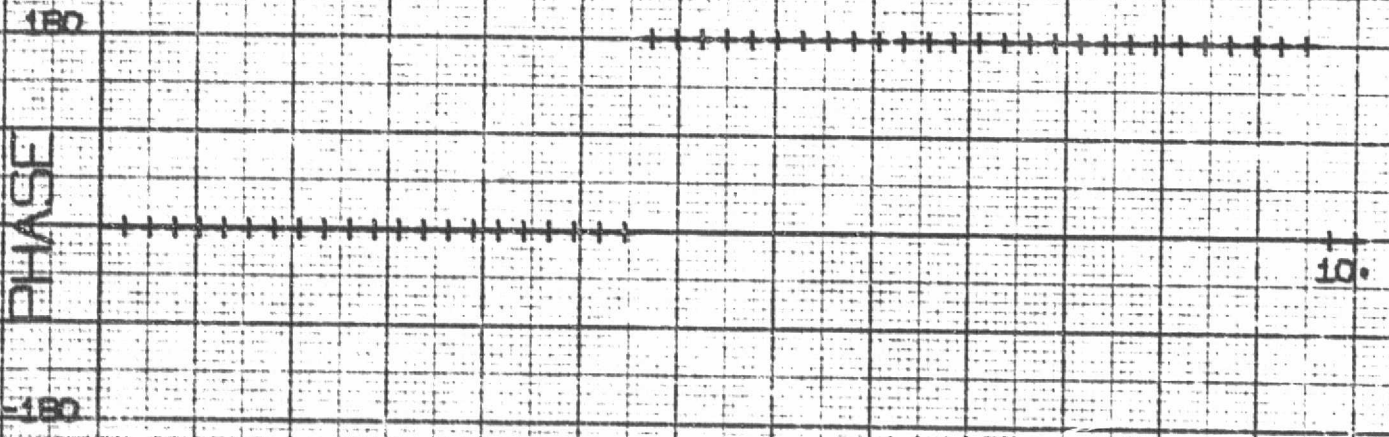

TARGET ORIENTATION	0.0
FOCUS SHIFT	0.500000
FRAC OBJECT HEIGHT	1.0000

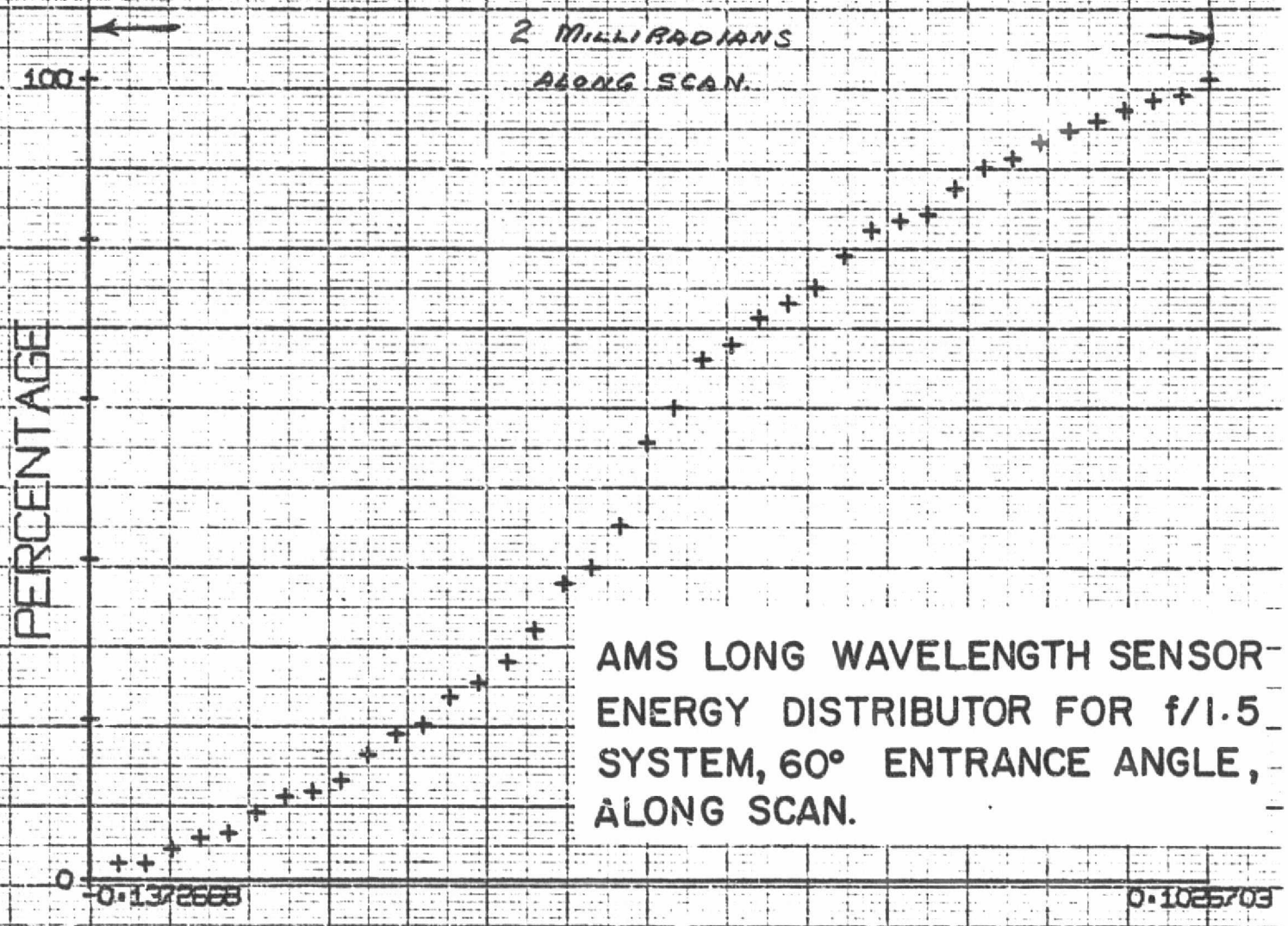

AMS LONG WAVELENGTH SENSOR-
ENERGY DISTRIBUTOR FOR f/1.5
SYSTEM, 60° ENTRANCE ANGLE,
ALONG SCAN.

KNIFE POSITION

ENKY

CHIEF RAY HEIGHT	63.7269
FOCUS SHIFT	0.500000
ORIENTATION ANGLE	0.0

ORIGINAL PAGE IS
OF POOR QUALITY

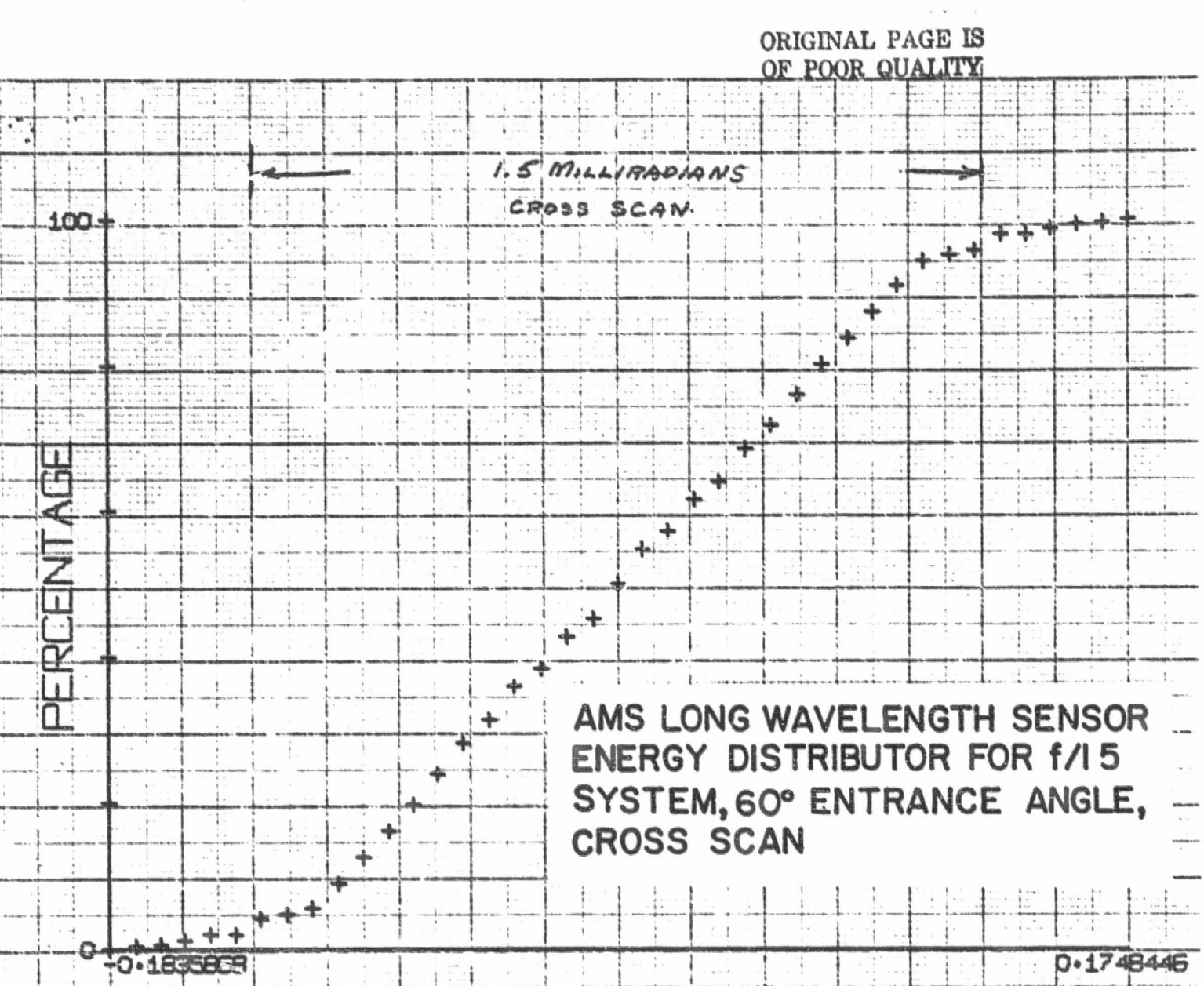

AMS LONG WAVELENGTH SENSOR ENERGY DISTRIBUTOR FOR f/15 SYSTEM, 60° ENTRANCE ANGLE, CROSS SCAN

KNIFE POSITION

ENKX

CHIEF RAY HEIGHT	63.7269
FOCUS SHIFT	0.500000
ORIENTATION ANGLE	0.0

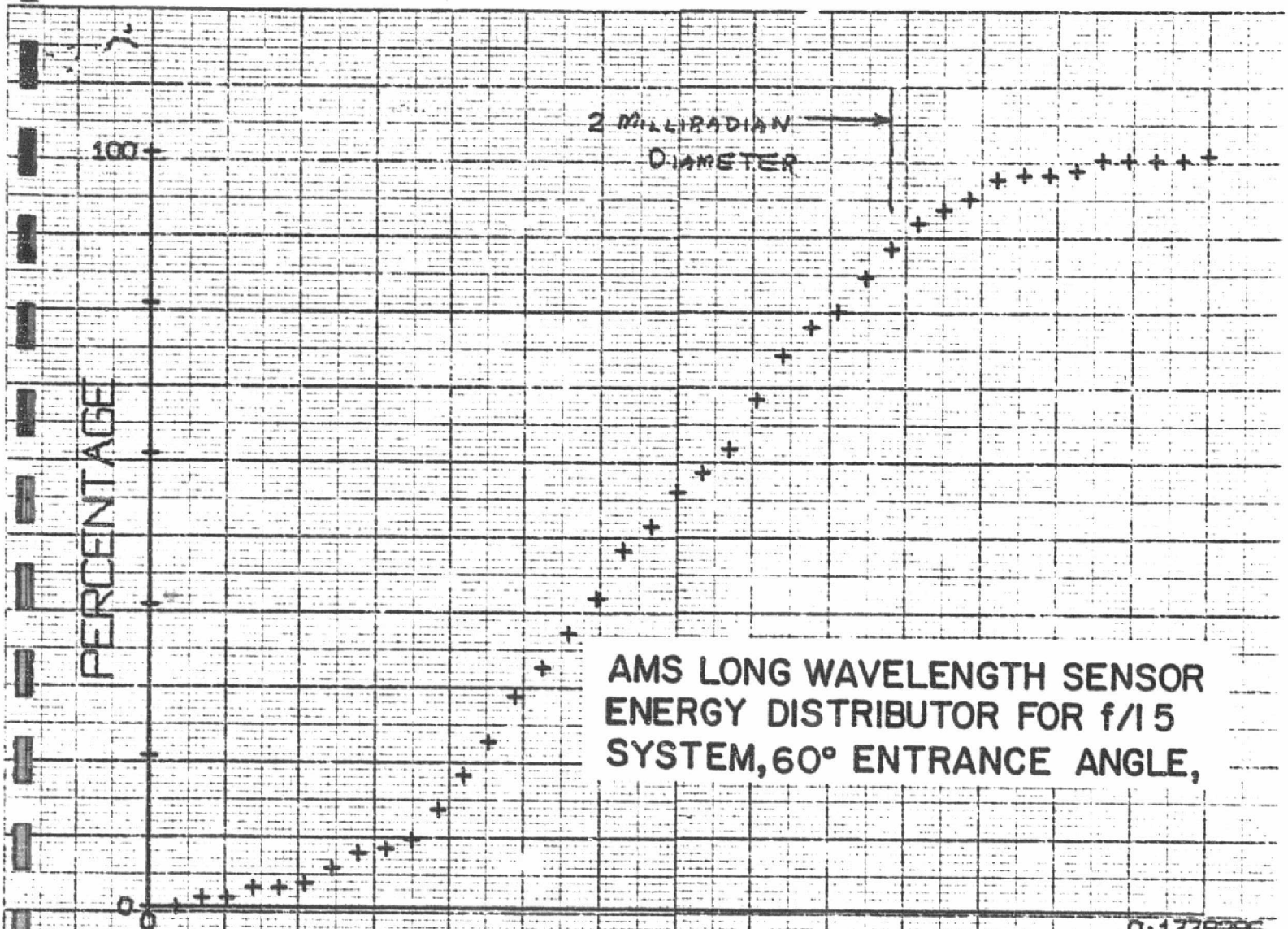

AMS LONG WAVELENGTH SENSOR
ENERGY DISTRIBUTOR FOR f/15
SYSTEM, 60° ENTRANCE ANGLE,

CHIEF RAY HEIGHT	63.7269
FOCUS SHIFT	0.500000
ORIGIN SHIFT	0.000000

APPENDIX C

SUBSYSTEM AND COMPONENT DATA

Galileo Electro-Optics Corp. Galileo Park, Sturbridge, Massachusetts 01518, (617) 347-9191

May 23, 1978

Mr. David Zink
Barnes Engineering Co.
30 Commerce Road
Stamford, Connecticut 06904

Subject: CCD Detector Array Application

Reference: Conversations with Mr. John Smith, Production Engineer for Galileo

Dear Mr. Zink:

Let me first apologize for Galileo and for Mr. Richard LeDuc of Sturgeon Company for not responding sooner with the information you had requested. By no means is this an everyday occurence but, as in most businesses, a breakdown in communications does come about once in a while. Let me assure you, Mr. Zink, this will not happen again.

Now, your CCR application of mating a 1,000 element fiber optic bundle, per copy of your sketched attached, to a CCD which measures 13 microns x 13 microns x 13 microns center is very feasible, per our production engineer, based on the information supplied. We would, however, require a more detailed set of specifications, and to get this project off the ground, would require approximately $25,000 to $45,000 in non-recurring engineering charges.

Again, I apologize for the delay in getting this information to you. I would also like to extend to you any and all assistance from both the Galileo marketing and engineering staff. Feel free to contact us for any reason.

Speaking for John Smith and myself, we look forward to working with you on this project.

Sincerely,

Konrad A. Lisi
Sales Engineer

KAL:dk

cc: C. DeLuca
J. Smith
L. Thompson
R. LeDuc

BARNES ENG

To: J. Smith
Galileo

From: D Zink
203-348-5381

< 3.0 mm

B

B

SECTION A-A

NOTE: FIBER ENDS MUST BE NEAR NORMAL TO SPHERICAL FOCAL SURFACE

60°

A

25 mm.

1.6 cm

1.6 cm

LESS

7 μm

CCD

< CCD DETECTOR ARRAY

16 x 16 μm CCD ELEMENT (x 1000)

FIBERS

POSSIBLE CONFIGURATION (BETTER FIBER PACKING DESIRABLE)

1 μm

etc

7 μm

etc

SECTION B-B

To: J. Smith
Galileo
from: D Zink
203-348-5381

SECTION A-A

NOTE: FIBER ENDS MUST BE
[illegible]

1.1 cm RADIUS

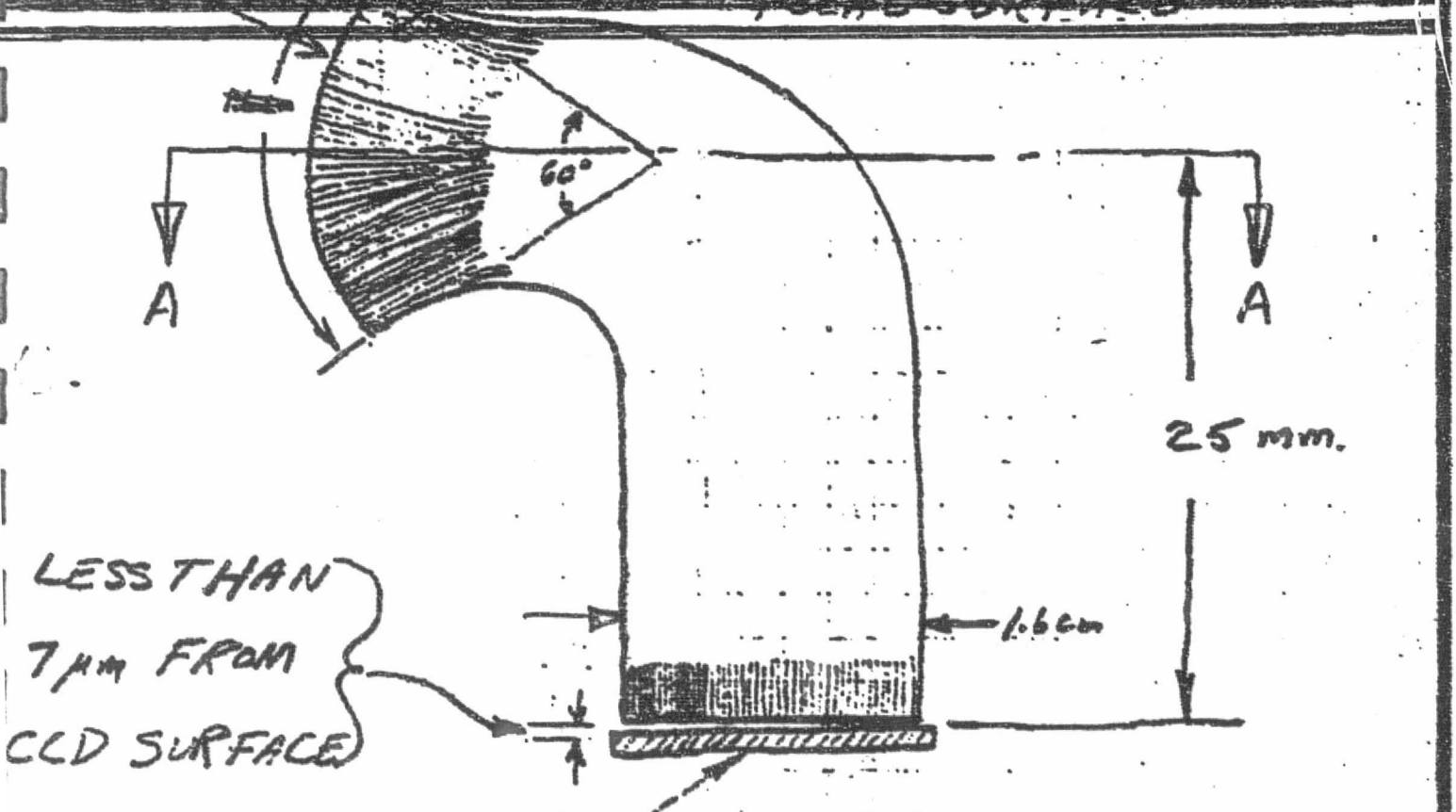

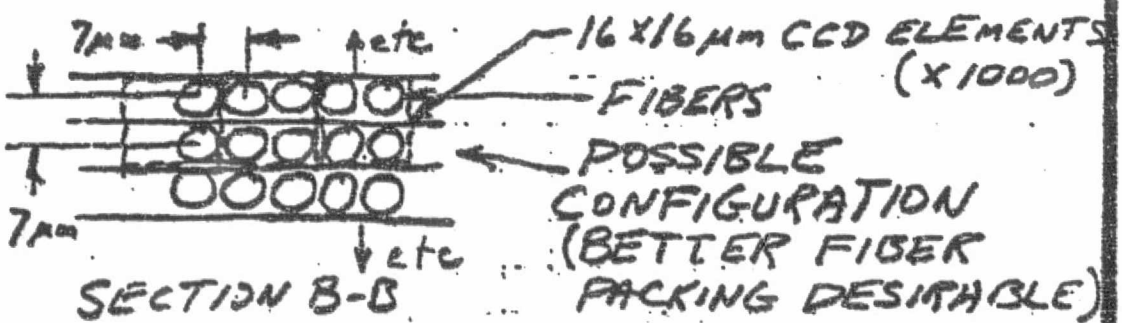

FIBER OPTICS ARRAY

CCD121H
1728-ELEMENT LINEAR IMAGE SENSOR
CHARGE COUPLED DEVICE

GENERAL DESCRIPTION — The CCD121H is a monolithic self-scanned 1728-Element Image Sensor designed for page scanning applications. The device provides a 200-line per inch resolution across an 8-1/2 inch page. Other intended applications are: facsimile readers, optical character recognition, as well as imaging applications that require high resolution, high sensitivity and high speed.

In addition to a row of 1728 sensing elements, the CCD121H chip includes: two charge transfer gates, two 2-phase analog shift registers, an output charge detector/preamplifier, and a compensation output amplifier. The 2-phase analog shift registers both feed the input of the charge detector resulting in sequential reading of the 1728 imaging elements.

The cell size is 13μ (0.51 mils) by 17μ (0.67 mils) on 13μ (0.51 mils) centers. The device is manufactured using Fairchild charge coupled device buried-channel technology.

- **DYNAMIC RANGE TYPICAL: 500:1 (PEAK-TO-PEAK), 2500:1 (rms)**
- **1728 ELEMENTS ON A SINGLE CHIP**
- **ON-CHIP PREAMPLIFIER AND COMPENSATION AMPLIFIER**
- **LOW POWER REQUIREMENTS**
- **ALL OPERATING VOLTAGES UNDER 15 V**
- **PACKAGED IN A 24-PIN DUAL IN-LINE HERMETIC PACKAGE**
- **LOW NOISE EQUIVALENT EXPOSURE**
- **WIDE RANGE OF VIDEO DATA RATE**
- **DIMENSIONALLY PRECISE PHOTOSITE SPACING**

CONNECTION DIAGRAM
DIP (TOP VIEW)

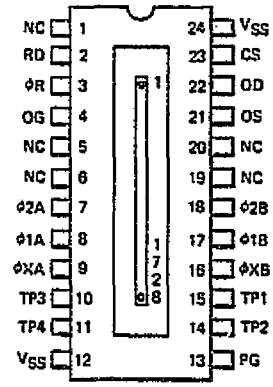

BLOCK DIAGRAM

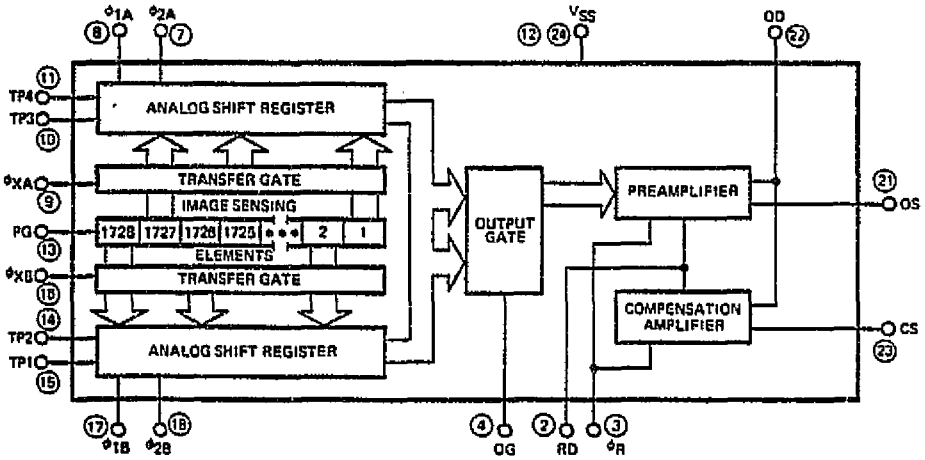

PIN NAMES

PG	Photogate
ϕ_{XA}, ϕ_{XB}	Transfer Gate Clocks
ϕ_{1A}, ϕ_{2A} ϕ_{1B}, ϕ_{2B}	Analog Shift Register Transport Clocks
OG	Output Gate
OS	Output Transistor Source
OD	Output Transistor Drain
CS	Compensation Transistor Source
ϕ_R	Reset Transistor Gate Clock
RD	Reset Transistor Drain
TP	Test Point
V_{SS}	Substrate (Ground)
NC	No Connection

464 ELLIS STREET, MOUNTAIN VIEW, CALIFORNIA 94042 (415) 962-5011 / TWX 910-379-6435

FAIRCHILD

 Printed in U.S.A. 253-11-0010-098 15M

ABSOLUTE MAXIMUM RATINGS (Above which useful life may be impaired)

Storage Temperature	−25°C to 100°C
Operating Temperature	−25°C to 55°C
Pins 3, 4, 7, 8, 9, 10, 13, 15, 16, 17, 18	−0.3 V to 12 V
Pins 2, 11, 14, 21, 22, 23	−0.3 V to 18 V

Caution Note: The device has limited built-in gate protection. It is recommended to control and minimize static charge buildup. Care should be taken to avoid shorting leads OS and CS to ground during operation of the device.

FUNCTIONAL DESCRIPTION —The CCD121H consists of the following functional elements illustrated in the Block Diagram:

Image Sensor Elements — A row of 1728 Image Sensor Elements separated by diffused channel stops and covered by a silicon photogate. Image photons pass through the transparent polycrystalline silicon photogate and are absorbed in the single crystal silicon by hole-electron pair production. The photon generated electrons are accumulated in the photosites. The amount of charge accumulated is a linear function of the incident illumination intensity and the integration period. The output signal will vary in this analog manner from a thermally generated noise background at zero illumination to a maximum at saturation.

Two Transfer Gates — Gate structures adjacent to the row of Image Sensor Elements. The charge packets accumulated in the image sensor elements are transferred out via the transfer gates to the transport registers. Alternating charge packages are transferred to the left and right (A and B) analog transport shift registers. The HIGH states of the transfer-gates must be contained by the HIGH state of the transport shift register clocks. The next light integration period is started when transfer gates go LOW.

Two 866-Bit Analog Shift Registers — One on each side of the row of Image Sensor Elements and separated from it by a Transfer Gate. The two registers are used to move the image generated charge packets serially from the sensor elements to the charge detector/preamplifier. The phase relationship of the last elements of the two shift registers provide for alternate delivery of charge packets to re-establish the serial sequence of the photosites.

A Gated Charge Detector/Preamplifier — Charge packets are transported to a precharged diode whose potential changes linearly in response to the quantity of the signal charge delivered. This potential is applied to the gate of the output n-channel MOS transistor producing a signal output at OS. The reset transistor is driven by a reset clock (ϕ_R) so as to recharge the charge-detector diode capacitance before the arrival of each new signal charge packet from the transport registers.

DEFINITION OF TERMS

Charge Coupled Device — A charge coupled device is a semiconductor device in which isolated charge-packets are transported from one position in the semiconductor to an adjacent position by sequential clocking by an array of gates. The charge-packets are minority carriers with respect to the semiconductor substrate.

Transfer Gate Clock ϕ_{XA}, ϕ_{XB} — The voltage waveform applied to the transfer gate to move the accumulated charge from the image sensor elements to the CCD shift registers.

Analog Shift Register Transport Clocks, ϕ_{1A}, ϕ_{2A}, ϕ_{1B}, ϕ_{2B} — The two sets of 2-phase clock applied to the gates of the CCD shift registers to move the charge packets received from the image sensor elements to the gated charge-detecting preamplifier.

Gate Charge Detector Preamplifier — The output circuit of the CCD121H which receives the charge packets from the CCD shift registers and provides a signal voltage proportional to the size of each charge packet. Before each new charge packet is sensed, a reset clock returns the output voltage to a base level.

Reset Clock ϕ_R — The voltage waveform required to drive the gated charge detector preamplifier.

Dynamic Range — The saturation exposure divided by the peak-to-peak noise equivalent exposure.

This does not take into account dark signal non-uniformities or average dark signal.
Dynamic range is sometimes defined in terms of rms noise. To compare the two definitions a factor of 4 to 6 is generally appropriate. (Peak-to-peak noise is approximately equal to 4 to 6 times rms noise.)

DEFINITION OF TERMS (Cont'd)

Peak-to-Peak Noise Equivalent Exposure — The exposure level which gives an output signal equal to the peak-to-peak noise level at the output in the dark.

Saturation Exposure — The minimum exposure level that will produce a saturated output signal. Saturation exposure is equal to the light intensity times the photosite integration time.

Spectral Response Range — The spectral band in which the response per unit of radiant power is more than 10% of the peak response.

Responsivity — The output signal voltage per unit exposure for a specified spectral type of radiation. Responsivity equals output voltage divided by exposure level.

Photoresponse Non-uniformity — The difference of the response levels of the most and the least sensitive element under uniform illumination. This is commonly expressed as a percentage of the saturation output voltage.

Average Dark Signal — The output signal level in the dark averaged over all elements and measured relative to the base line output voltage established by the reset clock. This is a linear function of the integration time. It is also strongly dependent on temperature. This is commonly expressed as a percentage of the saturation output voltage.

Dark Signal Non-uniformity — Maximum deviation of the output voltage of any element from the background level in the dark. This is commonly expressed as a percentage of the saturation voltage.

Saturation Output Voltage — The maximum signal output voltage.

Integration Time — The time interval between the falling edges of any transfer pulse ϕ_{XA} and ϕ_{XB} as shown in the timing diagram. The integration time is the time allowed for the photosites to collect charge.

Output Signal Range — The output signal range is defined as OSR = $V_{sat} - (t_{INT} + t_{Transport})$ X Rate of Average Signal Offset where: t_{INT} = Integration Time; $t_{Transport}$ = time necessary to transfer the charge packets from the analog shift registers and is equal to $\frac{1728}{f\phi_R}$. Integration time (t_{INT}) does not necessarily equal transfer time ($t_{Transport}$). If long integration times are required, $t_{Transport}$ should be minimized (increase $f\phi_R$) to maximize OSR.

Average Signal Offset — Average signal offset is a dc offset of the output voltage (due to the average leakage current in the CCD registers) which increases linearly with the transfer time.

TEST LOAD CONFIGURATION

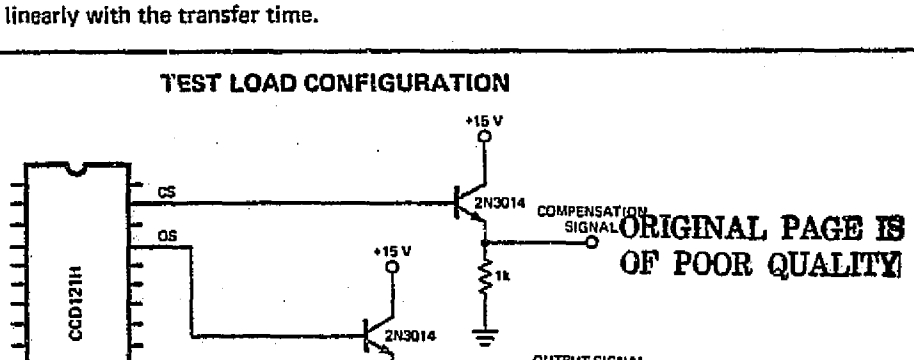

DC CHARACTERISTICS: $T_A = 25°C$

SYMBOL	CHARACTERISTIC	RANGE			UNITS	CONDITIONS
		MIN	TYP	MAX		
V_{OD}	Output Transistor Drain Voltage	14.5	15.0	15.5	V	
V_{RD}	Reset Transistor Drain Voltage	11.5	12.0	12.5	V	Note 1
V_{OG}	Output Gate Voltage	4.5	5.0	5.5	V	
V_{PG}	Photogate Voltage	10.0	10.3	10.5	V	
TP1, TP3	Test Points		0.0		V	Connect to V_{SS}
TP2, TP4	Test Points	14.5	15.0	15.5	V	

CLOCK CHARACTERISTICS: T_A = 25°C.

SYMBOL	CHARACTERISTIC	RANGE			UNITS	CONDITIONS
		MIN	TYP	MAX		
$V_{\phi 1AL}$,$V_{\phi 1BL}$ $V_{\phi 2AL}$,$V_{\phi 2BL}$	Analog Shift Register Transport Clocks LOW	0.0	0.5	0.8	V	Notes 2, 3
$V_{\phi 1AH}$,$V_{\phi 1BH}$ $V_{\phi 2AH}$,$V_{\phi 2BH}$	Analog Shift Register Transport Clocks HIGH	7.5	8.0	8.5	V	Note 3
$V_{\phi XAL}$	Transfer Gate Clock LOW	0.0	0.5	0.8	V	Notes 2, 3
$V_{\phi XAH}$	Transfer Gate Clock HIGH	7.5	8.0	8.5	V	Note 3
$V_{\phi RL}$	Reset Clock LOW	0.0	0.5	0.8	V	Notes 2, 3
$V_{\phi RH}$	Reset Clock HIGH	7.5	8.0	8.5	V	Note 3
$f_{\phi 1A}$,$f_{\phi 1B}$ $f_{\phi 2A}$,$f_{\phi 2B}$	Maximum Analog Shift Register Transport Clock Frequency		5.0		MHz	Notes 4, 5
$f_{\phi R}$	Maximum Reset Clock Frequency (Output Bit Rate)		10.0		MHz	Notes 4, 5

AC CHARACTERISTICS: T_A = 25°C, $f_{\phi 1} = f_{\phi 2}$ = 0.5 MHz, $f_{\phi R}$ = 1 MHz, t_{INT} = 1.78 ms, $t_{TRANSPORT}$ = 1.73 ms, See Note 14.

SYMBOL	CHARACTERISTIC	RANGE			UNITS	CONDITIONS
		MIN	TYP	MAX		
DR	Dynamic Range	250	750 ~~300~~			Notes 6, 7
NEE	Peak-to-Peak Noise Equivalent Exposure		2×10^{-3}		$\mu j/cm^2$	Note 7
SE	Saturation Exposure		1.5 ~~1.5~~		$\mu j/cm^2$	Note 7
SR	Spectral Response Range Limits		0.45–1.05		μm	
R	Responsivity		0.5 ✓		V per $\mu j/cm^2$	Notes 9, 10, 11
PRNU	Photoresponse Non-uniformity		±25	±50	mV	Note 8
ADS	Average Dark Signal		5.0	25	mV	Note 12
DSNU	Dark Signal Non-uniformity		20	50	mV	Note 13
V_{sat}	Saturation Output Voltage	500	750 ✓	1000	mV	Notes 9, 10
V_O	Output DC Level		7.5		V	
P	Power Dissipation		165		mW	V_{OD} = 15 V
Z	Output Impedance		1000		Ω	
N	Peak-to-Peak Noise		1.0	~3	mV	
RSO	Rate of Average Signal Offset		2.5		mV/ms	

NOTES:
1. $V_{\phi RH}$ should track V_{RD}.
2. Negative transients on the clocks below 0.0 V may cause an increase in apparent dark signal.
3. $C_{\phi XA} = C_{\phi XB} = C_{\phi 1A} = C_{\phi 1B} = C_{\phi 2A} = C_{\phi 2B} \cong 400$ pF, $C_{\phi RA} = C_{\phi RB} \cong 10$ pF.
4. The resulting data output frequency is twice that of each analog shift register clock, $f_{\phi 1A}$, $f_{\phi 2A}$, $f_{\phi 1B}$, $f_{\phi 2B}$.
5. Minimum clock frequency is limited by increase in dark current which reduces output signal range OSR. See curves.
6. The dynamic range is measured by taking the ratio of the saturation output voltage to the peak-to-peak noise of the device in the dark. Because of the high degree of linearity of the device the dynamic range measurement is also approximately equal to the ratio of the saturation exposure to the peak-to-peak noise equivalent exposure.
7. 1 $\mu j/cm^2$ = 0.02 fcs at 2854°K, 1 fcs = 50 $\mu j/cm^2$ at 2854°K.
8. Measurement is done at ≈ 350 mV output level. Measurement excludes first and last elements but includes both registers' outputs.
9. See test load configurations.
10. See definition of terms.
11. For 2854°K light source.
12. See curve.
13. DSNU has similar integration time and temperature dependence as ADS.
14. It is recommended to use an infrared blocking filter to obtain minimum PRNU and crosstalk.

PHOTOELEMENT DIMENSIONS

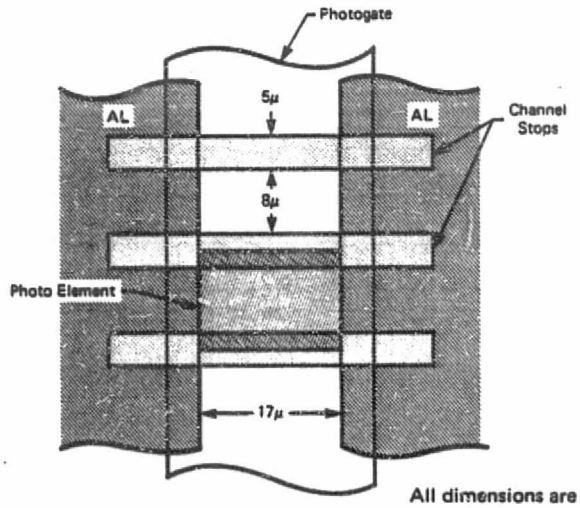

All dimensions are typical values

TYPICAL PERFORMANCE CURVES

OUTPUT SIGNAL LEVEL VERSUS INTEGRATION TIME 2854°K TUNGSTEN SOURCE

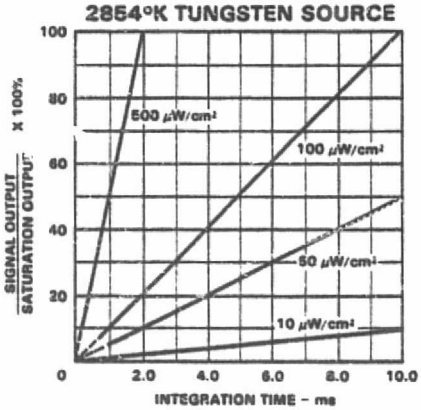

AVERAGE DARK SIGNAL VERSUS INTEGRATION TIME

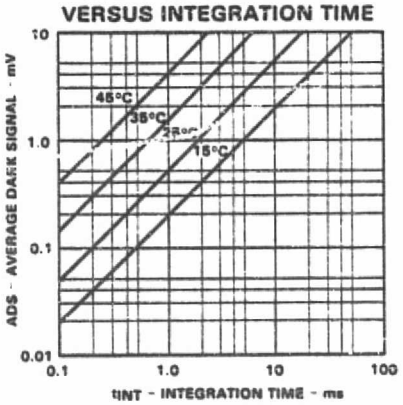

TYPICAL SPECTRAL RESPONSE

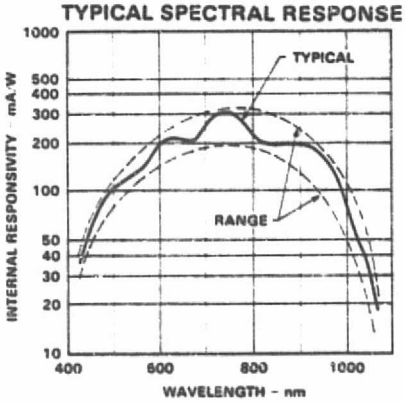

Note 1. Internal responsivity is related to the responsivity at the output through integration time and preamp charge-to-voltage conversion gain. of 3.8V/pC

Note 2. Internal responsivity pertains to photoelement signal only; it excludes the shift in black reference level produced by long wavelength radiation.

C·i·t

3.8V/pA·t

MODULATION TRANSFER FUNCTIONS FOR TWO BROADBAND ILLUMINATION SOURCES

SPATIAL FREQUENCY – CYCLES/mm

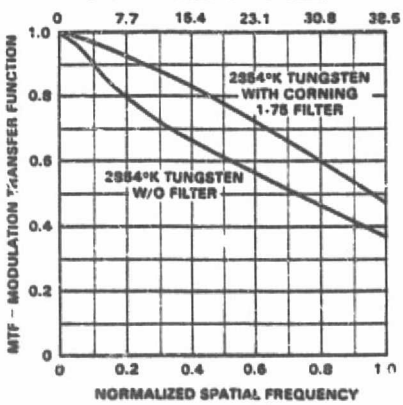

The Corning 1-75 filter has the following typical transmittance spectral characteristic: >85% at <600 nm, 60% at 700 nm, 30% at 800 nm, 5% at 900 nm and <2% at >1000 nm.

MODULATION TRANSFER FUNCTIONS FOR NARROW BAND ILLUMINATION SOURCES

SPATIAL FREQUENCY – CYCLES/mm

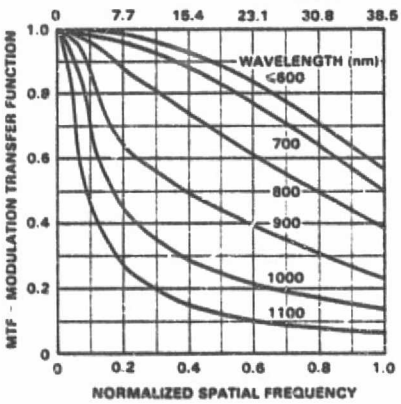

PHOTOELEMENT DIMENSIONS

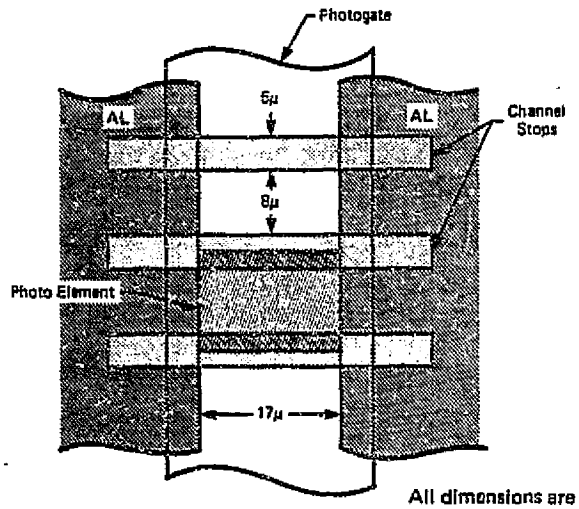

All dimensions are typical values

TYPICAL PERFORMANCE CURVES

OUTPUT SIGNAL LEVEL VERSUS INTEGRATION TIME 2854°K TUNGSTEN SOURCE

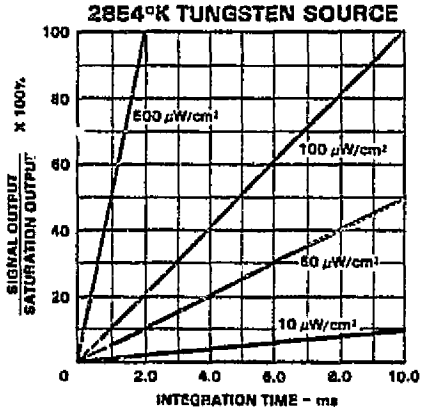

AVERAGE DARK SIGNAL VERSUS INTEGRATION TIME

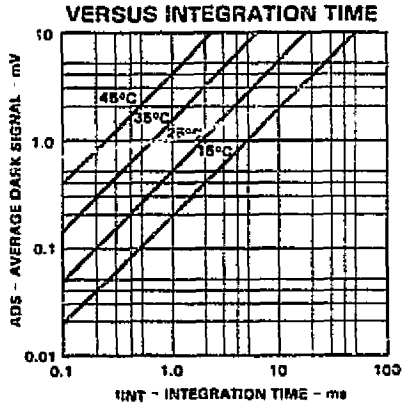

TYPICAL SPECTRAL RESPONSE

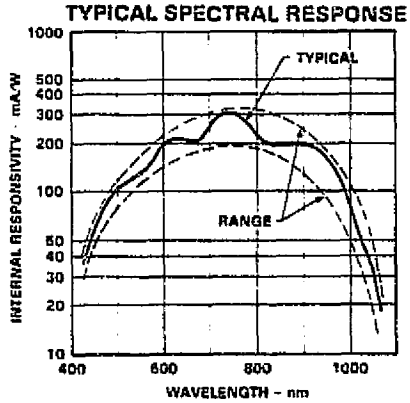

Note 1. Internal responsivity is related to the responsivity at the output through integration time and preamp charge-to-voltage conversion gain. of 3.8V/pC

Note 2. Internal responsivity pertains to photoelement signal only; it excludes the shift in black reference level produced by long wavelength radiation.

c·i·t

3.8V/pA·t)

MODULATION TRANSFER FUNCTIONS FOR TWO BROADBAND ILLUMINATION SOURCES

SPATIAL FREQUENCY – CYCLES/mm

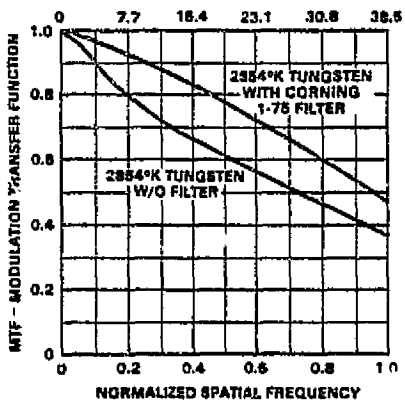

The Corning 1-75 filter has the following typical transmittance spectral characteristic: >85% at <600 nm, 60% at 700 nm, 30% at 800 nm, 5% at 900 nm and <2% at >1000 nm.

MODULATION TRANSFER FUNCTIONS FOR NARROW BAND ILLUMINATION SOURCES

SPATIAL FREQUENCY – CYCLES/mm

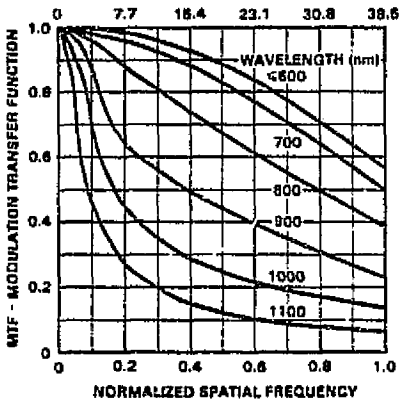

TIMING DIAGRAM DRIVE SIGNALS

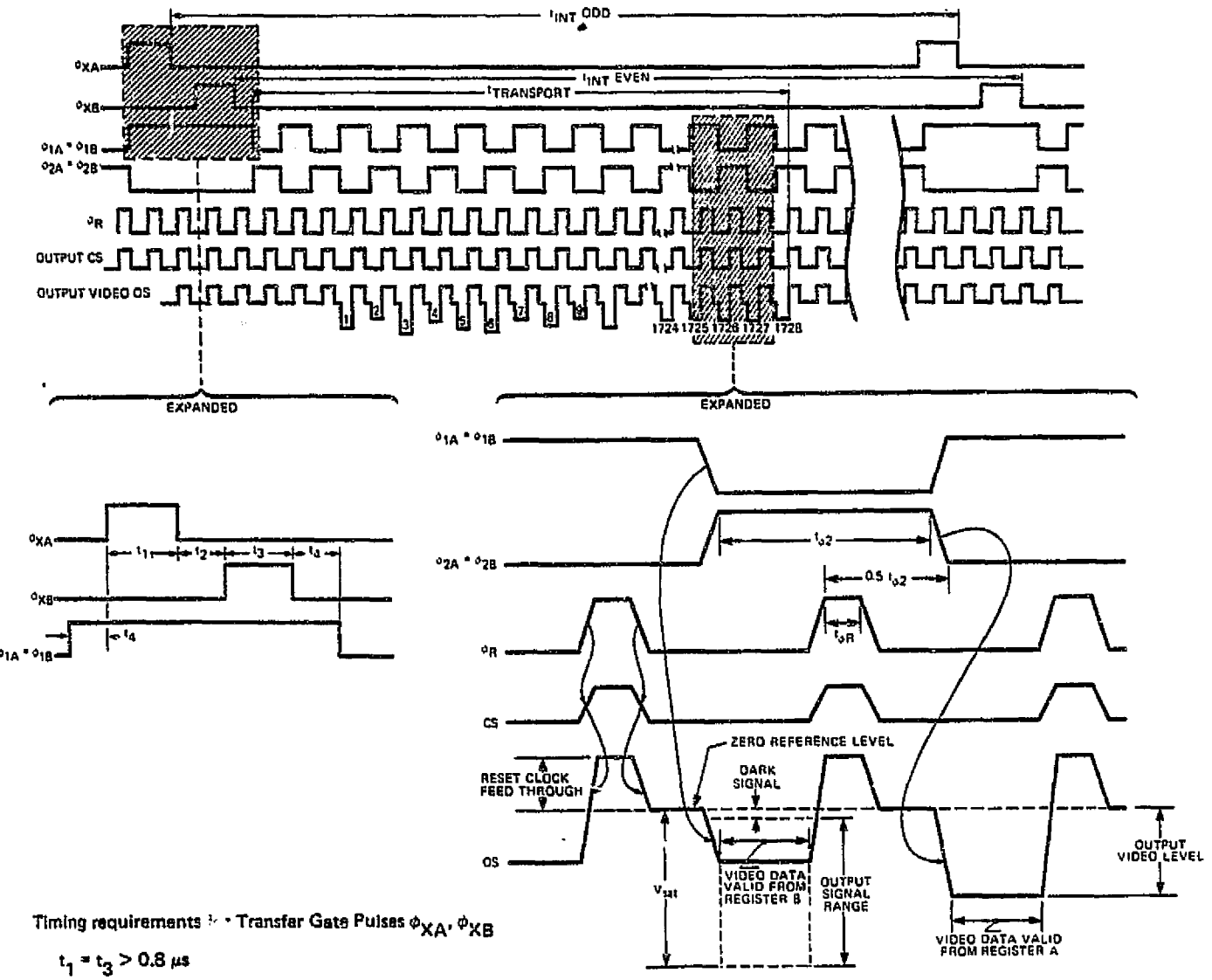

Timing requirements for Transfer Gate Pulses ϕ_{XA}, ϕ_{XB}

$t_1 = t_3 > 0.8\ \mu s$

$t_2 = t_4 > 0.1\ \mu s$

Timing requirements for Reset Pulse ϕ_{RA}

$t_r = t_f < 0.3\ (t\phi_R)$

$0.25\ (t\phi_2) < t\phi_R < 0.5\ (t\phi_2)$

Timing requirements for $\phi_{1A} = \phi_{1B}$

$0.1\ (t\phi_2) < (t_r = t_f) < 0.4\ (t\phi_2)$

CIRCUIT DIAGRAM

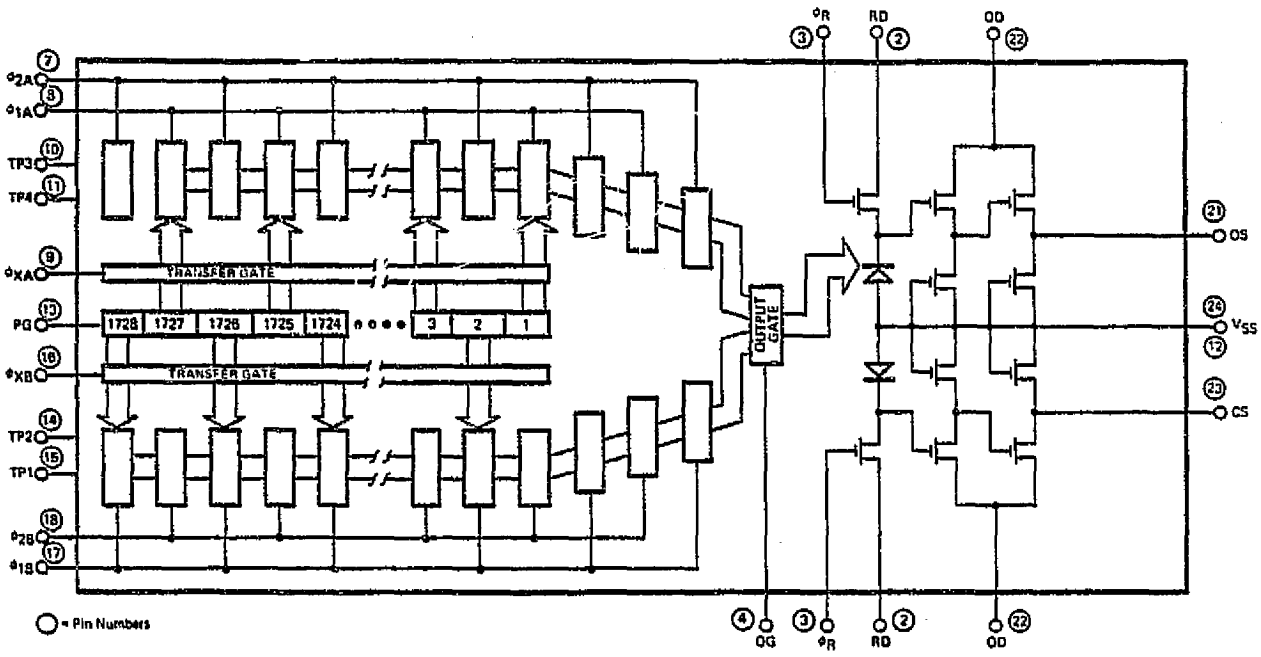

PACKAGE OUTLINE
24-Pin Dual In-line Hermetic Package

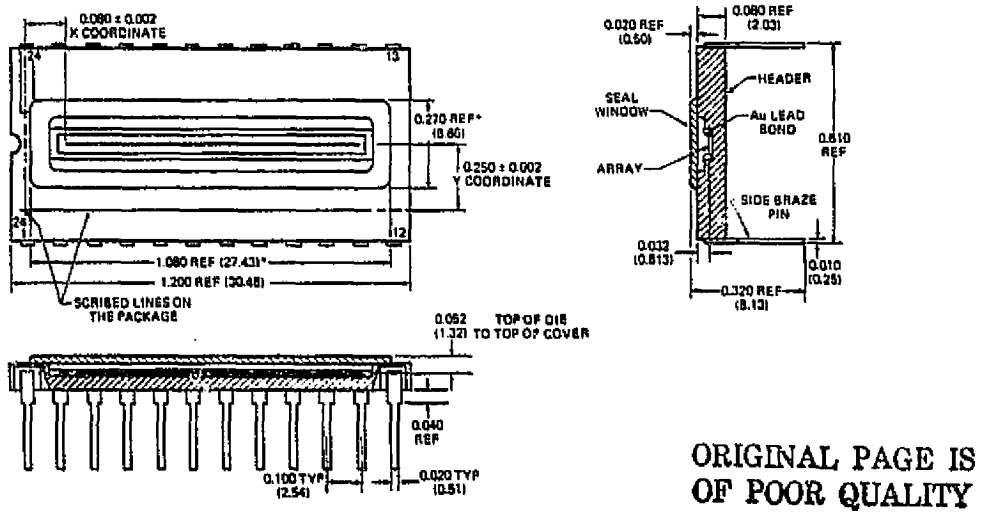

ORIGINAL PAGE IS
OF POOR QUALITY

NOTES:

All dimensions in inches (bold) and millimeters (parenthesis). Header is black ceramic (Al_2O_3). Transparent portion of package is glass. The CCD121H hermetic package carries the number "24" close to pin 1 of the device. This number should not be confused with pin 24 of the device is connected to V_{SS} (substrate).

ORDER INFORMATION – Order CCD121HC where "H" stands for hermetic package and "C" is commercial temperature range. The CCD121HC is the replacement for the CCD121DC. The two devices are pin-for-pin compatible. The output on-chip amplifier of the CCD121H is an improved design (over the CCD121) providing a higher saturation output voltage of typically 750 mV.

Also available is a printed circuit board that includes all the necessary clocks, logic, drivers and video amplifiers to operate the CCD121H. The printed circuit board is fully assembled and tested and requires three power supplies for operation (+5 V, +15 V and −15 V). The printed circuit board order code is: CCD121HB.

FAIRCHILD

CRITICAL EXPOSURE LEVELS FOR FAIRCHILD CCD 121 H

(Based on Typical Values Shown on Data Sheets)

(Source Fairchild Semiconductor)

		CCD 121H	UNITS
Saturation Exposure	N_{SAT}	1.2×10^{6}	el/pix
2800°K Radiation			
Photometric Units		1.0×10^{-2}	fc s
Radiometric Units		5×10^{-7}	J cm^{-2}
Peak Spectral Radiation		1.6×10^{-7}	J cm^{-2}
per Element		0.34	pJ
Sensitivity (Notes 1, 2)			
2800°K Radiation			
Photometric Units		3×10^{-4}	fc s
Radiometric Units		1.5×10^{-8}	J cm^{-2}
Peak Spectral Radiation		5×10^{-9}	J cm^{-2}
per Element		10	fJ
Noise Equivalent Exposure (Note 2)			
2800°K Radiation			
Photometric Units		6×10^{-5}	fc s
Radiometric Units		3×10^{-9}	J cm^{-2}
Peak Spectral Radiation		1.0×10^{-9}	J cm^{-2}
per Element		2.0	fJ

(1) Sensitivity is defined as the exposure level at which the signal level equals the peak-to-peak random noise level. This is approximately the lowest exposure level at which full resolution can be obtained. The peak-to-peak random noise level is approximately five times the RMS noise level.

(2) These noise-related exposure levels are based on noise measured within the video period of each element period; and at the test frequency specified in each data sheet. Major noise, in this case, is input-capacitance noise.

CCD131

ORIGINAL PAGE IS OF POOR QUALITY

1024-ELEMENT LINEAR IMAGE SENSOR

CHARGE COUPLED DEVICE

GENERAL DESCRIPTION – The CCD131 is a monolithic self-scanned 1024 Element Image Sensor designed for page scanning applications. The device provides a 120 line per inch resolution across an 8-1/2 inch page.

The device is also intended to be used for facsimile readers, optical character recognition, as well as imaging applications that require high resolution, high sensitivity and high speed.

In addition to a row of 1024 sensing elements, the CCD131 chip includes: two charge transfer gates, two 2-phase analog shi.. registers and two gated charge integrators that provide at the output typically a 1 V swing.

The cell size is 13 μ (0.51 mils) by 13 μ (0.51 mils) on 13 μ (0.51 mils) centers. The device is manufactured using Fairchild charge coupled device buried channel technology and packaged in a 24 pin hermetically sealed DIP with a glass window.

- DYNAMIC RANGE 500:1 TYPICAL
- 1024 ELEMENTS ON A SINGLE CHIP
- LOW POWER REQUIREMENTS
- ON-CHIP AMPLIFIER PROVIDING A 1 V TYPICAL OUTPUT SWING
- ALL OPERATING VOLTAGES UNDER 15 V
- PACKAGED IN 24-PIN DUAL IN-LINE HERMETIC PACKAGE
- LOW NOISE EQUIVALENT EXPOSURE
- WIDE RANGE OF VIDEO DATA RATE
- DIMENSIONALLY PRECISE PHOTOSITE SPACING
- ADDITION OF SIMPLE OUTPUT NETWORK PROVIDES CONTINUOUS VIDEO INFORMATION

CONNECTION DIAGRAM
DIP (TOP VIEW)

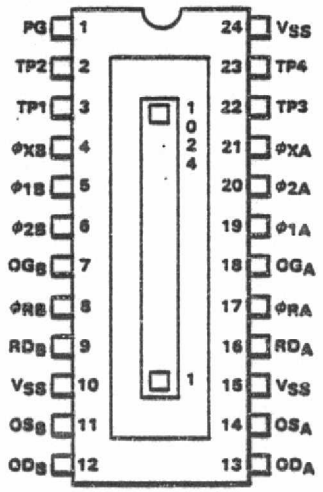

BLOCK DIAGRAM

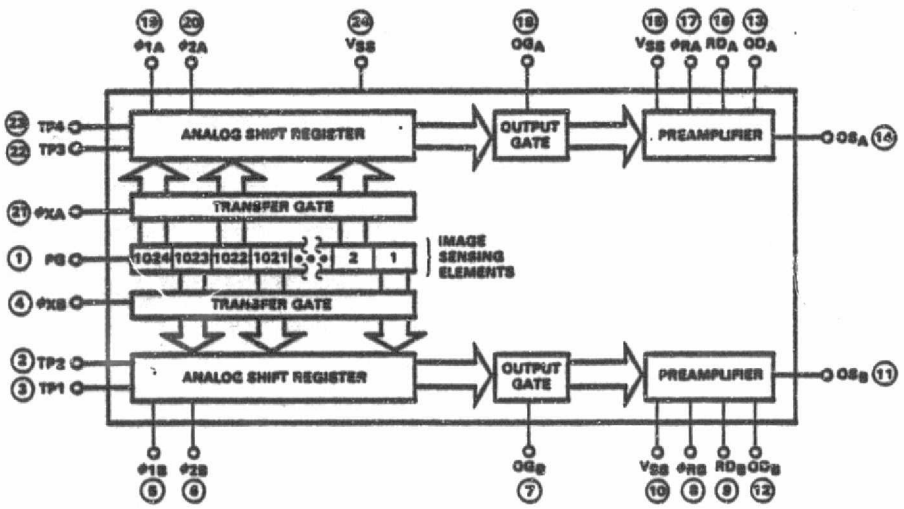

PIN NAMES

PG	Photogate
Φ_{XA}.Φ_{XB}	Transfer Gate Clocks
Φ_{1A}.Φ_{2A} Φ_{1B}.Φ_{2B}	Analog Shift Register Transport Clocks
OG_A.OG_B	Output Gates
OS_A.OS_B	Output Transistor Sources
OD_A.OD_B	Output Transistor Drains
Φ_{RA}.Φ_{RB}	Reset Transistor Gate Clocks
RD_A.RD_B	Reset Transistor Drains
TP	Test Point
V_{SS}	Substrate (Ground)

464 ELLIS STREET, MOUNTAIN VIEW, CALIFORNIA 94042 (415) 962-5011 / TWX 910-379-1925

FAIRCHILD SEMICONDUCTOR

 Printed in U.S.A. 2025-11-0002-016 15M

ABSOLUTE MAXIMUM RATINGS

Storage Temperature	−25°C to 100°C
Operating Temperature	−25°C to 55°C
Pins 1, 3, 4, 5, 6, 7, 8, 17, 18, 19, 20, 21, 22	−0.3 V to 12 V
Pins 2, 9, 11, 12, 13, 14, 16, 23	−0.3 V to 18 V
Pins 10, 15, 24	Ground

Caution: The device has limited built-in gate protection. It is recommended to control and minimize static charge build-up. Care should be taken to avoid shorting leads OS_A and OS_B to the positive supply (15 V) or ground.

FUNCTIONAL DESCRIPTION – The CCD131 consists of the following functional elements illustrated in the Block Diagram:

Image Sensor Elements – A row of 1024 image sensor elements separated by diffused channel stops and covered by a silicon photogate. Image photons pass through the transparent polycrystalline silicon photogate and are absorbed in the single crystal silicon by hole-electron pair production. The photon generated electrons are accumulated in the photosites. The amount of charge accumulated is a linear function of the incident illumination intensity and the integration period. The output signal will vary in this analog manner from a thermally generated noise background at zero illumination to a maximum at saturation.

Two Transfer Gates – Gate structures adjacent to the row of image sensor elements. The charge packets accumulated in the image sensor elements are transferred out via the transfer gates to the transport registers. Alternating charge packets are transferred to the right and left (A and B) analog transport shift registers. The HIGH states of the transfer gates must be contained by the HIGH state of the transport shift register clocks. The next light integration period is started when transfer gates go LOW.

Two 516-Bit Analog Shift Registers – One on each side of the row of image sensor elements and separated from it by a Transfer Gate. The two registers are used to move the image generated charge packets serially from the sensor elements to the charge detector/preamplifier. The phase relationship of the last elements of the two shift registers provide for alternate delivery of charge packets to re-establish the serial sequence of the photosites.

Two Gated Charge Detector/Preamplifier – Charge Packets are transported to the output charge detector/preamplifier through the output gate. A precharged diode potential changes linearly in response to the quantity of signal charge delivered. This potential is applied to the gate of the first of a two-stage source follower (as shown in the circuit diagram). The output voltage corresponding to the charge packet is present at the source of the output transistor (Pins OS_A and OS_B).

DEFINITION OF TERMS

Charge Coupled Device – A charge coupled device is a semiconductor device in which isolated charge-packets are transported from one position in the semiconductor to an adjacent position by sequential clocking of an array of gates. The charge packets are minority carriers with respect to the semiconductor substrate.

Transfer Gate Clocks ϕ_{XA}, ϕ_{XB} – The voltage waveform applied to the transfer gate to move the accumulated charge from the image sensor elements to the CCD shift registers.

Analog Shift Register Transport Clocks ϕ_{1A}, ϕ_{2A}, ϕ_{1B}, ϕ_{2B} – The two sets of 2-phase clock applied to the gates of the CCD shift registers to move the charge packets received from the image sensor elements to the gated charge-detector preamplifiers.

Gated Charge Detector Preamplifiers – The output circuits of the CCD131 which receive the charge packets from the CCD shift registers and provide a signal voltage proportional to the size of each charge packet. Before each new charge packet is sensed the reset clocks return the output voltage to a base level (zero reference level).

Reset Clocks ϕ_{RA}, ϕ_{RB} – The voltage waveforms required to drive the gated charge detector preamplifiers.

Dynamic Range – The saturation exposure divided by the peak-to-peak noise equivalent exposure. This does not take into account dark signal non-uniformities or average dark signal. Dynamic range is sometimes defined in terms of rms noise. To compare the two definitions, a factor of 4 to 6 is generally appropriate. (Peak-to-peak noise is approximately equal to 4 to 6 times rms noise).

Peak-to-Peak Noise Equivalent Exposure – The exposure level which gives an output signal equal to the peak-to-peak noise level at the output in the dark.

Saturation Exposure – The minimum exposure level that will produce a saturated output signal. Saturation exposure is equal to the light intensity times the photosite integration time.

Spectral Response Range – The spectral band in which the response per unit of radiant power is more than 10% of the peak response.

Responsivity – The output signal voltage per unit exposure for a specified spectral type of radiation. Responsivity equals output voltage divided by exposure level.

Photoresponse Non-uniformity – The difference of the response levels of the most and the least sensitive element under uniform illumination. This is commonly expressed as a percentage of the saturation output voltage.

Average Dark Signal – The output signal level in the dark averaged over all elements and measured relative to the base line output voltage established by the reset clock. This is a linear function of the integration time. It is also strongly dependent on temperature. This is commonly expressed as a percentage of the saturation output voltage.

Dark Signal Non-uniformity – Maximum deviation of the output voltage of any element from the background level in the dark. This is commonly expressed as a percentage of the saturation voltage.

Saturation Output Voltage – The maximum signal output voltage.

Integration Time – The time interval between the falling edges of any transfer pulse ϕ_{XA} and ϕ_{XB} as shown in the timing diagram. The integration time is the time allowed for the photosites to collect charge.

Output Signal Range – The output signal range is defined as OSR = $V_{sat} - (t_{INT} + t_{Transfer}) \times$ Rate of Average Signal Offset where: t_{INT} = Integration Time; $t_{Transfer}$ = time necessary to transfer the charge packets from the analog shift registers and is equal to $516/f_{\phi R}$. Integration time (t_{INT}) does not necessarily equal transfer time ($t_{Transfer}$). If long integration times are required, $t_{Transfer}$ should be minimized (increase $f_{\phi R}$) to maximize OSR.

Average Signal Offset – Average signal offset is a dc offset of the output voltage (due to the average dark signal in the CCD registers) which increases linearly with the transfer and integration time.

TEST LOAD CONFIGURATION

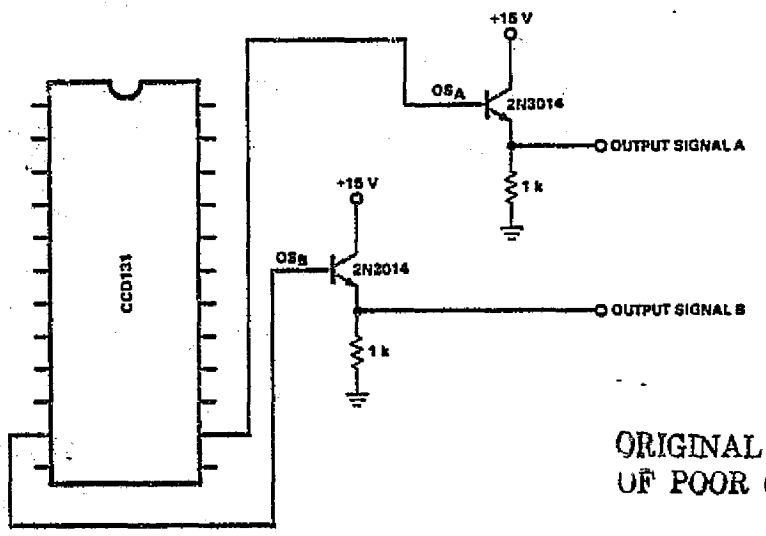

PHOTOELEMENT DIMENSIONS

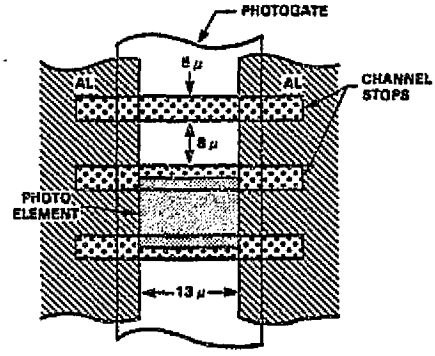

All dimensions are typical values

AVERAGE DARK SIGNAL VERSUS INTEGRATION TIME AT DIFFERENT TEMPERATURES

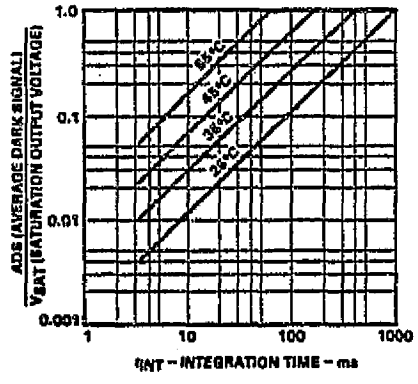

SPECTRAL RESPONSE

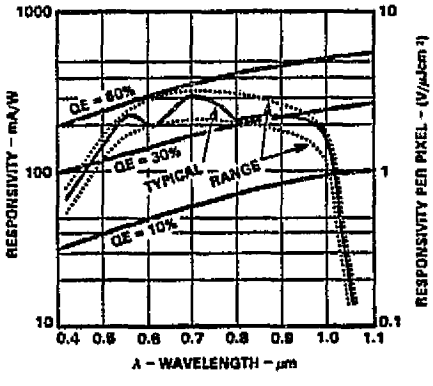

SQUARE WAVE RESPONSE IN PHASE

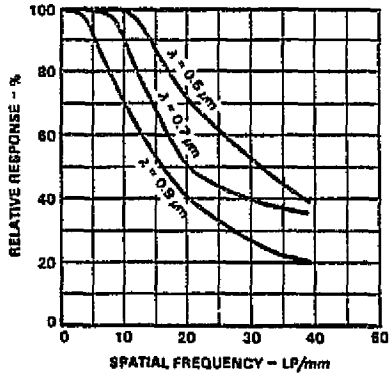

DC CHARACTERISTICS: $T_A = 25°C$

SYMBOL	PARAMETER	RANGE			UNITS	CONDITIONS
		MIN	TYP	MAX		
V_{ODA},V_{ODB}	Output Transistor Drain Voltage	14.5	15.0	15.5	V	
V_{RDA},V_{RDB}	Reset Transistor Drain Voltage	14.5	15.0	15.5	V	See Note 1
V_{OGA},V_{OGB}	Output Gate Voltage	4.5	5.0	5.5	V	
V_{PG}	Photogate Voltage	8.5	9.0	9.5	V	
TP1, TP3	Test Points		0.0		V	Connect to V_{SS}
TP2, TP4	Test Points	14.5	15.0	15.5	V	

CLOCK CHARACTERISTICS: $T_A = 25°C$

SYMBOL	PARAMETER	RANGE			UNITS	CONDITIONS
		MIN	TYP	MAX		
$V_{\phi 1AL}$,$V_{\phi 1BL}$ $V_{\phi 2AL}$,$V_{\phi 2BL}$	Analog Shift Register Transport Clocks LOW	0.0	0.5	0.8	V	Notes 2, 3
$V_{\phi 1AH}$,$V_{\phi 1BH}$ $V_{\phi 2AH}$,$V_{\phi 2BH}$	Analog Shift Register Transport Clocks HIGH	7.0	8.0	9.0	V	Note 3
$V_{\phi XAL}$,$V_{\phi XBL}$	Transfer Gate Clock LOW	0.0	0.5	0.8	V	Notes 2, 3
$V_{\phi XAH}$,$V_{\phi XBH}$	Transfer Gate Clock HIGH	7.0	8.0	9.0	V	Note 3
$V_{\phi RAL}$,$V_{\phi RBL}$	Reset Clock LOW	0.0	0.5	0.8	V	Notes 2, 3
$V_{\phi RAH}$,$V_{\phi RBH}$	Reset Clock HIGH	11	12	13	V	Note 3
$f_{\phi 1A}$,$f_{\phi 1B}$ $f_{\phi 2A}$,$f_{\phi 2B}$	Maximum Analog Shift Register Transport Clock Frequency		12		MHz	Notes 4, 5
$f_{\phi RA}$,$f_{\phi RB}$	Max. Reset Clock Frequency		12		MHz	Notes 4, 5

AC CHARACTERISTICS: $T_A = 25°C$ $f_{\phi 1} = f_{\phi 2} = f_{\phi R} = 2.5$ MHz, $t_{INT} = 768\ \mu s$, $t_{TRANSFER} = 204.8\ \mu s$

SYMBOL	PARAMETER	RANGE			UNITS	CONDITIONS
		MIN	TYP	MAX		
DR	Dynamic Range		500			Notes 6, 7
NEE	Peak-to-Peak Noise Equivalent Exposure		2×10^{-3}		$\mu j/cm^2$	Notes 7
SE	Saturation Exposure		1.0		$\mu j/cm^2$	Notes 7
SR	Spectral Response Range Limits		0.45–1.05		μm	
R	Responsivity		1.0		V per $\mu j/cm^2$	Notes 9,10,11
PRNU	Photoresponse Non-uniformity		±6.0	±10	% of V_{sat}	Note 8
ADS	Average Dark Signal		1.0	3.0	% of V_{sat}	
DSNU	Dark Signal Non-uniformity		3.0	5.0	% of V_{sat}	
V_{sat}	Saturation Output Voltage	700	1000		mV	Note 9
P	Power Dissipation		165		mW	$V_{OD} = 15$ V
Z	Output Impedance		1000		Ω	
N	Peak-to-Peak Noise		2.0		mV	
RSO	Rate of Average Signal Offset		10		mV/ms	

NOTES:

1. $V_{\phi RH}$ should track V_{RD}.
2. Negative transients on the clocks below 0.0 V may cause an increase in apparent dark signal.
3. $C_{\phi XA} = C_{\phi XB} = C_{\phi 1A} = C_{\phi 1B} = C_{\phi 2A} = C_{\phi 2B} = 200$ pF, $C_{\phi RA} = C_{\phi RB} = 10$ pF.
4. The resulting data output frequency is twice that of each analog shift register clock, $f_{\phi 1A}$, $f_{\phi 2A}$, $f_{\phi 1B}$, $f_{\phi 2B}$, $f_{\phi RA}$, $f_{\phi RB}$.
5. Minimum clock frequency is limited by increase in dark current which reduces output signal range OSR. See curves.
6. The dynamic range is measured by taking the ratio of the saturation output voltage to the peak-to-peak noise of the device in the dark. Because of the high degree of linearity of the device the dynamic range measurement is also approximately equal to the ratio of the saturation exposure to the peak-to-peak noise equivalent exposure.
7. 1 $\mu j/cm^2$ = 0.02 fcs at 2854°K, 1 fcs = 50 $\mu j/cm^2$ at 2854°K.
8. Measurement is done at 50% of saturation output level. Measurement excludes first and last elements but includes both registers outputs.
9. See test load configuration.
10. See definition of terms.
11. For 2854°K light source.

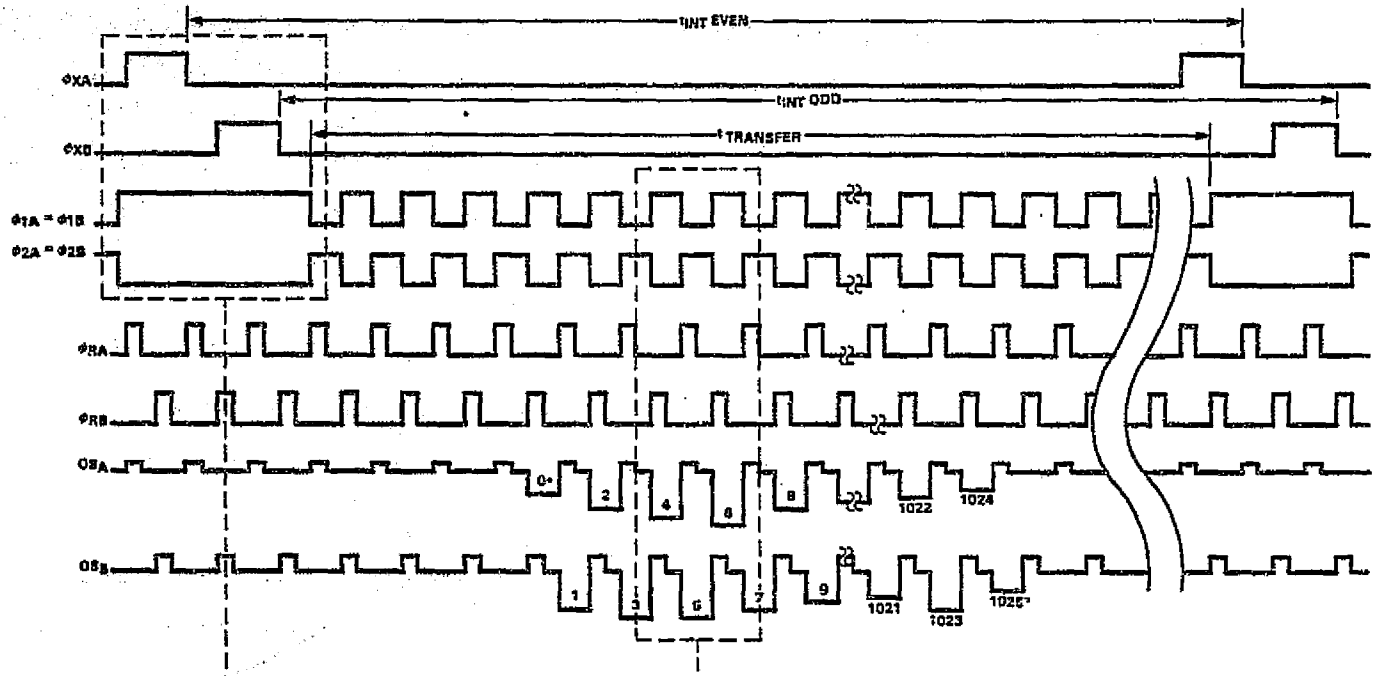

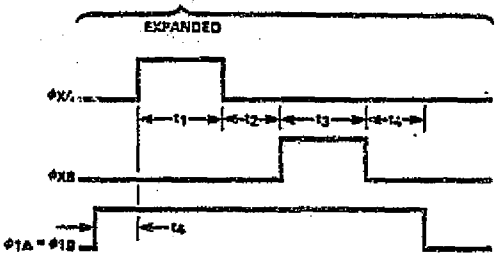

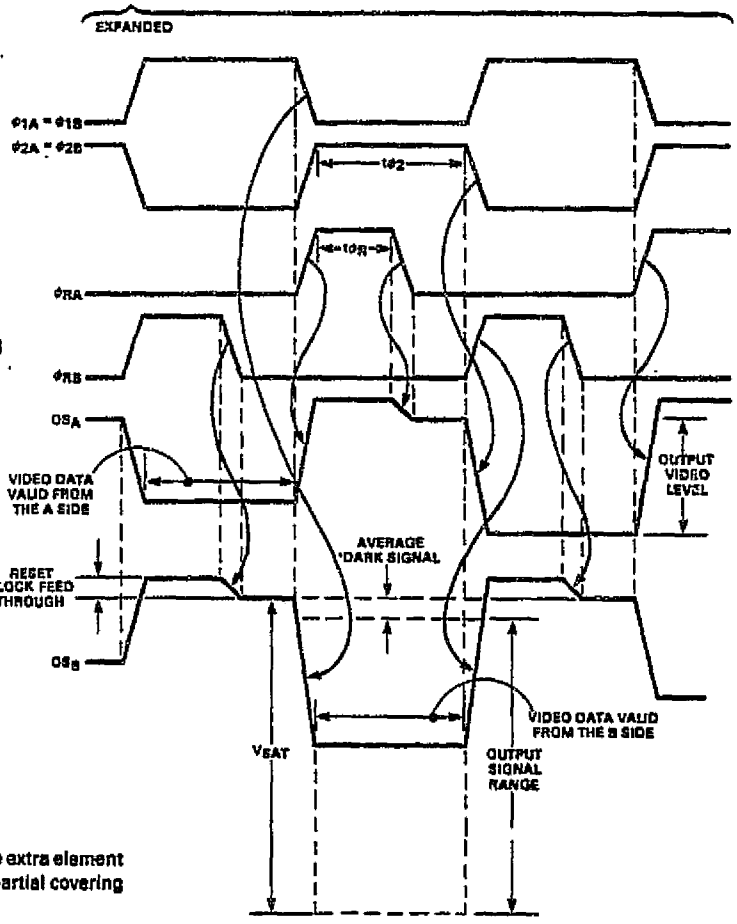

Timing requirements for Transfer Gate Pulses ϕ_{XA}, ϕ_{XB}

$t_1 = t_3 > 0.8\ \mu s$

$t_2 = t_4 > 0.1\ \mu s$

Timing requirements for Reset Pulse ϕ_{RA}, ϕ_{RB}

$t_r = t_f < 0.3\ (t_{\phi R})$

$0.5\ (t_{\phi 2}) < t_{\phi R} < 1.0\ (t_{\phi 2})$

Timing requirements for $\phi_{1A} = \phi_{1B}$

$0.1\ (t_{\phi 2}) < (t_r = t_f) < 0.4\ (t_{\phi 2})$

*NOTE: At each end of the 1024 photoelements there exists one extra element (0 and 1025). These elements are partly illuminated due to a partial covering of opaque aluminum.

CIRCUIT DIAGRAM

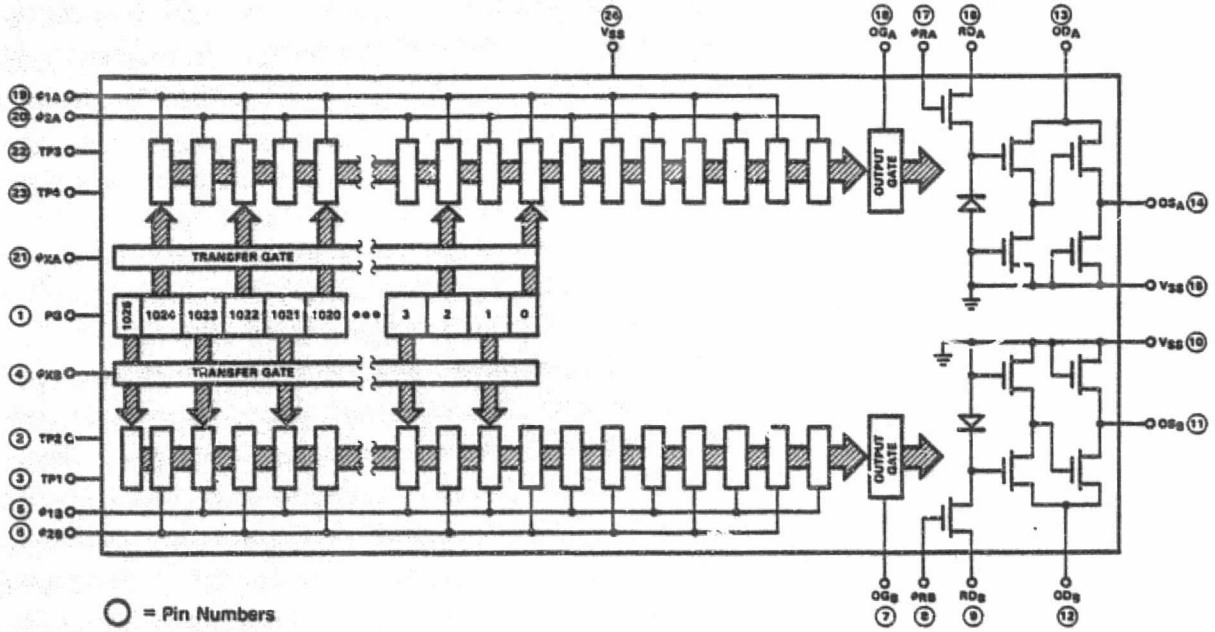

PACKAGE OUTLINE

24-Pin Dual In-line Hermetic Package

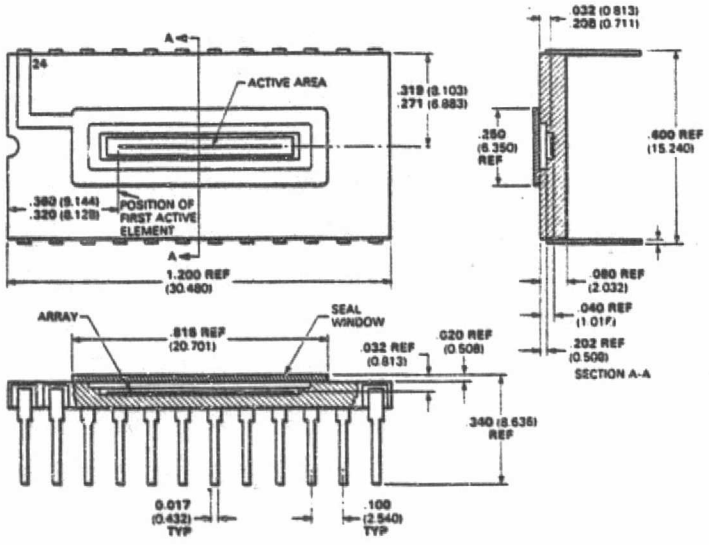

NOTES:
All dimensions in inches (bold) and millimeters (parentheses)
Header is black ceramic (Al_2O_3).
Transparent portion of package is glass

RETICON® CHARGE COUPLED PHOTODIODE ARRAYS
CCPD-256, CCPD-1024, CCPD-1728

Until now, users of solid-state image sensors have had to choose between devices optimized for low-noise readout (CCD) and devices with optimized sensor characteristics (photodiode arrays).

Although the low output capacitance of CCD imagers simplifies low-level signal extraction, the CCD sensing elements have a number of serious drawbacks: The semi-transparent electrode covering the sensing area causes gross optical interference effects throughout the visible spectrum and, in addition, absorbs strongly at short wavelengths, drastically reducing the blue response. In addition, CCD imagers have relatively low saturation charge, limiting their signal handling capability, and they typically have high dark currents which restrict their use to short integration times (high scan rates).

While self-scanned photodiode arrays have a high output capacitance which makes low-level signal extraction more difficult, these devices have nearly ideal sensor characteristics. They have the full silicon spectral response including blue and UV and are free of interference effects. They have a large signal handling capability, have little cross-talk or blooming, and have low dark currents.

Reticon has now successfully combined the advantages of the CCD and photodiode array technologies to produce for the first time a truly optimized family of solid-state image sensors. Our new CCPD™ (*C*harge *C*oupled *P*hoto-*d*iode) devices utilize diffused photodiode sensors which are essentially identical to those used in other Reticon products, but incorporate CCD readout registers and output buffer amplifiers for low-noise signal extraction. In addition, CCPD devices contain an anti-blooming gate which not only suppresses blooming but can also be used to set the integration period independently of the line rate.

CCPD devices are available with 256, 1024, or 1728 sensor elements on 16 μm centers. All three devices are mounted in 22-pin dual-in-line ceramic packages with ground and polished optical windows, and all have identical pin configurations.

Key features of Reticon's CCPD Devices include the following:

- **256, 1024, or 1728 elements on a single chip**
- **Dimensionally precise 16 μm x 16 μm picture elements**
- **Low power requirements**
- **Plus 12 and minus 5 volt supplies**
- **On-chip preamplifier**
- **Wide dynamic range: typically 500:1 (peak-to-peak), 2500:1 (rms)**
- **Low noise-equivalent-exposure**
- **Video sample rates up to 5 MHz**
- **Up to 40 msec integration time**
- **Smooth spectral response**
- **Useful response in blue and UV**
- **High resistance to blooming**
- **Standard 22-pin ceramic dual-in-line package**
- **High volume production process**

FUNCTIONAL DESCRIPTION

The CCPD pin configuration is shown in Fig. 1 and a simplified schematic diagram is shown in Fig. 2. The sensing elements are a row of diffused p-n junction photodiodes spaced on 16 μm centers and interdigitated into a sensing aperture 16 μm wide.

Light incident on the sensing aperture generates photocurrent which is integrated and stored as a charge on the capacitance of each of the photodiodes. If the charge accumulated on any diode exceeds a saturation value, the excess is shunted to V_{DD} through the anti-blooming gates V_{AB}, thus avoiding blooming effects.

At the end of each integration period, the charges on all the diodes are simultaneously switched through transfer gates $\emptyset_T$ into one of two CCD analog shift registers for readout. The odd diodes are switched into one register and the even diodes into the other. Immediately after this parallel transfer, a new integration period begins.

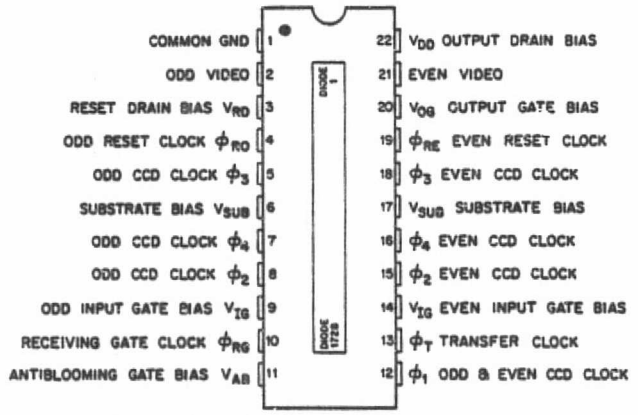

Figure 1. Pin configuration (identical for CCPD-256, 1024, and 1728)

RETICON CORPORATION 910 Benicia Avenue, Sunnyvale, California 94086
Phone: (408) RET-ICON, (408) 738-4266, TWX: 910-339-9343

RETICON CHARGE COUPLED PHOTODIODE ARRAYS
CCPD-256, CCPD-1024, CCPD-1728

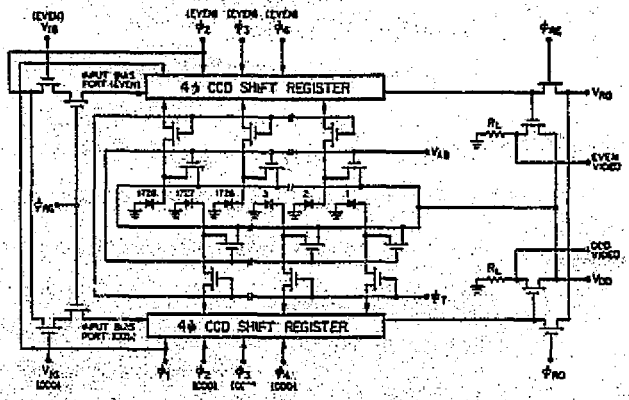

Figure 2. Schematic diagram of CCPD. Load resistors R_L are connected externally

Readout is accomplished by clocking the CCD shift registers so that the charge packets are delivered sequentially into two on-chip charge-detection circuits. The registers deliver the charge packets alternately, allowing the inactive charge detector to be reset to a fixed level by ϕ_R while the opposite detector is active. The outputs of the two detectors may then be multiplexed off-chip to obtain a stepwise-continuous video signal.

OPERATION

In the usual mode of operation, the CCPD requires four clock phases, a transfer gate pulse, and two dc voltages (-5V and +12V). The four-phase clock waveforms should swing between 0 and +12 volts with timing as shown in Figs. 3A and 3B. The falling edges of ϕ_1 and ϕ_3 should be delayed (or stretched) as shown in Fig. 3B to insure smooth transfer of charge. ϕ_2 and ϕ_4 are non-critical. The time between the transfer-gate pulses determines the integration time as shown in Fig. 3C.

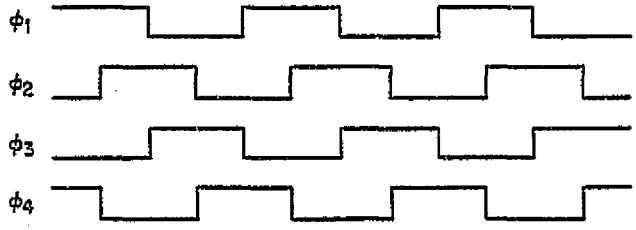

Figure 3A. Four-phase CCD clock timing diagram

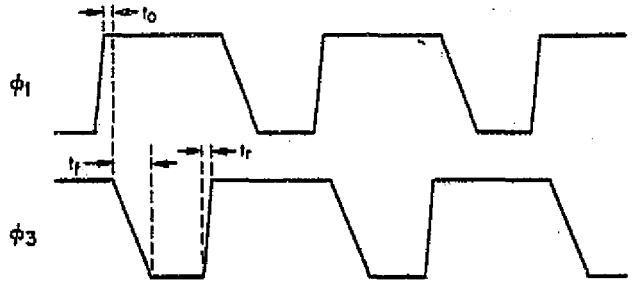

t_r = RISE TIME
t_o = OVER LAP TIME
t_f = FALL TIME

$t_r < 15$ nsec
$0 < t_o < 10$ nsec
$20 < t_f < 40$ nsec

Figure 3B ϕ_1 and ϕ_3 clock edges for optimum performance. ϕ_2 and ϕ_4 are non-critical

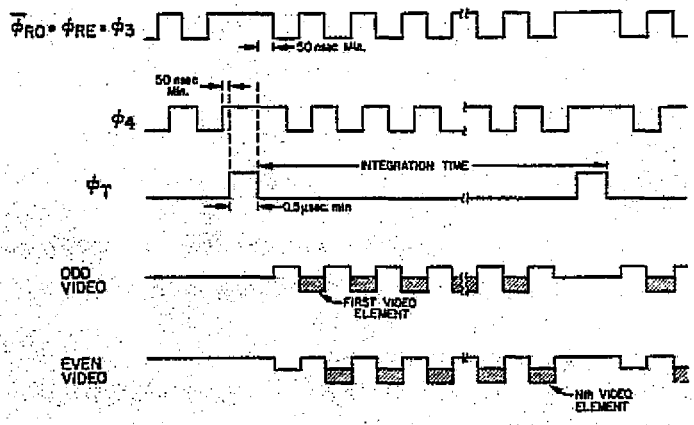

NOTE: $\phi_{RE} = \overline{\phi_{RO}} = \phi_3 = \overline{\phi_1}$ ONLY IN TIMING. FOR OPTIMUM OPERATION, THE RESET CLOCKS, ϕ_{RO} AND ϕ_{RE}, SHOULD BE CLOCKED THROUGH SEPARATE SOURCE RESISTORS (SEE TEXT).

Figure 3C. Timing relationship of transfer pulse, CCD transport clocks, reset clocks, and video outputs.

The transfer pulse should swing between -4 and +5 volts and have a width greater than 1 μsec. In order to transfer the charge from the photodiodes into the CCD register, the ϕ_3 and ϕ_4 clocks should remain high during the blanking and transfer interval, as shown in Fig. 3C. This same figure also shows ϕ_{RE}, the even reset clock, and its relationship to ϕ_4 and ϕ_3 clocks as well as the odd and even video outputs. The odd and even output reset clocks ϕ_{RO} and ϕ_{RE} are derived from the same sources as ϕ_1 and ϕ_3 and are nominally synchronous, respectively, except that they do not have the falling-edge delay of Fig. 3B, and will require a separate MOS driver for optimum performance. See Fig. 10 for an example of a circuit for deriving these clocks. A bias charge level is required in the CCD registers to obtain optimum operation. This charge is supplied by biasing the inputs to the registers (Pins 9 and 14) with a small positive voltage in the range of 0 to 2.5 volts. Also, in order to balance the dc output levels of the two registers, it is convenient to adjust one input level relative to the other. Resistive dividers (potentiometers) may be used since very little current is required.

The output gate (Pin 20) draws negligible current. It also may be biased, through a resistive divider, to a voltage (non-critical) of from 2 to 2.5 volts.

The substrate (pins 6 and 17) is held at -5 volts; the common reference (Pin 1) and the anti-blooming gate (Pin 11) are at ground; and the output amplifier drain, Pin 22, is at +12 volts. The reset drain (Pin 3) normally is connected to +12 volts, but may be at an intermediate level if desired.

In some applications, it may be desirable to define an integration period shorter than the read-out time. This may be accomplished by resetting the diodes with the anti-blooming gate. At the desired reset time V_{AB} is pulsed to +5 volts for at least one μsec and then back to ground. The integration period is then the time between the trailing edge of the V_{AB} pulse and the trailing edge of the next ϕ_T pulse.

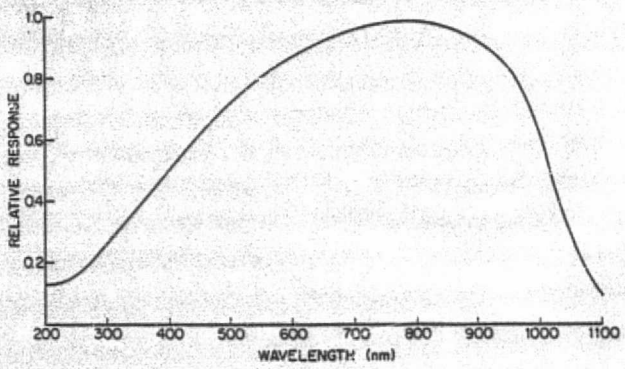

Figure 4. Relative spectral response

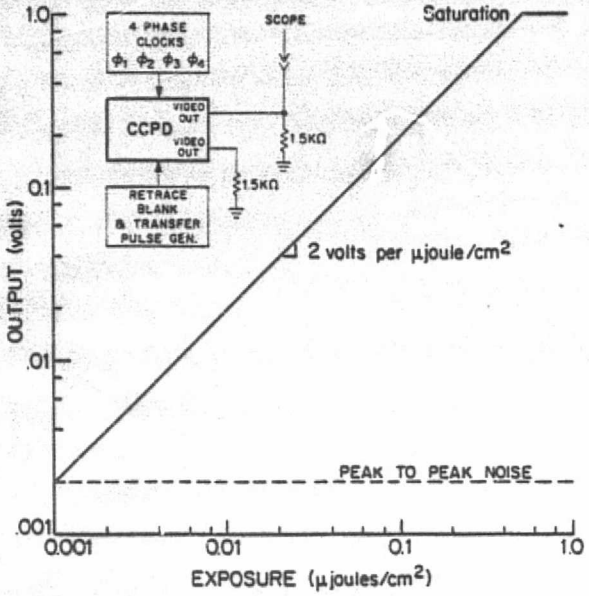

Figure 5. Typical transfer characteristic. Insert shows circuit used for noise measurement

PERFORMANCE

Typical performance characteristics are shown in Figs. 4 through 9. Spectral response shown in Fig. 4 is typical of high quality silicon photodiodes and does not exhibit the interference effects and loss of blue response characteristic of CCD sensors. Transfer characteristics showing the noise level, saturation, and the reciprocity between light intensity and integration time are shown in Figs. 5 and 6. It is obvious that longer integration times may be used to detect lower light levels. However, this approach is ultimately limited by dark leakage current which is integrated along with the photocurrent. At room temperature, dark current will contribute less than 1% of a saturated signal for integration times up to about 30 msec (corresponding to approximately 60 KHz scan rate for a 1728 element array). Figures 7A and 7B show dark scans at 1 MHz and at 100 KHz. The fact that dark signal remains negligible even at the lower scan rate is characteristic of the low dark current capability inherent in the CCPD technology.

Figure 8 is an oscilloscope photograph illustrating the full wave boxcar-type video output with a single cell illuminated by a 1/2 mil diameter light spot. The output impedance of the CCPD is shown in Fig. 9.

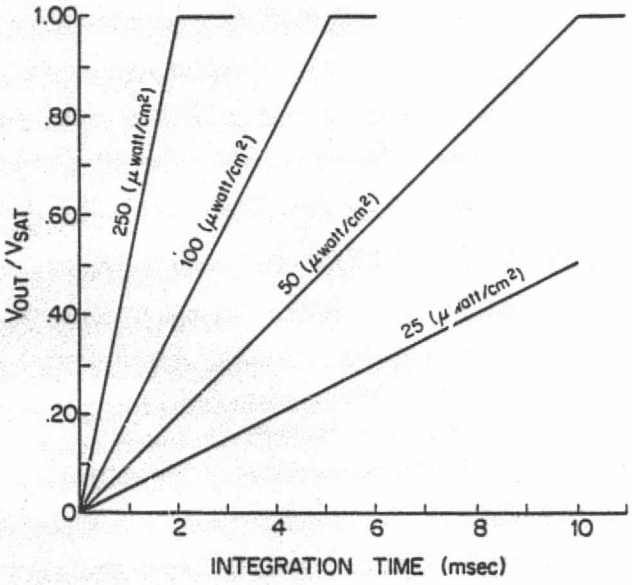

Figure 6. Output voltage as a function of integration time and light intensity (2870°K tungsten source measured using a detector with flat response and a 370 to 1040 nm bandwidth)

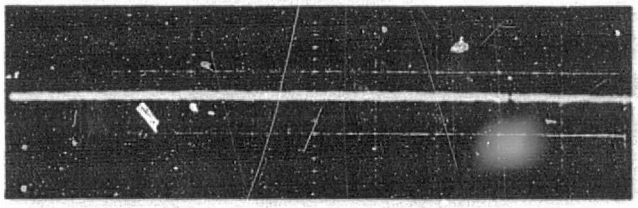

Figure 7A. Dark scan of CCPD-1728 at 1 MHz sample rate Circuit of Fig. 10, 50 mV/division.

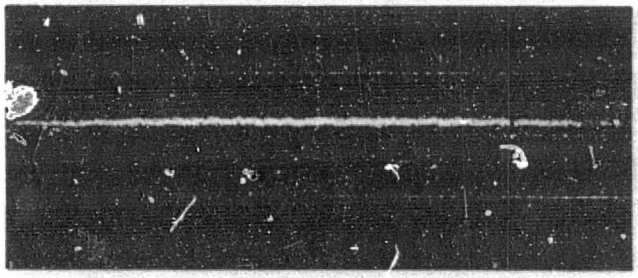

Figure 7B. Dark scan of CCPD-1728 at 100 KHz sample rate Circuit of Fig. 10, 50 mV/division.

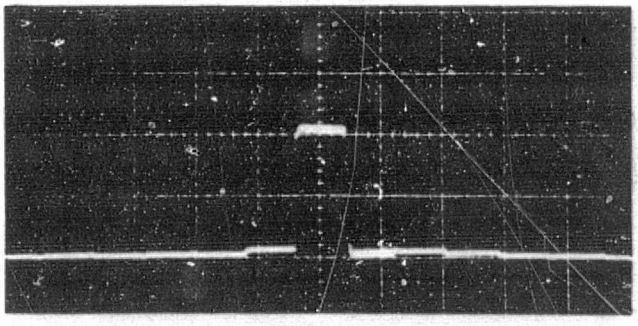

Figure 8. Expanded oscilloscope photograph showing video output waveform. Circuit of Fig. 10, 0.5 V per division.

CIRCUITS

A complete schematic diagram of a suitable evaluation circuit for the CCPD is shown in Fig. 10. This circuit requires +5 and ±12 volt power supplies. All clock phases are generated by dividing the master clock which can be set at any frequency up to 5 MHz. The transfer pulse ϕ_T is generated by counting clock pulses. The count may be set by rocker switches to vary the integration time, as desired, up to 2045 clock periods. The output circuit has a gain of 2 so that the saturation voltage is approximately 2 volts and the peak-to-peak noise level is approximately 4 mv. This evaluation circuit (Model RC701) is available from RETICON on a 4.5 x 5.6 inch printed circuit card.

ELECTRICAL CHARACTERISTICS

SYMBOL	PARAMETER		MIN	TYP	MAX	UNITS	NOTES
V_{RD}	Reset Drain Bias		–	12	–	Volts	
V_{DD}	Output Drain Bias		–	12	–	Volts	
V_{OG}	Output Gate Bias		–	2	2.5	Volts	
V_{IG}	Input Gate Bias		–	2	2.5	Volts	1
V_{AB}	Anti-Blooming Gate Bias		–	0	–	Volts	
V_{SUB}	Substrate Bias		-5.25	-5	-4.75	Volts	
$\phi_1, \phi_2, \phi_3, \phi_4$	CCD Transport Clocks	High	–	12	–	Volts	
		Low	-0.3	0	+0.5	Volts	
ϕ_T	Transfer Clock	High	3	5	7	Volts	
		Low	-5	-4	-3.5	Volts	
ϕ_{RE}, ϕ_{RO}	Reset Clocks	High	–	12	–	Volts	
		Low	-0.3	0	+0.5	Volts	
ϕ_{RG}	Receiving Gate Clock	High	–	12	–	Volts	
		Low	-0.3	0	+0.5	Volts	
f_s	Video Sample Rate		–	–	5	MHz	2

PERFORMANCE CHARACTERISTICS

SYMBOL	PARAMETER	MIN	TYP	MAX	UNITS	NOTES
DR	Dynamic Range	–	500	–	–	3
E_{NE}	Peak-to-Peak Noise Equivalent Exposure	–	1×10^{-3}	–	$\mu J/cm^2$	4
E_{SAT}	Saturation Exposure	–	0.6	–	$\mu J/cm^2$	4
	Spectral Response Range Limits	–	0.2–1.1	–	μm	
R	Responsivity	–	2	–	V per $\mu J/cm^2$	4, 5
	Photoresponse Non-Uniformity	–	±7	–	%	4, 6
V_{DARK}	Average Dark Signal	–	10	–	mV	7
	Dark Signal Non-Uniformity	–	10	–	mV	7
V_{SAT}	Saturation Output Voltage	–	1	–	V	5
P	Power Dissipation D.C.	–	70	–	mW	
R_O	Output Impedance	–	1500	–	Ohms	8
N_{PP}	Peak-to-Peak Noise	–	2	–	mV	9

1. The odd and even input gate biases may be adjusted differentially to achieve an odd/even balance in the video output.
2. The video sample rate is twice the frequency of the CCD transport clocks ϕ_1, ϕ_2, ϕ_3, and ϕ_4.
3. Dynamic range is referred to peak-to-peak noise. It is approximately 5 times higher when referred to rms noise.
4. Light source is a 2870°K tungsten lamp, measured using a detector with flat response and a 370 to 1040 nm bandwidth.
5. 1.5 Kohm load resistors and V_{DD} = 12 volts.
6. Measured with uniform illumination at approximately 50% of saturation.
7. At 20°C with 30 msec integration time. Dark signal and dark signal non-uniformity are proportional to integration time, and approximately double for every 7°C increase in temperature.
8. See Fig. 9.
9. Peak-to-peak noise is approximately 5 times rms noise.

TYPICAL CAPACITANCE DATA (10 Volts Bias)

CAPACITANCE	PIN NO.	CCPD 256	CCPD 1024	CCPD 1728	UNITS
ϕ_1	12	125	500	850	pF
ϕ_2 (each side)	8,15	35	135	225	pF
ϕ_3 (each side)	5,18	80	325	550	pF
ϕ_4 (each side)	7, 16	35	135	225	pF
ϕ_{RO}, ϕ_{RE}	4,19	3	3	3	pF
ϕ_T	13	20	80	135	pF
Video Outputs	2, 21	4.5	4.5	4.5	pF

ABSOLUTE MAXIMUM RATINGS (Above which useful life may be impaired)

Storage Temperature	−25°C to 100°C
Operating Temperature	−25°C to 55°C
Voltage on any pin with respect to substrate	−0.3 V to 18 V

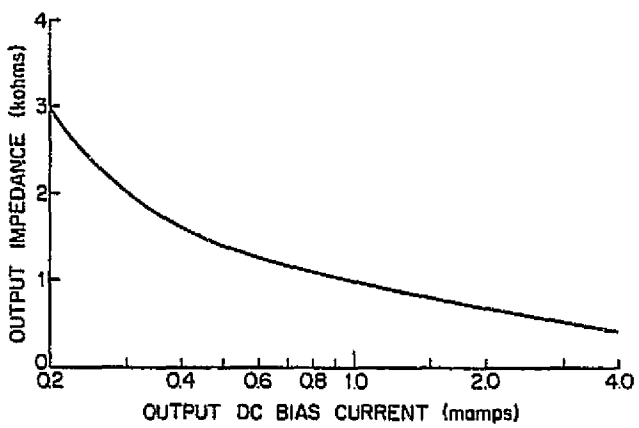

Figure 9. Output impedance as a function of dc bias current. With V_{DD} = 12 volts and R_L = 1.5 Kohms, the bias current is approximately 2 mA

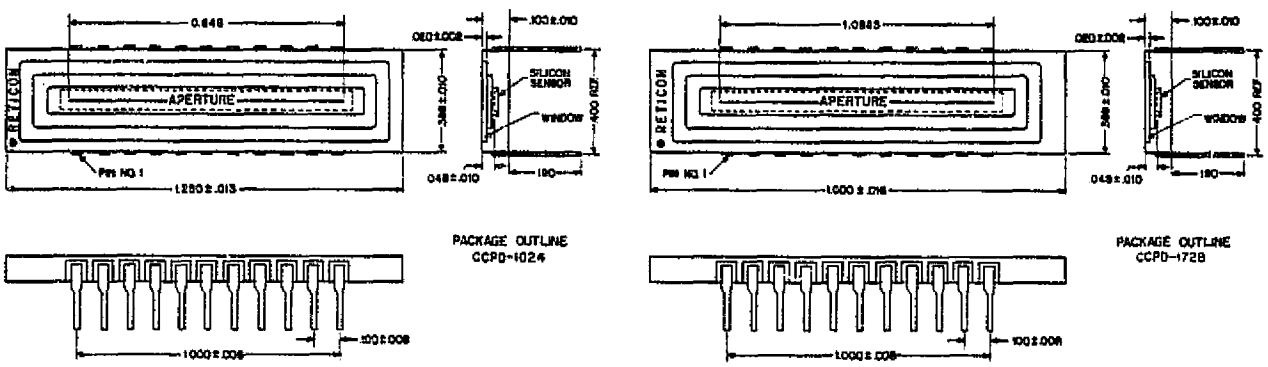

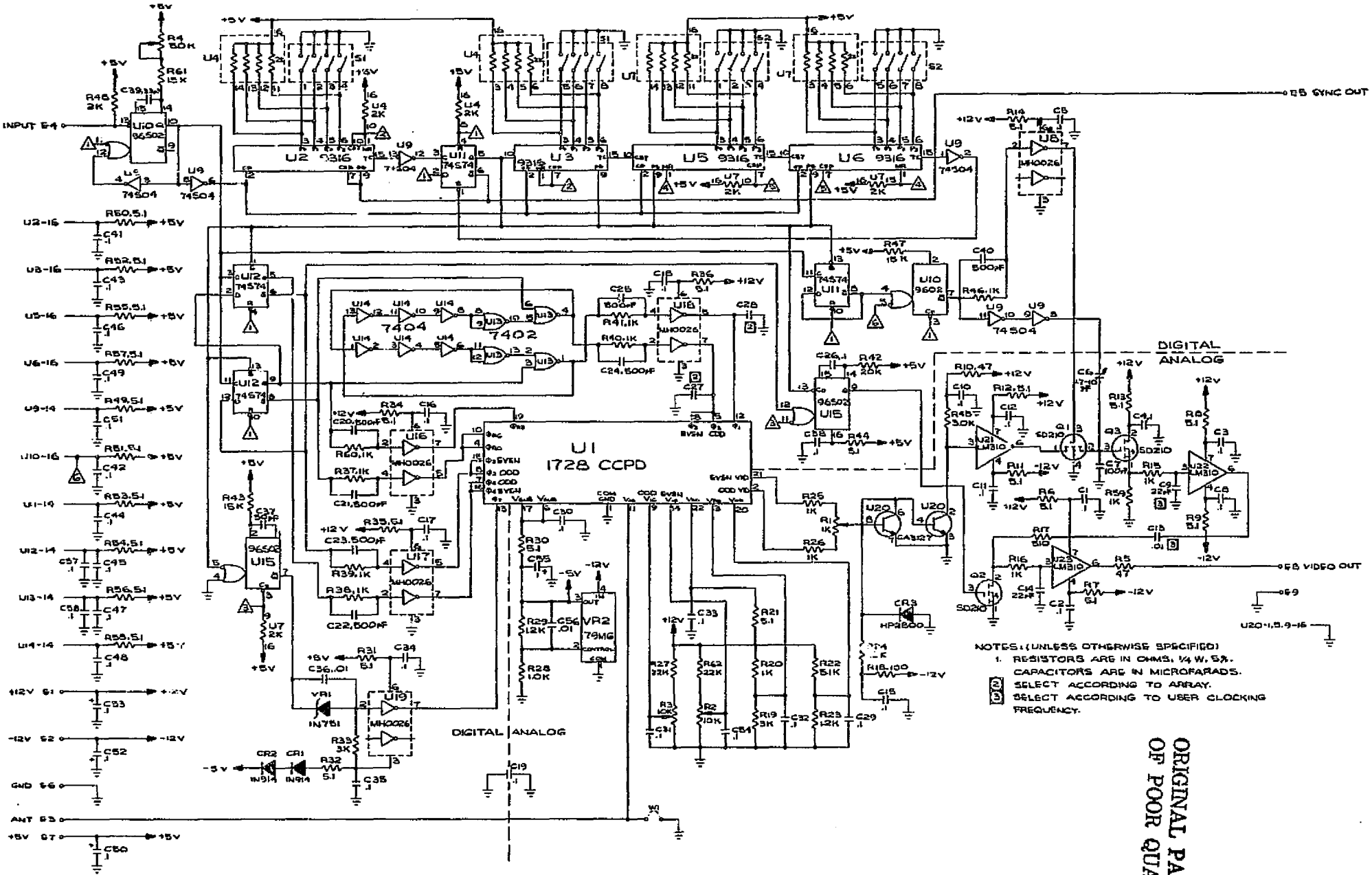

Figure 10. Model RC701 Evaluation Circuit, schematic diagram

ORIGINAL PAGE IS
OF POOR QUALITY

TRW

MONOLITHIC VIDEO A/D CONVERTER

ADVANCE INFORMATION

MODEL : TDC1007J

The TRW TDC 1007J is an 8 bit fully-parallel (flash) A/D converter capable of digitizing an analog signal at rates from dc to 30 megasamples per second (MSPS). It will accurately sample, without an external sample-and-hold circuit, input signals with frequency components up to 7 MHz (comparator 3 dB bandwidth of 35 MHz).

A single convert signal controls the operation of the unit, which consists of 255 clocked comparators, combining logic, and an output buffer register. Recovery from a full scale step input occurs within 20 nsec. Controls are provided for straight binary or offset 2s complement output coding, in true or inverted sense.

The TDC1007J is patented (No. 3283170), with other patents pending.

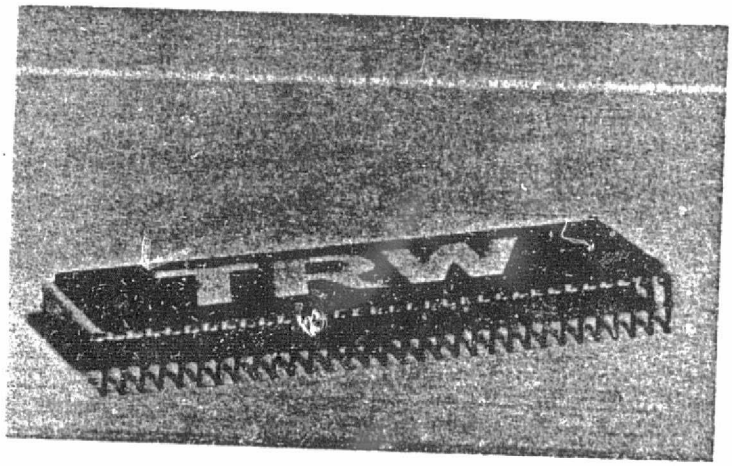

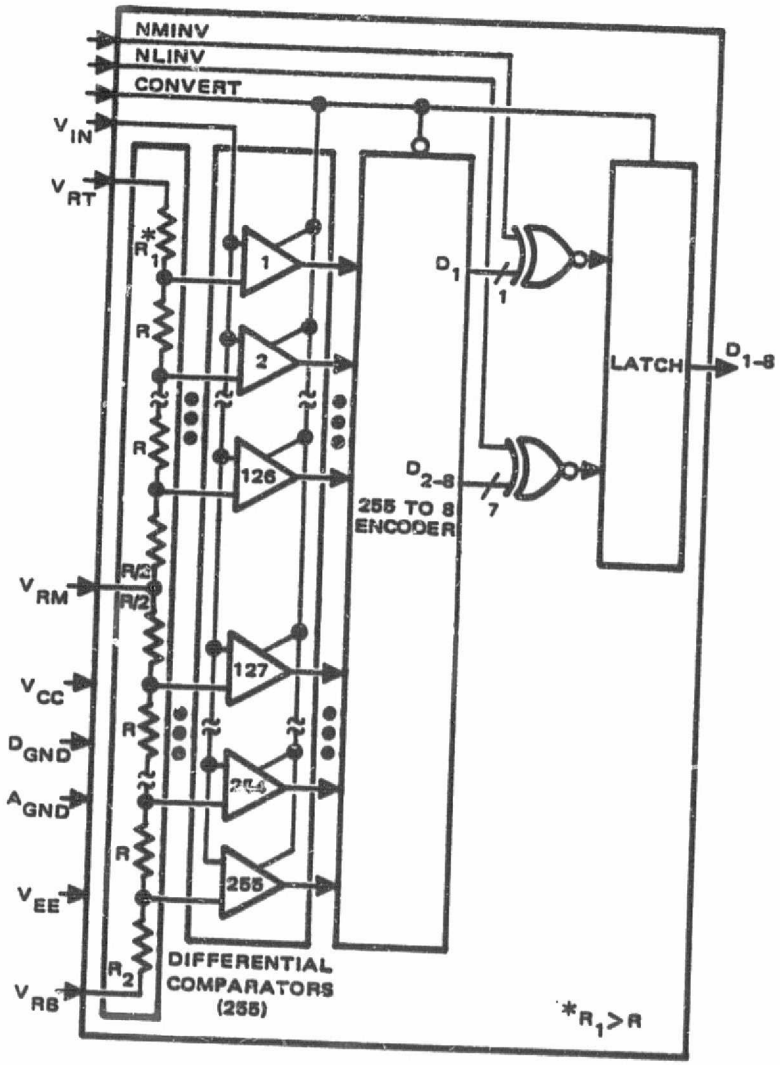

FEATURES

- 8 bit resolution
- 30 Megasamples/second
- No sample-and-hold circuit required
- Differential phase 1^o
- Differential gain 1%
- Binary or 2s complement output
- Monolithic, bipolar, TTL
- 64-pin ceramic DIP
- 2.0 W power dissipation

APPLICATIONS

- Video data conversion
  - 3X or 4X NTSC color
  - 3X or 4X PAL color
- Radar data conversion
- High speed multiplexed data acquisition

TRW LSI PRODUCTS
P.O. BOX 1125, REDONDO BEACH, CALIFORNIA 90278
(213) 535-1831

TDC1007J MONOLITHIC VIDEO A/D CONVERTER

SPECIFICATIONS

absolute maximum ratings

Supply voltage, V_{CC}	0.0 to +7.0 V
V_{EE}	0.0 to -7.0 V
Input voltage, digital	-0.5 to +5.5 V
analog; signal	+0.5 to -2.5 V
reference	+0.5 to -2.5 V
Output voltage	-0.5 to +7.0 V
Temperature, operating, ambient	0 to +70°C
junction	+175°C
lead, soldering (10 seconds)	+300°C
storage	-65 to +150°C

recommended operating conditions

Parameter	MIN	NOM	MAX	UNIT
Supply Voltage, V_{CC}	+4.5	+5.0	+5.5	V
V_{EE}	-5.75	-6.0	-6.25	V
Reference Input, V_{RT}	-1.1	0	+0.1	V
V_{RB}	-0.9	-2.0	-2.1	V
Operating Ambient Temperature Range	0	+25	+70	°C

electrical characteristics

Parameter	Test Conditions	TDC 1007 MIN	TDC 1007 NOM	TDC 1007 MAX	UNIT
V_{IH} High level input voltage		2.0			V
V_{IL} Low level input voltage				0.8	V
V_{OH} High level output voltage	V_{CC} = NOM, I_{OH} = -0.4 mA	2.4			V
V_{OL} Low level output voltage	V_{CC} = NOM, I_{OL} = 4.0 mA			0.4	V
I_{IH} High level input current	V_{CC} = MAX, V_{IH} = 2.4 V			75	µA
I_{IL} Low level input current	V_{CC} = MAX, V_{IL} = 0.4 V			-0.85	mA
I_{CC} Supply current	V_{CC} = MAX			25	mA
I_{EE} Supply current	V_{EE} = MAX		-300	-400	mA
R_{IN} Analog input impedance	V_{EE} = MAX	5.0		∞	KΩ
C_{IN} Analog input capacitance				300	pF
I_{BI} Analog input bias current	V_{EE} = MAX			0.5	mA
V_{IN} Analog input voltage		0.0		-2.0	V
I_{RT} Reference bias current	V_{EE} = MAX	16		30	mA
I_{RB} Reference bias current	V_{EE} = MAX	-16		-30	mA

switching characteristics, V_{CC} = 5.0, V_{EE} = -6.0 V

Parameter	Test Conditions	TDC 1007 MIN	TDC 1007 NOM	TDC 1007 MAX	UNIT
τ_{delay}, aperture delay			10		nsec
τ_D, digital output delay			30	45	nsec
τ_{PW}, convert pulse width		20			nsec
Maximum convert frequency		20	30		MHz

typical transfer characteristics over operating temperature range

Parameter	Test Conditions		UNIT
DC linearity errors		±0.5	LSB
AC linearity (Maximum spurious signal strength below full scale)	DC to 3.6 MHz*	55	dB
	3.6 MHz to 6 MHz*	50	dB
Noise power ratio	DC to 5 MHz white noise bandwidth, 500 kHz slot frequency	35	dB
Transient recovery time	Full scale step input	20	nsec

* Full scale input/rms noise

TRW | LSI PRODUCTS

ANNOUNCING

TDC1007J

A MONOLITHIC VIDEO A/D CONVERTER

AVAILABLE FOR DELIVERY IN APRIL 1978

PRICING

QUANTITY	1–9	10–49	50–99	100–499
PRICE	$745	$642	$558	$485

ALSO AVAILABLE

TDC1007PCB

FOR VIDEO A/D CONVERTER EVALUATION

A fully-tested printed circuit board containing the TDC1007J, a voltage reference, and a buffer amplifier to match the converter to 50, 75, 93, or 1KΩ. Input ranges of 1, 2, 5, and 10 V, positive or offset, are accommodated. Provisions are made for level shifting and gain adjustment. Power supplies of ±15 V and +5 V are required. The price is $845, including the TDC1007J.

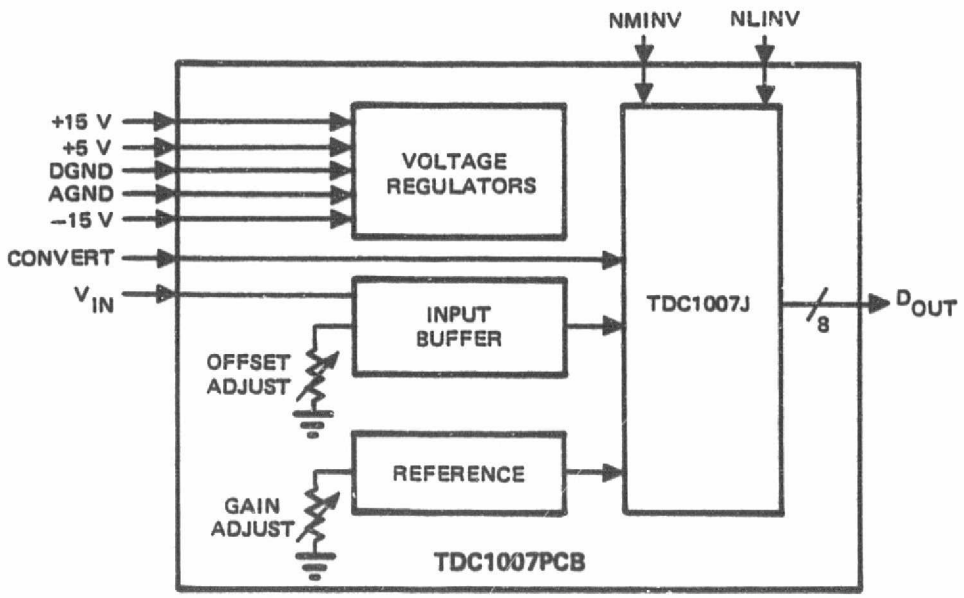

TRW LSI PRODUCTS
P.O. BOX 1125, REDONDO BEACH, CALIFORNIA 90278
(213) 535–1831

TDC1007J MONOLITHIC VIDEO A/D CONVERTER

PACKAGE INFORMATION

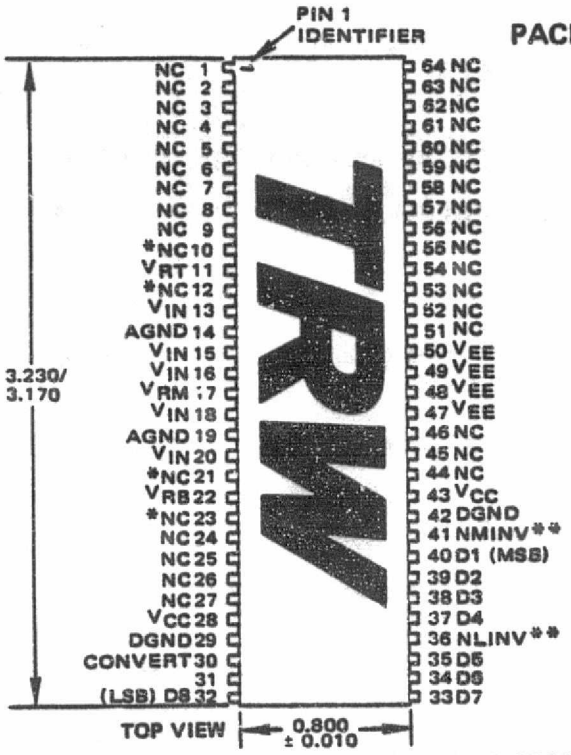

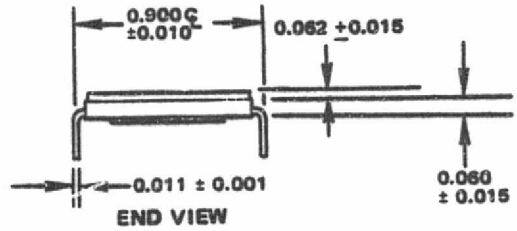

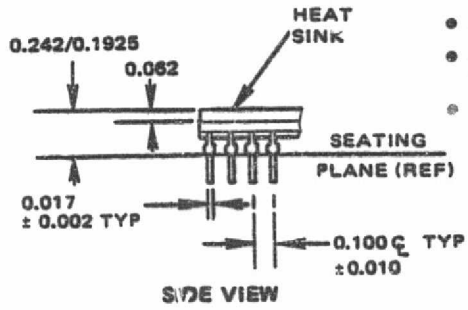

NOTES:

- DIMENSIONS IN INCHES
- ALL POWER AND GND PINS MUST BE CONNECTED.
- DGND IS +5V GROUND AND REFERENCES TTL I/O BUFFERS ONLY

*RECOMMENDED CONNECTION TO ANALOG GROUND FOR INTERELECTRODE SHIELDING

**CODE INVERSION INPUTS TIE TO +5 V FOR NORMAL OPERATION

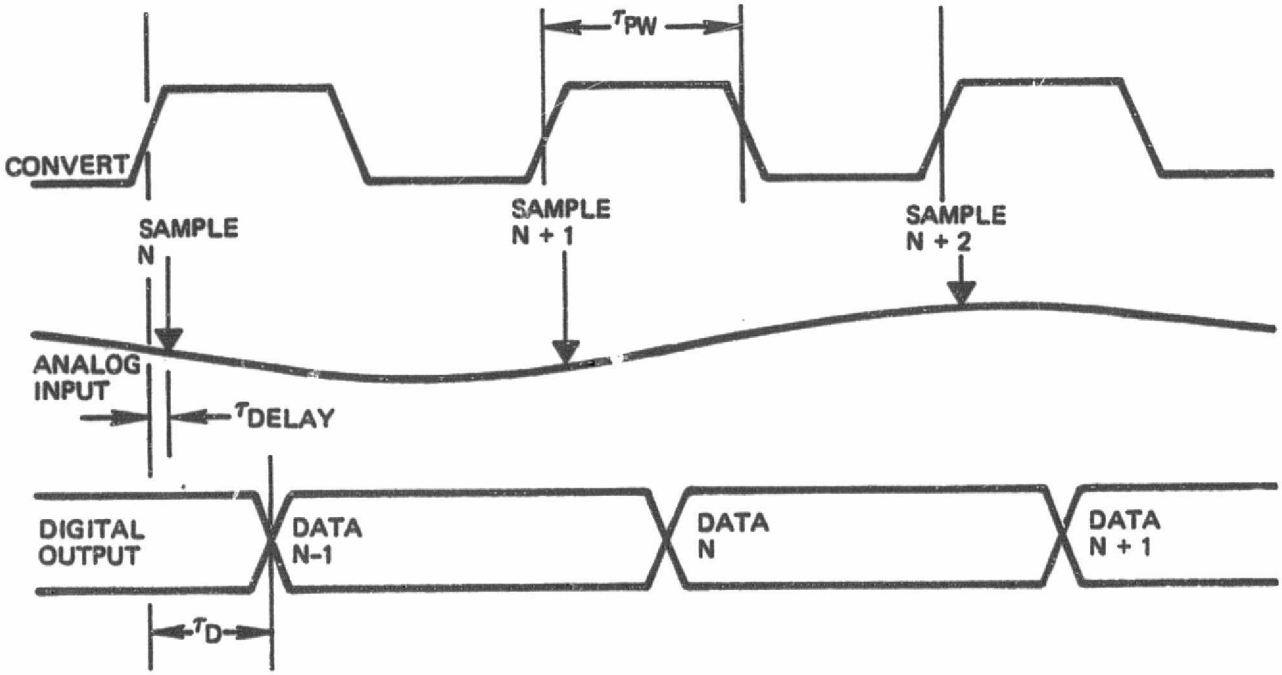

NORTH AMERICAN SALES OFFICES

ALABAMA, Huntsville	(205) 772-9656
ARIZONA, Phoenix	(602) 971-6250
CALIFORNIA, Los Angeles	(213) 478-0183
Menlo Park	(415) 321-9050
Tustin	(714) 832-4952
COLORADO, Westminster	(303) 426-0890
CONNECTICUT, Orange	(203) 795-3515
Rowayton	(203) 853-4466
FLORIDA, Ft. Lauderdale	(305) 721-1700
Orlando	(305) 857-3650
ILLINOIS, Elk Grove Village	(312) 593-0200
INDIANA, Fort Wayne	(219) 432-5591
Indianapolis	(317) 359-9283
Kokomo	(317) 453-3592
IOWA, Cedar Rapids	(319) 393-8703
KANSAS, Prairie Village	(913) 236-4646
Wichita	(316) 686-6685
KENTUCKY, Louisville	(502) 897-1569
MARYLAND, Baltimore	(301) 420-1241
MASSACHUSETTS, Waltham	(617) 890-3232
MICHIGAN, Grand Rapids	(616) 942-5420
Southfield	(313) 559-5454
St. Joseph	(616) 983-7337
MINNESOTA, Minneapolis	(612) 835-5454
MISSOURI, St. Louis	(314) 432-2830
NEBRASKA, Lincoln	(402) 474-5151
NEW MEXICO, Albuquerque	(505) 265-7759
NEW YORK, Rochester	(716) 461-3070
NORTH CAROLINA, Charlotte	(704) 527-1344
OHIO, Cincinnati	(513) 521-2290
Columbus	(614) 888-9396
Dayton	(513) 298-9546
Middleburg Heights	(216) 826-4424
OREGON, Beaverton	(503) 643-1644
PENNSYLVANIA, Bala Cynwyd	(215) 667-3400
Pittsburg	(412) 344-7277
TENNESSEE, Greeneville	(615) 639-6154
TEXAS, Austin	(512) 451-2959
Dallas	(214) 387-3030
Houston	(713) 772-5541
UTAH, Salt Lake City	(801) 943-5650
VIRGINIA, Richmond	(804) 288-8334
WASHINGTON, Bellevue	(206) 454-0300
WISCONSIN, Wauwatosa	(414) 475-7755
CANADA:	
MANITOBA, Winnipeg	(204) 775-3354
ONTARIO, Toronto	(416) 494-5445
QUEBEC, Montreal	(514) 341-6420

INTERNATIONAL SALES OFFICES

ARGENTINA, Buenos Aires	404122
AUSTRALIA, Kingsgrove N.S.W.	500111
AUSTRIA (See Germany)	
BELGIUM, Brussels	6600012
BRAZIL, Sao Paulo	2409211
DENMARK, Herler	842000
FINLAND, Helsinki	640641
FRANCE, Paris	7581111
GERMANY, Munich	503007
HONG KONG	281521
ISRAEL, Tel Aviv	444572
ITALY, Monza	360021
JAPAN, Tokyo	4615121
NETHERLANDS, Amsterdam	934824
NEW ZEALAND, Wellington	51279
NORWAY, Oslo	157550
SOUTH AFRICA, Capetown	457656
Johannesburg	6181027
SPAIN, Madrid	2425204
SWEDEN, Stockholm	248340
SWITZERLAND, Zurich	429900
TAIWAN, Taipei	7512062
UNITED KINGDOM, London	9025941

TRW LSI PRODUCTS
P.O. BOX 1125, REDONDO BEACH, CALIFORNIA 90278
(213) 535-1531

THE PERTEC T1000
BRINGING COST-EFFECTIVE VACUUM COLUMN TRANSPORTS TO DATA PROCESSING

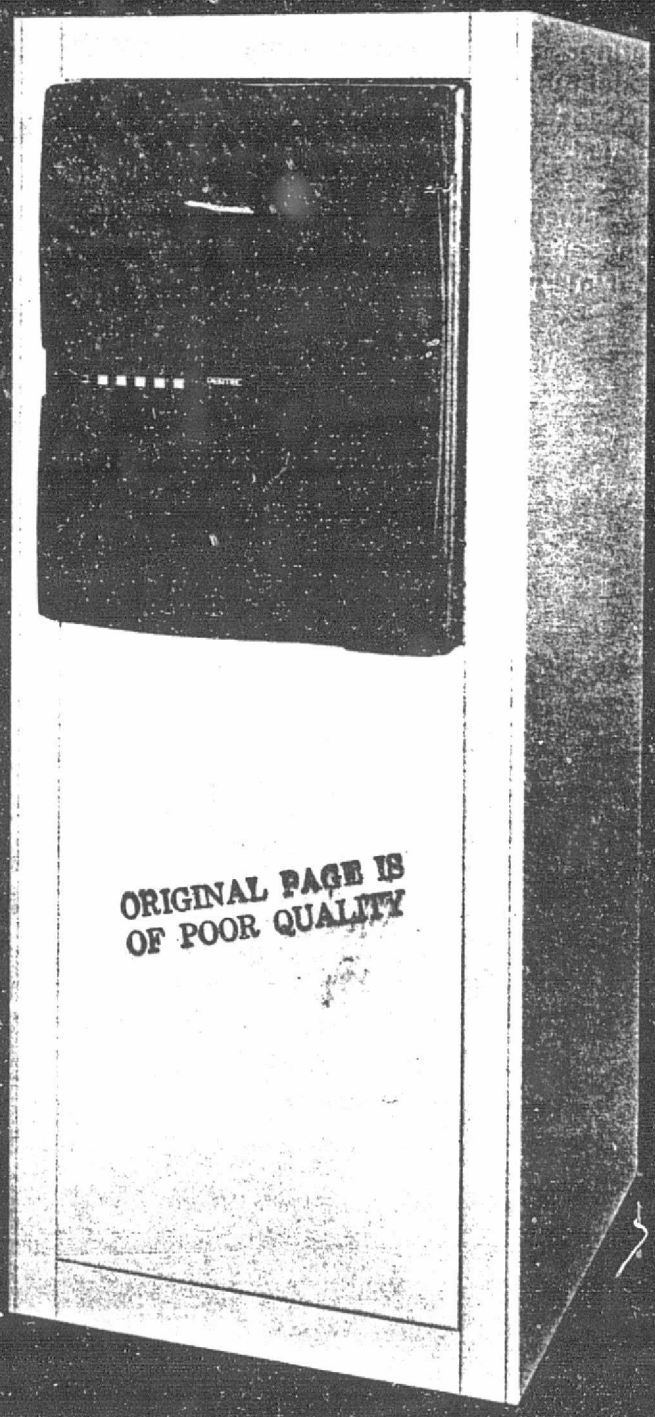

Jim Caporizo, Sales Engineer

PERTEC
a division of Pertec Computer Corporation

35 West Lane, Stamford, Connecticut 06905
Phone (203) 348-3949, [illegible]
Telex 965975

THE PERTEC T1000

The PERTEC T1000 Series Tape Transports are truly the world's first advanced design vacuum column transports. Specifically designed to meet today's and tomorrow's data processing system requirements, there's a T1000 to suit your OEM needs.

- **Standard Speeds from 1.905 to 3.175 m/s (75 to 125 ips)**
- **Dual PE/NRZI Format**
- **Dual GCR/PE Format**
- **Automatic Tape Threading**
- **Vacuum Capstan**
- **Air Bearings at All Turnaround Points**
- **Additional Buffer Pocket**
- **Optical Capstan Tachometer**
- **Automatic Load Point Seek**
- **Front Access to Electronics**
- **0.3- or 0.5-inch IRG Capability**
- **Optional Self-test Features**
- **Optional Internal PE/NRZI Formatter**

Performance You've Been Waiting For. Now you can have your choice of speeds, from 1.905 to 3.175 m/s (75 to 125 ips), to meet the application requirements of higher performance, minicomputer-oriented data processing systems. The T1000 Series is the perfect extension of Pertec's T9000 Series Vacuum Column Tape Transports which offer speeds from 0.952 to 1.905 m/s (37.5 to 75 ips).

The T1640 transports write and read 63 cpmm (1600 cpi) in PE format, and 32 cpmm (800 cpi) in NRZI format. The T1940 transports write and read 246 cpmm (6250 cpi) in GCR format, and 63 cpmm (1600 cpi) in PE format. You save the cost of separate transports for each format and have the media compatibility needed in today's market.

Smooth, Reliable Tape Handling. The exclusively designed Pertec vacuum capstan prevents tape slippage even with the short starts and stops required for 7.62 mm (0.3 inch) IRGs. There is no tape creep across the head in either on- or off-line modes. The vacuum capstan also smooths out acceleration and deceleration to provide maximum reliability and positive tape handling.

When unloading the tape, the vacuum is automatically turned off and the tape is slowly and quietly wound onto the supply reel, eliminating high-speed unload tape damage.

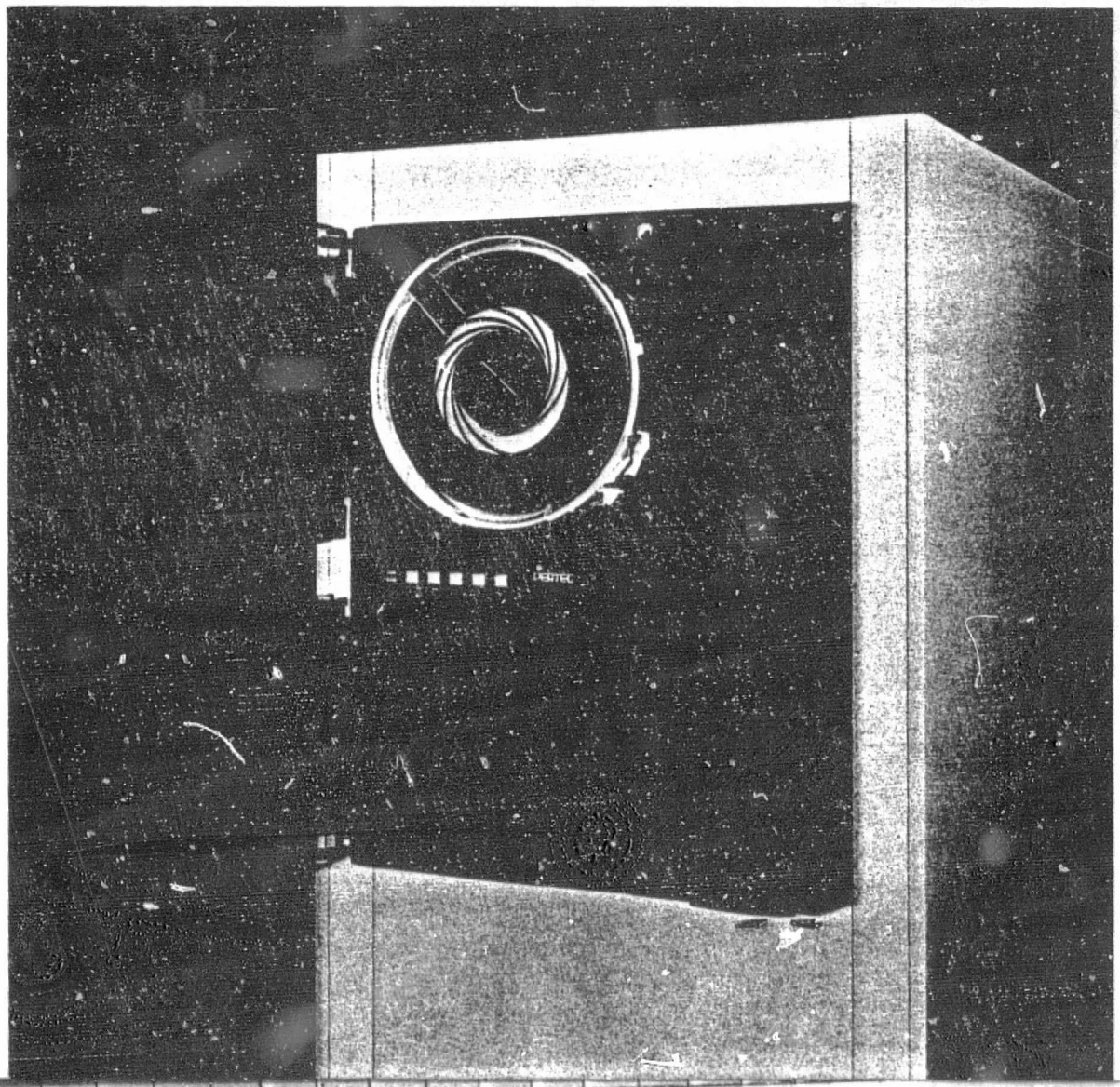

All vacuum column turnaround points use air bearings; ceramic guides are used at all critical tape edge points. During rewind, the tape path dynamics prevent tape from being in contact with the head. Thus, tape wear and system friction are minimized — assuring you better system performance.

By using the vacuum to draw particles from the tape and from the surface of the tape cleaner, you're assured effective tape cleaning and superb data reliability.

The Pertec exclusive additional buffer pocket provides additional tape storage for fast starts and stops. It also aids in providing the 7.62 mm (0.3 inch) inter-record gaps required for GCR. In addition, the buffer assures extremely low transient start/stop profiles.

The T1000 is the only transport in its class to use an optical tachometer in the capstan servo. This feature is generally found in servo designs of the more expensive plug-compatible type transports. The optical tachometer provides more positive speed control and precise controller reference when generating the short GCR gaps.

Pertec Reliability. The MTBF of the T1000 is greater than 2500 hours by design. No mechanical relays — no incandescent lamps. The use of solid state LED displays removes high-failure components from the system thus lowering maintenance costs.

Longer head life with far less downtime is obtained from Pertec's hard-coated, read after write head.

Reduced tape path and media wear is achieved by use of air bearings and ceramic guides.

Linear vacuum transducers operate on a vacuum differential providing linear operation of reel servos. This results in a more positive servo response and reduced power consumption.

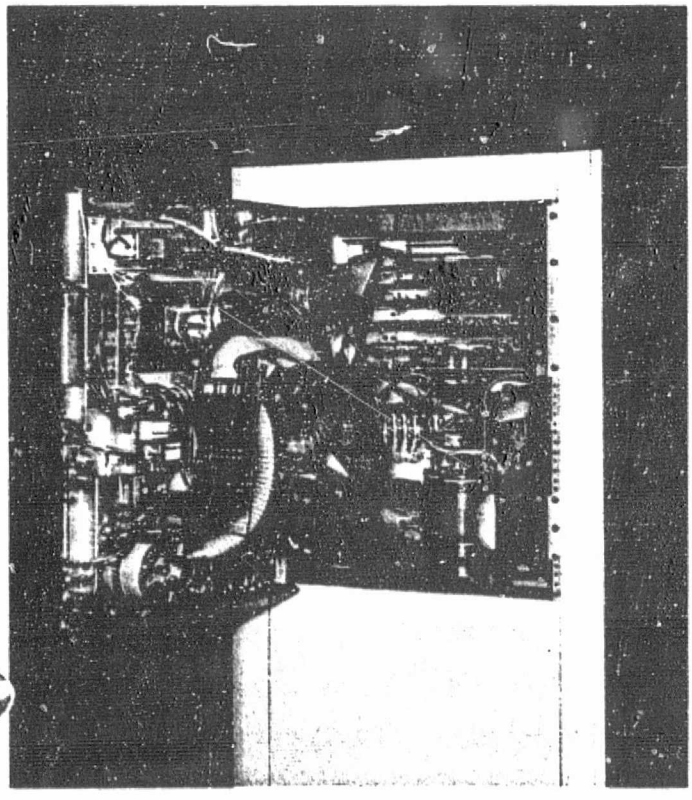

Customer Convenience. The T1000 automatically loads both Easy Load #1 and #2* cartridges. It also automatically threads 267 mm (10½ inch) open reels. Thus, your customer doesn't have to wait for the next reload or waste time threading tape. Reel sizes of 216 mm (8½ inches) and 178 mm (7 inches) are automatically threaded after tape has been manually placed in the loading slot. After the loading sequence is complete, tape will automatically seek load point.

A front panel 4-position select switch provides ease of address change.

Built-in daisy chain capability allows the T1000 to function in a multiple unit configuration.

Minimal dynamic skew is achieved by configuring head and tape guide geometry consistent with IBM and ANSI requirements. The head plate is adjustable for azimuth correction of skew.

Quality Assurance You Can Count On. On every product, Pertec pre-tests each circuit board and all critical components at the subassembly level. Prior to shipping, each T1000 Tape Transport is *burned in* for 40 hours minimum to force infant component failures to occur before shipment. Following quality control checkout, every T1000 must pass the fully computerized acceptance test criteria of our Quality Assurance Department. Only after vertification that all parameters of the performance specifications have been met is the T1000 approved for shipment to you. This care and attention assures you of a unit that will perform day after day, year after year.

Easy Serviceability. Modular electronics makes troubleshooting simple and reduces downtime and MTTR. All electronics and assemblies are accessible from the front to facilitate easy servicing. With Pertec's exclusive test plug on each module, fault isolation and repair of circuits has been greatly simplified.

Optional self-test maintenance controls can be built in to aid in adjustment of read pre-amp gains, skew window monitor, capstan and reel servo adjustments, and verifying that read and write circuits are functioning. This extremely sophisticated option makes adjustments easy and lowers your costs as well as your customers' cost of ownership.

For comprehensive unit troubleshooting, Pertec offers an external plug-in tester. This compact unit operates from the transport power. It has built-in capability to verify proper transport operation while in the off-line mode.

The maintenance manual shipped with each unit contains comprehensive operating descriptions, schematic drawings, and test and adjustment procedures to make repairs easy and economical.

Formatted Series. If you prefer, have Pertec supply an internal data formatter which contains the necessary data timing and control functions normally provided in an external tape control unit. Through the simplified data formatter interface, the user can transfer data to and from PE/NRZI transports without having to concern himself with any of the tape related housekeeping or data recovery logic. Since the interface is the same for the PE/NRZI formatter, only one control unit need be designed. Your local Pertec sales engineer can also provide you with the necessary formatter data.

* Easy Load #1 and #2 Cartridges are Registered Trademarks of IBM.

PERTEC

a division of Pertec Computer Corporation

9600 Irondale Avenue, Chatsworth, California 91311
Phone (213) 999-2020 / TWX 910-494-2093

WESTERN REGION SALES:
Irvine, California 91316, 17835 Ventura Boulevard, Suite 111 • (213) 996-1333 • TWX:910-493-2075
San Mateo, California 94402, 1670 Amphlett Boulevard, Suite 310 • (415) 349-9184 • TELEX 349389 DYNALOCSMT

CENTRAL REGION SALES:
Ann Arbor, Michigan 48104, 3001 South State Street, Suite 603 • (313) 668-7980 • TWX:810-223-2405
Rosemont, Illinois 60018, 6300 North River Road, Suite 102 • (312) 696-2460 • TWX:910-253-5918
Dallas, Texas 75240, 13500 Midway, Suite 403 • (214) 387-2817 • TWX:910-860-5236

EASTERN REGION SALES:
Hudson, New Hampshire 03051, 1001 Executive Drive • (603) 883-2100 • TWX:710-228-7681
Stamford, Connecticut 06905, 35 West Lane • (203) 348-3949 • TWX:710-474-3277
Malvern, Pennsylvania 19355, P.O. Box 229 • (215) 644-4910 • TWX:510-668-5034
Maitland, Florida 32751, 235 South Maitland Avenue, Suite 107 • (305) 647-6150 • TWX:810-853-5035

EUROPEAN SALES:
United Kingdom, 10 Portman Road, Reading, Berkshire RG3 1 DU • UK-Reading (734) 582115 • TELEX: UK-847101

Policy Note: Pertec reserves the right to change specifications at any time. It is Pertec policy to improve products as new techniques and components become available.

76813 (Revised 5-77)

Model Selection Chart and Data Transfer Rate

DATA FORMAT	DATA DENSITY	DATA TRANSFER RATE (KHZ)				MODEL NO.
		1.905 m/s (75 ips)	2.540 m/s (100 ips)	2.857 m/s (112.5 ips)	3.175 m/s (125 ips)	
PE/NRZI	63/32 cpmm (1600/800 cpi)	120/60	160/80	180/90	200/100	T1640-98
PE/NRZI	63/32 cpmm (1600/800 cpi)	120/60	160/80	180/90	200/100	FT1640-98*
GCR/PE	246/63 cpmm (6250/1600 cpi)	468/120	625/160	703/180	781/200	T1940-96

*Includes Internal Formatter.

Optional Features for Added Flexibility.
Self-test Maintenance Controls. For on-site verification of read and write circuits and adjustments.

Running Time Meter. Registers blower-on time for maintenance purposes.

Voltage Change. For the different international voltage requirements.

Customer Logo. We're proud of our name, but we'll insert your logo to enhance recognition of your company.

Industry Standard Interface. The T1000 Tape Transports use the same Pertec 3-connector interface which has been adopted as an industry standard. It is plug-to-plug compatible with Pertec T9000 Vacuum Column Tape Transports as well as our other transports. Also, the transport may be interfaced via 34-pin ribbon cable connectors for long cable lengths and built-in daisy chain capability.

Increase Your Sales and Profits by Building the Pertec T1000 Series Tape Transports Into Your Next System. If your systems move tape, look to the company that moves more tape transports than any other independent manufacturer in the world. If you're planning to penetrate the mini data processing market, you'll find that one of our basic configurations with available options offers you the best buy. In addition, our world-wide sales/service organization is ready to offer you added support when you need it.

Match the features, specifications, and benefits of the T1000 Vacuum Column Tape Transport with your system requirements. Call the Pertec sales engineer in your area — he's qualified to assist you in your selection of peripherals. Or, write PCC Pertec, 9600 Irondale Ave., Chatsworth, California 91311. For immediate assistance call (213) 999-2020.

Pertec T1000 Series Vacuum Column Tape Transport Specifications

Reel Size	178, 216, and 267 mm (7, 8½, and 10½ inch) Open Reels, or Easy Load #1 and #2* Cartridges
Number of Tracks	9-track, IBM Compatible
Recording Mode	GCR/PE or PE/NRZI
Data Density	246/63 cpmm (6250/1600 cpi) or 63/32 cpmm (1600/800 cpi)
Tape Speed	1.905, 2.540, 2.857, and 3.175 m/s (75, 100, 112.5, and 125 ips)
Instantaneous Speed Variation	±3% Forward and Reverse
Long Term Speed Variation	±1% Forward, ±2% Reverse
Start/Stop Time	1.5 ±0.1 msec in GCR mode at 125 ips or 3.0 ±0.35 msec in PE/NRZI mode at 125 ips
Start/Stop Displacement	4.83 ±0.51 mm (0.19 ±0.02 inch)
Rewind Time	80 seconds maximum; 65 seconds nominal
Tape Description	
Width	12.7 mm (0.5 inch)
Thickness	38.1 micrometers (1.5 mil)
Type	Computer Grade. ANSI Spec X3.40-1973
Environment	
Operating Temperature	5° to 44°C (40° to 112°F)
Relative Humidity	30 to 80% (non-condensing)
Altitude	0 to 2134 m (0 to 7,000 feet)
Mechanical Description	
Mounting	Standard EIA Rack Mount
Weight	113 kg (250 pounds)
Height	622 mm (24½ inches)
Width	483 mm (19 inches)
Depth (Behind Panel)	584 mm (23 inches); 635 mm (25 inches) for GCR
Electrical Description	
Electronics	All Solid State
Interface	DTL-, TTL-Compatible Logic (Low True)
Power	190/250v ac, 48 to 52 Hz or 58 to 62 Hz, 10A Continuous

*Easy Load #1 and #2 Cartridges are Registered Trademarks of IBM.

AMPEX

AR-1700
2-MHz/600-kHz airborne/mobile instrumentation recorder

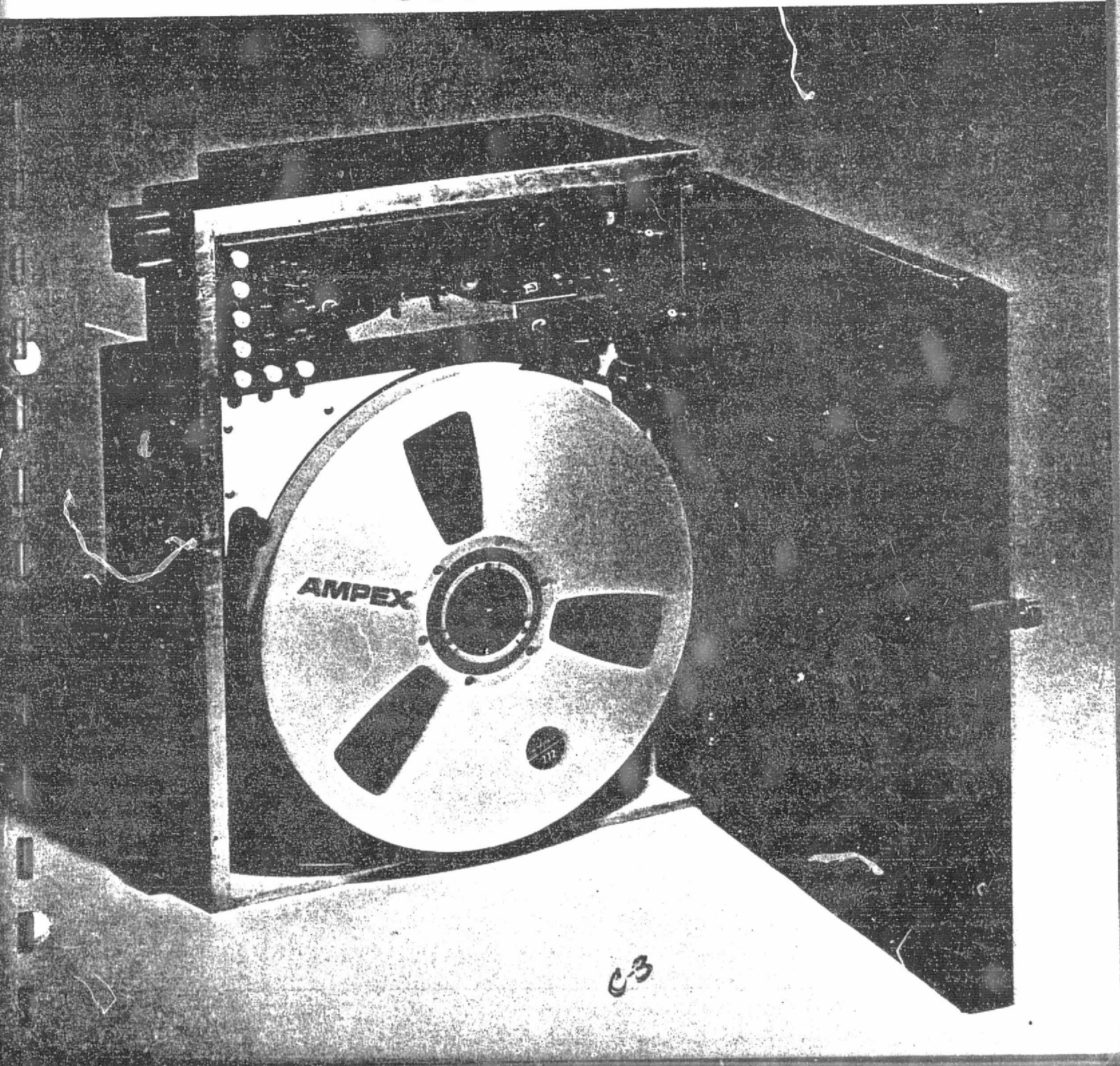

C-3

AR-1700

Extremely rugged multi-track intermediate or wideband recorder/reproducer with new versatility — new flexibility

- Third generation recorder of time-proven design — with new state-of-the-art improvements for more versatile, unparalleled performance.
- Major advancement in modular construction allows simplified maintenance — the AR-1700 can be disassembled and reassembled in less than an hour.
- Designed to meet MIL standards for airborne, shipboard or mobile applications.
- IRIG Wideband II and Intermediate Band signal electronics.
- Coaxial reel design saves space, allows use of large capacity 14-inch reels for long recording time, 100% more than 10½-inch reels.
- Closed loop drive for exceptional time base accuracy, low flutter, and jitter.
- Standard version for ½- or 1-inch tape (7 or 14 IRIG tracks), intermediate band or wideband (28 tracks also available on special order).
- Integral record electronics, reproduce heads and preamps. Separate modular reproduce electronics package available for adding full reproduce capability.

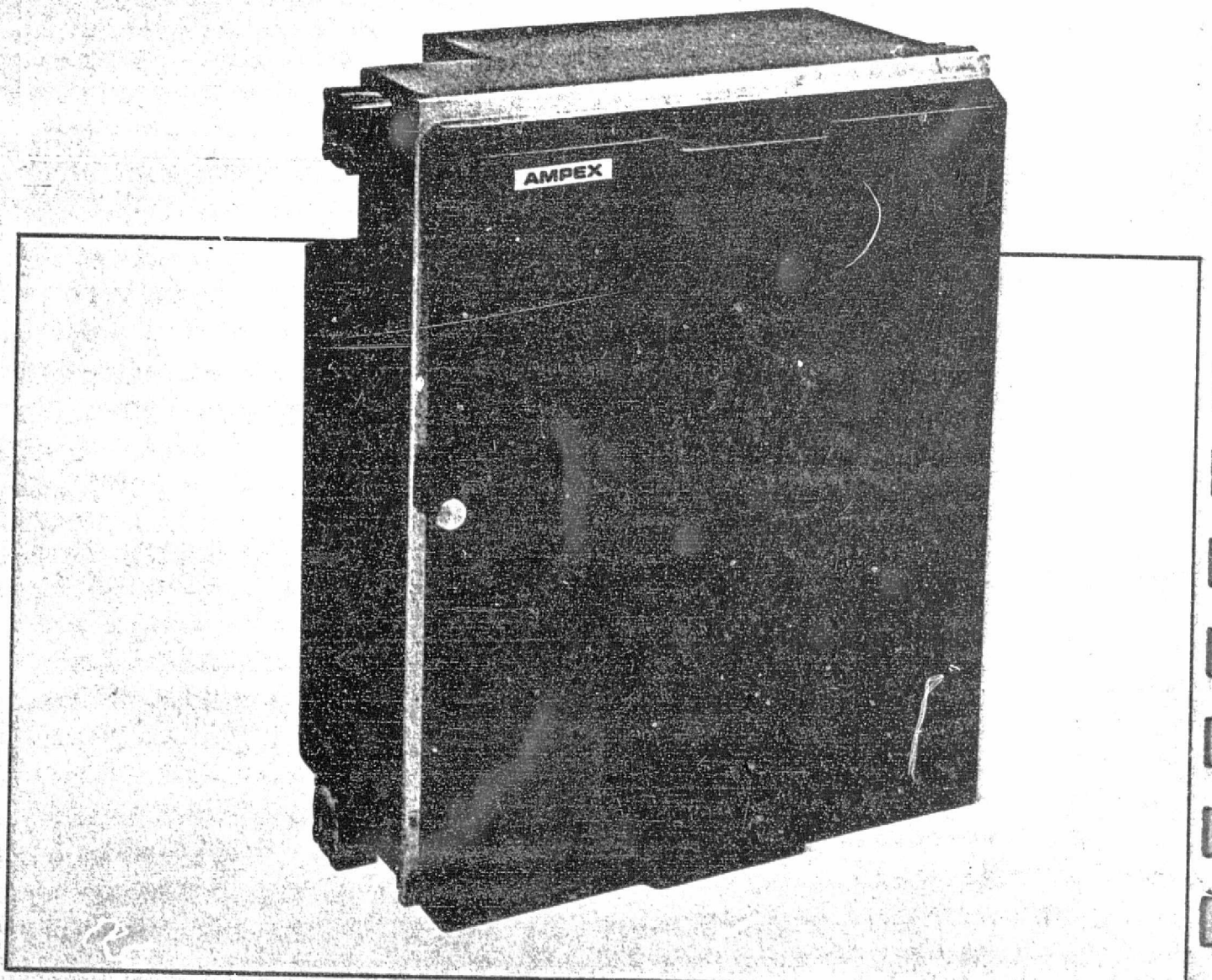

HBR-3000 System

AMPEX

For high bit rate data recording applications

U.S. GEOLOGICAL SURVEY TOPOGRAPHIC MAP 1:250,000

ERTS 0.8-1.1 μm IMAGE 27 JULY 72

Ampex HBR-3000 System - high bit rate (HBR) data recording for airborne or base applications

The recording of digital or digitized analog signals at high bit rates, with recording times of 20 minutes or more, is an established requirement for many commercial and defense applications. The Ampex High Bit Rate (HBR-3000) system has been developed to satisfy this requirement. Digitized signals are recorded in a space division multiplexed format on a conventional longitudinal recorder. During reproduce mode, the data is reassembled to its original format either in real time or at speeds compatible with data reduction devices. Conventional airborne or laboratory tape transports may be used along with proven digital electronics to provide the optimum systems approach to high bit rate recording.

Standard systems are available to accept either serial or parallel data streams at rates up to 96 Megabits/second. Higher rates are available on a custom basis. Incoming data is fanned out to the appropriate number of recorded tracks to maximize tape utilization. A single master channel for each group of 12 recorded tracks is used in conjunction with system generated sync information to minimize overhead requirements. Miller^2(M^2) coding is available to assure minimum error rate. Constant packing density on tape, an extremely valuable feature to minimize adjustments and to facilitate tape interchange, is achieved by controlling tape speed from the data clock. This frees the system from speed limitations imposed by VCO (voltage controlled oscillator) type systems. In the HBR-3000 system, response to data rate changes is limited only by the slew rate of the tape transport.

During reproduce, tape speed is also controlled by the data clock. Tape information is decoded and then deskewed to eliminate any transport/head generated time base errors. The multiplexed channels are then reformatted to the original input configuration. The Ampex HBR-3000 system has been designed to offer the utmost flexibility to meet the requirements of bit rate, record time and reliability.

Data format

The system provides for serial or parallel data streams alone or in combination. On a 14 track IRIG compatible record/reproduce system, a serial data stream is fanned out to a maximum of 12 data tracks with one track reserved as a master channel for deskew overhead.

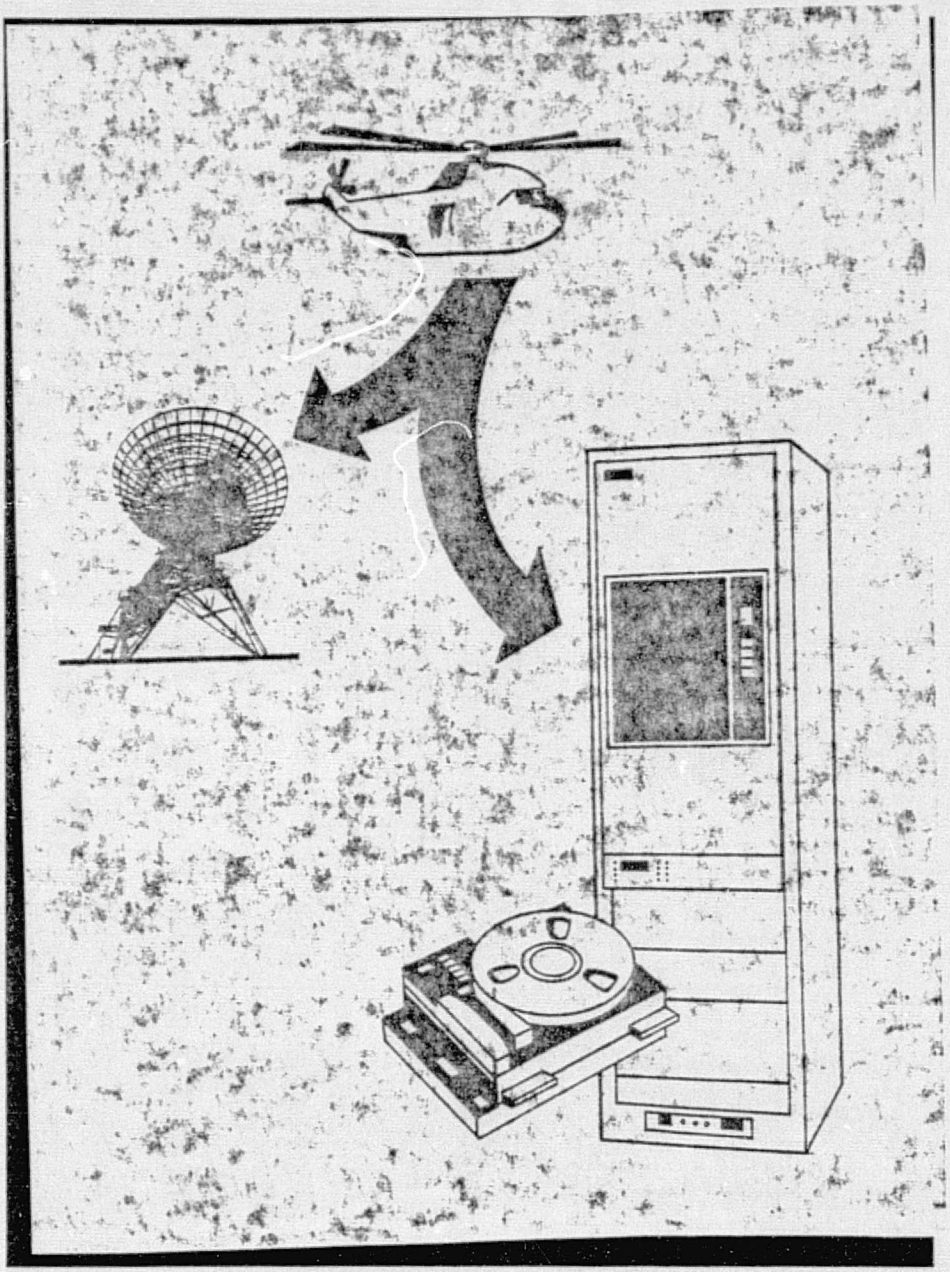

One additional track is available for voice or time code recording. If desired, the number of tracks utilized for HBR recording may be reduced, making additional tracks available for analog data recording as required.

If two or more serial data channels are required in the application, 28 track head configurations are available providing for 24 tracks of data, 2 master channels and 2 ancillary data channels. As in the 14 track configuration, HBR tracks may be replaced by analog data tracks as desired.

For parallel data applications, the HBR-3000 again offers optimum flexibility. Depending upon data reliability requirements, each track of the HBR-3000 system can accommodate up to 4 Megabits per second per channel.* As with the serial input system, up to 24 tracks are available on tape for data recording and a total data rate of 96 Megabits/second can be recorded at a packing density of 33.3 Kbits/inch* and a tape speed of 120 inches/second.

*User data bits as opposed to systems requiring overhead in data.

AR-1700

Extremely rugged multi-track intermediate or wideband recorder/reproducer with new versatility — new flexibility

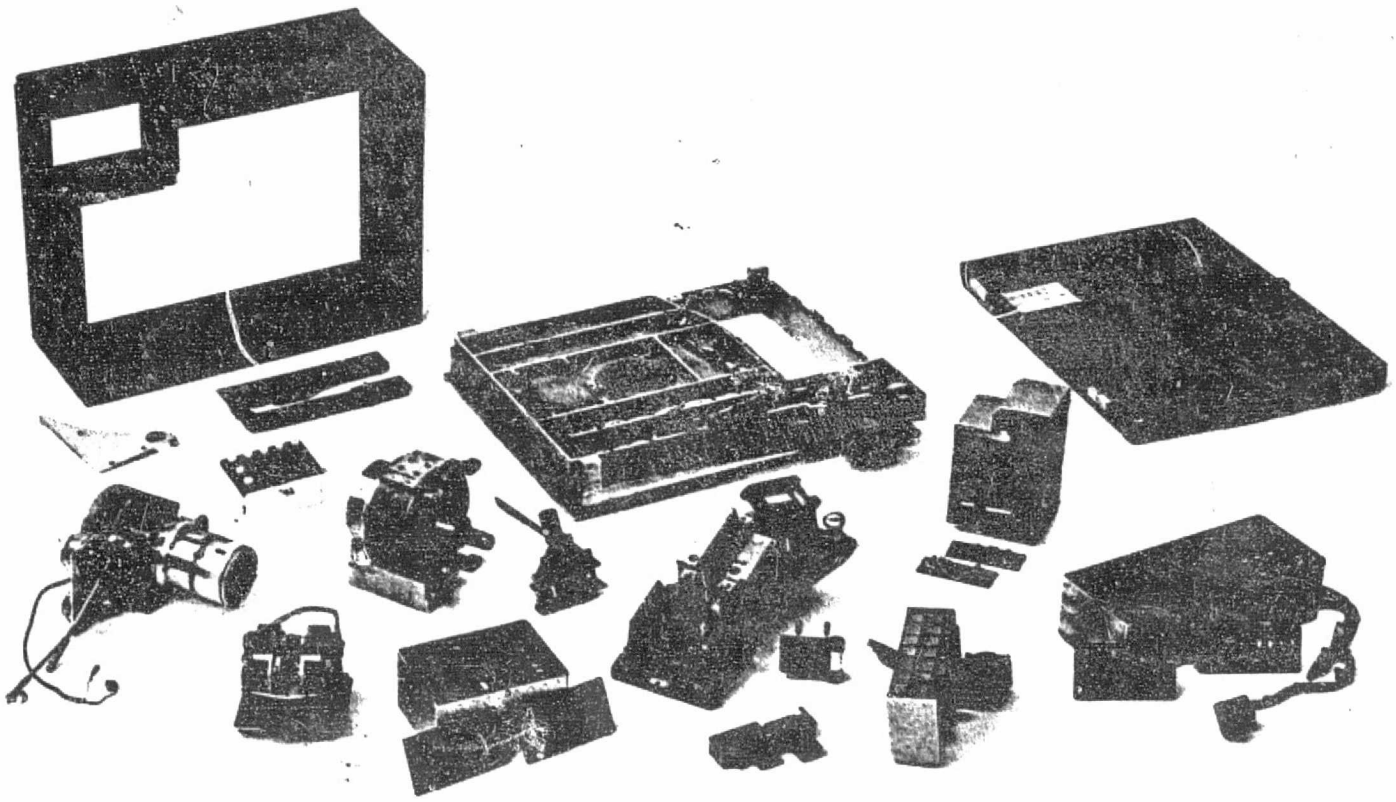

New concept in maintainability

The AR-1700 has been designed to place emphasis on configuration flexibility and maintainability through the use of total modular construction. All modular subassemblies are attached by quick release connectors. The AR-1700 can be disassembled and completely reassembled in less than one hour by a qualified field technician. Modular construction as designed in the AR-1700 greatly adds to the maintainability and reliability of the system and decreases "down time" if maintenance is required.

AMPEX

Ampex Corporation
Data Products Division
401 Broadway
Redwood City, California 94063
(415) 367-2011

U.S. Sales Offices:

ALABAMA, Huntsville (205) 837-3702. CALIFORNIA, Glendale (213) 240-5000, Sunnyvale (408) 733-2900. FLORIDA, Cocoa Beach (305) 783-1811. ILLINOIS, Elk Grove (312) 593-6000. MARYLAND, Bethesda (301) 530-8800. MASSACHUSETTS, Waltham (617) 890-2040. NEW JERSEY, Hackensack (201) 489-7400 (from New York City, phone 736-6116). NEW MEXICO, Albuquerque (505) 266-8749. OHIO, Dayton (513) 254-6101. TEXAS, Dallas (214) 637-5100, Houston (713) 774-8714.

International Sales or Service Companies:

ARGENTINA, Buenos Aires 46-9029. AUSTRALIA, Sydney 439-4077. BELGIUM, Nivelles 067 22 49 21. BRAZIL, Rio de Janeiro 242-3795. CANADA, Bramalea (416) 791-3100. COLOMBIA, Bogota 43 82 43 and 41 43 84. FRANCE, Boulogne 609 91 55. GERMANY (FEDERAL REPUBLIC), Frankfurt (Main) 60581. GREECE, Athens 67 78 160. HONG KONG, Kowloon K 678051-3. ITALY, Rome (06) 51 38 341, Milan 02 165 15 41 2 3 4. JAPAN, Tokyo 03 264-7331. LEBANON, Beirut 340-820. MEXICO, Mexico City 539-68-70 71 72. NETHERLANDS, Utrecht 030-61 29 21. SOUTH AFRICA, Johannesburg 838 7640. SWEDEN, Sundbyberg 08 28 29 10. SWITZERLAND, Fribourg 037 22 73 31. UNITED KINGDOM, Reading, Berkshire (0734) 85200.

PRINTED IN U.S.A.—D139R—11/76

ELECTRONICS AND HEADS

State-of-the-art design for signal compatibility and accuracy.

The new AR-1700 electronics take advantage of the latest solid-state technology to insure maximum reliability over a wide range of temperature and operational extremes. Highly reliable microcircuits are used whenever possible. All electronics boards are small, lightweight, require low power, and are easily removed for service.

2 MHz for improved predetection capability.

Two different signal electronics are available: Intermediate Band electronics and Wideband II electronics. Intermediate Band electronics (600 kHz at 120 ips) use a single operational amplifier design allowing greater density in packaging so that up to 28 IB tracks can be installed within the transport enclosure. Wideband electronics increase frequency response to 2 MHz at 120 ips. The 2-MHz recording capability is essential to preserve sidebands in predetection recording and for many pulse recordling applications.

Standard AR-1700's can be supplied with reproduce heads and preamps for signal monitoring and reproduce electronics interface. Record electronics for six-speed operation are included in each module. All six speeds are electrically switchable from the front panel transport speed selector or from an optional remote control unit.

IRIG compatible heads

The heads are IRIG compatible with either 7- or 14-track configurations for ½- or 1-inch tape. Intermediate band 28-track heads (1-inch tape) are also available.

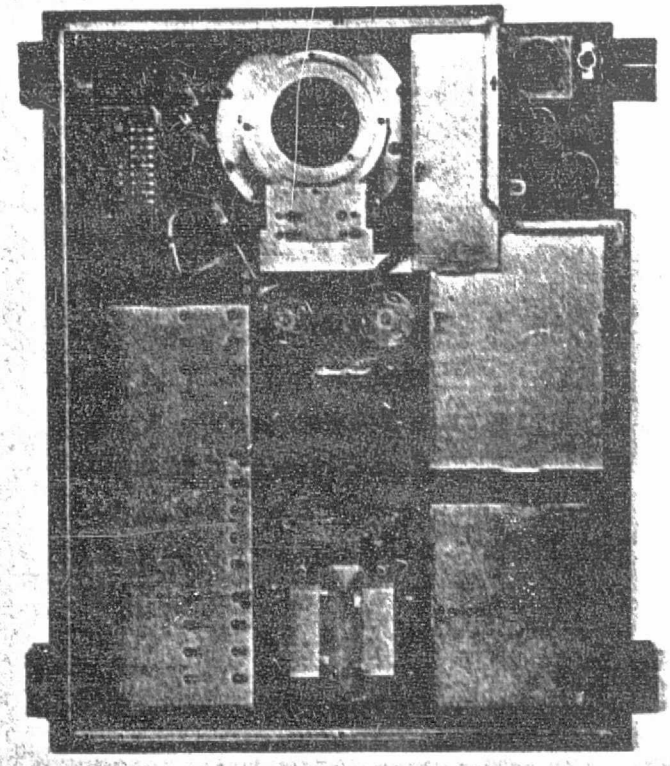

Access to AR-1700 electronics card racks is from rear of transport. Up to 28 tracks of IRIG Intermediate Band Direct Record Electronics may be mounted in the AR-1700.

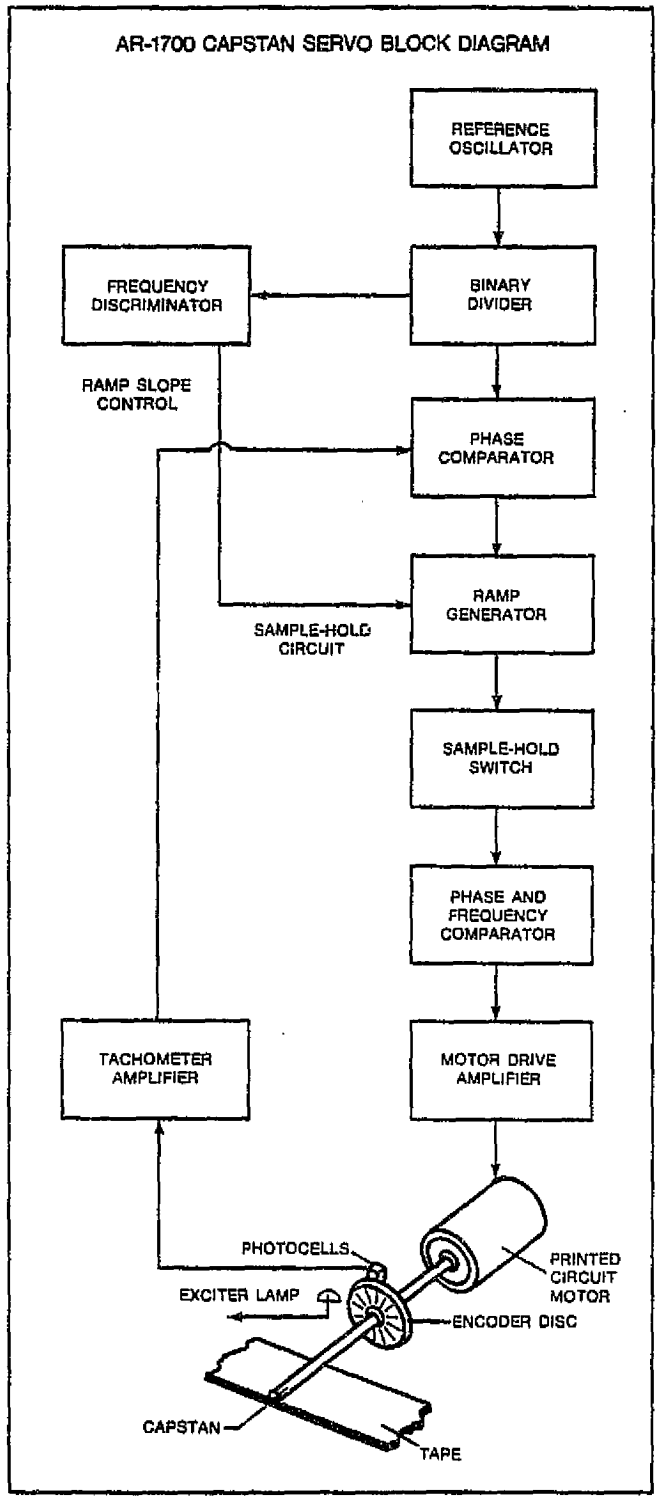

HIGHLY ACCURATE TAPE SPEEDS WITH ADVANCED CAPSTAN SERVO

The capstan servo is a phase comparator, sample-and-hold system that maintains a constant capstan rotational velocity and thus a constant tape speed. The servo maintains constant capstan speed by comparing the output of a tachometer encoder disc mounted on the capstan shaft, with an output derived from a crystal controlled oscillator. By comparing the frequency and phase of the integral reference with the frequency and phase of the tachometer signal, an error signal is generated and used to control the current to the capstan motor and therefore, tape speed and position.

AMPEX

May 15, 1978

Mr. David Zink
Barnes Engineering Corp.
30 Commerce Road
Stamford, CT 06904

Dear Dave:

We are enclosing some preliminary information on the Airborne High Density Digital Recording System for your scanner. The Ampex AR-1700 is the recorder we discussed but will be integrated with the Miller Digital Recorder Electronics to handle a 3.25 Mb/s per system stream.

We have a Monitor Box which is roughly half the size of the AR-1700 package to select the individual channels recorded. In other words, we can provide the recording system in (3) packages consisting of:

The basic recorder
The Digital Electronics, and
The Monitor Box.

All you have to provide is the sync clock and the data to be recorded.

If you have any further questions, please do not hesitate to give us a call or Mr. Jim Kelly at 301-530-8800.

Yours very truly,

AMPEX CORPORATION

Fred S. Korb

FSK:rlc

Encl.

cc: J. Kelly

Ampex Corporation • 75 Commerce Way • Hackensack, New Jersey 07601
Telephone (201) 489-7400 • N.Y. (212) 736-0116 • TWX 710-990-5143

Constant packing density

For maximum recording efficiency with minimum adjustment and reliable tape interchange, the HBR-3000 system design provides for a constant packing density on tape regardless of input data rate variations.

The Ampex HBR-3000 employs the use of the input data clock to generate a tape speed reference. If the input rate varies, the tape speed is varied to insure a constant packing density on tape. This not only provides for the maximum recording time for the packing density selected, but once set up, to reproduce a particular data rate. Other data rates may be recorded and reproduced at that data rate with no additional set-up/adjustment required.

Low bit error rates (BER)

The bit error rate (BER) in any high density digital system is a function of many variables that must be of concern to the system designer. These include the type of tape used, track width and response of the head assembly, bit packing density, type of coding used, transport skew characteristics and the nature of the data being recorded.

The BER requirements of any given application may vary according to the application and the user should be able to select those parameters critical to his application. The Ampex HBR-3000 system provides the widest range of selectivity of key elements effecting BER.

No data pattern sensitivity

In digitizing slowly changing sensor data, or pictorial data from TV, radar or satellites, repetitive patterns rich in low frequency components are generated. Unless compensated for, these data patterns produce high bit error rates and loss of essential data when recorded and reproduced on magnetic tape.

Ampex has developed the M² coding technique to completely eliminate the DC pattern sensitivity usually associated with recording NRZ derived codes. Coded data is faithfully recorded on tape regardless of data pattern; during reproduce, data is decoded and returned to the user in its error free form. No sophisticated DC restoration circuitry is required. Only the Ampex HBR-3000 offers this feature.

Time base expansion

If the data reduction facility is not able to cope with the extremely high data rates at acquisition, then time base expansion is an essential requirement of a high bit rate system. The Ampex HBR-3000 system takes advantage of the constant packing density on tape and makes use of an externally generated data clock to control tape speed in the reproduce mode. Thus, the HBR-3000 system is able to supply electrically switchable output rates, matched to the exact user requirements, without system adjustment.

Ancillary data channels

In addition to the digital data stream, time code reference and other ancillary data may be required. The Ampex HBR-3000 system offers flexibility in terms of track allocation and the use of conventional analog record/reproduce electronics.

Machine/machine compatibility

Whether the application involves airborne data acquisition for ground reproduction, or strictly a lab environment operation, machine to machine compatibility is an essential requirement of a high density record/reproduce system. The Ampex HBR-3000 system insures this compatibility in two ways. Track registration is a function of closely maintained head tolerances and tape transport dynamics—both products of Ampex experience for over 25 years. The second essential ingredient to machine compatibility is constant density recording on tape. All alignments, equalization and variables associated with changes in data rates are located in the reproduce side of the system, thus insuring faithful reproduction regardless of recording conditions.

Application flexibility

Whether the need is to record a high bit rate serial data stream from a satellite, a digitized video signal from an optical scanner, or simply to improve signal to noise ratios by increasing data word lengths, the Ampex HBR-3000 offers the flexibility to cope with changing requirements as they develop. Consider the following:

- The ability to accept either a serial or parallel data stream by merely pressing a button.
- The assurance of constant packing density on tape as input data rates vary or change.
- The simplicity of changing packing density by switch selection should a change in record time or margin be desired.
- The availability of a digital bit synchronizer/decoder which permits the reproduction of data in real time or at some non-binarily related data rate.
- The ease of system expansion or modification by adding the required electronics cards.
- The confidence of machine-machine compatibility.

FLEXIBILITY—that only comes from years of experience in instrumentation magnetic tape recording.

Human engineering

The HBR-3000 system has been designed for operation on a day to day basis by personnel who have limited experience with this type of equipment. During critical stages of a mission, little time is available for tape recorder "fiddling." The HBR-3000 system design has taken these factors into account. Wherever possible, alignment and adjustment have been eliminated. A simplified on line diagnostic/mode select panel is provided for verifying key operating parameters. Easily readable indicator lights give an instantaneous readout of system performance at any time. The HBR-3000 system has been designed by experienced engineers for use by inexperienced engineers!

Ampex high performance transports – PLUS – Ampex HBR-3000 electronics

FR-3000—advanced design laboratory recorder

High performance, the utmost in data reliability and long term trouble-free operation—these are advantages which for years have been taken for granted by users of this top of the line Ampex Instrumentation recorder. HBR-3000 High Bit Rate systems for ground installation use this well proven tape transport to achieve the high packing density/low error rate performance required in today's digital instrumentation applications.

The FR-3000 transport affords cross-play compatibility with all other Ampex portable or stationary instrumentation recording systems, including airborne equipment and IRIG compatible recorders.

Digital interface

The Digital Process Bay in the HBR-3000 systems provides the interface between the multiple serial or parallel NRZ data streams and the record/reproduce electronics. In the input mode, data is fanned out to the appropriate number of data tracks, prior to encoding and sync insertion, to insure maximum recording efficiency on tape. During reproduce, deskewed data is reformatted to its original NRZ format, time base corrected to the user clock, thus providing a true user transparent system.

AR-700/1700—rugged, proven airborne recorders

For airborne high bit rate digital data acquisition applications, HBR-3000 electronics can be used in conjunction with AR-700/1700 tape transports designed for hostile environments. The digital electronics are contained in a separate shock mounted unit which may be located where desired.

These advanced transports of proven design and performance offer reduced size and weight, lower power consumption and increased versatility and reliability. Recording time of 15 minutes or more is available at full bandwidth; longer times are proportional to reduced tape speed/bandwidth requirements.

Airborn digital interface

This shock mounted assembly provides the digital interface between the airborne recorder and the digital data stream. The unit accepts the serial or parallel NRZ data plus clock, adds sync information, creates the necessary master channel and encodes the data prior to recording.

The airborne HBR-3000 systems also include a reproduce monitor amplifier and a 14 x 1 or 28 x 1 switch permitting selection of any track for monitor/verification purposes. This monitor capability greatly facilitates set-up and maintenance of the airborne system.

HBR-3000 system block diagram

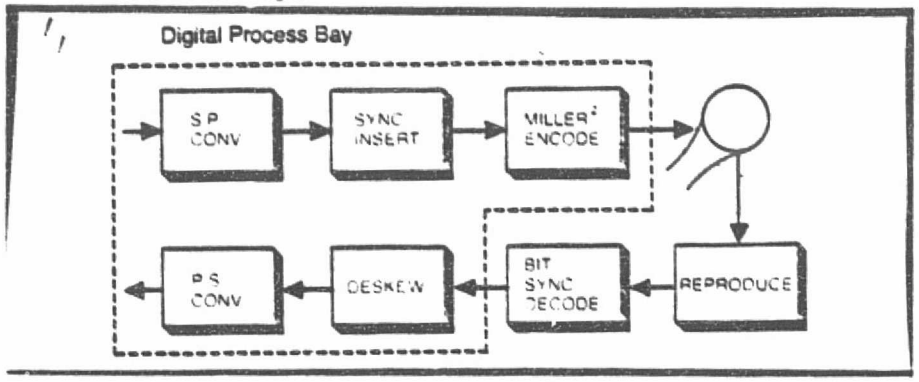

The HBR-3000 electronics—key to reliability

The HBR-3000 system is an electronic system designed to accept digital data in the high megabit range for recording on airborne or laboratory tape transports. The system features high packing density recording for maximum record time, Miller or M² coding for minimum error rates, and variable time base expansion for ease of data reduction. Incoming data—serial or parallel—is fanned out to optimize tape track utilization. Sync information is added and data is encoded prior to recording on tape. In the reproduce mode, signals are amplified, decoded to NRZ-L format, and sync is removed as part of the deskew process prior to parallel-serial conversion.

Digital process bay

Each bay will service up to 12 digital data tracks and contains the serial-parallel converter, sync insertion, Miller/M² encoders, deskew and parallel-serial printed wiring assemblies.

Serial-parallel converter. Each digital Process Bay contains a single serial-parallel converter PWA. Input data streams and data clock are fed to the converter for fanout as required. Each board contains a DIP switch which programs the number of tracks on tape for digital data as required by the application. Data clock information is also used to derive a capstan drive signal allowing the system to track the incoming data and provide a constant bit packing density without operator intervention.

Sync Inserter. Prior to recording, data is formatted to allow for deskewing by inserting sync words into each track every 512 bits: On inserting the sync word, data at that point is transferred to a master channel or overhead track. One overhead track is used for up to twelve data tracks, one sync inserter PWA is included in each Digital Process Bay.

Encoder. The M² Encoder PWA contains hybrid encoders capable of generating either Miller or M² coded data streams to the head drivers. The selection of codes to be used is programmable at the user's option, although at high packing densities the DC free M² code will give the best results with regard to BER and is felt to be far superior to any other codes yet available for these applications. Compatibility with existing Miller systems is inherent in the design.

Reproduce amplifier bay

The Reproduce Amplifier Bay is similar to conventional analog direct reproduce amplifier bays, but has been designed specifically for high bit rate applications. The bay will accommodate up to 16 reproduce amplifiers whose function it is to amplify the low level digital signals read from tape prior to the decode and deskew functions. Each reproduce amplifier contains six speed, electrically switchable equalizers capable of being adjusted over a ±50% range on either side of the nominal tape speed.

Bit sync decoder bay

Clock recovery and decoding is accomplished in the bit sync/decoder PWA located in the Bit Sync Decoder Bay. One bit sync/decoder card is used for each track on tape, including the master channel. The unit will decode either Miller or M² and provides NRZ-L data plus clock to the deskew electronics.

Deskew electronics

The deskew electronics, mounted in the Digital Process Bay, realign the data on a bit-by-bit basis. Each deskew PWA handles two tracks of data. With the aid of an external bit rate clock, the deskew electronics time base correct the data, removing timing perturbations caused by the tape transport. Deskewing and time base correction are accomplished by storing the data in shift registers with sufficient correction capability for timing errors related to the record/reproduce process. During the deskew process, sync words are removed as data is reformatted.

Parallel-serial converter

A parallel-serial converter, also located in the Digital Process Bay, commutates the data channels after reproduce and deskew to reformat the high bit rate data to its original configuration. One converter is required per Digital Process Bay, and it is user programmable to conform to tape format requirements.

On-line diagnostic/mode select panel

To simplify setup and test procedures, an on-line diagnostic/mode select panel is provided that permits selection of individual record/reproduce lines. The complete input-output path for a selected line can be tested. Alternately, the tape and heads can be bypassed in the electronics-electronics (E-E) mode. The serial-parallel-serial converters and sync/deskew circuits can also be bypassed in order to test specific functions on selected line.

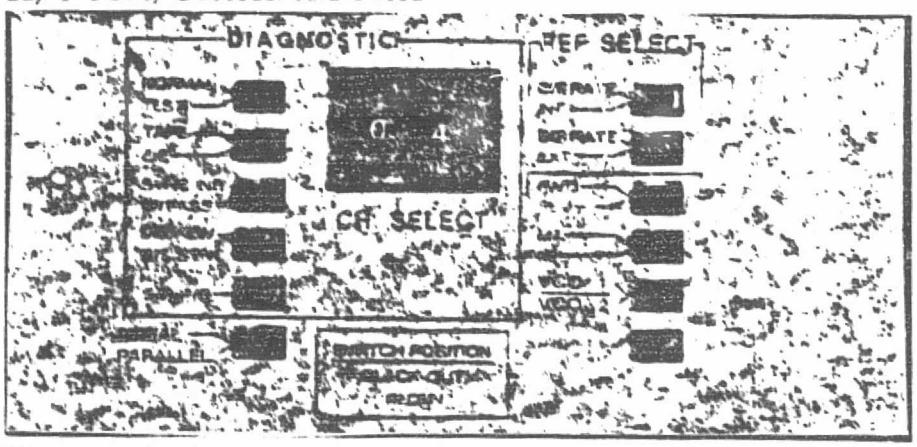

Diagnostic/mode select panel

HBR-3000 System exclusives

DC free M² coding for highly correlated data

Magnetic reproduce heads rely on flux change to sense the information recorded on a magnetic media. Conventional NRZ-L data containing strings of continuous "0" would appear as a DC level if recorded directly without some form of coding. Various coding schemes have been developed that essentially force flux changes according to a set of logical rules. In 1970 Ampex introduced the Miller code as the most efficient method of coding digitized information in applications requiring high reliability and packing density. The Miller code is widely used in both data processing and instrumentation applications, and is, with slight variation, the predominant code used in most digital computer disks.

With the advent of digitized video and other highly correlated graphic information, such as satellite scan information, it became apparent that certain pattern configurations generated codes with an extremely high DC content resulting in unacceptable error rates.

Now, from Ampex again, has come the most important advance to resolve the problem of unique pattern sensitivity at high bit packing densities—the M² code. M² effectively removes the DC component found in other coding schemes, a vital factor when repetitiously recording certain code patterns.

The Miller and M² codes are complementary. The HBR-3000 encoder circuitry will provide either as a result of operator choice. Any Miller coded data can be played back through the decoder circuitry since it includes both Miller and M² capability without operator intervention. It is a straight forward system—no exotic bit insertion, bit reversal or scrambling techniques are needed.

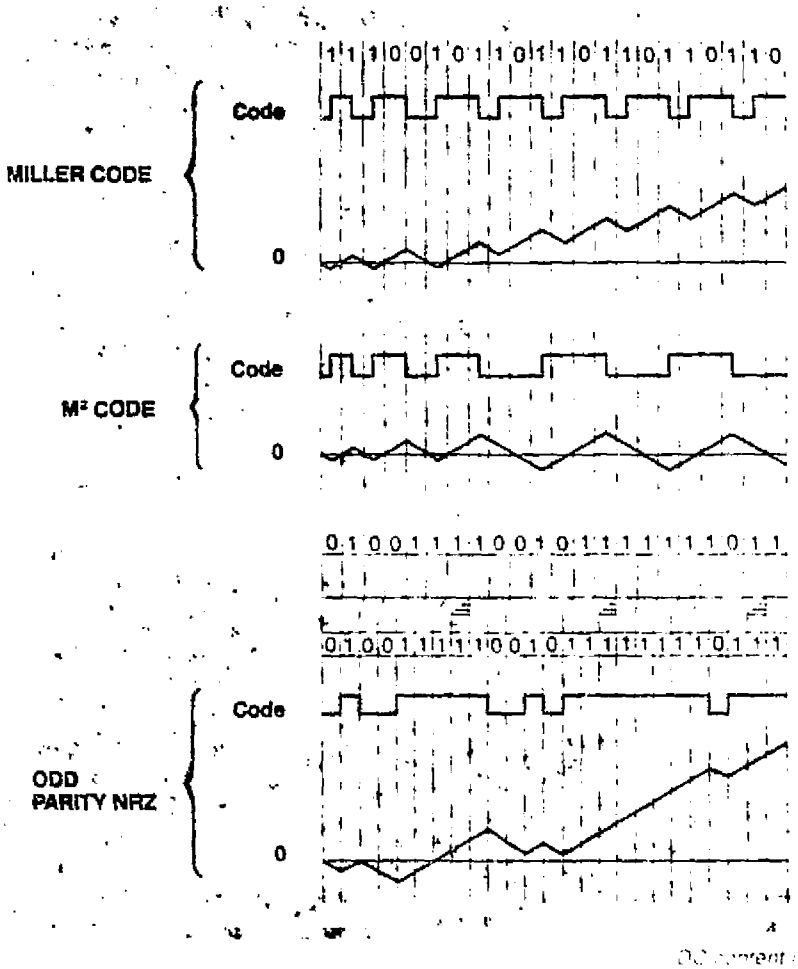

DC component in codes

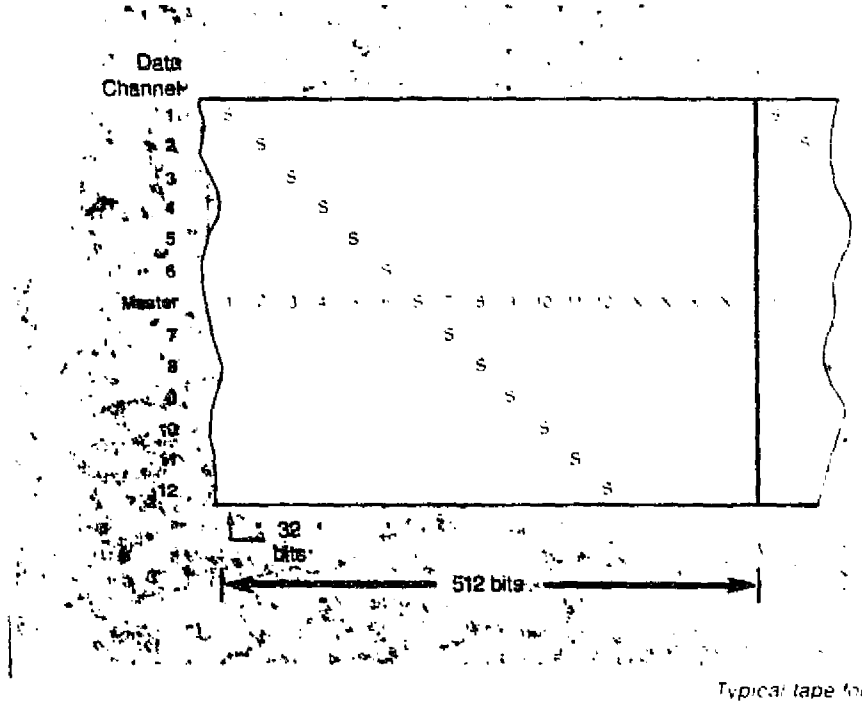

Typical tape format

Dedicated master channel for time base correction data

Data arriving at the input to the record/reproduce system is in a time correlated sequence that must be preserved. Tape recorders, being electromechanical devices, have inherent time related errors that must be taken into account. These timing errors are often compounded when data is recorded on one system and reproduced on another.

The Ampex HBR-3000 system totally eliminates these timing errors through the use of a master channel/sync word system as illustrated. Parallel data streams arrive at the input to the sync inserter where a unique 32 bit sync word is sequentially inserted in each of the data streams. As data is replaced by the sync word in each of the parallel data streams, the replaced data is recorded on the master channel, thus preserving the continuity of the data. The process is repeated every 512 bit intervals, a spacing far wider than the accumulated error tolerances in the record/reproduce process.

During reproduce, individual tracks are out of sync with respect to each other due to the mechanical errors of skew and inter-track time displacement error. The deskew logic detects the unique sync word in each track, corrects it, replaces the data from the master channel and stores the decoded data in registers for simultaneous clocking out by the internal clock in its original format.

HBR-3000 System—design nomograph

The key parameters of a High Bit Rate record/reproduce system are (a) data rates, (b) reliability or bit error rates, and (c) record time available. To achieve these objectives within the state-of-the-art of current technology, many choices are available. The design nomograph has been provided to assist the application engineer in determining these trade offs. Some examples of its use follows.

Assume a user system generates a serial stream of 32 Megabits/sec per channel, limited primarily by TTL logic. The principle of space multiplexed recording is to distribute, or fan out, the high bit rate input over some number of tracks on tape. The first step, therefore, is to decide on the number of tracks to be allocated for data. If all 24 available tracks are to be allocated to a single 32 Megabit/sec data channel, then the resultant track data rate is 1.33 Megabits/sec per track. It should be noted that two or more 32 Megabit / sec channels could be satisfied by reducing the number of tracks allocated to each. In this instance, two or three such data channels could be recorded on 12 or 8 tracks per channel resulting in bit rates of 2.67 or 4.0 Megabits / sec per track respectively.

Similarly, consider an application that requires an eight bit word to be recorded at a 2 Megabyte/sec rate (2 Megabits/sec parallel input). If each parallel data channel is allocated a single track on tape, the resultant bit rate is 2 Megabits /sec per track. If 24 tracks are available on tape, each parallel data line is allocated three tracks and the resultant track rate is reduced to .667 Megabits/second.

Having determined individual track rates, a packing density consistent with bit error rate requirements must be selected. Standard configurations provide for a track rate of 4 Megabits/sec at 33.3k bits/inch resulting in a nominal tape speed of 120 inches/sec. Tape speed and tape length available then determine total recording time available from a single reel of tape. At a tape speed of 120 inches/second with 10,500 feet of tape available, maximum record time would be 17.5 minutes.

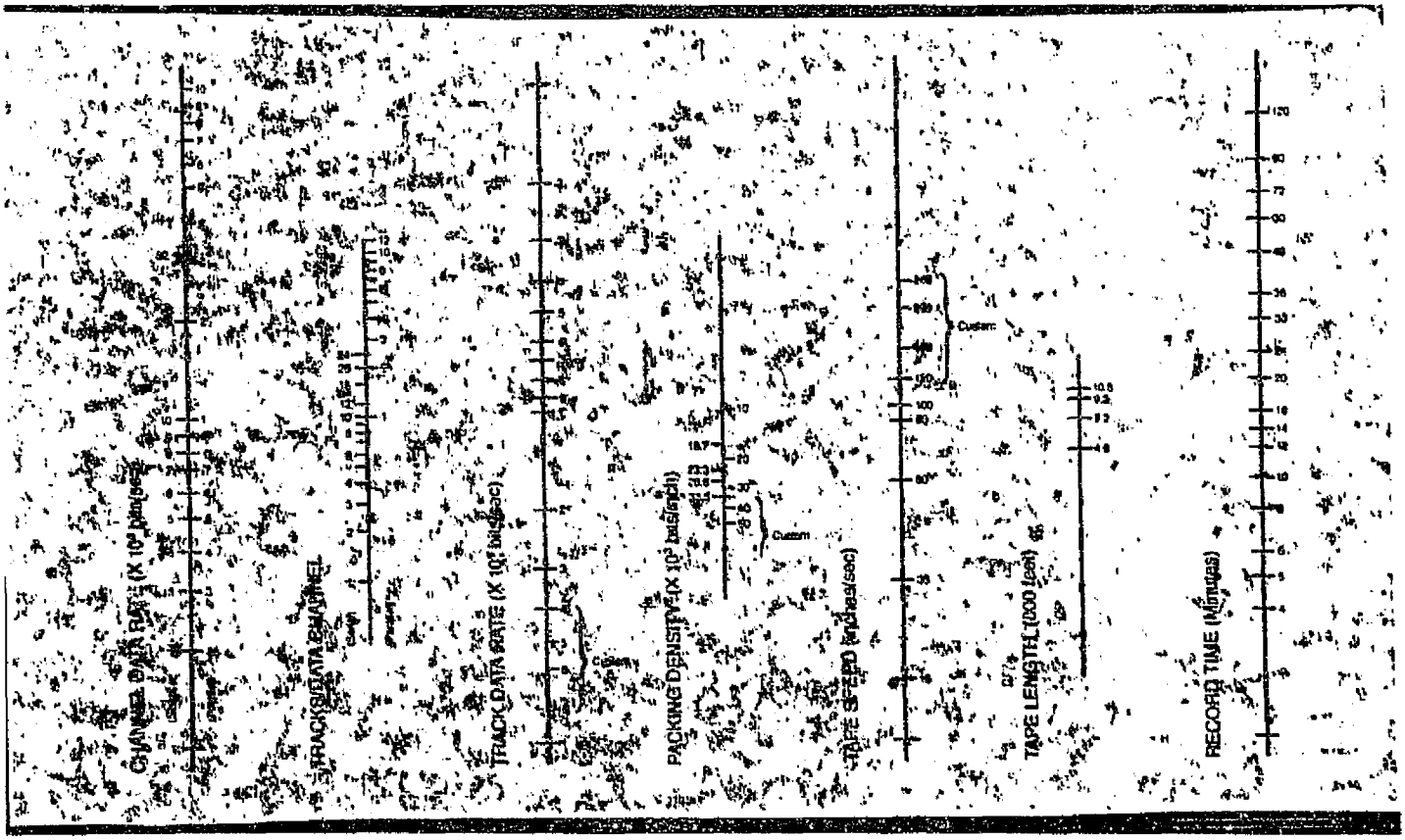

HBR-3000 system design nomograph

Sales offices

For additional information, contact the Ampex sales office listed below:

U.S. SALES OFFICES

ALABAMA
4306 Governors Drive S.W.
Suite "C"
Huntsville, AL 35805
(205) 837-3702

CALIFORNIA
500 Rodier Drive
Glendale, CA 91201
(213) 240-5000

1020 Kifer Road
Sunnyvale, CA 94086
(408) 733-2900

FLORIDA
1355 N. Atlantic Avenue
Suite 120
Cocoa Beach, FL 32931
(305) 783-1811

ILLINOIS
2201 Lunt Avenue
Elk Grove Village, IL 60007
(312) 593-6000

MARYLAND
10215 Fernwood Road
Bethesda, MD 20034
(301) 530-8800

MASSACHUSETTS
391 Totten Pond Road
Waltham, MA 02154
(617) 890-2040

NEW JERSEY
75 Commerce Way
Hackensack, NJ 07601
(201) 489-7400

NEW MEXICO
1200 Pennsylvania N.E., Suite D
Albuquerque, NM 87110
(505 266-8749

OHIO
4130 Linden Avenue
Dayton, OH 45432
(513) 254-6101

TEXAS
1615 Prudential Drive
Dallas, TX 75235
(214) 637-5100

INTERNATIONAL SALES AND SERVICE COMPANIES

ARGENTINA
Ampex Electronica S.A.
Cerrito 836 9th Floor
Casilla de Correo 5403
Buenos Aires, Argentina
Telephone: 46-9029 or 40-7881

AUSTRALIA
Ampex Australia Pty. Ltd.
4 Carlotta Street
Artarmon
Sydney NSW 2064
Telephone: 439-4077

BELGIUM
Ampex S.A.
Rue de L'Industrie
B-1400 Nivelles
Belgium
Telephone: 067/2249.21

BRASIL
Ampex Do Brasil Electronica Ltda.
Conjunto 1.502-15 Andar, Bloco D
Rua Mexico, 31
20.000—Rio de Janeiro
Brasil
Telephone: 242-3795

CANADA
Ampex Canada Ltd.
132 East Drive
Bramalea Ontario, Canada
Telephone: (416) 791-3100

COLOMBIA
Ampex de Colombia S.A.
Apartado Aereo No. 29613
Carrera 10 No. 19-64
Oficina 409/410
Bogota, D.E. Colombia
Telephone: 43-82-32 and 41-43-84

FRANCE
Ampex S.A.R.L.
17-23, rue du Dome
92100 Boulogne
France
Telephone: 609-9155

GERMANY (Federal Republic)
Ampex Europa GmbH
6000 Frankfurt, (Main)
Walter-Kolb-Str. 9-11
Germany (Federal Republic)
Telephone: 60581

GREECE
Ampex World Operations S.A.
260 Kifissias Avenue
P.O. Box 45, Halandli (1)
Athens, Greece
Telephone: 67 18 160

HONG KONG
Ampex World Operations S.A.
1801-1805 Star House
8 Salisbury Road
Kowloon, Hong Kong
Telephone: 3-678051-3

ITALY
Ampex Italiana S.p.A.
Via Turati, 6
Milano-20121
Italy
Telephone: (02)65.15 41-2-3-4

Ampex Italiana S.p.A.
Via Del Minatori
Casella Postale Zur 720
Roma, Italy
Telephone: (06)54-69-91

JAPAN
Ampex Japan Ltd.
3, Kojimachi 3-Chome
Chiyoda-Ku
Tokyo, Japan 102
Telephone: 03-264-7331

MEXICO
Ampex De Mexico, S.A. de C.V.
Apartado Postal 13-615
Division del Norte No. 1832
Mexico 13, D.F.
Telephone: 539-68-70/71/72

NETHERLANDS
Ampex B.V.
2505 Utrecht
Zamenhofdreef 65A
Netherlands
Telephone: 030-61.29.21

SOUTH AFRICA
Ampex South Africa (Pty.) Ltd.
8th Floor, Standard House
67 Simmonds St.
Johannesburg 2001
South Africa
Telephone: 838-7640

SWEDEN
Ampex A.B.
Rissneleden 8
P.O. Box 7056
S-172 07 Sundbyberg
Sweden
Telephone: 08/28 29 10

SWITZERLAND
Ampex World Operations S.A.
1701 Fribourg
Rue de Romont 29
P.O. Box 1031
Switzerland
Telephone: 037-22.73.31

UNITED KINGDOM
Ampex Great Britain Ltd.
Acre Road
Reading, Berkshire
England
Telephone: (0734) 85200

UNITED STATES
Ampex International
401 Broadway (Box 4000)
Redwood City, CA 94063
Telephone: (415)

AMPEX

Ampex Corporation
Data Products Division
401 Broadway
Redwood City, California 94063
(415) 367-2011

LITHO IN U.S.A. D-322 7-77

VRR·421

Video Characteristics

Video Record/Reproduce
One channel (DC-6 MHz) capable of recording "transient free" instrumentation data or video formatted data of multiline rates (511-1023 lines per frame).

Input/Output Level
1 V-p-p terminated into 75 Ohms

Bandwidth
10 Hz to 6 MHz ±1.5 dB

Signal-to-Noise
40 dB p-p to RMS

Time Base Stability
5 nanoseconds RMS

Distortion
−25 dB

Amplitude Linearity
±5%

Record Time
60 mins.

Audio Characteristics

Audio Record
Two channels of audio capable of recording signal frequencies from 60 Hz to 12 kHz.

Input Level
0 dBm 600 ohms balanced or unbalanced.

Frequency Response
60 Hz to 12 kHz ±3 dB

Signal-to-Noise
40 dB p-p to RMS

Distortion
3% at normal record level.

Operating Features

Controls
Standby; Record; Play; Rewind; Fast Forward; Power ON/OFF; EOT/BOT; Calibrate.

Start Time
Stabilized Playback Video in 8 seconds or less.

Power Requirements
115/230 V AC; 47 to 63 Hz.

Recording Medium
1" tape, 1.13 mil overall thickness video tape, "B" wrap.

Reel Size
NAB 8", 10.5", or 12.5".
Note: Record Time specified for 10.5" reel

Configuration

Size
Console—31" x 19" x 17.5"
Rack—6 ft., 19" EIA

Weight
Console—165 lbs.
Rack—<400 lbs.

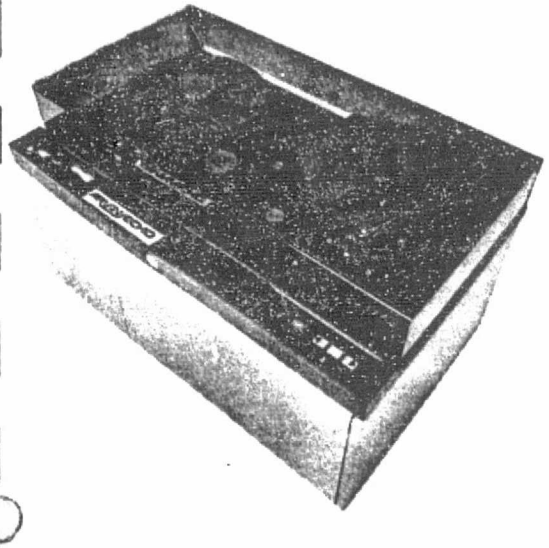

ARVIN/ECHO™
ECHO SCIENCE CORPORATION
an ARVIN SYSTEMS, INC. company
485 E. Middlefield Road, Mt. View, California 94043
Tel: (415) 961-7143 TWX: 910-379-6499

Universal Instrumentation Video Recorder/ Reproducer WRR-421

WRR-421

The WRR-421 Recorder/ Reproducer employs Arvin/Echo's segmented helical scanning recording format with a Pilot signal, which is utilized to provide all timing information independent of data format. For the WRR-421, Arvin/Echo has incorporated its unique "transient free" record feature, thus broadening the recorder's adaptability to mission parameters. The system makes use of the Echo scanner assembly which achieves Quad writing speeds in conjunction with long life ferrite heads and standard one-inch Gamma Ferric Oxide video tape, providing a cost effective system with exceptional quality performance. The WRR-421 Recorder/ Reproducer can be used alone for lab analysis or for reproducing tapes recorded on the ARVIN/ ECHO WR-221 or WR-521.

The WRR-421 can record virtually any type of signal.

Radar
Forward-looking, ground mapping, multimode radars. Radar video with horizontal and vertical sweep waveforms multiplexed in one channel.

Electro-Optic Sensor
Forward-Looking Infra-Red (FLIR)

Television
Low Light Level Television (LLLTV); All EIA Multi-Line Television Standards.

Multiplexed Narrow Band Data
FDM/TDM, AM, FM, suppressed carriers, etc.

Digital
Digital data rates up to 10×10^6 bits per second with Bit Error Rates (BER) $< 1 \times 10^{-5}$.

Audio
Audio annotation on Channel I and event or timing information on Channel II. Optional audio bandwidths up to 30 KHz available.

Details regarding the size, weight, and performance characteristics of the WRR-421 are indicated under the specifications on the reverse side.

ARVIN/ECHO™

REFAC electronics corporation

MICROMINIATURE LAMPS

BULLETIN 3001 B

PINLITE® THE WORLD'S SMALLEST INCANDESCENT LAMP

- ECONOMICAL
- SMALL SIZE
- LOW POWER
- SHOCK PROOF
- VIBRATION RESISTANT
- FAST RESPONSE TIME
- LONG LIFE
- VARIOUS COLORS AVAILABLE
- LOW VOLTAGE
- SPECIAL DESIGNS

ACTUAL SIZE
PINLITE ®

PINLITE® LAMP SPECIFICATIONS

L = Lens Axial = No Prefix

MODEL	VOLTAGE V	CURRENT mA	BULB LENGTH INCHES (MM)	BULB DIA. INCHES (MM)	LEAD DIA. INCHES (MM)	PULSE RESPONSE TO 50% (MILISECONDS)	LIGHT OUTPUT (MILLILAMBERT)	RESISTANCE COLD 'HOT (OHMS)	LIFE (HOURS)
L12-12	1.25	12 ±2	.080 (2.03)	.030 (0.76)	.004 (0.10)	5	45	13/104	1000
L15-30	1.5	30 ±4	.080 (2.03)	.030 (0.76)	.004 (0.10)	7	160	5.5/50	1000
L15-45	1.5	45 ±5	.080 (2.03)	.030 (0.76)	.004 (0.10)	10	220	4/33	1000
15-15	1.5	15 ±2	.070 (1.78)	.015 (0.38)	.003 (0.07)	5	60	11/100	800
30-30	3	30 ±3	.125 (3.18)	.030 (0.76)	.005 (0.13)	7	250	10/100	1000
60-20	6	20 ±3	.250 (6.36)	.040 (1.02)	.005 (0.13)	10	400	30/300	2000

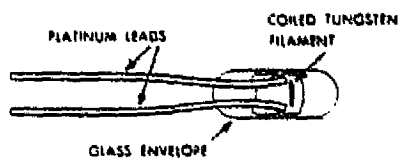

LENS LAMP

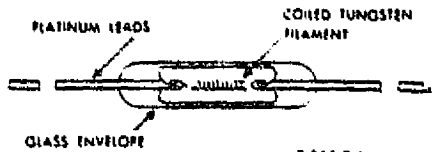

AXIAL

MICROMINIATURE LAMPS

REFAC electronics corporation
P.O. SOX 809 • WINSTED, CONNECTICUT 06098
WEST HILL ROAD • BARKHAMSTED, CONNECTICUT 06098
(203) 379-2731 TWX: 710-449-6464

BULLETIN 6-101C

Off-Axis Collimator Model 6-101

Calibrates, Tests and Aligns
Electro-Optical Systems and Instruments

Special Features

- ☐ No obscuration and low transmission losses
- ☐ Includes a set of precision, wheel-mounted entrance apertures
- ☐ Special mirror coatings available for specific spectral regions
- ☐ Accepts infrared, visible and ultraviolet sources
- ☐ Spectral Range — 0.25 micron to beyond 16 microns
- ☐ High angular resolution

Typical Applications

- ☐ Checkout, alignment and calibration of missile homing systems
- ☐ Image evaluation (infrared, visible, ultraviolet) of optical systems
- ☐ Multi-sensor alignment and calibration
- ☐ Radiometer calibration
- ☐ Field of view plotting and alignment of electro-optical systems
- ☐ Boresighting optical instruments to complete systems

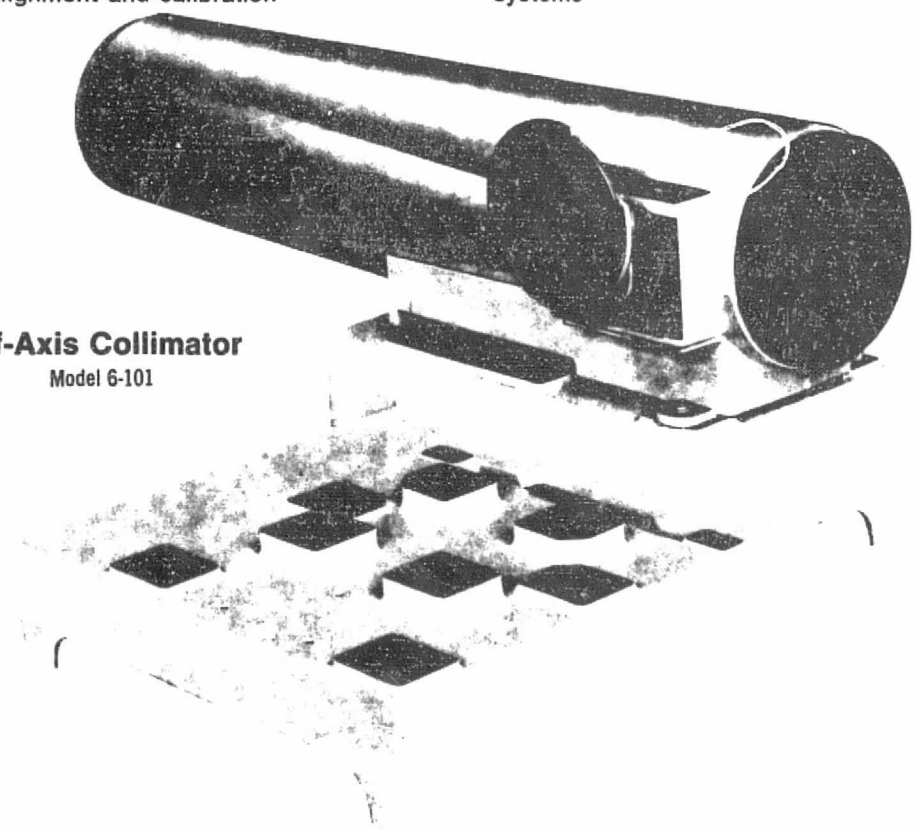

Off-Axis Collimator
Model 6-101

Description

The Model 6-101 Off-Axis Collimator is an optical system designed to calibrate and test electro-optical instruments and systems which receive radiation from both near and distant targets.

The Model 6-101 is normally used with a radiation reference source to simulate accurately the radiation characteristics — color temperature, irradiance and target size — of remote targets. Although it is primarily intended to collimate infrared energy by producing a uniformly intense beam of parallel radiation, this system can also collimate energy in the visible and ultraviolet spectral regions.

The radiation beams produced by this Off-Axis Collimator do not suffer from excessive transmission loss, as do those produced by refractive optical systems. In addition, the Model 6-101's parallel rays are free from areas of obscuration, which normally occur in Cassegrain and Newtonian systems.

This collimation system employs a plane reflecting mirror and a 4.8-inch diameter, f/5.3 off-axis paraboloidal mirror with a focal length of 25.6 inches (nominal). Both of these mirrors can be coated with any one of three optical coatings for high reflectivity in specific spectral regions. In the standard Model 6-101, an aluminum coating with silicon monoxide overcoating is used. Two other coatings, offering high reflectivity in specific spectral ranges, are high-purity aluminum with a magnesium fluoride overcoating and gold with or without silicon monoxide overcoating. Both are readily available at extra cost. (A 2-inch by 2-inch reflectivity sample of these coatings can be supplied for a slight additional charge.)

In operation, radiation from the reference source enters the Collimator through the selected entrance aperture and is reflected by the plane mirror toward the concave mirror where it is collimated and redirected toward the exit aperture. (Figure 1).

The optical system in the standard 6-101 has an angular resolution of 0.2 milliradian, which is sufficient for many applications of this Off-Axis Collimator. However, this instrument can also be supplied with an angular resolution of 0.1 milliradian or better on special order.

Accessories for the 6-101 Collimator include auxiliary radiation interrupting devices, such as two-speed or variable-speed radiation modulators. In addition, spectral filters of the interference-type can be provided mounted to filter wheels.

Design Considerations

The Model 6-101 Off-Axis Collimator consists of a lightweight, cast aluminum tube which contains the system optics — a plane reflecting mirror and an off-axis, concave, paraboloidal mirror — and a universal mounting plate.

Both mirrors are coated simultaneously with the coating surface which provides optimum reflectance in the wavelength region of interest. Before the assembly of each Collimator, mirror reflectance is measured. A curve showing measured reflectance versus wavelength is then prepared and supplied with the Collimator. Using this curve, collimator transmittance may then be calculated by squaring the measured value of reflectance at each wavelength.

The standard coating for the Collimator mirror surfaces is evaporated aluminum overcoated with silicon monoxide. This coating provides high reflectance from about 0.3 micron in the ultraviolet region to beyond 16 microns in the infrared, with exception of a dip at about 0.8 micron due to the characteristic absorption of aluminum. Attenuation below 0.3 micron is attributable to both the aluminum and the silicon monoxide.

The ultraviolet coating, available on special order, is composed of high-purity aluminum and a thin overcoating of magnesium fluoride. High reflectance is provided from 0.2 micron through the visible and infrared wavelengths, although the dip at 0.8 micron, due to the aluminum, is present.

For applications where the absorption band at 0.8 micron is objectionable, a special infrared coating is available. This coating is a film of gold overcoated with silicon monoxide. Reflectance with this coating is high from about 0.6 micron throughout the infrared wavelength region.

Figures 2, 3, and 4 show transmittance versus wavelength curves for both standard and special coated mirrors.

The entrance aperture wheel of the Model 6-101 Off-Axis Collimator is located at one side of the aluminum tube and is positioned perpendicular to the optical axis. This aperture wheel has seven precisely etched openings graduated in area to permit changes of up to 1000-to-1 in input flux density.

A wide range of radiation reference sources, including the Barnes Models 11-100T, 11-101T, 11-120T, 11-200T and 11-201T, are easily and accurately positioned on the Collimator's universal mounting plate. Spectral and tungsten sources can also be used with the Model 6-101.

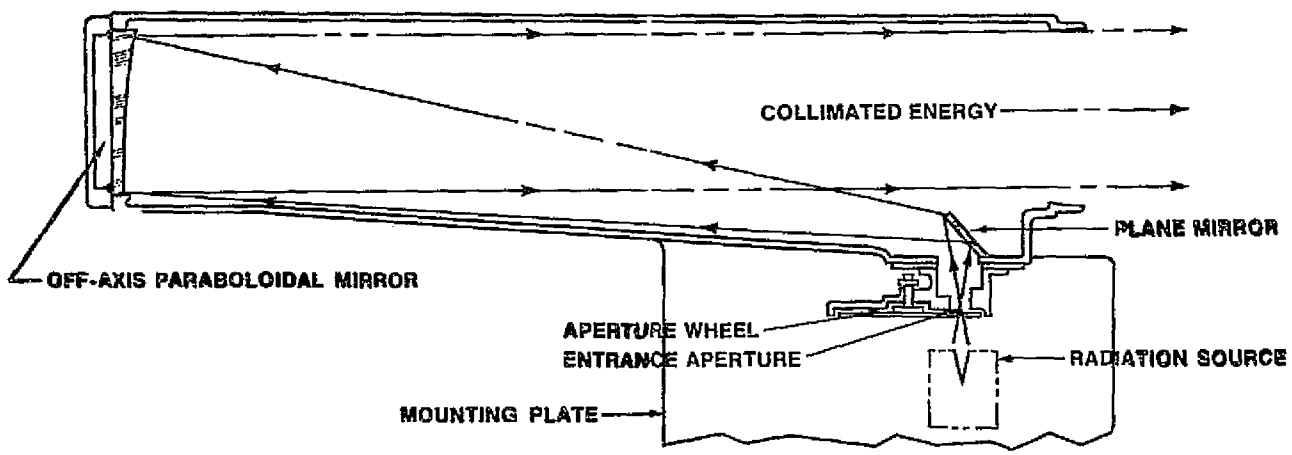

Figure 1 — Optical Schematic of Model 6-101 Off-Axis Collimator.

Specifications *(Note 1)*

OPTICAL DATA

Main Mirror:
- Type ..... Off-Axis Paraboloid
- Diameter *(inches)* 4.8
- Focal Length *(inches)* ..... 25.6 nominal
- f/number 5.3
- Surface Treatment *(Note 2)* Evaporated aluminum with silicon monoxide overcoat

Auxiliary Mirror:
- Type ..... Plane
- Size *(inches)* ..... 1 x 1¼
- Surface Treatment *(Note 2)* Evaporated aluminum with silicon monoxide overcoat

Optical Transmittance ..... See Figure 2 and text, Page 3

Resolution *(Note 3)* ..... 0.2 milliradian

Entrance Apertures *(Note 4)*

	Diameter (Inches)	Area (cm^2)	Area Ratio
Aperture #1	0.0081	0.333×10^{-3}	1
Aperture #2	0.0141	1.00×10^{-3}	3
Aperture #3	0.0256	3.33×10^{-3}	10
Aperture #4	0.0444	10.0×10^{-3}	30
Aperture #5	0.0810	33.3×10^{-3}	100
Aperture #6	0.141	100×10^{-3}	300
Aperture #7	0.256	333×10^{-3}	1000

MECHANICAL DATA

Main Housing:
- Dimensions *(inches)* ..... 8(H) x 9½ (W) x 28(L)
- Weight *(pounds)* 13¾

Base Plate:
- Dimensions *(inches)* ..... 5¾(H) x 20(W) x 17½ (L)
- Weight *(pounds)* 13½

NOTES

1. These specifications describe equipment previously furnished and are subject to change. Please request confirmation of these data at time of purchase.
2. Upon request, one of the two coatings described below can be provided at additional cost.
   a. Special ultraviolet coating consisting of a rapidly deposited high-purity aluminum with an overcoating of magnesium fluoride.
   b. Special infrared coating consisting of a specially prepared gold film with an overcoating of silicon monoxide. For maximum reflectance around 1 micron, and also between 8 and 10 microns, the silicon monoxide overcoat may be omitted.
3. On special order, this instrument can be supplied with a resolution of 0.1 milliradian or better.
4. A rotatable entrance aperture wheel permits the selection of the aperture diameters listed. Settings also indicate the area in square centimeters. Other diameters can be provided on special order.

Typical Reflectance for Each Mirror Used in Model 6-101 Off-Axis Collimators

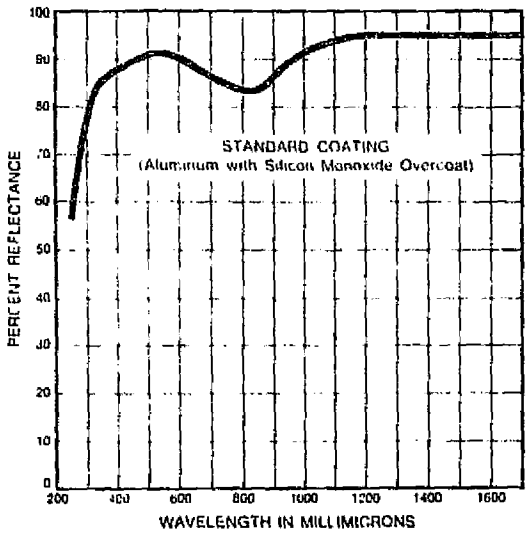

Figure 2 — Typical reflectance curve for standard aluminum and silicon monoxide overcoat.

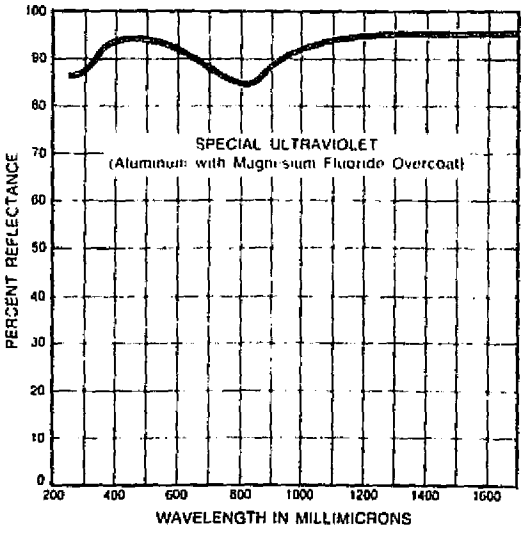

Figure 3 — Typical reflectance curve for special ultraviolet coating (high-purity aluminum and magnesium fluoride overcoat).

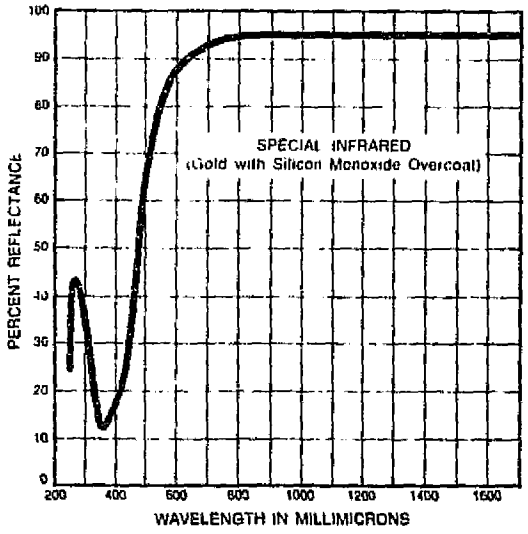

Figure 4 — Typical reflectance curve for special infrared coating (gold and silicon monoxide overcoat). See Note 25.

Accessories

To extend the capabilities of the Model 6-101 Off-Axis Collimator into other areas of optical investigation and measurement, the following accessories are available on special order.

- ☐ Sources: infrared blackbody, NBS tungsten and spectral sources (ultraviolet to infrared)
- ☐ Radiation Modulators (two-speed and variable)
- ☐ Filter Wheel assembly with Interference or Neutral Density Filters
- ☐ Resolution targets or patterns on aperture wheel assembly in place of apertures
- ☐ Manually-operated iris diaphram (from 0.475-in. to 4.8 inches) in exit aperture opening
- ☐ Shutters, compur-type

BARNES
Barnes Engineering Company
30 Commerce Road

Bulletin 11-035A

BARNES

Radiation Reference Source Model 11-210

- 50 - 1000°C
- Emissivity of .99 ±.01
- One Inch Aperture
- One Year Warranty
- Stable and Accurate

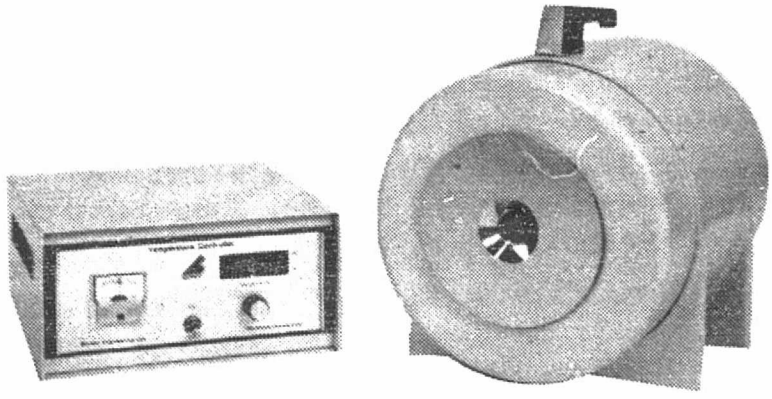

The calibration of infrared instruments requires sources of radiation with known intensities and spectral distributions. Such sources must remain stable and accurate under varying laboratory and field conditions. The Barnes Model 11-210 Radiation Reference Source and Controller meets these requirements.

The Model 11-210 Source uses the proven cylindrical/conical cavity. With sophisticated design and careful fabrication techniques, radiation characteristics close to blackbody conditions are obtained. Unlike competitive sources which claim only nominal value cosine law distribution, the Model 11-210 precisely follows cosine law distribution over the central 15° cone. This minimizes alignment problems and assures accurate calibration.

Any temperature in the range from 50 to 1000°C may be set into the Controller. Cavity temperature is monitored with a platinum resistance probe sensed in the Controller. The Controller automatically adjusts electrical power to heat the cavity in the Source and maintains it at the selected temperature. The Controller design is of the zero-crossover proportional rate type which performs switching only while AC power is going through zero. This eliminates radio frequency interference due to switching transients.

The 11-210 Source and Controller are fabricated using quality and rugged components. Each unit is tested and certified using standards traceable to the National Bureau of Standard. Workmanship and material are guaranteed for one year.

Accessories

Cavity temperature can be monitored externally. For this purpose, Barnes can provide a Platinum/Platinum Rhodium thermocouple probe. The probe is available factory installed or in kit form for customer installation. Alternately, a Thermocouple and Reference is available. Factory installed, it includes a precision platinum thermocouple and electronic temperature reference. When connected to a conventional voltmeter, cavity temperature can be obtained.

When chopped radiation is required, the 11-210 can be used with the Barnes Variable Speed Modulator. The Modulator consists of a motor assembly, speed controller and chopper wheel. Seven chopper wheels are available and provide chopping rates from 0.5 to 30,000 cps.

The 11-210 Source mounts directly on the Barnes Aperture Plate Assembly. With its seven precision apertures, one can conveniently obtain 1000/1 attenuation in emitted radiation at any temperature setting.

The Source, Modulator and Aperture Plate may also be mounted to the Barnes off-axis 4.8" Collimator, Model 6-101, forming a complete and flexible simulator system.

Specifications

Temperature Range	50 - 1000 °C
Aperture	1" Diameter (2.5 cm)
Emissivity	.99 $\pm$ 0.1
Absolute Accuracy of Calibration	$\pm$5 °C @ 1000 °C
Reset Accuracy	$\pm$1 °C @ 1000 °C
Longterm Stability (105 to 125 V and Ageing)	Better than $\pm$1 °C
Power	485 Watts Warm-up 275 Watts Operation
Warm-up Time (Ambient to 1000 °C)	90 minutes
Ambient, Controller	0 to 40 °C
Ambient Source	-40 to 60 °C
Source Case Temperature	5 °C above ambient
Aperture Plate Temperature	50 °C a 1000 °C
Size: Source	$11\frac{1}{2}$ x $10\frac{1}{2}$ x $12\frac{1}{2}$ inches (29 x 27 x 32 cm)
Controller	$5\frac{1}{2}$ x 10 x 10 inches (14 x 25 x 25 cm)
Weight: Source	25 lbs (11 kgs)
Controller	10 lbs (4.5 kgs)

Barnes Engineering Company
30 Commerce Road
Stamford, Connecticut 06904
Telephone 203 348-5381